Kari Ravnestad Kjørholt

Optimization of Hemocompatible Thin Film Coatings for Biomedical Applications

Master's thesis in Materials Science and Engineering
Supervisor: Ragnhild Elizabeth Aune
Co-supervisor: Julia Glaum

June 2021

Master's thesis

NTNU
Norwegian University of Science and Technology
Faculty of Natural Sciences
Department of Materials Science and Engineering

NTNU
Norwegian University of
Science and Technology

Kari Ravnestad Kjørholt

Optimization of Hemocompatible Thin Film Coatings for Biomedical Applications

Master's thesis in Materials Science and Engineering
Supervisor: Ragnhild Elizabeth Aune
Co-supervisor: Julia Glaum
June 2021

Norwegian University of Science and Technology
Faculty of Natural Sciences
Department of Materials Science and Engineering

NTNU
Norwegian University of
Science and Technology

Preface

Throughout the last century, scientists have developed medical devices that can be used for medical treatments or even replace parts of the human body or bodily functions. This advance was only made possible by the use of biocompatible materials, and today a broad range of materials are used in the industry of biomedical devices. Metals, ceramics, polymers and composites are all used both with and without surface modifications aiming to improve the materials performance in the human body.

This Thesis is a continuation of work performed by the present author during her Specialization Project (SP) entitled "*Development of TiN Thin Film Coatings for Biomedical Applications*" (2020) and has aimed to optimize TiN thin film coatings for use on blood contacting biomedical devices. The work is part of a larger project led by Professor Ragnhild E. Aune which aims to improve the material properties of various biomedical devices. The Thesis is intended to support work performed by PhD Candidate Maren K. Fossum, and as a result some choices made throughout the present work were thus influenced by her work.

The developed coatings have been deposited on substrates of medical grade thermoplastic polyurethane. The structure, surface morphology, chemical composition, mechanical properties and biocompatibility of the coatings have been characterized. The materials have also been exposed to a simulated body fluid to examine possible material degradation due to prolonged presence in the human body.

The tasks performed in the present work have been the following:

1. Reproducing two TiN coatings first developed during the present author's SP.

2. Characterization of the initial coatings.

3. Evaluation of the performance of the coatings with respect to the non-coated reference substrate.

4. A first-step optimization of the most promising coating by development of a third TiN coating.

5. Characterization of the newly produced coating, as well as a commercial Diamond-Like Carbon (DLC) reference coating and the non-coated reference substrate.

Abstract

The use of biomedical devices has provided vast benefits to the human population in the decades since the scientific field first was developed. However, the bio- and hemocompatibility of existing devices should be further improved to reduce the risk of complications. The present work has focused on 30 nm thick TiN thin film coatings produced using RF magnetron sputtering for use on blood-contacting biomedical devices. The coatings have been deposited on two types of medical grade thermoplastic polyurethane (Carbothane) substrates. The first generation of coatings, TiN (A) and TiN (B), were deposited on the thicker substrates using balanced and unbalanced magnetron sputtering, respectively, at 80 W. Further, coating TiN (C) was deposited on the thinner substrates using the balanced magnet configuration at 120 W and was later compared to a 50 nm thick commercial DLC coating deposited on the same substrates.

The TiN coatings are believed to have a lower than stoichiometric nitrogen content, and SEM analysis revealed excellent coating coverage and that all coatings followed the large-scale surface morphology of the substrates. The substrates showed significant surface roughness in the form of directional lines in a regular pattern, which was more prominent for the thinner substrates. Micrometer sized $BaSO_4$ particles protruded the surface of the thicker substrates. Further, cracks were found in all TiN coatings, suggesting that they are brittle and have suboptimal bio- and hemocompatibility. Coating TiN (C) was significantly more cracked than TiN (A) and TiN (B) while no cracks were found in the DLC coating where particles agglomerated in a distinctive pattern. However, cross section analysis revealed that coating TiN (C) was homogeneous in thickness and followed the surface morphology of the substrate on a nanometer scale, while much porosity was observed below the DLC coating along with Carbothane degradation, believed to be caused by the coating procedure.

The contact angle with water of the thicker substrate was reduced from $101° \pm 2°$ by applying coating TiN (A) ($80° \pm 2°$) and TiN (B) ($89° \pm 1°$), thus suggesting that coating TiN (A) is the most biocompatible. The contact angle measurements of the thinner substrates ($120° \pm 3°$) had greater uncertainty due to significant surface roughness, but both coatings TiN (C) and DLC reduced the contact angles to $93° \pm 3°$ and $97° \pm 3°$, respectively.

Friction testing revealed that the TiN (C) and DLC coatings improved the friction properties compared to the non-coated reference substrates. Coatings TiN (A) and TiN (B) did also improve the friction properties, but not to the same extent. The friction coefficients were, however, much more stable across the surface for these coatings. The DLC coating had a lower friction coefficient (0.28 ± 0.01) than the TiN (C) coating (0.42 ± 0.01), and the non-coated reference substrate (0.59 ± 0.05). The stability of the measurements also suggested excellent coating adhesion, with a slightly lower stability of the measurements performed on the DLC coating compared to the TiN coatings. The coating adhesion was further evaluated to be sufficient for all coatings.

Tensile testing revealed that neither the deposition of coating TiN (C) or DLC, nor their exposure to the PBS solution, damaged the favorable mechanical properties of Carbothane. Moreover, no correlation was found between the duration of sample exposure to the PBS solution and the surface morphology. However, the time between the end of the exposure and the analysis of the surface morphology was observed to correlate with the degree of material degradation on the thicker non-coated reference substrates. ICP-MS analysis of the liquid solution resulting from the exposure study revealed an increasing leaching of Ba from all samples as a function of the exposure time in the PBS solution, as well as a decrease in the S concentration after 24 hours for all samples. The TiN coatings were also established to release small amounts of Ti into the PBS solution during the first 10 minutes of being exposed.

TiN thin film coatings thus show promise in improving the bio- and hemocompatibility of blood-contacting medical devices compared to the non-coated materials, and outperforms the commercial DLC coating in some respects, but further optimization is needed.

Sammendrag

Bruken av biomedisinsk utstyr har gitt store fordeler til den menneskelige befolkningen i tiårene siden det vitenskapelige feltet først ble utviklet. Bio- og hemokompatibiliteten til eksisterende utstyr burde derimot forbedres ytterligere for å redusere risikoen for komplikasjoner. Dette arbeidet har fokusert på 30 nm tykke TiN tynnfilm overflatebelegg produsert ved RF magnetron pådamping til bruk på biomedisinsk utstyr som skal være i kontakt med blod. Overflatebeleggene har blitt deponert på to typer substrater av termoplastisk polyuretan av medisinsk grad (Carbothane). Først generasjon med overflatebelegg, TiN (A) og TiN (B), ble deponert på tykkere substrater ved bruk av henholdsvis balansert og ubalansert magnetron pådamping ved 80 W. Overflatebelegg TiN (C) ble videre deponert på tynnere substrater ved bruk av den balanserte magnet konfigurasjonen ved 120 W, og ble senere sammenlignet med et 50 nm tykt kommersielt DLC overflatebelegg deponert på samme type substrater.

TiN overflatebeleggene antas å ha et lavere enn støkiometrisk innhold av nitrogen, og SEM-analyse avslørte god dekning av overflaten og at de fulgte stor-skala overflatemorfologien til substratene. Substratene fremviste betydelig overflateruhet i form av rette linjer i et gjentagende mønster, som var mer fremtredende i de tynne substratene. $BaSO_4$-partikler av mikrometerstørrelse stakk opp av overflaten av de tykkere substratene. Videre ble det funnet sprekker i alle overflatebeleggene av TiN, noe som indikerer at de er sprø og har suboptimal bio- og hemokompatibilitet. Overflatebelegg TiN (C) var betydelig mer sprukket opp enn TiN (A) og TiN (B), mens ingen sprekker ble funnet i overflatebelegget av DLC hvor partikler agglomererte i et distinktivt mønster. Analyse av tverrsnittene avslørte derimot at overflatebelegg TiN (C) hadde homogen tykkelse og fulgte overflatemorfologien til substratet på nanometerskala, mens mye porøsitet ble observert under overflatebelegget av DLC sammen med degradering av Carbothane materialet, som antas å være et resultat av deponeringsprosessen.

Kontaktvinkelen med vann til de tykkere substratene ble redusert fra $101°\pm2°$ ved å påføre overflatebelegg TiN (A) ($80°\pm2°$) og TiN (B) ($89°\pm1°$), hvilket indikerer at overflatebelegg TiN (A) er mest biokompatibelt. Kontaktvinkelmålingene av de tynnere substratene ($120° \pm 3°$) var mer usikre på grunn av den betydelige overflateruheten, men deponering av både overflatebelegg TiN (C) og DLC reduserte kontaktvinkelen til henholdsvis $93°\pm3°$ og $97° \pm 3°$.

Friksjonstesting avslørte at overflatebelegg TiN (C) og DLC forbedret friksjonsegenskapene sammenlignet med referansesubstratene uten overflatebelegg. Overflatebelegg TiN (A) og TiN (B) forbedret også friksjonsegenskapene, men ikke til samme grad. Friksjonskoeffisientene var derimot mye mer stabile over overflaten for disse overflatebeleggene. Overflatebelegget av DLC hadde en lavere friksjonskoeffisient (0.28 ± 0.01) enn overflatebelegg TiN (C) (0.42 ± 0.01) og substratet uten overflatebelegg (0.59 ± 0.05). Stabiliteten til målingene indikerte også utmerket heft av overflatebelegget, med en noe lavere stabilitet av målingene utført på overflatebelegget av DLC sammenlignet med overflatebeleggene av TiN. Heften er evaluert til å være tilstrekkelig for alle overflatebelegg.

Strekktesting avslørte at verken deponering av overflatebelegg TiN (C) eller DLC, eller eksponering av prøvene for PBS løsning, skadet de gunstige mekaniske egenskapene til Carbothane. Det ble det ikke funnet en korrelasjon mellom lengden på eksponeringstiden for PBS og overflatemofologien. Det ble derimot funnet en korrelasjon mellom tiden fra avsluttet eksponering til analyse av overflatemorfologien og graden av degradering av de tykkere referansesubstratene uten overflatebelegg. ICP-MS-analyse av den flytende løsningen fra eksponeringsstudien avslørte en økende lekking av Ba med økende eksponeringstid og en reduksjon i konsentrasjonen av S etter 24 timer eksponering for alle prøver. Det ble også fastslått at overflatebeleggene av TiN avga små mengder av Ti til løsningen innen 10 minutter etter eksponering for PBS.

Tynnfilm overflatebelegg av TiN er dermed lovende i forhold til å forbedre bio- og hemokompabiliteten til medisinsk utstyr som skal være i kontakt med blod, og noen av egenskapene er bedre enn egenskapene til det komersielle overflatebelegget av DLC, men videre optimalisering er nødvendig.

Acknowledgments

As I finish this Thesis and my five years of studies at NTNU I wish to express my sincere appreciation to those who have been part of making this such an enlightening and wonderful experience. I imagine it will stand out as a truly defining part of my life.

I am deeply grateful to my supervisor Professor Ragnhild E. Aune and my co-supervisor Julia Glaum. Thank you for always sharing your expertise and for giving me words of encouragement. You have been of great motivation throughout this Thesis. I would also like to thank you for introducing me to the interesting field of biomaterials. Without you I would have not had the chance to explore this fascinating and far-reaching topic.
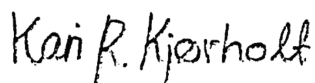
I also want to thank PhD Candidate Maren K. Fossum for sharing my frequent frustrations, and for motivating me to keep going. The early mornings and late evenings in the laboratories would not have been the same without you. Your work ethics inspire me.

Thank you to PhD Candidate Muhammad Ibrahim for sharing all your interest and practical experience, and for always taking the time to help me when I needed it.

I am also grateful for the support and immense patience of senior engineer Johannes Ofstad at the Department of Materials Science and Engineering. I am sorry for always introducing new problems to your work schedule. To senior engineer Cristian Torres Rodriguez and PhD Candidate Chandrahaasan Kattuputhur Soundararajan at the Department of Mechanical and Industrial Engineering and the engineers at NanoLab: Thank you for always taking my questions seriously and for taking the time and putting in the effort to answer them thoroughly. I would also like to thank senior engineer Anica Simic at the Department of Chemistry for sharing your expertise about ICP-MS and for letting Maren and I esentially move into your laboratory for a month.

I also find it necessary to thank the professors and other staff at the Department of Materials Science and Engineering for teaching me all I know about materials. Thank you for investing time in me and for creating such a warm and inspiring work environment.

Lastly, I would like to thank my parents for always believing in me, and brother for always keeping me grounded. A special thanks also goes out to my friends and classmates for sharing these years with me, and for making every moment better.

Kari R. Kjørholt

Kari Ravnestad Kjørholt

18.06.2021 Trondheim, Norway

List of Figures

List of Tables

Nomenclature

Abbreviations

CAUTI - Catheter-Associated Urinary Tract Infections

CDC - US Centers for Disease Control and Prevention

CLABSI - Central Line-Associated Bloodstream Infections

CVC - Central Venous Catheter

CVD - Chemical Vapor Deposition

DC - Direct Current

DCV - Direct Current Bias

DLC - Diamond-Like Carbon

EDS - Energy Dispersive X-ray Spectroscopy

EELS - Electron Energy Loss Spectroscopy

FDA - US Food & Drug Administration

FEGSEM - Field Emission Gun Scanning Electron Microscopy

FIB - Focused Ion Beam

FTIR - Fourier Transform Infrared Spectroscopy

FWD - Forwarded Power

GI-XRD - Grazing Incidence X-Ray Diffraction

HAI - Healthcare-Associated Infections

HiPIMS - High Impulse Power Magnetron Sputtering

ICP-MS - Inductively Coupled Plasma Mass Spectroscopy

LVFESEM - Low Vacuum Field Emission Scanning Electron Microscope

NAO - UK National Audit Office

NHS - UK National Health Service

PBS - Phosphate Buffered Saline

PICC - Peripherally Inserted Central Catheter

PVD - Physical Vapor Deposition

PVC - Polyvinyl Chloride

REF - Reflected Power

RF - Radio Frequency

SEM - Scanning Electron Microscopy

SSI - Surgical Site Infections

STEM - Scanning Transmission Electron Microscopy

TCKT - Transfercenter für Kunststofftechnik GmbH

TEM - Transmisson Electron Microscopy

TPU - Thermoplastic Polyurethane

VAE - Ventilator-Associated Events

XPS - X-ray Photoelectron Spectroscopy

Medical Terms

Artery - Blood vessel responsible for carrying oxygen-rich blood away from the heart and to the body [1].

Biocompatibility - The ability of a material to perform with an appropriate host response in a specific application [2].

Biofilm - A thin but robust layer of mucilage adhering to a solid surface and containing a community of bacteria and other microorganisms [3].

Carcinogenic - Producing or tending to produce cancer [4].

Central Venous Catheter - A thin, flexible tube that is inserted into a vein, and guided into a large vein above the right side of the heart called the superior vena cava. It is used to give intravenous fluids, blood transfusions, chemotherapy, and other drugs as well as taking blood samples [5].

Chandler Loop - *In-vitro* rotating blood flow loop model for the assessment of biomaterial hemocompatibility [6].

Coagulation - The process of blood clot formation [7].

Fibrogenic - Promoting the development of fibers [4].

Cytotoxic - Toxic to cells [8].

Genotoxic - Toxic to DNA [9].

Heart Palpitations - Heartbeats that suddenly become more noticeable but are most commonly harmless [10].

Hemocompatibility - Compatibility with blood [11].

Hemolysis - The breakdown of red blood cells [12].

In-vitro - Made to occur outside the living organism, *i.e.* in an artificial environment such as within a glassware, a test tube, *etc.* [7].

In-vivo - Made to occur within the living organism [7].

Metallosis - Aseptic fibrosis, local death of tissue, or loosening of a device secondary to metal corrosion and release of wear debris [13, 14, 4].

Myocardial Infarction - Occurs when the blood flow to the hearth is blocked, usually due to buildup of fat, cholesterol and other substances, and can damage parts of the hearth muscle. Myocardial infarction is also called hearth attack [15].

Myocardial Ischemica - Occurs when the blood to the hearth is reduced, usually due to partial or complete blockage of the hearth's arteries, and prevents the hearth muscle from receiving enough oxygen and thus reduces its ability to pump blood [15].

Neurotoxic - Toxic to the nerves or nervous tissue [4].

Pathogen - A specific agent that causes disease such as a virus or bacterium [4].

Plasma - The liquid component of blood that is a mixture of water, sugar, fat, protein and salts. It transports blood cells, nutrients, waste products, antibodies, clotting proteins, chemical messengers such as hormones, and proteins throughout the body [16].

Platelets - A blood component consisting of small fragments of cells that help the blood coagulation process [16].

Red Blood Cells - The most abundant cells in the blood accounting for 40-45 percent of the blood volume. They contain the protein hemoglobin, which carries oxygen from the lungs to the body and returns carbon dioxide to the lungs [16].

Restenosis - A reoccurring narrowing or blockage of an artery that was previously treated for blockage due to a buildup of plaque, leading to restricted blood flow [17].

Thrombosis - The formation of a blood clot within a blood vessel which prevents blood from flowing normally through the circulatory system [18].

Vein - Blood vessel responsible for carrying blood low in oxygen from the body and back to the hearth to be reoxygenated [1].

White Blood Cells - Cells that protect the body from infection and constitute about 1 percent of the blood volume. The two most common types of white blood cells are neutrophils and lymphocytes [16].

Whole Blood - Whole blood consists of red blood cells, white blood cells, and platelets suspended in a protective yellow liquid known as plasma [19].

Other Terms

Osmolarity - The number of solute particles per 1 L of solvent [20].

References

[1]   Scott Frothingham. *Artery vs. Vein: What's the Difference?* Website. Accessed: 13.04.2021. Apr. 2018. URL: https://www.healthline.com/health/artery-vs-vein.

[2]   "Biomaterials Science: An Introduction to Materials in Medicine". In: ed. by Buddy D. Ratner et al. Third. Academic Press, 2013. Chap. Biomaterials Science: A Multidisciplinary Endeavor.

[3]   Oxford Lexico. *Biofilm.* Website. Accessed 21.12.2020. URL: https://www.lexico.com/definition/biofilm.

[4]   Merriam-Webster. *Dictionary.* Website. Accessed: 09.06.2021. URL: https://www.merriam-webster.com/.

[5]   National Cancer Institute. *Central Venous Access Catheter.* Website. Accessed 15.03.2021. URL: https://www.cancer.gov/publications/dictionaries/cancer-terms.

[6]   Jessica Yau et al. *Investigating a Chandler Loop System for Thrombogenicity Testing of Biomaterials.* Tech. rep. US Food and Drug Administration, University of Maryland College Park.

[7]   BiologyOnline. *Biology Dictionary.* Website. Accessed 14.06.2021. 2020. URL: https://www.biologyonline.com/dictionary.

[8] William C. Shiel. *Medical Definition of Cytotoxic*. Website. Accessed 21.12.2020. URL: https://www.medicinenet.com/cytotoxic/definition.htm.

[9] European Comission. *Genotoxic*. Website. Accessed 21.12.2020. URL: https://ec.europa.eu/health/scientific_committees/opinions_layman/en/electromagnetic-fields/glossary/ghi/genotoxic-genotoxicity.htm.

[10] National Health Service. *Heart palpitations and ectopic beats*. Website. Accessed: 18.04.2021. Oct. 2019. URL: https://www.nhs.uk/conditions/heart-palpitations/.

[11] V. Kumar et al. "6 - Surface analysis technique for assessing hemocompatibility of biomaterials". In: *Hemocompatibility of Biomaterials for Clinical Applications*. Ed. by Christopher A. Siedlecki. Woodhead Publishing, 2018, pp. 119–161. ISBN: 978-0-08-100497-5. DOI: 10.1016/B978-0-08-100497-5.00006-9.

[12] MedlinePlus. *Hemolysis*. Website. Accessed 21.12.2020. 2020. URL: https://medlineplus.gov/ency/article/002372.htm.

[13] Catarina A. Oliveira, Isabel S. Candelária, and Filipe Caseiro-Alves. "Metallosis: A diagnosis not only in patients with metal-on-metal prostheses". In: *European Journal of Radiology Open* 2 (2015), pp. 3–6.

[14] James Drummond, Phong Tran, and Camdon Fary. "Metal-on-Metal Hip Arthroplasty: A Review of Adverse Reactions and Patient Management". In: *Journal of Funtional Biomaterials* 6.3 (Sept. 2015), pp. 486–499.

[15] Mayo Clinic. *Diseases and Conditions*. Website. Accessed: 09.06.2021. URL: https://www.mayoclinic.org/diseases-conditions.

[16] *Blood Basics*. Website. Accessed 15.03.2021. URL: https://www.hematology.org/education/patients/blood-basics.

[17] Nancy Moyer. *What Is Restenosis?* Website. Accessed: 18.04.2021. Jan. 2019. URL: https://www.healthline.com/health/restenosis.

[18] North American Thrombosis Forum. *What is Thrombosis?* Website. Accessed 21.12.2020. 2020. URL: https://natfonline.org/patients/what-is-thrombosis/.

[19] National Institutes of Health. *Whole Blood*. Website. Accessed 21.12.2020. 2020. URL: https://clinicalcenter.nih.gov/blooddonor/donationtypes/whole_blood.html.

[20] Bruce M. Koeppen and Bruce A. Stanton. "1 - Physiology of Body Fluids". In: *Renal Physiology (Fifth Edition)*. Ed. by Bruce M. Koeppen and Bruce A. Stanton. Fifth Edition. Philadelphia: Mosby, 2013, pp. 1–14. ISBN: 978-0-323-08691-2. DOI: 10.1016/B978-0-323-08691-2.00001-6.

Contents

Chapter 1

Introduction

Since the use of biomaterials based on scientific principles first came into use in the late 1940s and early 1950s, rapid advances in within both medicine and technology have improved life expectancy and life quality [1, 2]. The field has grown quickly, and today the function of almost every major body system can be replaced, supported and/or improved by biomaterials [3]. Along the way, not only has the life quality been improved for millions of people, but millions of human lives have also been saved [1].

However, the population is expected to age in virtually every country in the world [4]. The number of persons over the age of 65 years is projected to double from 2019 to 2050, increasing this share of the population from 9% to 16% respectively. Though recent studies indicate that health care expenditures are more closely related to proximity to death rather than age itself, it cannot be denied that health care costs will rise as the large generation of people born between 1946 and 1964 age [5]. The UN has estimated that a financial pressure will be put on the welfare state if they should continue to provide the same benefits as today [4]. A projection by the OECD Health Division (2019) found that health expenditure is expected to rise from an average of 9% in 2017 to 11% in 2040 and that an average of 19% of the public budgets in OECD countries should be dedicated to health to fund the increase [6]. Government officials are thus faced with the challenge of controlling the health care expenditures, while improving the effectiveness and efficiency of the system without compromising on the quality or accessibility of care.

This challenge also calls for further advances in medicine and medical technology. Although cutting-edge technology and development of completely new treatments are certainly a part of the solution, much can also be done by making improvements to already existing treatments. Despite the numerous benefits of biomedical devices, their use does not come without disadvantages, as discussed in further detail later in the preset work. To improve the quality of treatments, a key focus should thus be improving the quality of biomedical devices. However, improved quality is often associated with increased device cost due to improved material quality or additional processing steps. Thus, it may not be obvious how improved properties correspond to the badly needed cost control of the

health sector.

Nevertheless, utilizing such improved products may reduce the overall healthcare costs. For example, it has been estimated that infections acquired while receiving healthcare, *i.e.*, healthcare-associated infections, cost the UK more than £1 billion annually and the US between \$28.4 to \$45 billion [7, 8]. If the frequency of such complications, some which are directly caused by medical devices, is reduced, it can mean huge financial savings for the governments[9]. It can both mean reduction in the length of a patient's hospital stays reducing strain on hospital capacity, lower antibiotics use slowing the emergence of antibiotic resistant bacteria, and otherwise decrease drug use. Of course, it would also be of great benefit to the patients themselves as they can get quicker and better treatment with a decreased risk of potentially painful and exhausting complications, allowing them to quicker return to society as healthy individuals. There is no question that this is a great challenge which will require cooperation between numerous scientific disciplines, but it is certainly also one with possibilities for great societal benefits.

1.1 Project Objectives

The present work has focused on reproducing and characterizing two TiN thin film coatings (TiN (A) and TiN (B)) developed as part of the present authors Specialization Project (SP) performed at NTNU (Norwegian University of Science and Technology, Trondheim, Norway) during the fall semester of 2020 [10]. Based on the obtained results, the properties of the coatings should be improved by developing a third TiN coating (TiN (C)). In addition, the use of a new substrate has been tested for coating TiN (C). The coatings are intended for medical grade polyurethane for use in blood contacting biomedical devices. The aim is to reduce complications such as infections, blood clotting and toxic effects related to presence of such biomedical devices in the human body over extended periods of time, and to reduce the number of devices failures while in use. The results have been evaluated with reference to the non-coated reference substrates, a commercial Diamond-Like Carbon (DLC) coating, and data available in the open literature.

Chapter 2

Background

2.1 The Complex Requirements for Materials Used in the Human Body

The requirements for materials used in implantable medical devices, also called biomaterials, were partly described in detail in the present author's Specialization Project [10]. This section will thus only give a brief summary of the main requirements for chemical, mechanical and surface properties as well as other requirements for biocompatibility.

The revelation that true inertness cannot be achieved between the human body and any material led the topic of biocompatibility to become an important one. One definition of biocompatibility is "*the ability of a material to perform with an appropriate host response in a specific application*" [1]. This definition emphasizes that the requirements for biocompatibility will change depending on the application and the surrounding environment. It also suggests that aiming for biocompatibility is not necessarily the same as aiming for inertness as "the appropriate host response" can vary, and an increasing number of biomaterials are intended to interact with the body or even degrade [11, 12, 13]. Thus, claims of biocompatibility for one application cannot be directly transferred to use for another, though it can be a natural starting point for further investigation.

The human body is a surprisingly harsh environment [12]. Materials must both withstand an extreme chemical environment which is both particularly reactive and corrosive due to an electrolyte with active biological species, free radicals and intermediate oxygen species. The material must thus be chemically stable and corrosion resistant. Materials implanted in the body for extended periods of time must also withstand potentially large stresses and/or a large number of loading cycles. Thus, mechanical properties such as creep strength, fatigue strength and resistance against wear become important. The materials must also have sufficient formability.

The surface properties of a material (*i.e.*, the surface chemistry, structure, morphology

and topography) will to a large extent determine the interactions with the human body [14, 15]. The interaction may also be affected by the thickness and density of the surface layer [11, 14]. Because the relevant forces (*i.e.*, electrostatic and van der Waals forces) only work in the range of a few tens of nanometers, any surface modification only needs to be of this scale as long as the integrity of the surface layer is intact [14]. In addition to sufficient chemical, mechanical and surface properties, there are several other requirements to be fulfilled for biocompatibility to be achieved. It must be noncarcinogenic, nontoxic and must not cause foreign-body reactions [12]. Unfortunately, the term is often used without sufficient proof, and Griesser [14] suggests discarding it altogether in favor of more specific terms.

If the material is intended to be in contact with blood, as the materials of interest for this project are, it should also be hemocompatible, *i.e*, not cause thrombosis or hemolysis. The factors influencing the hemocompatibility as well as possible complications following the lack of hemocompatibility are described in sections 2.3 and 2.5, respectively.

It is also worth noting that the materials will seldom subside in the body as a pure material, but will be part of a medical device, possibly made up of several different materials [1]. That may give rise to effects other than those found when the materials are present separately. The device will also have a certain geometry, including sharp edges, that may affect its performance and should also be considered [14]. The duration of the intended interaction between the material and the human body is also of interest as the material may degrade or otherwise change while implanted [1]. Thus, to have successful utilization and application of a medical device, a full assessment of both the biological and physical needs of each device must be made [1, 13].

2.2 The System for Ensuring the Safety and Reliability of Medical Devices

The regulations for medical devices vary depending on where in the world you are. Though the Chinese and Indian markets are expected to grow quickly over the next 10 years, the US and European markets are still the two significantly largest ones with 48% and 27% market share in 2018, respectively [16, 17]. Thus, this section will present the regulations within the US and the European Union to describe the regulatory routes medical devices must pass through to get access to the two most important markets.

2.2.1 US Regulations

A medical device is defined by the U. S. Food & Drug Administration (FDA) as:

> *An instrument, apparatus, implement, machine, contrivance, implant, in-vitro*

reagent, or other similar or related article, including a component part, or accessory which is: (. . .) intended for use in the diagnosis of disease or other conditions, or in the cure, mitigation, treatment, or prevention of disease, in man or other animals, or intended to affect the structure or any function of the body of man or other animals, and which does not achieve its primary intended purposes through chemical action within or on the body of man or other animals and which does not achieve its primary intended purposes through chemical action within or on the body of man or other animals and which is not dependent upon being metabolized for the achievement of its primary intended purposes [18].

The medical device market in the US has been under regulation of the FDA since the 1976 Medical Device Amendments [19]. These regulations came into place following a disaster with the Dalkon shield contraception device that injured thousands of women. As of 2020, the FDA has established classifications for about 1,700 different generic types of devices and the medical devices are classified into three main categories according to the risk the device poses to the patient based on the intended use and indications for use (*e.g.*, by device labeling or indications gives orally during product sale) [20]. Higher risk devices are subjected to stricter regulation to assure that the devices are safe and effective.

Class I devices are the lowest risk of the three categories and include devices such as thermometers, bandages, and tongue depressors [20, 21]. Class II devices are higher risk than those categorized as Class I and includes devices such as most orthopedic prosthetics, insulin pumps, vascular graft prosthesis and diagnostic intravascular catheters.

Class III devices are those that pose the greatest risk to the patient [20]. According to the FDA: "*Class III devices are those that support or sustain human life, are of substantial importance in preventing impairment of human health, or which present a potential, unreasonable risk of illness or injury.*" [22]. Such devices include breast prosthesis, atrial defibrillators, pacemakers, ventricular and cardiopulmonary bypass devices, and contact lenses intended for extended wear up to 30 days [21]. They are required to go through a premarket approval (PMA) process before the device can be marketed, which requires sufficient valid scientific evidence of the device's safety and effectiveness for the intended application [22]. However, there are certain exceptions: If the device is substantially equivalent to an already legally marketed device (referred to as the predicate), it can be cleared through a 510(k) premarket notification, and can thus be marketed in the US [23]. The submitters of such an application must support their claims that the device is similar to one or more such predicates, meaning that the new device is as safe and effective. To get market clearance, the 510(k) premarket notification does not require clinical data (though it can be included) but can also rely on non-clinical performance data (*e.g.*, sterility, biocompatiblity evaluation, electromagnetic compatibility, and engineering performance testing). A 510(k) premarket notification is also required for Class I and II devices, though there are plenty of exceptions. (74% of Class I devices are exempt from this process [20].)

2.2.2 EU Regulations

Within Europe, five countries stood for almost two thirds of the medical device market in 2019: Germany (19.2%), France (14.4%), Italy (13.8%), Spain (9.2%) and UK (9.2%) [17]. It is estimated that there are more than 500,000 medical devices on the EU market, giving an indication of the market's vast scale [24]. As in the US, the EU also divides medical devices into categories based on the risk level for the patient and/or the public in case of device failure [25]. According to the European framework, there are four classes of medical devices: Class I (*e.g.*, simple bandages and wound products), Class IIa (*e.g.*, syringes for pump infusion), Class IIb (*e.g.*, anesthesia machines) and Class III (*e.g.*, stents). The level of regulatory control depends on the category, and the highest risk devices (*i.e.*, Class III) are naturally subject to the most stringent pre- and post-market requirements.

The EU regulations for medical devices and *in-vitro* diagnostic medical devices are currently going through a transition phase that began in May of 2017 [24]. Two new regulations will completely replace the previous three directives within May of 2022, though some exceptions extend until May of 2025. As the last directives were passed in the 1990's, the new regulations are designed to catch up with the scientific and technological process in the field and are meant to ensure a higher level of protection for EU citizens while still encouraging innovation [24, 26, 27]. There have also been problems with divergent interpretations of the directives across the European market and certain concerns about product performance, but as regulations do not have to be transposed into national laws, as directives do, this risk will be reduced [26, 28].

Broadly speaking, the new legislation will put more emphasis on a safety throughout the medical device life-cycle. The new regulations will not remove any existing requirements, but they will include stricter pre-market controls for high-risk devices, an extensive EU database and a tracing system on medical devices, stricter rules for clinical evidence and stronger post-market surveillance [28, 29]. The independent third parties which perform the conformity assessment procedures (called Notified Bodies) will also need to meet stricter criteria, in particular with regards to clinical competence [27, 28].

2.3 The Blood Coagulation System

Blood has several essential functions in the human body. It brings nutrients and oxygen to the lungs and tissues, helps fight infection through transporting cells and antibodies, carries waste products to the kidneys and liver, and regulates the body temperature. Further, it is crucial that the blood can coagulate if the human body is exposed to trauma as the coagulation prevents excessive blood loss [30]. The vascular system is finely tuned and depends on several components and interconnected mechanisms which balance procoagulant and anticoagulant factors. When a biomedical device is introduced into the bloodstream, this balance of the finely tuned system may shift, which can lead

to complications that work against the aim to heal the body, as is discussed in Section 2.5 [31, 32, 33]. Thrombosis is a common reason for failure of biomaterials, and the most serious limitation in the use of blood-contacting devices [32, 34, 35].

In this section the components of the blood coagulation system will be briefly introduced. The aim is not to give an in-depth explanation of the numerous components and subsystems (as such is done elsewhere [32, 33, 36, 37, 38]), but to give sufficient insight into the material properties that affects blood coagulation in contact with artificial surfaces. This insight should be the basis for understanding the material properties that can and/or should be tailored to improve the hemocompatibility of blood contacting medical devices.

2.3.1   The Mechanisms of Blood Coagulation

Blood mainly consists of platelets, plasma, white and red blood cells. Whole blood is a mixture of about 55 percent plasma and 45 percent blood cells [30]. In turn, the plasma contains about 300 different proteins [37]. Thus, it is not surprising that the blood coagulation pathway is complex. Hemocompatibility is an essential property of biomaterials and can be measured by the interaction between the material and the various blood components [11].

Thrombus formation can be triggered by artificial surfaces through a number of mechanisms as illustrated in Figure 2.1 [33, 37]. The process is initiated by protein adsorption on the surface, which in turn will lead to adhesion of platelets and white blood cells [33, 11]. Factor XII, a clotting factor and plasma protein, will also set off both complement activation (through the conversion of prekallikrein to kallikrein) and thrombin generation [33, 39]. Thrombin generation and activation of white blood cells can both enhance complement activation. Both the activated complement and activated white blood cells can contribute to a local inflammatory response. The activated white blood cells can also contribute to fibrin formation. Further, thrombin also promotes platelet activation and induces fibrin deposition. The resulting thrombus is a platelet aggregate deposited on the surface which is stabilized by fibrin strands. The mechanism of thrombosis is similar, but not identical in the veins and the arteries [38]. For example, the composition of the venous thrombus differs from that of arterial thrombus. Thrombosis may also occur more rapidly on surfaces implanted in the veins as the blood velocity is lower and thus the residence time in the veins is higher.
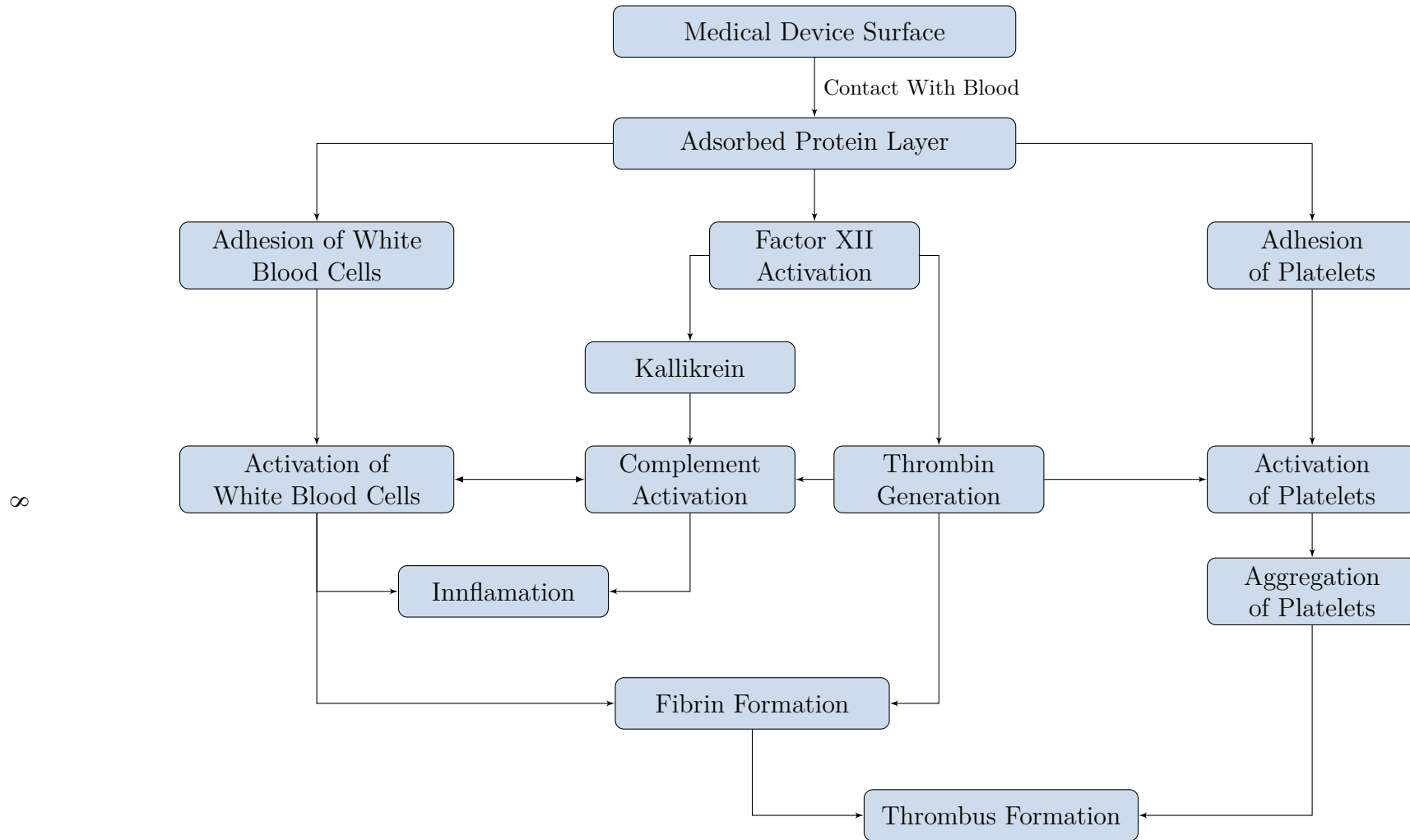
Figure 2.1: When an artificial surface, like that of a biomaterial in a medical device, is introduced into the vascular system it triggers a number of subsequent reactions that eventually lead to thrombus formation and/or inflammation.

Source: [33]

As protein adsorption is the first step towards thrombus formation, and initiates the subsequent, usually catastrophic effects described above, the mechanism of protein adsorption will be described in further detail [32, 33]. If preventive measures are not taken all surfaces will be covered with a thin layer of proteins (2-10 nm) within a few seconds upon blood contact. The protein layer can have protein concentrations 1000-fold higher than that of plasma and will vary in composition over time as surface adsorption often is reversible, though the variations over days and weeks are poorly understood. The layer composition is also complex: It does not reflect the protein composition of the plasma and will vary from surface to surface, making it unpredictable.

Blood contains predominately negatively charged proteins where some have a strong affinity for surfaces [14]. Surfaces should be designed to promote adhesion of desirable proteins and resist nonspecific protein adsorption [32]. Fibrinogen is one of the first plasma proteins to deposit on artificial surfaces [33]. The presence of fibrinogen is undesirable in the protein layer, as it has a prominent role in mediating platelet adhesion and activation [32]. Thus, surfaces that eliminate fibrinogen adsorption should have increased hemocompatibility. It has also been found that some of the materials that resist the adsorption of fibrinogen and the subsequent platelet adhesion also are less active in promoting clotting of the intrinsic system of coagulation, adding an extra benefit to such a material property. Materials that adsorb less than 5 ng/cm^2 of fibrinogen are thought to resist platelet adhesion and such materials have recently been reported. However, the degree of protein resistance required to reach hemocompatibility is not well established.

There are also other proteins that may initiate and/or propagate coagulation which are also undesirable [32]. Some proteins inhibit coagulation (*e.g.*, antithrombin, thrombomodulin and activated protein C) and would therefore be favorable. Other desirable proteins include albumin, plasminogen and t-PA. Albumin is another key protein that, along with fibrinogen, is found on most of the investigated surfaces. It was previously believed that the protein resisted adhesion and activation of platelets under all conditions, but more recent research has disproved this claim. If albumin attaches to a surface, it can become conformationally altered over time, thus exposing binding sites for platelets in the albumin structure. However, the short-term effect of resisting platelet adhesion may still be significant for albumin.

The dynamics of the protein adsorption and the protein layer composition will depend on the chemical and physical properties of the surface (*e.g.*, surface charge, wetting properties and topography) as well as the protein properties (*e.g.*, size, charge and conformational stability) [11, 14, 32, 33]. However, the dependence on these properties is not well understood, in particular the influence of protein properties. The following paragraphs will however discuss what is known about the effect of surface properties on hemocompatibility.

2.3.2 The Effect of Wetting Properties and Surface Charge

The wetting properties and surface charge will play a key role in the interaction with blood. One reason for this is that water is a vital component of blood, and the first molecule that absorbs to the functional groups of the surface when blood comes in contact with a biomaterial [32]. It is the thermodynamic stability of the interaction between the water molecules and the surface that determines if the biomolecules will replace the water and adsorb to the surface instead. Both non-polar hydrophobic surfaces and surfaces with a net surface charge favor the replacement of water with biomolecules, albeit due to different mechanisms. The mechanism will also vary between surfaces of positive and negative charge, though both activate blood coagulation. *In-vitro* experiments have also shown that autoactivation of FXII was enhanced on negative surfaces with hydrophilic properties as well as hydrophobic properties [40].

Further, proteins bind more tightly to hydrophobic surfaces than hydrophilic surfaces [32]. This is also the case for fibrinogen, which can explain the adhesion of platelets to hydrophobic surfaces [37]. However, this trend has not been observed consistently and the wetting properties is not the only factor affecting protein adsorption. Fluorinated polymer surfaces with contact angles ranging from 80° to 120° showed increased adsorption of fibrinogen with increasing contact angle [32]. On the other hand, a hydrophilic PMMA surface (contact angle approximately 70°) showed a much higher fibrinogen adsorption than the fluorinated polymer surface. Xu and Siedlecki [41] found a step dependence of wetting properties on protein adhesion to LDPE. The adhesion forces of key proteins (*i.e.*, bovine serum albumin, fibrinogen and human FXII) was shown to be stronger on surfaces with $\theta > 60 - 65°$ than for the surfaces with contact angles below 60°. Superhydrophobic surfaces ($\theta > 150°$) should be treated as a separate category as the mechanism for resisting protein adsorption is believed to be different [32, 42]. The material-plasma interface will trap air, and though the proteins may attach to the plasma-air interface, they will be easily washed away. However, the plasma-air interface may itself affect the proteins and induce the formation of emboli downstream of the surface.

Thus, neutrally charged hydrophilic surfaces are the most resistant to protein adsorption as the free-energy state of the adsorbed water is sufficiently low for the displacement to be thermodynamically favorable [32].

2.3.3 The Effect of Surface Topography

Surface topography has also been shown to affect the absorption of proteins onto the surface [43]. It has, however, proved difficult to find a general trend in the protein absorption to patterned surfaces, but studies have found low protein absorption to surfaces with nano-scaled roughness while the absorption was increased on substrates with micrometer sized roughness. It is believed that the nano-scaled roughness has this effect due to the similar dimensions of proteins and substrate structure. Hydrophobic surfaces have also shown a particular surface roughness dependence on protein adsorption: The

adsorption has proved to be extremely rapid on flat surfaces, but the adsorbed proteins are washed off at rough surfaces due to the increased shear rate [32]. Though the effect of surface topography is not easily described, it is worth noting that changing the surface roughness may also affect the wetting properties of the surface as described in section 2.7.1.

2.3.4 Further Considerations

There is still much that is unknown about the interactions between biomaterials and blood. One such factor is the time dependence of protein resistance. It is speculated that even if a material resists protein adsorption initially, platelet adhesion and activation will become significant over time due to conformational changes that occur as the proteins age on the material surface [32]. It is not known if the proteins must adsorb reversibly or at least be continuously exchanged with other proteins to avoid this aging effect. The time dependence of protein resistance is crucial as it dictates if the materials can be used for long-term applications or for short-term applications only. More data is also needed on the *in-vivo* performance of protein resistant surfaces as most experiments performed this far have only been using *in-vitro* methods. If *in-vitro* methods are used, protein resistance should be evaluated using plasma or blood, not simple protein solutions, as these do not capture the full complexity of the system.

Further, it is not known if it is sufficient to resist fibrinogen adsorption to achieve hemocompatibility or if the surface must be resistant to other proteins as well [32]. We also do not know if surfaces that resist protein and platelet adhesion also resist blood clotting through the intrinsic pathway of coagulation. The influence of the surface properties may also be drastically reduced after the surface is fully covered, though the trend has not been observed consistently [32, 44]. We also have much to learn about how we can exploit our knowledge about blood and the cardiovascular system to provide medical devices with improved hemocompatibility. Lastly, it is worth noting that it is not only the surface itself that can cause thrombosis: It can also be initiated by flow disturbances caused by biomedical devices in the veins or arteries [38].

2.4 The Use of Biomedical Devices in Blood Contacting Applications

2.4.1 Biomedical Devices for Blood Contacting Applications

There are numerous medical devices used for cardiovascular applications and in the bloodstream, and they are crucial for diagnosing and treating serious medical conditions. Central Venous Catheters (CVCs) are thin, flexible tubes inserted into veins [45]. They are used to take blood samples and give treatments such as drugs, intravenous fluids and

blood transfusions. To reduce the number of needle sticks a patient has to experience, they may stay in the human body for weeks or even months. CVCs are very frequently used (*e.g.*, in cancer patients), and estimates say that over 5 million CVCs are inserted every year in the US alone, with an average dwell time of about 3 days [37, 46]. The global market is also expected to grow from an estimated $763 million in 2020, with more than 27 million CVCs inserted, to $860 million by 2026 [47].

Pacemakers are typically inserted to treat bradycardia, slow beating hearts [48]. This is a condition that typically affect people over the age of 60 years and can lead to the blood flow to the brain and body being too low. The resulting symptoms include fainting, dizziness, fatigue, shortness of breath, and intolerance for exercise. In extreme cases, a slow beating heart can even be fatal. A major study found that there were over one million pacemakers implanted globally in 2009 [49]. The US was the nation with the most implants (over 235,000), followed by Germany (over 76,000), France (over 48,000) and Italy (almost 45,000). China also had over 40,000 implanted pacemakers. These numbers are expected to grow in the future due to the aging population and an increase in this type of hearth conditions [50].

If the heart valves are diseased or damaged, they could be replaced by prosthetic heart valves, with a large variety of options available [51]. The valves may become dysfunctional due to valve stiffness, or they can leak, causing symptoms like dizziness, chest pain, heart palpitations, difficulties breathing, swelling, or fluid retention that causes rapid weight gain [52]. Though valve replacements do not come without risk, they can increase the life quality of patients, and each year about 280,000 valve substitute procedures are performed worldwide with 90,000 of them performed in the US [51, 52]. It is particularly important for valve substitutes that they have excellent hemodynamics, are highly thromboresistant and very durable.

Further, other common medical devices for cardiovascular applications include stents used to treat restenosis, cardiopulmonary bypass machines used to oxygenate blood during cardiac surgery, blood oxygenators, vascular grafts, intra-aortic balloon pumps, hemodialysis systems and total artificial hearts [13, 32, 53, 54]. The importance of such medical devices is thus accentuated by the scale of their use and the severity of the conditions they treat.

2.4.2 State-of-the-Art Materials for Blood Contacting Biomedical Devices

Synthetic biomaterials can be divided into metals, ceramics, composites, and polymers [55]. In addition, several materials from animals or the plant world are being used. One advantage with these materials is that they are similar to the materials in the body, and they usually do not have problems with toxicity like many synthetic materials. However, they can have problems with immunogenic and natural polymers are particularly prone to degradation and decomposition at below their melting point which significantly limits their formability.

Heart valves can also be made of various carbon materials, such as pyrolytic carbon [56]. Such carbons are mechanically durable and have shown to be highly thromboresistant and compatible with blood cells as the surface absorb blood proteins without altering them and do not influence plasma proteins or the activity of plasma enzymes.

Polymers are widely used for blood contacting applications [55]. As these devices are not load bearing, the inferior strength of polymers compared to metals and ceramics is not a significant disadvantage as other mechanical properties are desired [54]. Thus, the high formability of most polymers are of greater advantage. Polymers like acetal, polyethylene and polyurethane are used in some pacemakers [55]. Other polymers like polyester, polytetrafluoroethylene and polyvinyl chloride (PVC) can also be used to replace artery segments if they are becoming blocked by the buildup of fatty deposits.

CVCs are typically made of either silicones or polyurethanes [57]. Of the two, polyurethanes are the most frequently used as they allow for high catheter strength while maintaining a delicate catheter design, though polyurethane catheters have shown higher infection and thrombosis rates. Silicone elastomers are more frequently used for venous access devices implanted over 6 weeks, but they display decreasing mechanical stability over time. Thus, there are pros and cons related to both materials. There is a large diversity of thermoplastic polyurethanes (TPUs) used for vascular catheters, including polyester-, polyether-, and polycarbonate-based variants as well as aromatic and aliphatic grades. The aliphatic grades soften, easily processable and colorable, and a wide variety of fillers can be used. On the other hand, the aromatic grades are stronger, more chemically resistant and kink resistant. Polyether-based polyurethanes of both aliphatic and aromatic grades will soften at body temperature, which is an advantage as it reduces the risk of vascular trauma while increasing patient comfort. These synthetic polymers are classified as chemically inert, and resistant to chemical and thermal degradation. However, studies performed by PhD Candidate Maren K. Fossum, affiliated at the Department of Materials Science and Engineering, NTNU, has revealed that the surface of such intravascular catheters becomes porous after prolonged *in-vivo* exposure as well as exposure to whole blood and NaCl solution, suggesting that the performance of the currently used materials is not optimal [58]. Similar observations have also been made by Verbeke et. al. [59]. It has also been shown that polyurethane, silicone, and PVC are not resistant to bacterial colonization and biofilm formation which can cause serious complications as discussed in Section 2.5 [57].

2.5 Complications Related to Biomedical Devices

2.5.1 Infections

Healthcare-associated infections (HAIs) are infections that patients acquire while receiving healthcare, and they are the most common complications affecting patients under hospital care and a leading cause of morbidity and mortality globally [57, 60]. HAIs are one of the

top ten causes of death in the US and there were more than 4.5 million cases in Europe in 2007[61]. In 2017, more than half a million infections associated with medical implants were acquired in hospitals in the US. That is more than half of the total HAIs [9].

Though the medical devices are supplied as sterile or sterilized before use, they can be contaminated by the environments in hospitals or other care facilities (which are known to be full of microorganisms that may even be multi-drug resistant) or by organisms present in or on the human body itself [2, 13] during handling and/or when inserted into the patient. Bacterial colonization typically arises from the skin flora. When the immune barrier of the skin is compromised (*e.g.*, through insertion of a CVC or other more serious surgical trauma), skin flora bacteria can quickly become infectious agents though they are typically part of the normal flora of the human body. As the medical device is previously uncolonized and does not have an immune system that fights off microorganisms like the human body, the bacteria can populate its surface without being challenged in an environment with plenty of nutrients, and a biofilm will subsequently form [2, 34, 44]. The initial attachment of bacteria is influenced by the causative pathogen, the presence of a conditioning film, and biomaterial surface properties which govern hydrophobic, electrostatic, and thermodynamic interactions. Silicon elastomers used in catheters are for example more prone to colonization by the *Candida Albicans* than polyurethane catheters [57]. Microorganisms in the biofilm form may further be more resistant to antibiotic treatment, and it can be difficult treat such infections as there is much diversity in the microorganisms and the infections tend to be a result of a several pathogens rather than one single species [2, 34].

The most common HAIs include Central Line-Associated Bloodstream Infections (CLABSI), Catheter-Associated Urinary Tract Infections (CAUTI), Surgical Site Infections (SSI), and Ventilator-Associated Events (VAE) [60]. The infection rates tend to vary with both device type and location in the human body [57]. CVCs have an infection rate of 3-8%, cardiac pacemakers one of 1-7% and vascular grafts an infection rate of 1-5% [2]. The mortality rate for CLABSI is estimated to be 12-25%, and each episode of infection will significantly increase the length of a patient's hospital stay and thus also significantly increase healthcare costs [34].

The UK National Audit Office (NAO) estimated that HAIs cost the UK National Health Service (NHS) more than £1 billion annually in a report released in 2009 [7]. A report by the US Centers for Disease Control and Prevention (CDC) released that same year puts the total direct annual medical costs of HAIs in US hospitals in the range of $28.4 to $45 billion [8]. That includes over 1.7 million HAIs, which of approximately 450,000 were CAUTI, over 290,000 were SSI, 92,000 were CLABSI and more than 5,000 were VAE [13]. Though the CDC reported a 31% decline in CLABSI in general acute care hospitals from 2015 to 2019, there is still a long way to go [62].

To prevent infections through optimization of the biomaterial, the biomaterials scientist should focus should be on preventing biofilm formation, but many biomaterials still remain vulnerable to bacteria colonization [2, 44]. However, there are other factors that may have a significant impact on infection rates. Infection prevention programs (including

education and training off staff, better hand and environmental hygiene, consistent post-surgery screening of patient health, and selection of appropriate medical devices and their placement) are promising and have shown to decrease patient mortality and morbidity [13, 34]. It has been estimated that such programs could reduce infection rates by up to 30%. Thus, such measures may have a larger effect on reducing medical device associated HAIs short-term than improvements in biomaterial surfaces.

2.5.2   Toxicity

Exposure to metals can cause various toxic effects, some even at low exposure levels [63]. Certain elements are neurotoxic, can cause cardiovascular disease and adverse effects to the kidneys, be carcinogenic, and harm the reproductive systems. Nevertheless, there are also adverse effects related to deficiencies of certain metals as metals are an intrinsic component of the environment that the human body has adapted to with evolution. The toxicity depends on several factors including the dose, the duration of exposure and whether the body can rid itself of the metal or if it accumulates in the body over time. It also depends on if the exposure is in the form compounds dissolved in a liquid (*e.g.*, water), a vapor phase or in the form of solid particles. If one is exposed to particles, the particle size may also be detrimental. Further, it may also matter if the metal is in its metallic form or part of a compound. The pathway of exposure will also matter. Typically, the exposure stems from external sources and occurs through inhalation or through intake of food and water. However, internal exposure from *e.g.*, medical devices is also possible.

Naturally, one should shy away from some of the most toxic elements when designing implantable medical devices. However, there are cases where toxic elements have been utilized in medical devices. Toxic effects from medical devices are often associated with orthopedic devices like hip implants. Metal-on-metal hip implants, typically made of a CoCrMo alloy, have given adverse local tissue reactions from the release of wear debris and metal ions and elevated cobalt levels in the body have caused adverse systemic health effects in individual patients [64]. The local effects include inflammatory responses and the development of psedotumors while the observed systemic effects include loss of sight and hearing, development of polyneuropathy and hearth failure. The frequency of such incidences of metallosis is not well reported, but it is generally estimated that 5% of hip prosthetics will need replacements due to the diagnosis [65]. In total, about 20% of metal-on-metal hip replacements will need to be revised within 10-13 years after insertion [66]. That is high compared to the less than 4% of metal-on-polyethylene implants that need revision 10 years after implantation. This difference is thought to be related to increased metal debris from the metal-on-metal implants, thus suggesting that the actual metallosis rates are higher than 5%. Such effects have however led to the adoption of implants made of non-metallic materials, namely polyethylene and ceramics [65]. Fortunately, tribocorrosion is not as problematic for blood-contacting medical devices as for many orthopedic implants, thus significantly reducing the constant release of new material from the devices. Nevertheless, the potential release of toxic substances from implanted medical

devices should be carefully risk assessed and monitored to avoid any adverse responses.

2.5.3 Thrombosis

Thrombosis is the formation of blood clots and can occur when blood comes in contact with medical devices as described in Section 2.3. If the blood clot remains in the vessel after formation, it is called a thrombus [67]. However, if the clot travels to another part of the body, it is called an embolism. In addition to causing device failure [37] the clots can get stuck in the blood vessels and restrict blood flow, and thus oxygen, to surrounding tissue or even critical organs [37, 67]. This can lead to tissue damage, destruction, or death in that area. Even if the blood vessel is not completely blocked, the consequences can still be critical in tissues like the heart and the brain and cause myocardial ischemia and/or myocardial infraction and stroke [38].

Like infections, thrombosis is associated with considerable morbidity and cost [57]. Healthcare-Associated Venous Thromboembolism affects approximately 900,000 Americans each year and leads to 100,000 premature deaths and $10 billion in the US alone [68]. The numbers are also expected to increase if preventive measures are not made. These cases are not all associated with the use of medical devices, but some certainly are. Venous thrombosis occurs in 1-7% of all patients with peripherally inserted central catheters (PICCs), with even higher rates in cancer patients, and can become evident due to pain and swelling in the arm [57]. More than 39% of patients with PICC lines had detectable thrombosis, though most of the cases were asymptomatic. This PICC-associated thrombosis has been reported to double hospital stays and thus increasing costs per patient substantially.

As the hemocompatibility of most medical devices today is suboptimal, clotting must be counteracted using short- or long-term treatment with systemic antiplatelet and anticoagulation drugs [32, 37, 43]. This causes an unpredictable balance between bleeding and thrombosis. It has also been suggested that there is a bidirectional relationship between catheter related thrombosis and catheter related blood stream infections [57]. A clinical analysis showed the risk of catheter-related sepsis was more than doubled when thrombosis occurred. The biofilm and attached microorganisms also enhance the thrombogenic process.

2.6 Approaches for Improving Bio- and Hemocompatibility

There are many possible approaches for improving the bio- and hemocompatibility of a biomedical device, and the main approaches are illustrated in Figure 2.2. First of all, one should consider making changes to the device design (*e.g.*, avoid sharp edges, change flow dynamics etc.) [14, 38, 61]. However, this may not always be possible. Another

is to change the device's bulk material or materials completely. As already mentioned, different materials interact with the human body in different ways. The downside is that it may not be possible to find a material with the required mechanical properties of the given device, that also fulfill the needs for surface properties and thus the interaction with the human body. Thus, surface modifications have been a common and promising approach that aims to uncouple the bulk and surface properties to obtain improved bio- and hemocompatibility while still maintaining the desired bulk properties [14, 43].
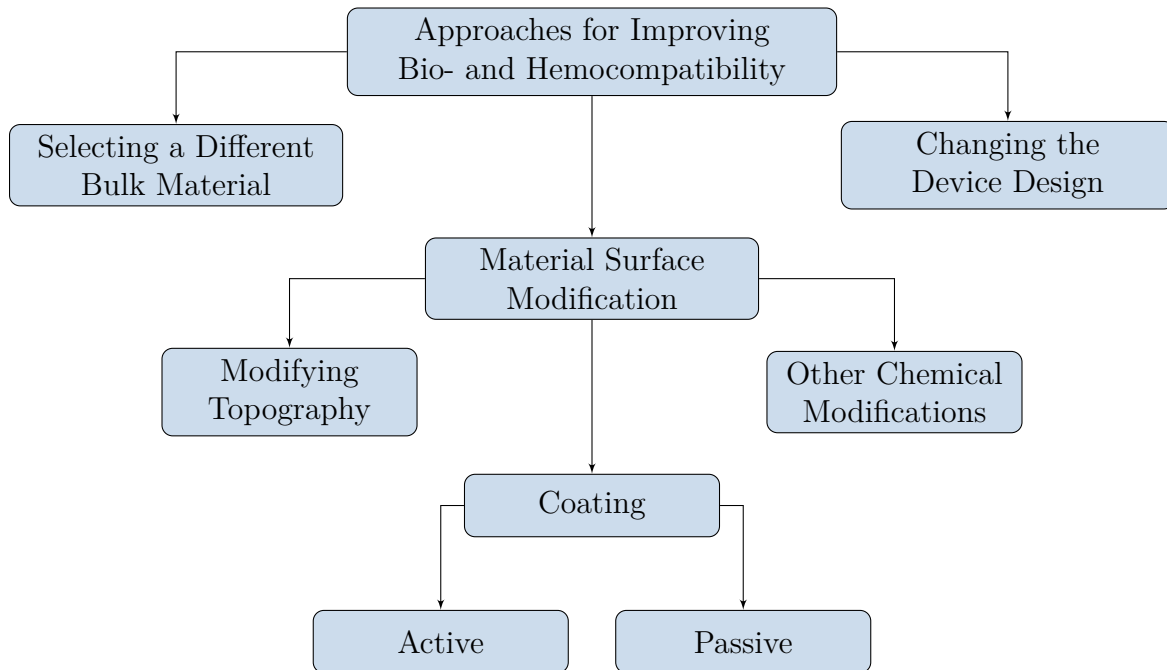
Figure 2.2: The main approaches to consider when aiming to improve the bio- and hemo-compatibility of biomedical devices.

As previously discussed, the surface properties are critical for the biological response to a biomedical device [14]. They are a major determining factor in the initiation for both bacterial colonization, the formation of biofilm, immune reactions, and the formation of thrombus [9]. Thus, numerous strategies and approaches for such surface modifications have been developed. The strategies include both active and passive coatings of both organic and inorganic origin, chemical surface modifications, or altering surface topography in both chemical and physical ways [11, 44]. Whether a coating is active, or passive is just one way to classify coatings. They can also be classified according to their aim (*e.g.*, antimicrobial, or anti-thrombotic), their material group (polymeric, ceramic, metallic, etc.), the character of the bonding between the coating and the substrate, or the production method. Chemical approaches for reducing protein adsorption on biomedical devices can decrease protein adsorption, and includes surface activation, oxidation, nitration, and carbonation [32].

Modifications to the surface topography can be done on a microscopic or nanoscopic scale and the topographic structured may be highly ordered or more disordered. Like proteins,

the attachment of pathogens to a surface is also dependent on the surface roughness [2]. Increased surface roughness gives better protection against shear forces and leaves an increased surface area for attachment. However, our understanding is far from complete when it comes to how the distribution of nanoscale morphology features and chemical functionalities affect the attachment of bacteria and the further development to a biofilm, in large due to the complexity of the system [44]. Because most surface treatments not just will alter the surface topography, but also the surface chemistry, it can be difficult to obtain surfaces of identical surface roughness but with different morphology. Thus, it can be challenging to assign changes in biological responses to morphology alone. It should also be mentioned that if a biofilm or protein layer first forms on a pattered surface, the biofilm may mask the desired topographical features and significantly reduce the desired anti-fouling properties of the surface.

Coating of the surface is a more common strategy. The coatings can roughly speaking be split into two categories, *i.e.*, active and passive coatings [34]. The active coatings may release substances from the surface or have a catalytic surface. The passive coatings are, as the name implies, more inert and chemically stable, and rely on preventing the initial adhesion of bacteria, protein, and platelets [69]. They can be polymeric, ceramic, metallic or carbon based. Active coatings can for example release anti-bacterial agents and anticoagulant agents like heparin into the local environment of the device. This could help reduce the use of blood thinners that leave a patient at risk of excessive bleeding or reduce infection risk and antibiotics use. However, active coatings are less stable than passive coatings and degrade more quickly over time.

As the state-of-the-art materials for CVCs, polyurethane and silicone, cannot resist biofilm nor thrombus formation, both antimicrobial and antithrombotic catheter coatings have been developed [57]. Of the implantable medical devices with claims of antimicrobial properties, almost all of them utilize antimicrobial agents. The use of such active technology can involve incorporation of the antimicrobial substance into the device surface, but also in the bulk material [34]. The use of antimicrobial coatings has revealed itself as one of the most effective approaches for preventing infections related to medical devices [9]. The coating of CVCs with heparin has also shown promise for reducing bacterial colonization and platelet and protein adsorption to the surface, reducing catheter related infections, though not reducing the frequency of catheter malfunction [57]. However, endpoint attachment of heparin on blood contacting biomaterials have shown to give an *in-vivo* long-term resistance to thrombosis (over 16 weeks).

Nevertheless, such active coatings do not come without drawbacks. If the amount of antimicrobial agent is too high, it could pose risk as most antimicrobial agents are very toxic and regulatory agencies have not approved them for use in implantable medical devices [34]. In addition, it is not clear if the use of slowly eluting antimicrobial compounds may contribute to the increasing problem of antibiotic resistant bacteria [61]. It also follows that biomaterial treatments based on active drug release have a limited lifetime of protection [70].

A novel approach of colonizing medical devices with healthy microbes to protect against

pathogenic organisms has been developed in recent years, and the progress of this approach will be interesting to follow in the coming years [61]. Researches have also investigated seeding endothelial cells to the surface of biomaterials, but it has proven challenging due to the stability, viability, and function of the technique, as well as the cell sourcing [37]. Other biologically inspired biomaterials are also relevant, where for example bioactive molecules are introduced onto the surface.

The use of passive coatings can give antifouling surfaces. Though they cannot kill microorganisms or inhibit the growth of them in the surrounding environment, they can reduce bacterial attachment and thrombus formation to limit device-related complications [9, 57]. As passive coatings are more chemically stable, they are also better suited to protect the medical devices against chemical and mechanical degradation. They mostly also avoid the issues of introducing toxicity and drug resistance, though toxic compounds may also leach from passive materials and accumulate in the body. However, also passive coatings have the issue of bacteria finding ways to overcoming the anti-fouling surface properties (*e.g.*, if there are coating defects) and can find ways to cover the surface. On the other hand, deposition of passive coatings is technically simpler, which is an advantage for commercialization and reducing the overall healthcare costs.

There are many different coating techniques, including Physical Vapor Deposition (PVD) methods (*i.e.*, evaporation, sputtering, molecular beam epitaxy) and Chemical Vapor Deposition (CVD) methods (available with various precursors, deposition conditions and energy forms applied) [71]. CVD techniques unfortunately often involve the use of toxic precursors, which can pose a treat if the precursors are not completely consumed or removed, thus their use for biological applications is limited [72]. Deposition of thin film coatings using magnetron sputtering is further discussed in Section 2.6.1.

Considering all these possible approaches, the passive coatings pose less risks and are more chemically and mechanically stable, thus giving a better chance of enhancing and/or maintaining the physical properties of the bulk material. As it is less challenging to get a surface modification approved by government legislators, rather than a whole new device material, applying a coating to a much-used material is a natural approach. It may also be easier to get approval for a passive coating rather than an active one as active interactions with the human body poses risks of its own. Passive coatings may also be more versatile, and the creation of a passive coating for blood contacting applications may also be a good starting point for coatings for other non-blood-contacting biomedical applications. The passive coatings can also work to improve the resistance to both infection and thrombosis while avoiding toxic effects.

2.6.1 Thin Film Coating Deposition by Magnetron Sputtering

Magnetron sputtering is a PVD method used for the deposition of thin films [71]. The technique gives high purity films and can be used to deposit metals, alloys and other compounds onto a wide variety of substrates [73]. There are many other advantages of

magnetron sputtering, including high deposition rates, extremely high adhesion of films, excellent coverage of small surface features, excellent coating uniformity and the ease of which the process can be automated. The great versatility and many advantages have led to the technique being used in many commercial applications (*e.g.*, fabrication of microelectronics and decorative coatings).

An inert gas, typically Argon (Ar), is introduced into the deposition chamber [71]. A discharge of Ar atoms is further initiated and maintained as the atoms are ionized by accelerated electrons. These electrons knock atoms or molecules from a target, which will deposit on the substrate and constitute the coating. A negative voltage is applied to the target which attracts positive ions which bind to the surface if the kinetic energy of the ions is sufficiently large [73]. The target and substrate are placed facing each other and both act as electrodes [71]. For reactive sputtering processes, a reactive gas can also be introduced into the chamber along with Ar to form a new compound with the target material [73]. Multi-elemental targets can also be applied.

There are several different magnetron sputtering techniques [73]. A Direct Current (DC) can be applied for pure metal targets, while isolators and semiconductors require the use of Radio Frequency (RF) power or pulsed DC. A variety of other techniques have also been developed. Magnetron sputtering can be used with different magnet configurations, *i.e.*, balanced and unbalanced modes. The magnets are used to control the electron positions, and thus control the plasma density in different regions. In the balanced mode, the plasma is confined close to the target while the unbalanced mode allows for a higher plasma density at the surface of the substrate. This results in the substrate being bombarded by ions in the unbalanced mode, which can influence both the structure and properties of the growing film [74, 75]. The thin film formation is also influenced by the magnetron sputtering process parameters, *i.e.*, the distance between the target and the substrate, the sputtering pressure and power, and the substrate temperature [76].

2.7   Characterization of Thin Film Coatings

Characterization of thin film coatings can me challenging due to small scale of the material in question, requiring high accuracy and precision of both instruments and the scientists involved. However, many methods have been developed, and a selection of these, also relevant for key biomaterial properties, are presented in the following section.

2.7.1   Wetting Properties

The wetting properties of a surface can tell us something about the surface energy of the material, describing the properties of the outer atomic layers (2–10 Å) [77]. The property is described by the contact angle, θ, between the solid surface, a liquid (often water) and a gas. As Figure 2.3 illustrates, θ is defined as the angle between the tangent of the liquid

droplet and the solid surface on which it is deposited. The contact angle is determined by the equilibrium between the three phases and described by Young's equation (Equation 2.1):

$$\gamma^{sv} = \gamma^{sl} + \gamma^{lv} \cos \theta \qquad (2.1)$$

where γ^{sl} is the solid/liquid interfacial energy, γ^{sv} is the solid/vapor interfacial energy and γ^{lv} is the liquid/vapor interfacial energy. The angle is often determined using a camera and further software image analysis. The contact angle can be measured with both static and dynamic methods such as static sessile drop, dynamic contact angle, dynamic sessile drop and Wilhelmy plate measurements [78]. If the contact angle is above 90° the surface is classified as hydrophobic, and contact angles below 90° denote hydrophilic surfaces [15, 79].
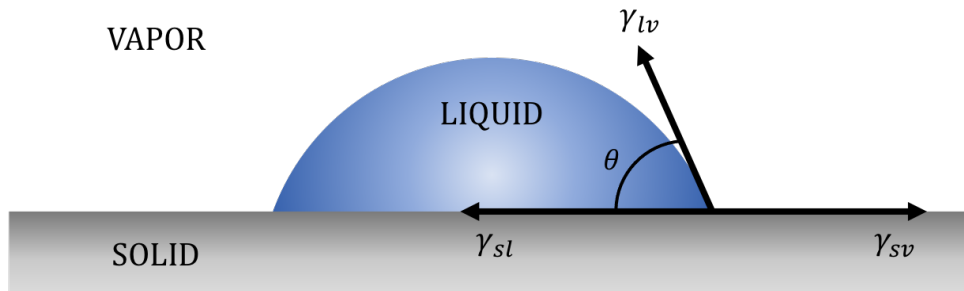
Figure 2.3: The equilibrium between the solid/liquid interfacial energy (γ^{sl}), the solid/-vapor interfacial energy (γ^{sv}) and the liquid/vapor interfacial energy (γ^{lv}) determines the contact angle θ.

Source: [80]

Though Young's equation describes an equilibrium state, the real system is metastable, and solvent may evaporate, particularly in an open lab atmosphere [81]. Such evaporation causes variability in the measurements, and the temperature and humidity should thus be controlled to ensure that the results are as reliable and reproducible as possible. Kinetic factors should also be considered, particularly for more viscous liquids, but water typically uses less than a second to reach the semi-static state. As Young's equation is only truly valid for ideal surfaces, the wetting properties can also be affected by factors like surface roughness and surface cleanliness [81, 82]. An ideal surface should also be non-deformable, non-porous, inert, insoluble, and non-reactive, but all these requirements are usually not fulfilled by real surfaces [77, 82]. Thus, the apparent contact angle observed on a real surface fall within an interval of angles called the contact angle hysteresis.

The contact angle can also be influenced by gravity factors if the drop volume is too large, simulating an increased wetting effect, but the use of drop volumes between 1 μL and 10 μL should have no effect on the static contact angle values [83]. Otherwise, if the surface is close to ideal the droplet volume will have no significant influence on the contact angle. However, a correlation between the drop volume and the contact angle can emerge if the

surface is non-ideal [84]. The contact angle can also depend on the solvent and vapor purity and the drop deposition method [77, 81].

Unfortunately, there is often much variation in the procedures used for measuring the wetting properties and variance between reported values are thus expected [81]. It is thus best practice to aim to reduce deviations from ideality and to report and evaluate the impact of any remaining deviations [77].

2.7.2 Friction Coefficient

Friction is a force that works to resist the sliding or rolling motion of one solid object over another [85]. The frictional force is proportional to the load that pushes the surfaces together, and the proportionality constant is called the coefficient of friction, μ. The friction that acts when the surfaces are in relative motion is called kinetic friction, while static friction arises between surfaces that do not move with respect to each other. The force needed to overcome kinetic friction (*i.e.*, to continue the motion) is always smaller than the smallest force needed to overcome static friction (*i.e.*, start the motion). The coefficient of friction is dependent on both the nature of the materials sliding or rolling against each other, and the surface roughness of these materials [78]. The coefficients are typically reported for specific material combinations (*e.g.*, aluminum on steel) with corresponding surface conditions (*e.g.*, clean and dry) [86].

2.7.3 Inductively Coupled Plasma Mass Spectroscopy (ICP-MS)

Inductively Coupled Plasma Mass Spectroscopy (ICP-MS) is a quantitative elemental analysis technique which can detect most elements in the periodic table [87]. There are only a few light elements that are not detectable by ICP-MS (*i.e.*, H, He, C, N, O, F, and Ne), and a few heavier elements that do not have naturally occurring isotopes which is necessary for detection [88]. The detection limits depend on the element but can be as low as parts per trillion or nanograms per liter [87, 88]. The high accuracy of the technique makes it suitable for detecting small trace amounts that may leach out of medical devices and accumulate in the body. Thus, it can be used to predict the toxicity of biomaterials.

The system consists of a sample introduction system, an ion source (typically argon plasma), a vacuum system and interface, ion optics with a mass spectrometer, and an ion detection system [87, 88]. The first two constituents are operated at atmospheric pressure while the remaining constituents are operated under high vacuum. The technique can analyze both solid, liquid and gaseous samples, though liquid samples are most used. The solid and liquid samples are converted into aerosol form using an ablation device and a nebulizer, respectively, while gases can be analyzed directly. The Inductively Coupled Plasma (ICP) fully decomposes the samples into its constituent elements and further ionizes these elements to singly charged ions. Liquid samples typically have an aqueous matrix containing nitric acid (and sometimes hydrochloric acid) to stabilize the elements

as an ionic solution. The ions are directed into the mass spectrometer (MS) where only one mass-to-charge ratio will be allowed to pass through at any given time. When the ions exit the MS they hit an electron multiplier, which serves as a detector, and signal intensities are compared to standards to determine elemental concentrations.

The level of total dissolved solids in a liquid sample should be below approximately 0.5% to avoid precipitation in the nebulizer or overloading of the plasma to avoid data collection issues though the data is lower [87]. Thus, sample dilution is commonly performed. There is a larger tolerance for lighter elements than for heavier elements as heavier elements effect the ion beam much more strongly, but the tolerance also depends on the instrument setup.

2.7.4 Adhesion and Cohesion

The cohesive and adhesive strength of coatings will determine their quality and service lifetime [89]. To evaluate coating adhesion, scratch testing is one of the most widely applied methods. The critical load (L_c) at which failure occurs is used as a quantitative measure to compare the cohesive and adhesive properties of coatings or even bulk materials, and the method is reproducible. The scratches are made with sphero-conical tips with tip radiuses typically ranging from 1 μm to 200 μm. A constant speed is used across the surface with a constant or progressively increasing load.

For tests with progressive loads, the critical load will be the smallest load where failure occurs [89]. If a test with constant load is performed the critical load is defined as the load where failure regularly occurs along the scratch track. The critical load will depend on the test specific parameters (*i.e.*, the loading rate, scratching speed, indenter tip radius, and indenter material) and the coating-substrate system (*i.e.*, the coating adhesion and cohesion, the friction coefficient between the surface and the indenter, substrate hardness and roughness, coating hardness and roughness, and coating thickness). Further, microscopic observation is the most reliable method to detect surface damage as it is possible to determine the difference between adhesive failure at the coating-substrate interface and cohesive failure within the coating. It should also be noted that the test conditions should be tailored to the relevant coating-substrate system.

2.8 Previous Development and Characterization of TiN Coatings

Two titanium nitride coatings (TiN) were developed and characterized as part of previous work by the present author. The coatings were deposited using RF magnetron sputtering. Chemical analysis (*i.e.*, Energy Dispersive X-Ray Spectroscopy (EDS), Grazing Incidence X-Ray Diffraction (GI-XRD) and Raman spectroscopy) confirmed the presence of TiN on the surface of the coated samples but did not reveal chemical differences between the

coatings [10]. Rietveld refinement of the diffractograms resulting from GI-XRD analysis confirmed these findings [90]. Analysis of the surface morphology using secondary electron imaging in Scanning Electron Microscopy (SEM) revealed that there was surface roughness in all samples in the form of directional lines in a regular pattern most likely originating from the processing method of the substrates [10]. It also revealed that $BaSO_4$ particles of micrometer scale protruded the substrate surface, but that the coatings appeared to be uniformly covering the substrate surfaces. However, both coating TiN (A) and TiN (B) showed signs of cracking, indicating that the coatings were brittle. This was further supported by SEM secondary electron analysis of the sample cross section which revealed coating fragments believed to stem from the cutting of the samples during sample preparation. Further, the contact angles with water were found to be $92° \pm 1°$ for the non-coated reference substrates, $64° \pm 7°$ for coating TiN (A), and $78° \pm 8°$ for coating TiN (B). As the coatings do not have optimal coating properties, improvements should be made before utilizing such TiN coatings for biomedical applications.

Chapter 3

Experimental Procedure

The experimental plan for the present project is presented in Figure 3.1, and each step will be thoroughly described in the following sections.

3.1   Materials

3.1.1   Substrate Material

All substrates used for the present work are produced using pellets of a medical grade thermoplastic polyurethane (TPU) – Carbothane. The pellets' specifications can be found in Appendix A. Carbothane was selected as a substrate material as work performed by Maren K. Fossum, PhD Candidate affiliated at the Department of Materials Science and Engineering, NTNU, revealed that it is similar to the material used in CVCs used for administration of cytostatic drugs to patients treated for breast cancer at Karolinska Hospital (KS) in Stockholm, Sweeden [58]. As these devices are much used, the optimization of the material surface properties is very relevant in relation to improving societal health care. The producer of the material, Lubrizol, claims that Carbothane has "*excellent oxidative stability, good mechanical properties and very good chemical resistance*" [91]. 20 wt% barium sulfate ($BaSO_4$) is added to the material to make it radio-opaque and it is of aliphatic form. Though not without the drawback of losing grounds for comparison, a decision was made to switch from using the substrates produced at NTNU to using substrates produced by Transfercenter für Kunststofftechnik GmbH (TCKT). This was done as Fossum also utilizes these substrates in her work with developing a coating for the material, and the results from the present work should thus be directly comparable to hers. As the new substrates are thinner, they are also more comparable to the CVCs.
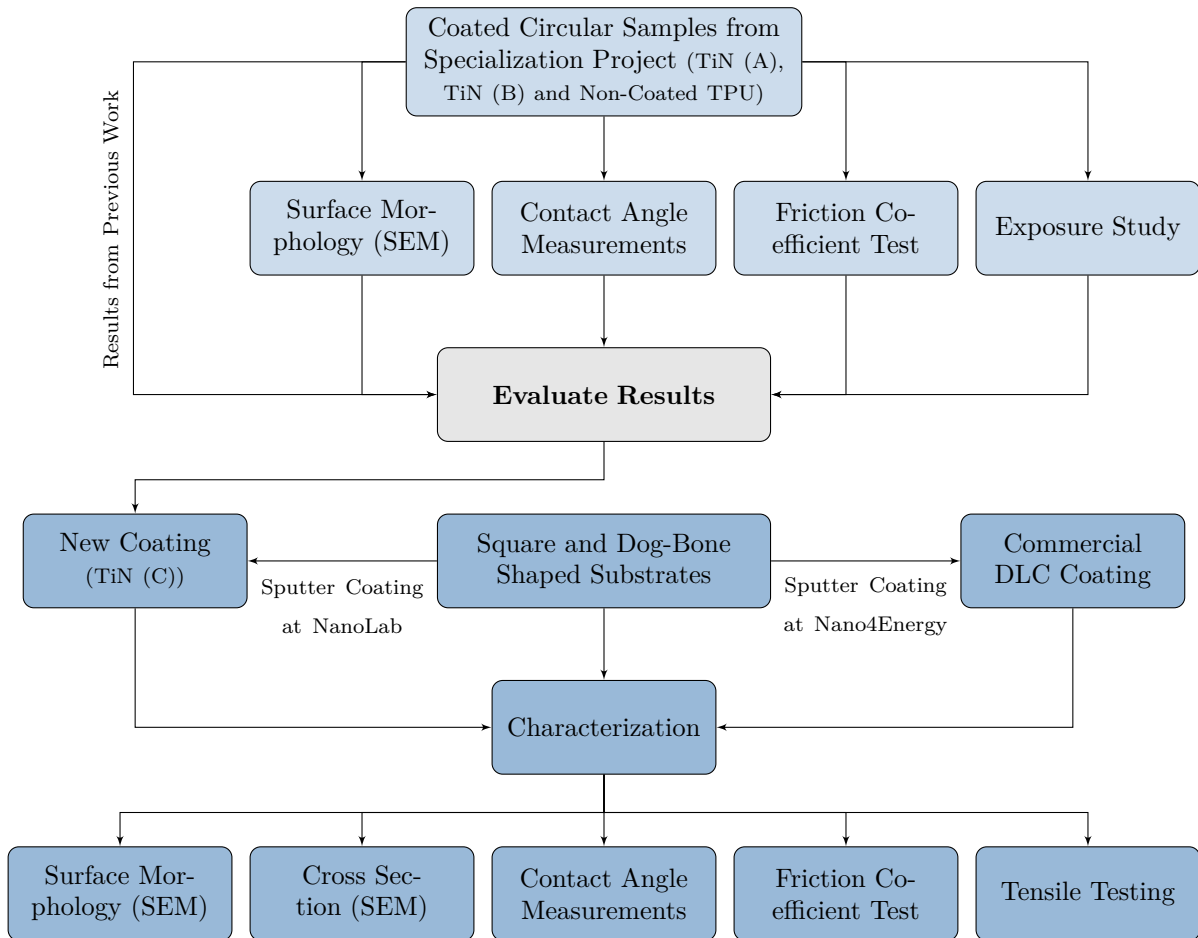
Figure 3.1: The project plan for the present activities. The light blue color signifies the thicker, circular substrates while the darker blue signifies the thinner, square and dog-bone shaped samples.

3.1.2 Coating Materials

Two 30 nm thick titanium nitride (TiN) thin film coatings (TiN (A) and TiN (B)) first developed as part of the present authors Specialization Project have been reproduced and further characterized as part of the present work. In addition, a third TiN coating (TiN (C)), also 30 nm, was developed as first-step optimization of the previous coatings. Coating TiN (C) has also been compared to a 50 nm commercial Diamond-Like Carbon (DLC) coating as it was applied to the same type of substrates.

The choice of these coating materials results from a literature study on the biocompatibility of coating materials performed as part of the forementioned Specialization Project. The literature study revealed that TiN is hard, wear and corrosion resistant and has a low friction coefficient [92, 93]. The material has also shown promising results in terms of reduced probability for infection, non-toxicity, non-hemolytic, non-irritant and anti-thrombotic properties for the systems tested [35, 93, 94]. Other claims of hemocompati-

bility and biocompatibility have also been made [43, 92].

The ceramic is often used as a coating to improve a substrate's surface properties, *i.e.*, to (i) harden and protect cutting and sliding surfaces, (ii) for decorative purposes due to the golden appearance of the stoichiometric TiN phase, and (iii) as a non-toxic exterior for medical instruments and implants. When applied to medical instruments, the surface tension is lowered giving the surface a more hydrophobic character, thus making the devices easier to clean. However, due to the intended interaction with blood, hydrophilic surfaces would be preferred. Nevertheless, the TiN surface has been shown to be more hydrophilic than the medical grade polyurethane used for blood contact applications today [10]. The wetting properties are thus improved in comparison to the state-of-the-art material.

DLC has a combination of the carbon bonds found in graphite (planar trigonal sp^2 bonds) and in diamond (tetragonal sp^3 bonds) and is an essentially amorphous form of carbon [95, 96]. DLC films possess a low surface roughness, have a low coefficient of friction and are hard, wear resistant and chemically stable [44, 96]. The material has shown promise as a candidate for biomaterial coatings for blood-contacting devices [44, 96, 97] as studies suggest good hemocompatibility, anti-bacterial properties and no inflammatory reactions were observed during *in-vitro* experiments [95, 96]. They can also be deposited onto polymer materials due to the possibility of low-temperature deposition and are relatively inexpensive. Literature also frequently mentions the excellent biocompatibility of DLC films [96, 97].

3.2 Compression Molding Substrates

Two compression molding techniques have been used for producing the substrates used for the present work. Coatings TiN (A) and TiN (B) have been deposited on the thicker, circular substrates while coatings TiN (C) and DLC were deposited on the thinner square and dog-bone shaped substrates.

3.2.1 Circular Substrates

Circular substrates (3.4 cm in diameter and 1 mm thick) were produced through compression molding of Carbothane pellets at 180° C. The pellets were dried in a vacuum chamber for a minimum of 4 hours in a vacuum chamber at 55°C before being dispersed in a steel mold. Further, the mold was placed between two steel plates only separated from the mold by Teflon sheets. The mold was then preheated to 180° C for 20 minutes without pressure applied, before 2.18 bar was applied for 10 minutes at the elevated temperature. The substrates were subsequently cut from the mold using a scalpel. [1]

---

[1]For further details on the process, see the present authors Specialization Project [10].

3.2.2 Square and Dog-Bone Shaped Substrates

The second production method was performed at TCKT and included compression molding of the pellets into sheets (10 cm x 10 cm) of approximately 150 μm to 500 μm thickness. A shearing-edge mold was used, exerting the pressure to the material directly, in combination with a Frekote 700NC mold release coating. The material was preheated to 180° C in the mold for 5 minutes at 2 bar hydraulic pressure, before the mold was transferred to a cooling press cooled by 15° C water where 65 bar was applied for 10 minutes. The sheets were then cut into square specimen of 2 cm x 2 cm or die cut into dog-bone shapes suitable for tensile testing. [2]

3.3 Coating Procedure

3.3.1 TiN Coatings

The TiN coatings were sputtered onto the Carbothane substrates at NanoLab at NTNU, Trondheim using a custom ATC-2200V sputter and evaporation tool from AJA International Inc. Before coating, the substrates were cleaned with distilled water and ethanol according to the cleaning procedure described in Appendix B. They were then attached to the instrument sample holder using double-sided tape as shown in Figure 3.2.
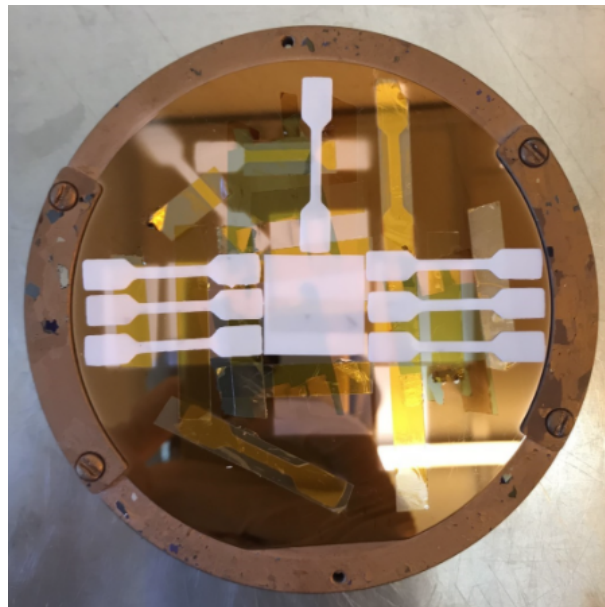
Figure 3.2: One square and seven dog-bone shaped Carbothane substrates attached to the sample holder used for sputtering by double-sided tape.

---

[2]For further details on the process, please contact Christoph Burgstaller (christoph.burgstaller@tckt.at) at Transfercenter für Kunststofftechnik GmbH (TCKT), Austria.

RF magnetron sputtering was used with either a balanced or unbalanced magnet configuration with a TiN target with a diameter of 5.08 cm. The sputtering parameters of the coatings reproduced from the Specialization Project (*i.e.*, TiN (A) and TiN (B)) and the new coating developed in this Thesis (*i.e.*, TiN (C)) are described and compared in Table 3.1. A Inficon SQM-16 Rate Monitor integrated in the sputter coater was used to find the sputter rate and thus the required sputter time to reach the desired 30 nm coating thickness.

Table 3.1: The sputtering parameters used for deposition of the titanium nitride coatings.

Sputtering Parameters	TiN (A)	TiN (B)	TiN (C)
Sputtering Power	80 W	80 W	120 W
Magnet Configuration	Balanced	Unbalanced	Balanced
Sputtering Time	60 min	55 min	35 min 45 sec
Argon Pressure	3 mTorr	3 mTorr	3 mTorr
Argon Flow Rate	67 sccm	67 sccm	67 sccm
Target - Substrate Distance	22 cm	22 cm	22 cm

To ensure stability of the deposition process, the substrate temperature, the Forwarded Power (FWD), the Reflected Power (REF), and the Direct Current Bias (DCV) were monitored approximately every 5 minutes. The FWD is the electrical power applied by the power supply, while REF is the power reflected back to the power supply. A two-capacitor matching unit will make sure the REF is as low as possible. The DCV is the direct current voltage that evolves across the target as a result of the RF voltage applied and initiates the sputtering process as it attracts ions. The ion energy, and thus the deposition rate, will generally be higher with higher DCV [98].

3.3.2 DLC Coating

The 50 nm thick DLC coating was applied by Nano4Energy SL using high impulse power magnetron sputtering (HiPIMS) from a pure graphite target in an Ar atmosphere [99]. This is a configuration where power is applied to the target in short pulses with cathode voltages above 500 V and frequencies between tens of Hz to several kHz, resulting in high peak power densities in the range of kW/cm^2. Such conditions have been shown to give ultra-smooth and dense films, improved coating adhesion to the substrate and the possibility for low-temperature synthesis of thin films. [3]

---

[3]For more details on HiPIMS and the coating procedure, please contact José Antonio Santiago Varela (joseantonio.santiago@nano4energy.eu) at Nano4Energy, Madrid, Spain.

3.4 Characterization

3.4.1 Scanning Electron Microscopy (SEM)

The surface morphology of the coated and non-coated substrates was analyzed using a Zeiss Supra 55VP Low Vacuum Field Emission Scanning Electron Microscope (LVFE-SEM). The built-in secondary electron detector was used to perform the topographic imaging. For statistical significance, three samples from each of the coated and non-coated surfaces were studied. To ensure that the results were representative of the surface morphology, several micrographs were taken at a chosen range of magnifications, *i.e.* at 50 000 X, 20 000 X, 10 000 X, 5000 X, 3000 X, 1000 X, 500 X and 100 X, for each sample.

The samples were cut into pieces of approximately 1 x 1 cm^2 and attached on a metallic sample holder using carbon tape as shown in Figure 3.3 to ensure sufficient electrical contact. As the samples are poor electronic conductors, a gold coating was further applied using an Edwards Sputter Coater S150B and the coating parameters presented in Table 3.2 to avoid charging during imaging. The thickness of the gold coating was measured to be 3.9±0.7 nm by a method described in detail in Appendix C. Further, a low accelerating voltage of 3 kV was used to secure the micrographs of coatings TiN (A) and TiN (B) and the corresponding non-coated reference substrate, while 2 kV acceleration voltage was used coating coatings TiN (C) and DLC as well as their non-coated reference substrate.

Table 3.2: Sputtering parameters used when applying gold coating to the samples before SEM analysis by the use of an Edwards Sputter Coater S150B.

Sputtering Parameter	Value
Sputtering Time	20 s
Argon Pressure	0.15 mbar
Voltage	18 kV
Current	18 mA

In addition, the cross section of samples coated with coatings TiN (C) and DLC were studied using a Helios G4 UX dual-beam Focused Ion Beam (FIB) from FEI with a Field Emission Gun SEM (FEGSEM). The work was performed by Per Erik Vollum at SINTEF Industry with an aim to investigate the coating homogeneity and adhesion and the substrate underneath. Because the focus of the study had turned to the optimized coatings at the time of this analysis, samples coated with coatings TiN (A) and TiN (B) were not included. Non-coated reference substrates were furthermore not analyzed as the bulk material of the coated samples was expected to be representative of the non-coated substrates.

When preparing the cross section lamellas, both samples were first coated with a thin Pt-Pd layer (80% Pt – 20% Pd) by a Cressington sputter coater to avoid charging while
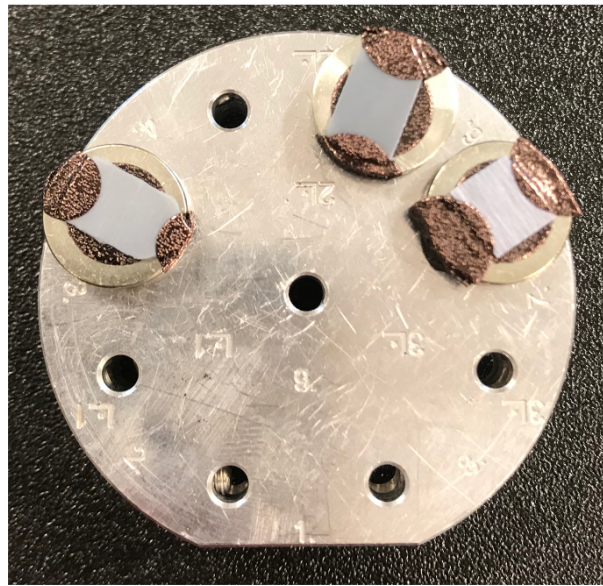
Figure 3.3: The samples are cut into appropriate size, attached to the metallic sample holder using carbon tape and coated with a gold coating to avoid charging during SEM analysis.

using the dual-beam FIB. Carbon protection layers were further deposited on top of the region of interest prior to cutting. The first part of the protection coating was deposited by electron assisted deposition to avoid ion-beam damage into the region of interest, while the second and thickest part of the carbon coating was deposited by Ga^+ ion beam assisted deposition. The cross section lamellas were cut out and transferred to dedicated Cu half grids using standard lift-out procedures. All course thinning was done at 30 kV acceleration voltage for the Ga^+ ions, while the final thinning was performed at 5 kV on either side of each lamella to minimize ion beam induced surface damage.

The FEGSEM was used to image the morphology of the prepared cross section lamellas using secondary electron imaging with approximately 4 mm working distance, a tilt between 50° and 54° and 0.10 nA current. An accelerating voltage of 3 kV and 5 kV was utilized for the samples coated with coating TiN (C) and DLC, respectively. [4]

3.4.2 Contact Angle Measurements (CAM)

The contact angle with water of the coated surfaces (*i.e.*, TiN (A), TiN (B), TiN (C) and DLC), as well as the non-coated reference surfaces (*i.e.*, both thick and thin substrates), was measured using a Krüss Drop Shape Analyzer 100. A HC10 humidity chamber was used in combination with a TC40 temperature chamber to ensure a reproducible and controlled environment of 25°C and 50% humidity. Each measurement was performed

---

[4]For more details on the cross section analysis, please contact Per Erik Vollum (PerErik.Vullum@sintef.no) at SINTEF Industry, Trondheim, Norway.

with a sessile drop volume of 4 μL at a rate of 0.16 mL/min, and all samples were stored in a desiccator prior to the measurements.

Between dosing and deposition of the droplet, a 5 second break was employed to ensure that the dosing was complete and thus facilitating a constant drop volume. Directly after the water droplet was deposited on the sample surface by moving the needle down for the drop to be picked up by the surface, the instrument camera took 10 images per second for 40 seconds. The contact angle was determined based on the Young-Laplace fitting method and image recognition performed by the Advance software [100]. The border between the drop shape and the sample surface, called the baseline, was set manually as the automatic baseline set by the software proved to be unstable. At least three drops were deposited onto each sample, and measurements were performed for at least three samples representative of each surface treatment for statistical purposes.

The wetting properties of the coatings deposited onto the thinner substrates (*i.e.*, TiN (C) and DLC) and the non-coated reference substrate were also measured at 37°C (*i.e.*, the temperature of the human body) and otherwise same conditions. This temperature change caused no significant change in wetting properties. However, a significant change in wetting properties was observed with the surface topography of these substrates (*i.e.*, the orientation of the directional lines in a regular pattern found in these samples as further discussed in Section 4.2). Hence, all measurements involving the thinner substrates were performed with the directional lines oriented parallel to the imaging direction, as is illustrated in Figure D.1. A further explanation of the investigation of the effect of temperature and substrate orientation and its results can be found in Appendix D.

The contact angle of the non-coated circular samples and coatings TiN (A) and TiN (B) were measured as a part of the present authors Specialization Project. However, new measurements were performed with the aforementioned parameters to confirm the wetting properties of the coatings and to improve the measurement quality, thus also improving the reliability of the results.

3.4.3 Friction Testing

The friction coefficients of all surfaces were characterized using a Hysitron TI 950 TriboIndenter with a Berkovich tip 20 μm in diameter. The load and displacement functions are presented in Figure 3.4 and show that the friction tests were performed at a maximum load of 1000 μN with a scratch length of 10 μm. The loading regime can be described by the following segments:

1. The tip moves 5 μm in the negative x-direction with no load applied to reach the scratch starting point.

2. The load is increased linearly from 0 μN to 1000 μN at a rate of 100 μN/s.

3. The tip holds for 5 seconds.

4. The tip scratches a 10 μm line in positive x-direction with the 1000 μN load applied at a rate of 20 μm/min.

5. The tip holds for 5 seconds.
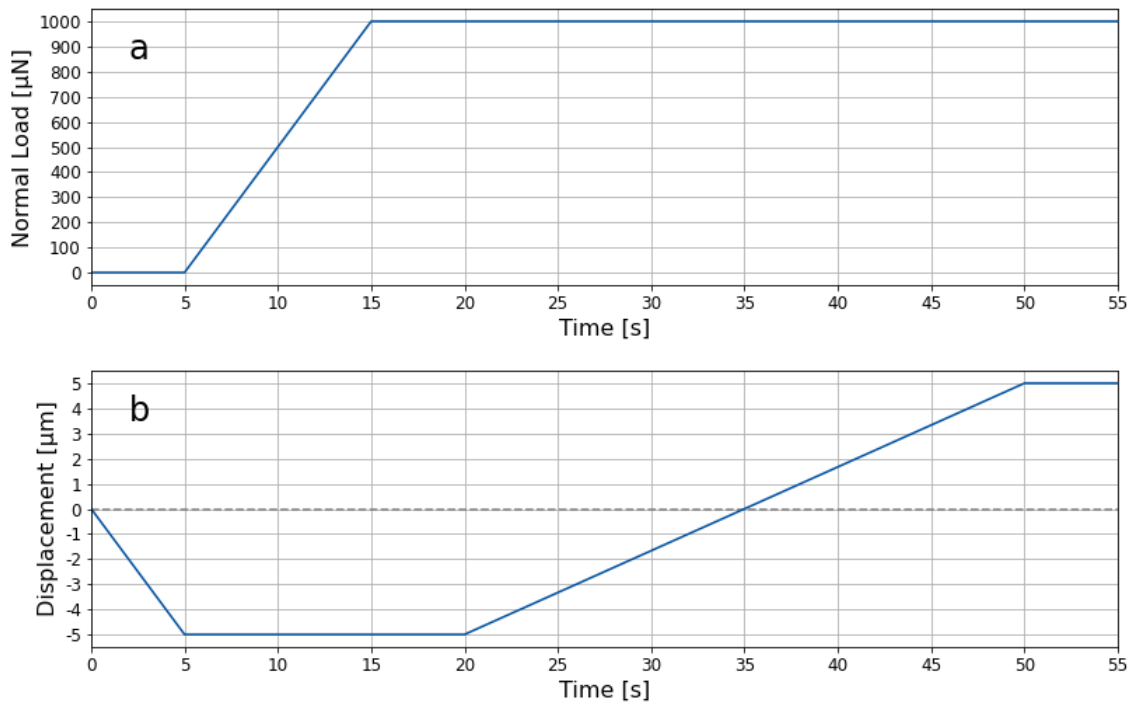
Figure 3.4: The (a) load and (b) displacement functions of the friction tests performed to find the material friction coefficient.

At least three tests were performed per sample, and at least three samples of each surface treatment were analyzed for statistical purposes. A 1 mm distance was employed between each scratch to ensure that possible surface variability was discovered, and that the analyzed area was not affected by previous measurements. The orientation of the directional lines in the thinner substrates proved to influence the stability of the results. Thus, these samples were aligned so that the directional lines were oriented parallel to the scratch direction to limit the effects of the substrate surface roughness and to determine the effect of the coatings.

The tip was calibrated using an 8 x 8 grid of indentations on fused silica 5 μm apart with loads varying linearly from 6 400 μN to 100 μN. The standard software refinement was set to give the best fit for lower loads as these are most relevant for the performed measurements. As the calibration gave conventional results no significant tips damage was indicated, and the tip area function was applied to all measurements.

3.4.4   Tensile Testing

Tensile testing can give well established mechanical properties such as elastic modulus, tensile strength and ductility [101]. The dog-bone shaped samples with and without coatings were tensile tested to determine if and how the coatings and coating processes affect the mechanical properties of the material. For each type of sample (*i.e.*, non-coated thin substrates, TiN (C) coated and DLC coated substrates), five samples were tested for statistical significance. Five non-coated substrates exposed to Phosphate Buffered Saline (PBS) solution for 49 days, as described in Section 3.5, were also tested to determine if the exposure to the solution altered the mechanical properties of the substrates. These samples were measured and weighed before the exposure to reveal possible swelling.

The tensile tests were performed at TCKT in Wels, Austria using a Zwick Roell Z0.5 instrument. The execution was according to ISO 527-2/5B/50 at room temperature with the atmospheric conditions otherwise according to ISO 291. The samples were shaped according to ISO 527-2 Typ 5B and the thickness of the samples was measured prior to analysis to account for the varying substrate thicknesses.

3.4.5   Testing of Other Mechanical Properties

Scratch testing was also attempted as it can give results on coating adhesion and cohesion, two important coating properties [89]. However, the group was unable to establish a reliable and reproducible method with the available equipment (*i.e.*, an Anton Paar Micro Scratch Tester with a 100 μm radius Rockwell diamond indenter and an Hysitron TI 950 TriboIndenter with a Berkovich tip 20 μm in diameter) due to the combination of a soft substrate and a nanometer-scaled hard coating. As a scratching procedure was performed with the Anton Paar Micro Scratch Tester for the present authors Specialization Project, SEM micrographs were collected of the scratched areas using the same imaging conditions as otherwise used throughout this Thesis. A selection of these micrographs is presented in Appendix E, along with micrographs from attempts of establishing a new method.

The coating hardness was also deemed to be an interesting property but attempts at establishing a method for measuring it using the TI 950 TriboIndenter with various tip geometries was not successful. This is in accordance with literature which states that the indentation depth should be below 10-15% of the film thickness to avoid substrate effects, and that it is hard to reliably measure meaningful values of coating hardness of coatings significantly thinner than 130-200 nm as the hardness decreases with decreasing indentation depths below 20 nm [102].

3.5 Exposure to Phosphate Buffered Saline (PBS)

To evaluate the produced coatings' biological response the coated and uncoated substrates were immersed in a Phosphate Buffered Saline (PBS) solution as an initial simulation of the environment in the human body. The PBS solution is a close match to the fluids found in the human body with regards to pH, osmolarity and ion concentrations [103]. Analysis of the liquid after exposure can reveal the compounds released from the substrates and coatings, predicting which compounds could be released into the blood stream. Studying the post-exposure surface morphology can also reveal changes to the material surface. The steps included in the exposure study are illustrated in Figure 3.5. Details on the PBS used in this project can be found in Appendix A.
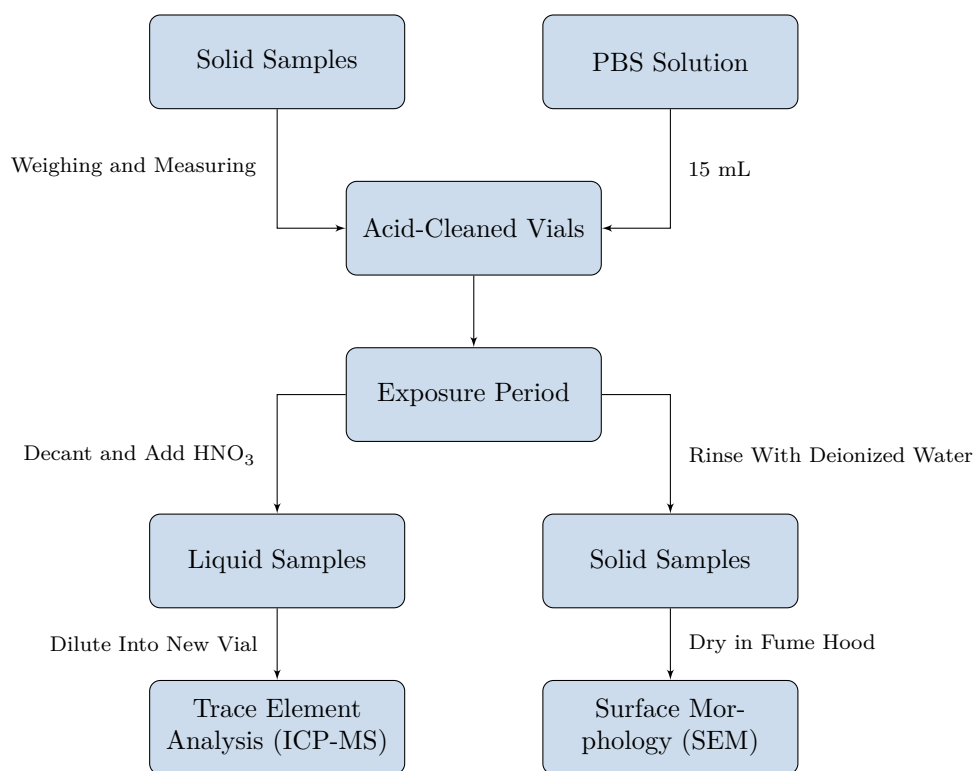
Figure 3.5: The activities performed in relation to the exposure study of the solid samples with Phosphate Buffered Saline (PBS).

The PBS solution was prepared by dissolving tablets in deionized water, according to the supplier instructions, and stored in an acid washed teflon container to avoid contamination of the solution. In total, 63 samples were cut to appropriate size and placed in separate acid washed vials filled with 15 ml of the PBS solution, before being placed in a heating cabinet, *i.e.*, 40 coated samples, 20 non-coated and 3 samples of unprocessed pellets. 3 vials were also only filled with the PBS solution as a reference. The heating cabinet was kept at a constant temperature of 37° C during the duration of the test. To simulate the

flow of liquid across the material surface, it was placed on top of a tilting table with a frequency of 10 RPM. Two samples of each of the two coatings, as well as two of the non-coated samples were removed at each time interval according to the protocol presented in Table 3.3.

Table 3.3: The plan for liquid exposure to PBS over different time intervals. Two samples are removed from the PBS solution at each time interval marked with X.

Sample	TiN (A)	TiN (B)	TPU	TPU Pellets	Only PBS
10 min	X	X	X		
30 min	X	X	X		
1 hr	X	X	X		
6 hrs	X	X	X		
12 hrs	X	X	X		
24 hrs	X	X	X		
3 days	X	X	X		
7 days	X	X	X		
10 days	X	X	X		
30 days	X	X	X	X	X

When removing the sample containers from the heating cabinet the liquid solution was poured into new acid washed vials. 5 drops of 65% of nitric acid (HNO$_3$) was added to obtain a solution of 0.1 M HNO$_3$ to preserve the samples awaiting further analyses. The solid samples were carefully rinsed with deionized water to remove any salt residues and stored plastic sample boxes cleaned with soap, ethanol and distilled water.

The chemical composition of the liquid samples was further analyzed using ICP-MS with an Agilent – 8800 ICP-MS Triple Quad. Following a full scan of the PBS solution (*i.e.*, determination of the concentrations of 66 elements), the concentrations of S, Ti, and Ba were determined. To avoid drift in the measurements, the samples were diluted 30 times by using Rainin E4 XLS+ electronic pipettes from Mettler Toledo before the analysis. 0.4 mL of each sample was mixed with 11.6 mL of a 0.1 M HNO$_3$ standard solution. Separate pipettes were used for the liquid samples and the HNO$_3$ solution, and the pipette tips used for liquid samples were changed between every sample to avoid cross contamination. The tips used for the HNO$_3$ solution were changed after every 20th sample. The instrument parameters utilized for the analysis can be studied in Appendix F.

The surface morphology of the solid samples was studied using SEM analysis using the method described in Section 3.4.1, with an acceleration voltage of 2 kV. One sample was analyzed for each of the ten time intervals, and an additional sample was analyzed for each of the selected time intervals (*i.e.*, 1 hour, 24 hours, 7 days and 30 days) for statistical significance. The sample surfaces were also imaged at various locations and magnifications to ensure that the micrographs were representative of the surface morphology.

As ICP-MS is an extremely sensitive technique, the accuracy of the sample analysis is

consequently sensitive to contamination. Therefore additional precautions were taken. Cutting boards, tweezers and the calipers were covered in plastic foil and the contact with tweezers and the caliper were also otherwise minimized. All work was performed in a laminar flow cabinet to further reduce contamination. To ensure that the samples were of similar size and to account for differences in weight of the solid samples, each of the samples were weighed and measured to find the mass and surface area before starting the exposure. The weight of the PBS solution included in each vial was also registered to find the exact liquid volume.

Chapter 4

Results

4.1 Sputtering Process

The color of the TiN (C) coating is grey as seen in Figure 4.1 and indistinguishable from that of coatings TiN (A) and TiN (B) when observed with the naked eye.
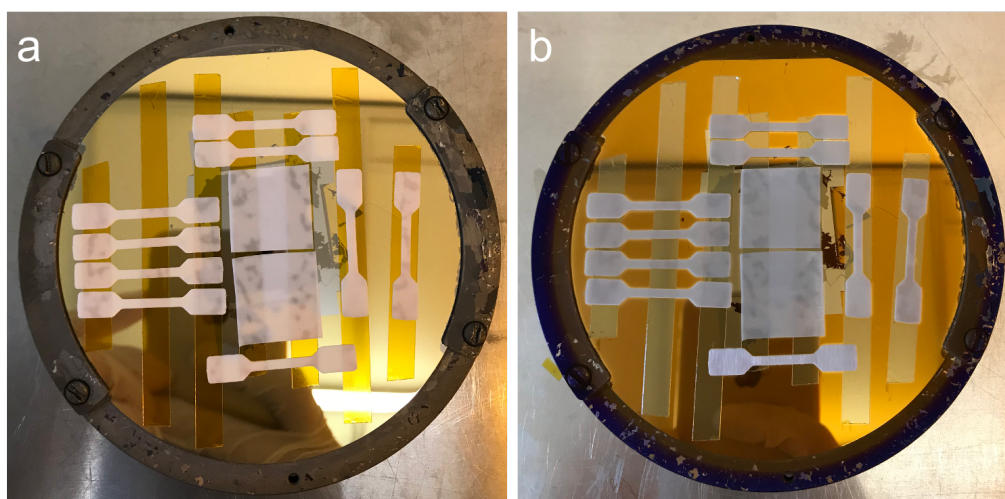
Figure 4.1: Images of samples attached to the sample holder used for sputtering (a) before and (b) after deposition of coating TiN (C).

Values for the substrate temperature, FWD, the REF and the DCV registered during the sputtering processes of the three TiN coatings are presented in Table 4.1.

Table 4.1: The values for the substrate temperature, the Forwarded Power (FWD), the Reflected Power (REF) and the Direct Current Bias (DCV) observed during the TiN sputtering processes.

Parameter	TiN (A)	TiN (B)	TiN (C)
Substrate Temperature	14-16°C	14-16°C	14-16°C
FWD	80 W	80 W	120 W
REF	0 W	0 W	0-1 W
DCV	192-195 V	260-264 V	239-244 V

4.2 Surface Morphology

All micrographs presented in the present section are the most representative of the respective samples at the respective magnification and were selected to display key features. A variety of micrographs taken at other magnifications as well as encountered irregularities are shown in Appendix G.

4.2.1 Coatings TiN (A) and TiN (B)

The surface morphology of the non-coated thicker reference substrates as well as samples coated with coatings TiN (A) and TiN (B) are presented at various magnifications in the following figures. All samples have significant surface roughness in the form of directional lines in a regular pattern as illustrated at 1 000 X magnification in Figure 4.2. These lines are also visible by the naked eye.
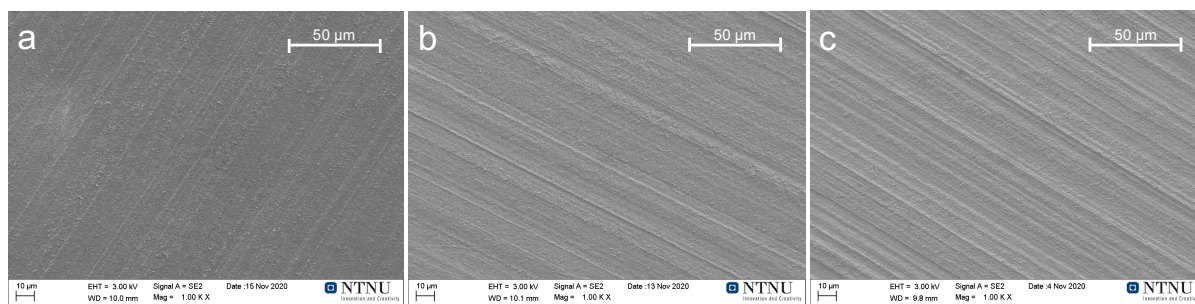
Figure 4.2: SEM micrographs of (a) the non-coated reference substrate, (b) samples coated with coating TiN (A) and (c) coating TiN (B) imaged at 1 000 X magnification.

The SEM micrographs of the surfaces taken at 20 000 X magnification presented in Figure 4.3 show particles protruding the surface in all samples. Further, Figure 4.4 shows cracks in both coatings.
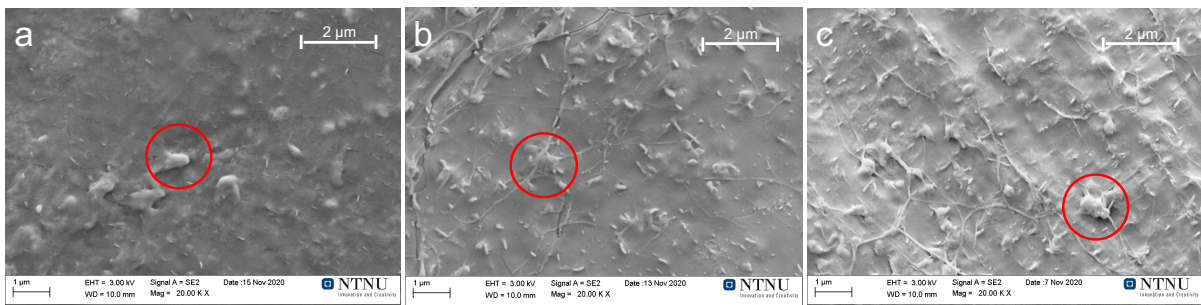
Figure 4.3: SEM micrographs of (a) the non-coated reference substrate, (b) samples coated with coating TiN (A) and (c) coating TiN (B) imaged at 20 000 X magnification.
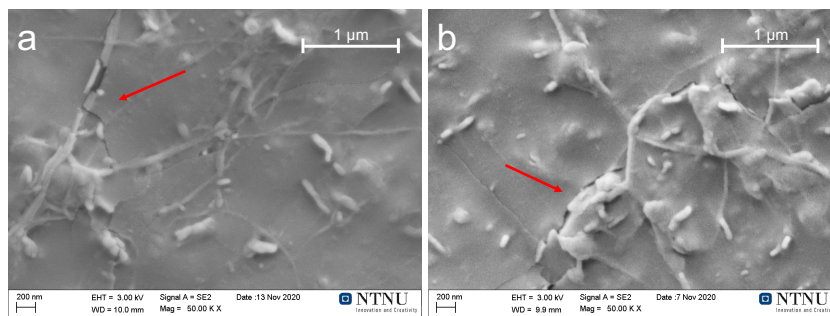
Figure 4.4: SEM micrographs of samples coated with (a) coating TiN (A) and (b) coating TiN (B) imaged at 50 000 X magnification.

4.2.2 Coatings TiN (C) and DLC

The surface morphology of the non-coated thinner reference substrates as well as samples coated with coating TiN (C) and DLC are presented in the following figures at various magnifications. All samples have significant surface roughness in the form of directional lines in a regular pattern as best illustrated at 500 X magnification (Figure 4.5) and 1 000 X magnification (Figure 4.6). These lines are also visible by the naked eye.
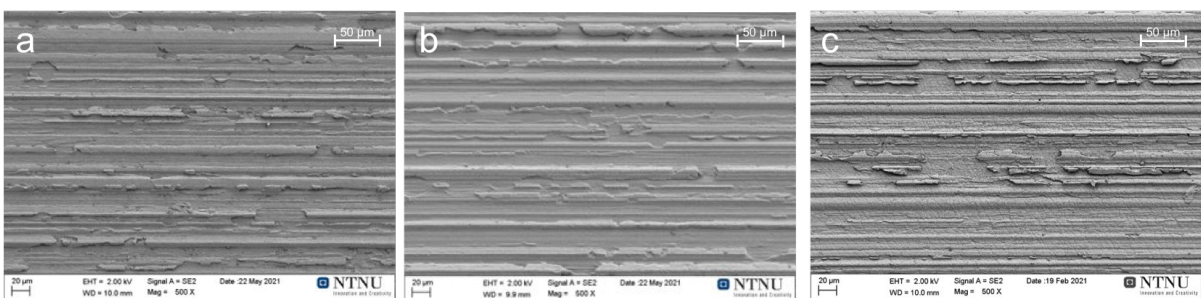
Figure 4.5: SEM micrographs of (a) the non-coated reference substrate, (b) samples coated with coating TiN (C) and (c) DLC imaged at 500 X magnification.

At higher magnifications (Figures 4.7, 4.8, and 4.9) other features also become evident. The non-coated reference substrate has significant surface roughness, even on a nanometer
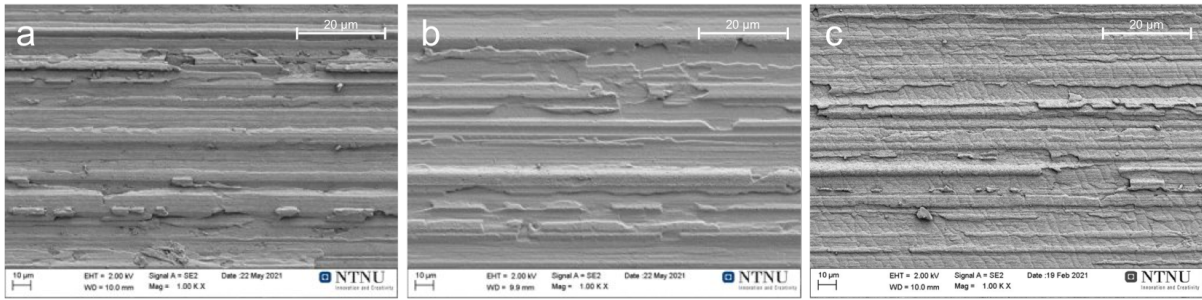
Figure 4.6: SEM micrographs of (a) the non-coated reference substrate, (b) samples coated with coating TiN (C) and (c) DLC imaged at 1 000 X magnification.

scale. The surfaces coated with TiN (C) are generally more even, have a semi-periodic pattern of cracks across the entire surface. The DLC coating has a structure where particles have agglomerated in a distinctive pattern best observed at 50 000 X magnification, which gives significant surface roughness, but the coating does not show signs of cracking.
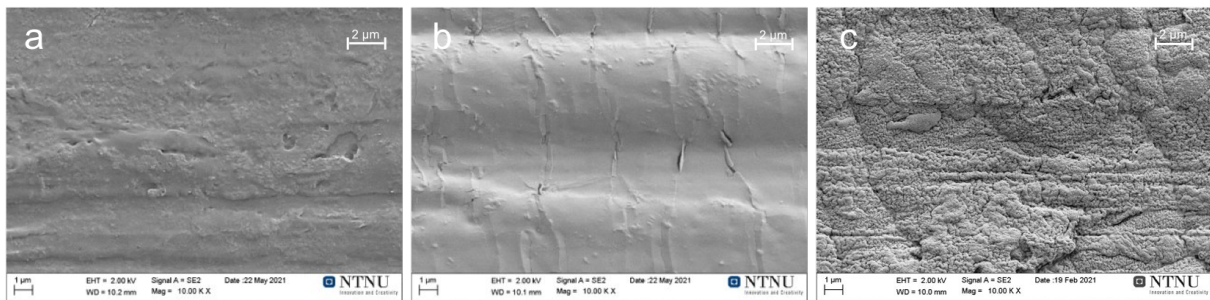
Figure 4.7: SEM micrographs of (a) the non-coated reference substrate, (b) samples coated with coating TiN (C) and (c) DLC imaged at 10 000 X magnification.
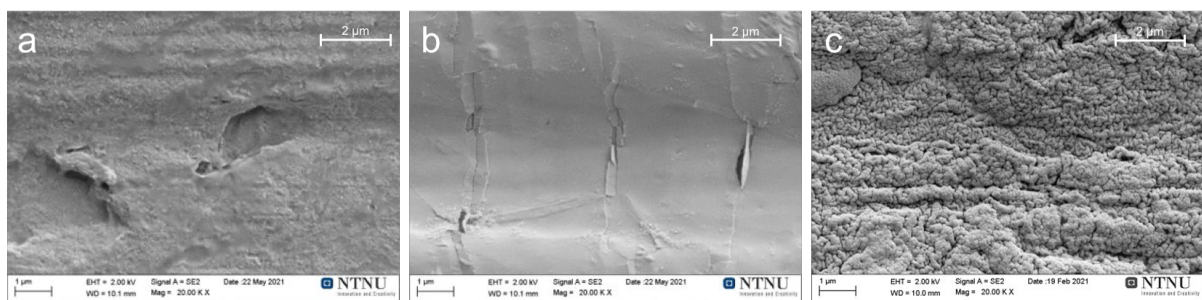
Figure 4.8: SEM micrographs of (a) the non-coated reference substrate, (b) samples coated with coating TiN (C) and (c) DLC imaged at 20 000 X magnification.
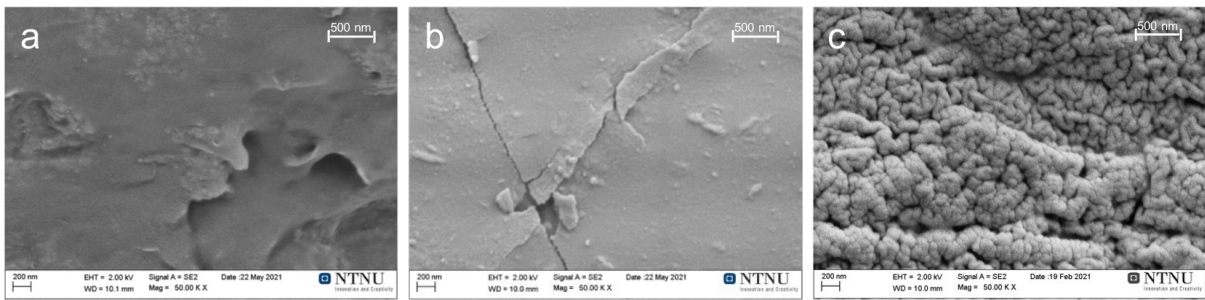
Figure 4.9: SEM micrographs of (a) the non-coated reference substrate, (b) samples coated with coating TiN (C) and (c) DLC imaged at 50 000 X magnification.

4.3 Cross Section Morphology

Micrographs of the cross section of a sample coated with coating TiN (C) are presented in Figures 4.10 where the cross section is imaged at 35 000 X, 120 000 X and 350 000 X magnification.
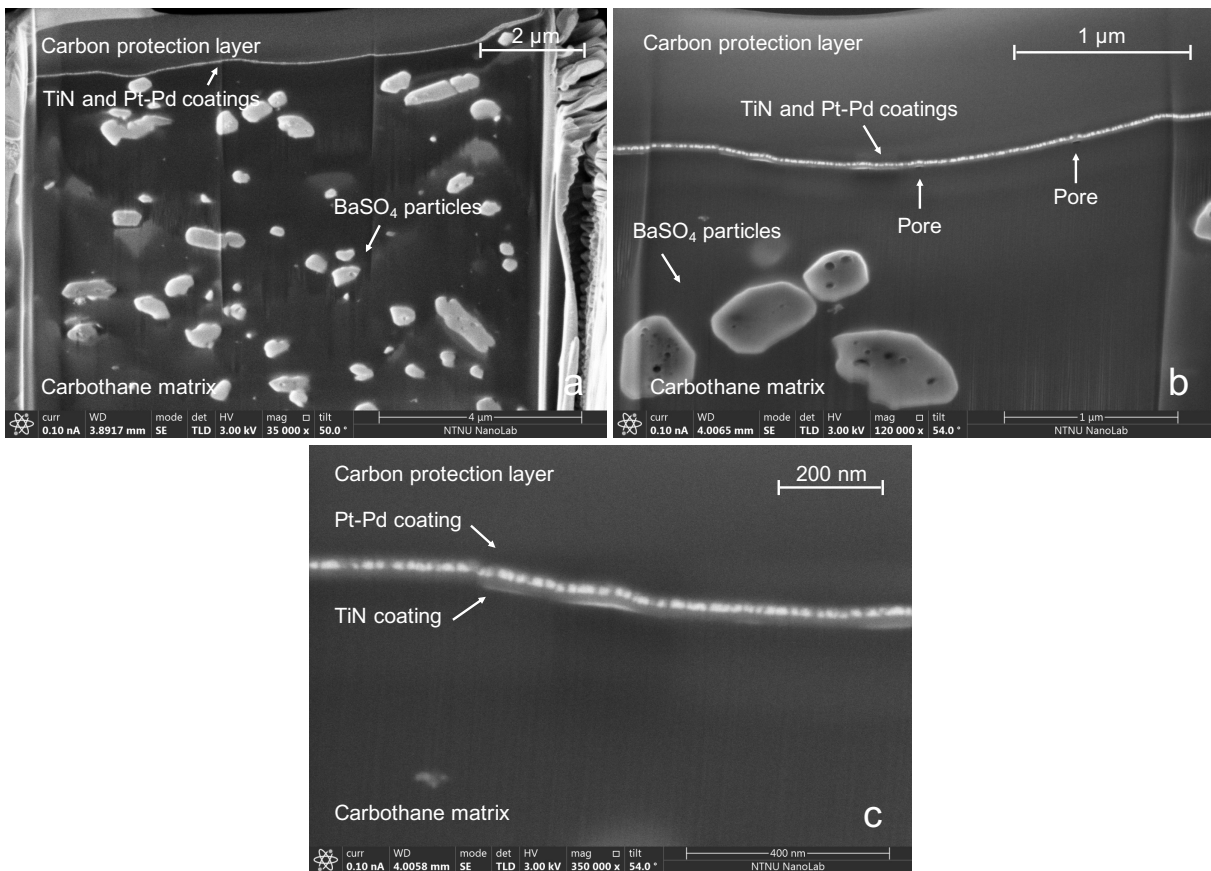
Figure 4.10: The cross section of a sample coated with TiN (C) imaged at (a) 35 000 X, (b) 120 000 X and (c) 350 000 X magnification using SEM.

The cross section of a sample coated with DLC coating is presented in Figure 4.11 where the micrographs are taken at 80 000 X and 100 000 X magnification.
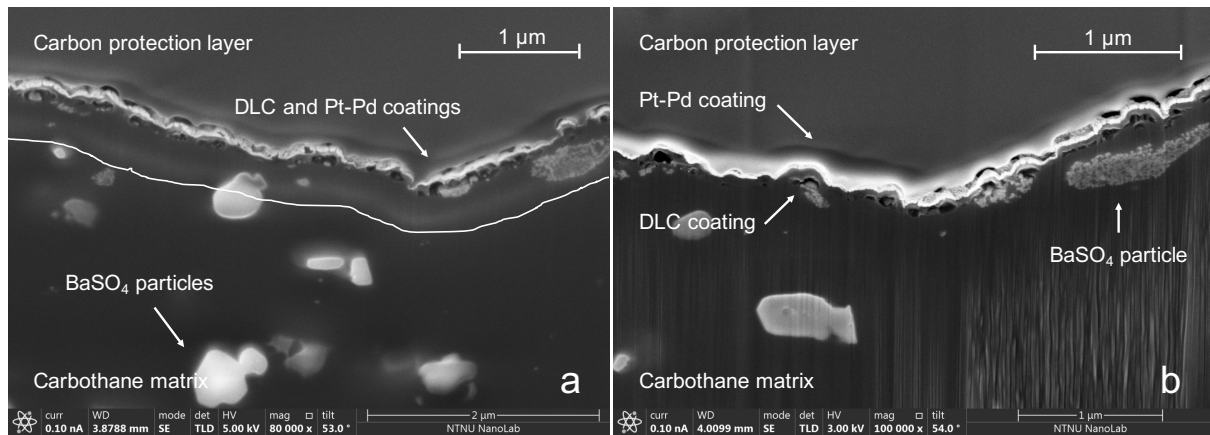
Figure 4.11: The cross section of a sample coated with DLC imaged at (a) 80 000 X and (b) 100 000 X magnification using SEM.

4.4 Wetting Properties

All drops showed a gradual decline in the contact angle with water over time, though with varying rate and rate stability. This is the origin of the standard deviation found within the measurements from each drop presented in the following subsections. The standard deviation from each drop has been considered when calculating the standard deviation for the average sample contact angle. A temporary increase in the humidity of a few percent was also registered directly after deposition.

4.4.1 Coatings TiN (A) and TiN (B)

The contact angle varied significantly between coatings TiN (A) and TiN (B) and the non-coated circular reference substrate. The reference substrate had the highest average contact angle ($101° \pm 2°$), followed by coating TiN (B) ($89° \pm 1°$) and coating TiN (A) ($80° \pm 2°$). The variance between the three different samples measured from each surface can be studied in Figure 4.12. Figure 4.13 also illustrates the difference between the surfaces by showing a selection of drops 10 seconds after deposition.
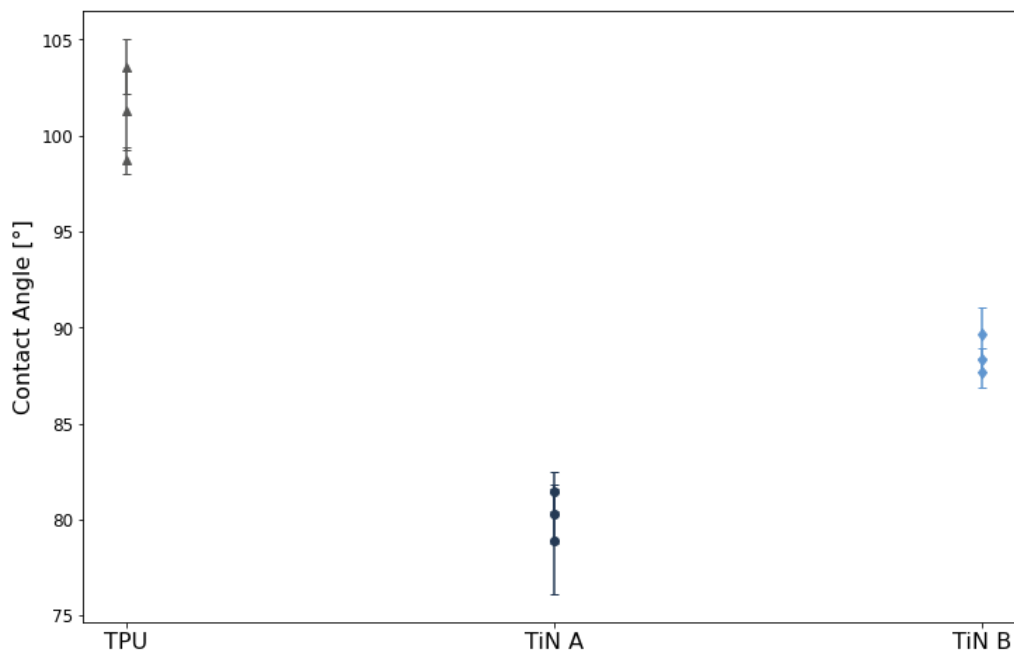
Figure 4.12: The measured contact angles with water of the non-coated reference substrate (TPU), and samples coated with coating TiN (A) and TiN (B) at 25°C and 50% humidity.
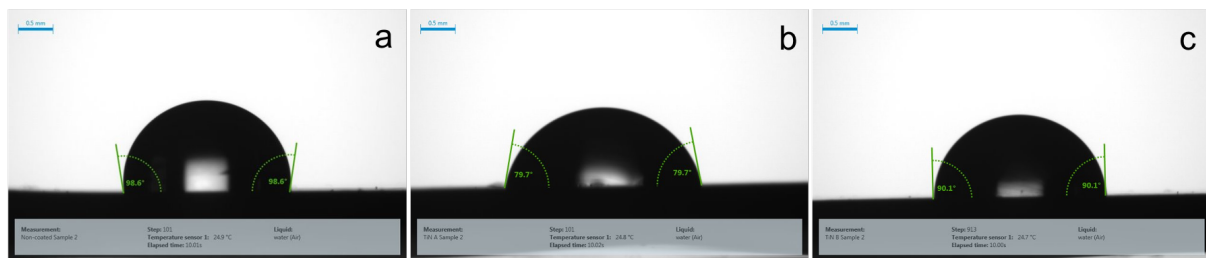
Figure 4.13: The images show water drops deposited on (a) a sample of the non-coated reference substrate, and samples coated with coating (b) TiN (A) and (c) TiN (B) at 25°C and 50% humidity. The images are taken 10 s after deposition and illustrate the variation between surfaces.

4.4.2 Coatings TiN (C) and DLC

The average contact angle was also higher for the non-coated thinner substrates (120°±3°) than for the substrates coated with DLC coating (97°±3°) and coating TiN (C) (93°±3°). The variance between the three different samples measured from each surface can be studied in Figure 4.14. Figure 4.15 also illustrates the difference between the surfaces by showing a selection of drops 10 seconds after deposition.
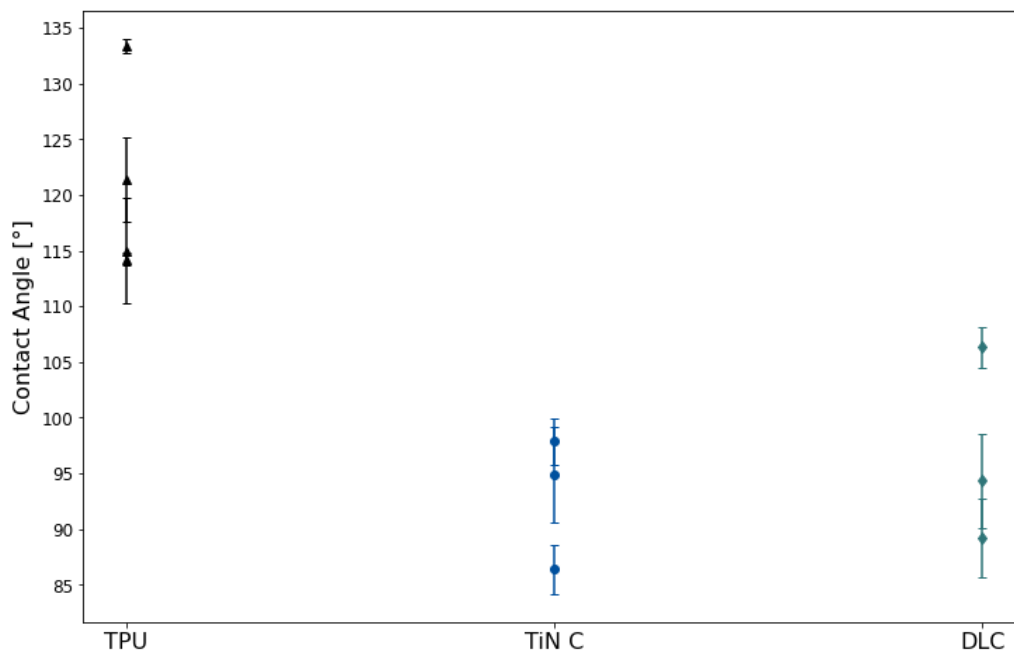
Figure 4.14: The measured contact angles with water of the non-coated reference substrate (TPU), and samples coated with coating TiN (C) and DLC at 25°C and 50% humidity. The directional lines in the substrates are oriented parallel to the imaging direction.
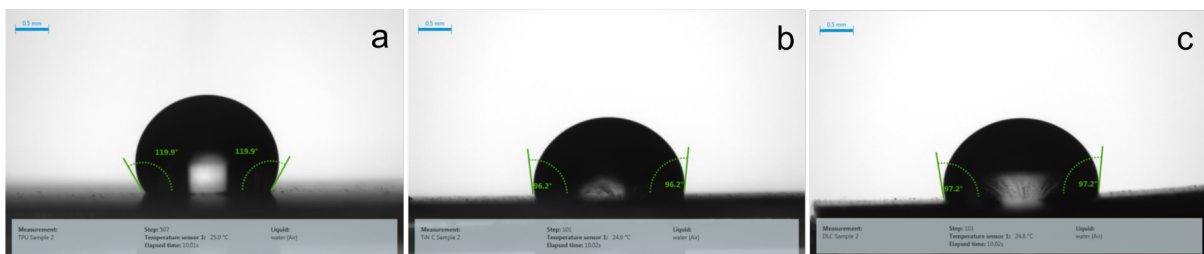
Figure 4.15: The images show water drops deposited on (a) a sample of the non-coated reference substrate, and samples coated with coating (b) TiN (C) and (c) DLC at 25°C and 50% humidity. The images are taken 10 s after deposition and illustrate the variation between surfaces. The directional lines in the substrates are oriented parallel to the imaging direction.

4.5   Coating Cohesion, Adhesion and Friction Properties

For the following section, the most representative results from each sample are presented. All results from all samples can be studied in Appendix H. The normal force and the lateral displacement were confirmed to be in correspondence with the experimental procedure for

all measurements. No changes to the scratched surfaces could visually be observed a result of the scratches using the built-in optical microscope.

4.5.1 Coatings TiN (A) and TiN (B)

The friction coefficients for coatings TiN (A) and TiN (B) as well as the corresponding non-coated reference substrate obtained from segment 4 described in Section 3.4.3 are presented in Figure 4.16. The average friction coefficient is 0.40 ± 0.03 for coating TiN (A), 0.39 ± 0.03 for coating TiN (B), and 0.44 ± 0.10 for the non-coated reference substrate. The average friction coefficient is calculated from 25 s to 50 s for the coated surfaces and 28 s to 50 s for the non-coated reference surfaces to ensure that equilibrium conditions are reached.
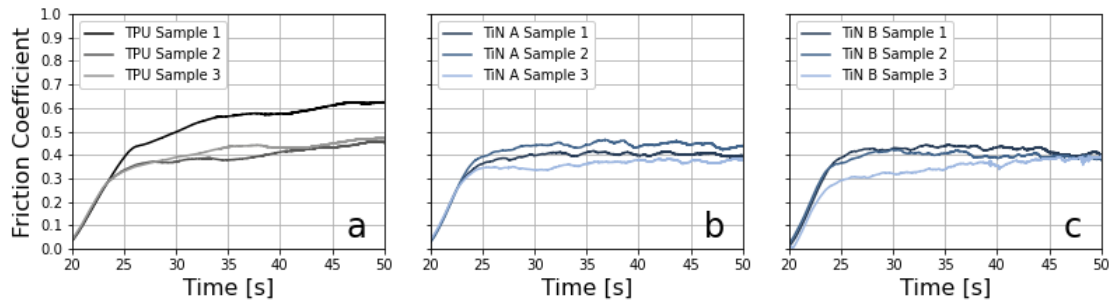
Figure 4.16: The friction coefficients of (a) non-coated reference substrates, (b) samples coated with coating TiN (A), and (c) samples coated with coating TiN (B). The most representative results has been chosen from each sample.

The normal displacements for coatings TiN (A) and TiN (B) as well as the corresponding non-coated reference substrate also obtained from segment 4 are presented in Figure 4.17. The normal displacement is approximately two orders of magnitude greater than the coating thickness.
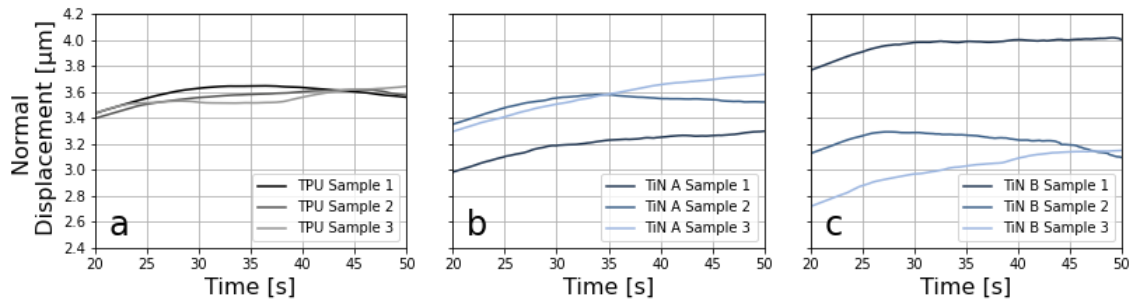
Figure 4.17: The normal displacement of (a) non-coated reference substrates, (b) samples coated with coating TiN (A), and (c) samples coated with coating TiN (B). The most representative results has been chosen from each sample.

4.5.2 Coatings TiN (C) and DLC

The friction coefficients for coatings TiN (C) and DLC as well as the corresponding non-coated substrate obtained from the same segment are presented in Figure 4.18. The average friction coefficient is 0.42 ± 0.01 for coating TiN (C), 0.28 ± 0.01 for DLC, and 0.59 ± 0.05 for the non-coated reference substrate. The average friction coefficient is calculated from 25 s to 50 s for the coating TiN (C), 24 s to 50 s for DLC and 28 s to 50 s for the non-coated reference surfaces to ensure that equilibrium conditions are reached.
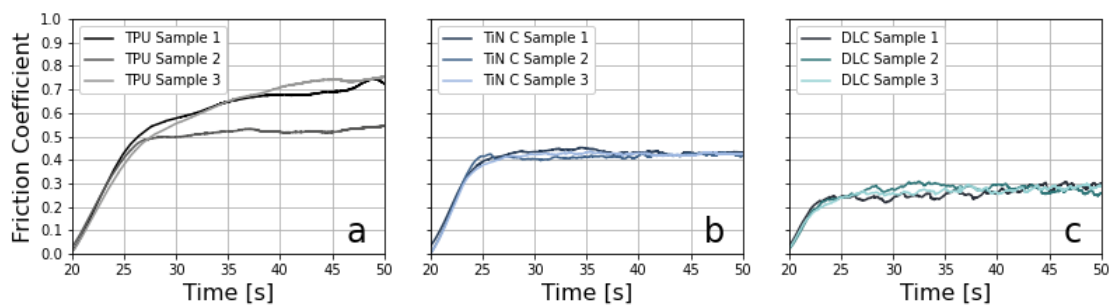
Figure 4.18: The friction coefficients of (a) non-coated reference substrates, (b) samples coated with coating TiN (C), and (c) samples coated with DLC. The most representative results has been chosen from each sample.

The normal displacement for coatings TiN (C) and DLC as well as the corresponding non-coated substrate obtained from the same segment are presented in Figure 4.19. The normal displacement is approximately two orders of magnitude greater than the coating thickness.
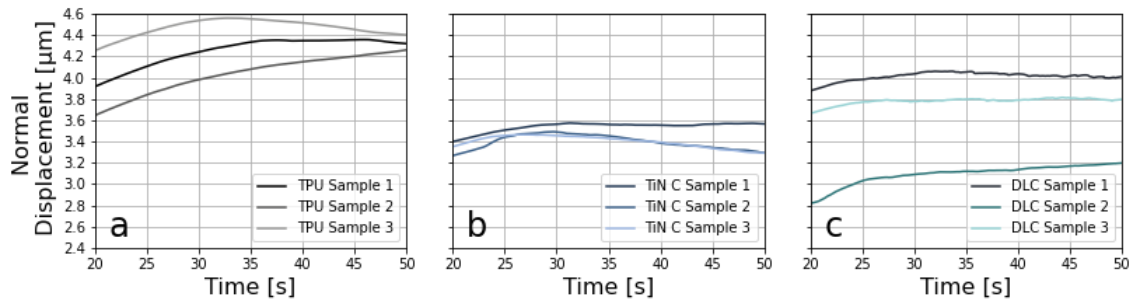
Figure 4.19: The normal displacement of (a) non-coated reference substrates, (b) samples coated with coating TiN (C), and (c) samples coated with DLC. The most representative results has been chosen from each sample.

4.6 Mechanical Properties

The average maximum stress and strain obtained after tensile testing are presented in Figure 4.20. The thickness of the samples used for tensile testing was found to vary between 150 μm and 430 μm. No swelling in the material of the non-coated samples exposed to PBS was measured, but due to the uncertainties in the measurement equipment and method, it cannot be concluded that no swelling occurred.
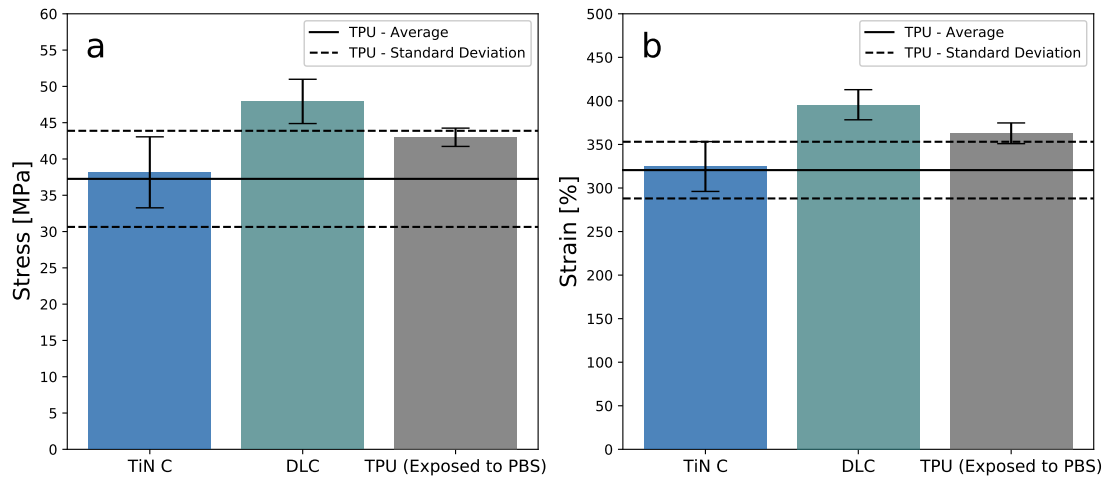
Figure 4.20: The average (a) maximum stress and (b) maximum strain for samples coated with coating TiN (C) and DLC as well as non-coated reference substrates (TPU) exposed to Phosphate Buffered Saline (PBS) for 49 days. The horizontal lines give the average values and standard deviation for non-coated reference substrates (TPU).

4.7 The Effect of Exposure to Phosphate Buffered Saline

4.7.1 Surface Morphology

The following micrographs are deemed to be the most representative of the respective surfaces (*i.e.*, TiN (A), TiN (B) and non-coated reference substrates), exposure times and magnifications. The micrographs presented in this section show samples exposed to PBS solution for 1 hour, 24 hours, 7 days and 30 days imaged at 20 000 X and 5 000 X magnification. Additional magnifications and the remaining time intervals can be studied in Appendix I.

Figures 4.21, 4.22 and 4.23 show SEM micrographs at 20 000 X magnification of samples with coating TiN (A), TiN (B) and non-coated substrates, respectively.
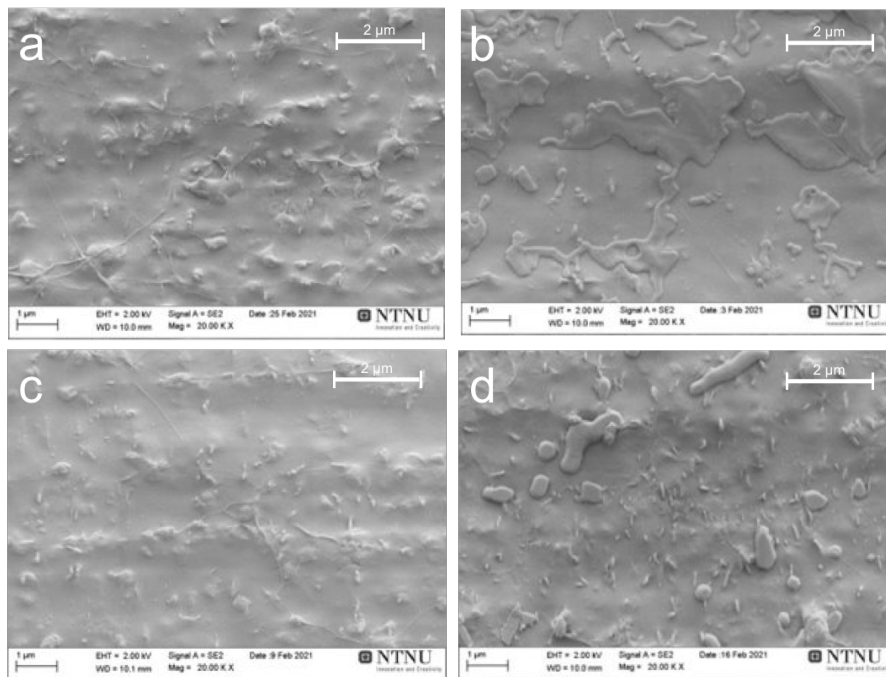
Figure 4.21: SEM micrographs of samples with coating TiN (A) exposed to PBS for (a) 1 hour, (b) 24 hours, (c) 7 days and (d) 30 days imaged at 20 000 X magnification.
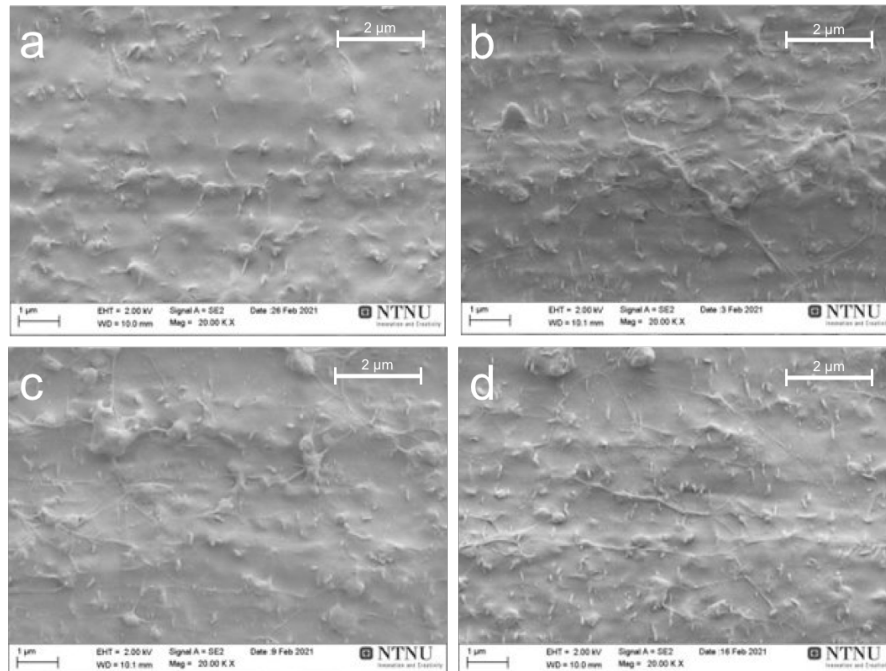
Figure 4.22: SEM micrographs of samples with coating TiN (B) exposed to PBS for (a) 1 hour, (b) 24 hours, (c) 7 days and (d) 30 days imaged at 20 000 X magnification.
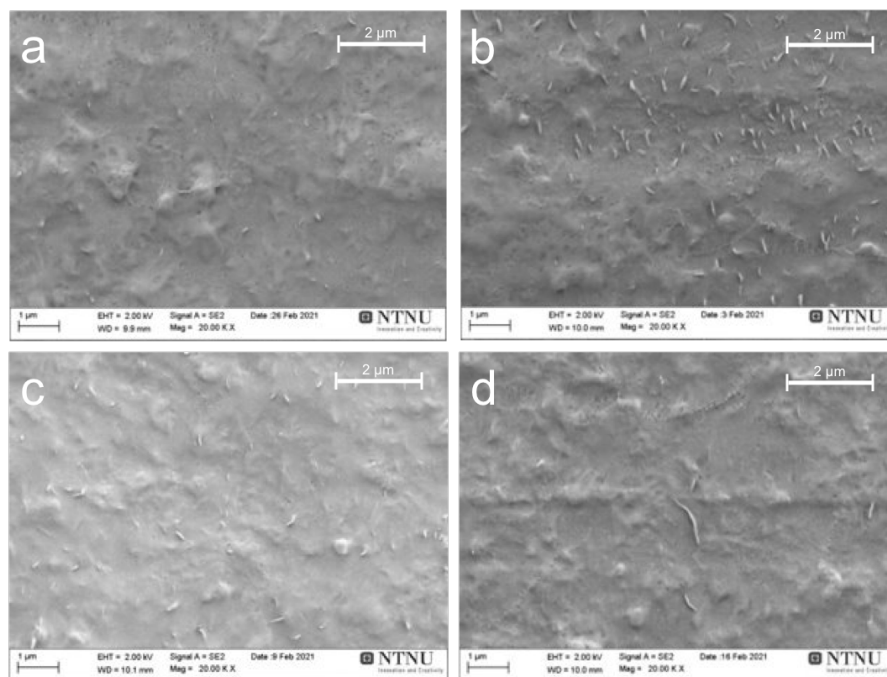
Figure 4.23: SEM micrographs of non-coated substrates exposed to PBS for (a) 1 hour, (b) 24 hours, (c) 7 days and (d) 30 days imaged at 20 000 X magnification.

Figures 4.24, 4.25 and 4.26 show SEM micrographs at 5 000 X magnification of samples with coating TiN (A), TiN (B) and non-coated substrates, respectively.
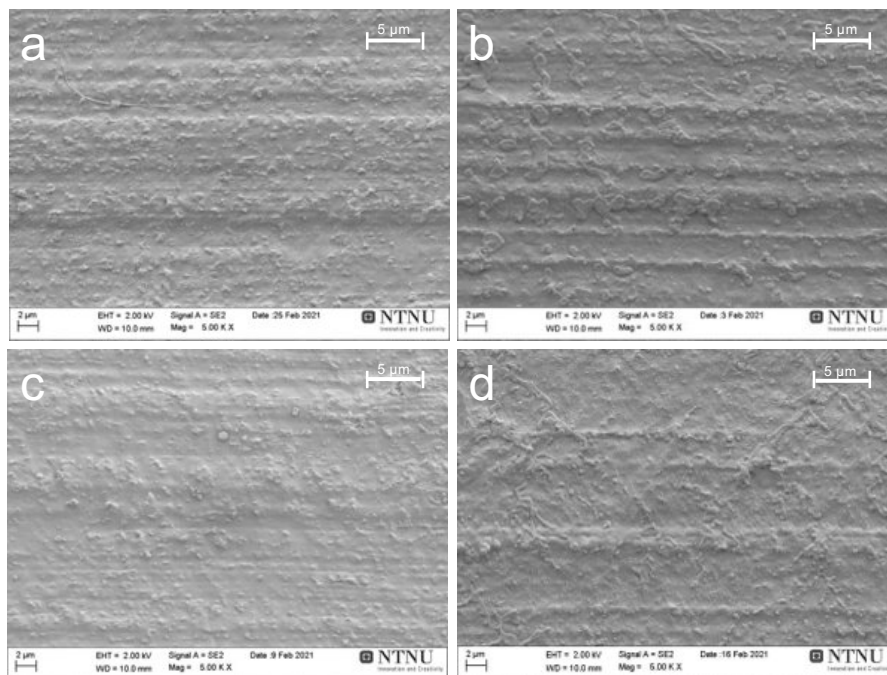
Figure 4.24: SEM micrographs of samples with coating TiN (A) exposed to PBS for (a) 1 hour, (b) 24 hours, (c) 7 days and (d) 30 days imaged at 5 000 X magnification.

NTNU
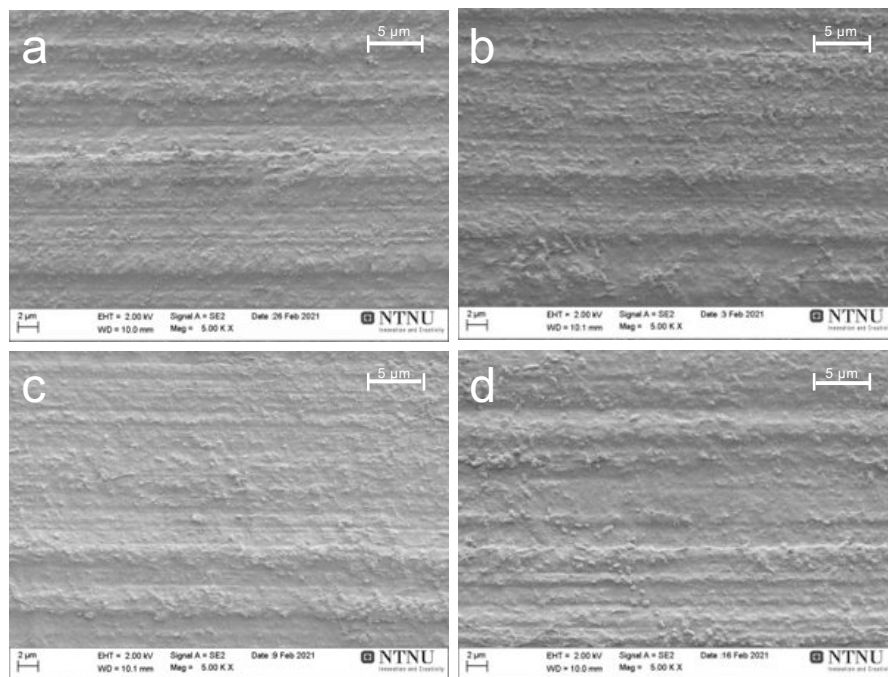
Figure 4.25: SEM micrographs of samples with coating TiN (B) exposed to PBS for (a) 1 hour, (b) 24 hours, (c) 7 days and (d) 30 days imaged at 5 000 X magnification.
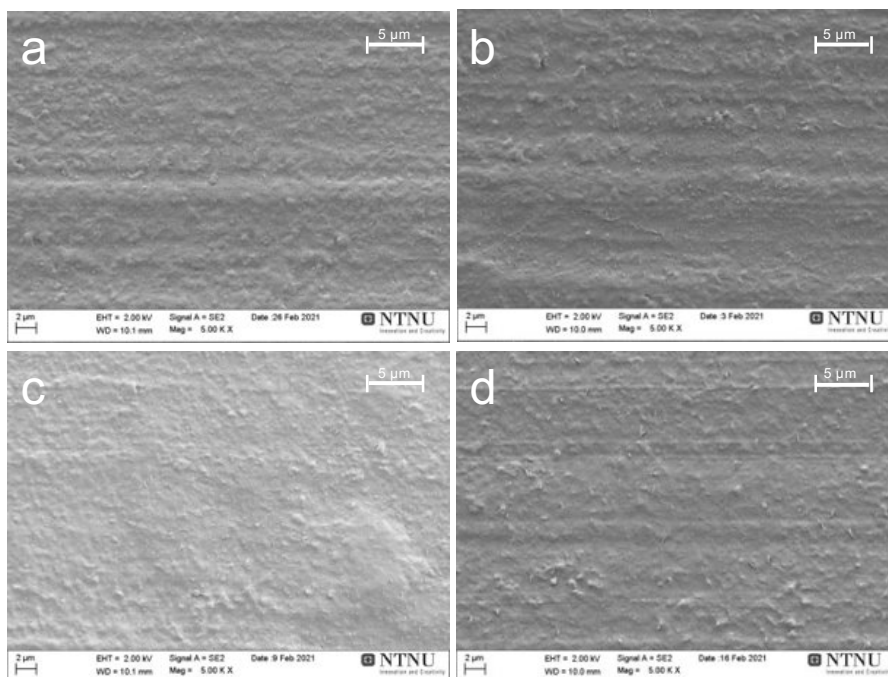
Figure 4.26: SEM micrographs of non-coated substrates exposed to PBS for (a) 1 hour, (b) 24 hours, (c) 7 days and (d) 30 days imaged at 5 000 X magnification.

The degree of degradation of the non-coated reference substrates appears to correlate

better with the timespan between the end of the exposure study and the SEM analysis than the duration of the exposure period itself. No such correlation has been identified for the coated samples. The exact time between these events are presented in Appendix I. The following figures present the samples exposed to PBS for 1 hour (Figure 4.27), 24 hours (Figure 4.28), 7 days (Figure 4.29) and 30 days (Figure 4.30) imaged at 20 000 X magnification. The samples analyzed between 3 days and 16 days after exposure end are compared to the samples analyzed between 94 days and 109 days after exposure.
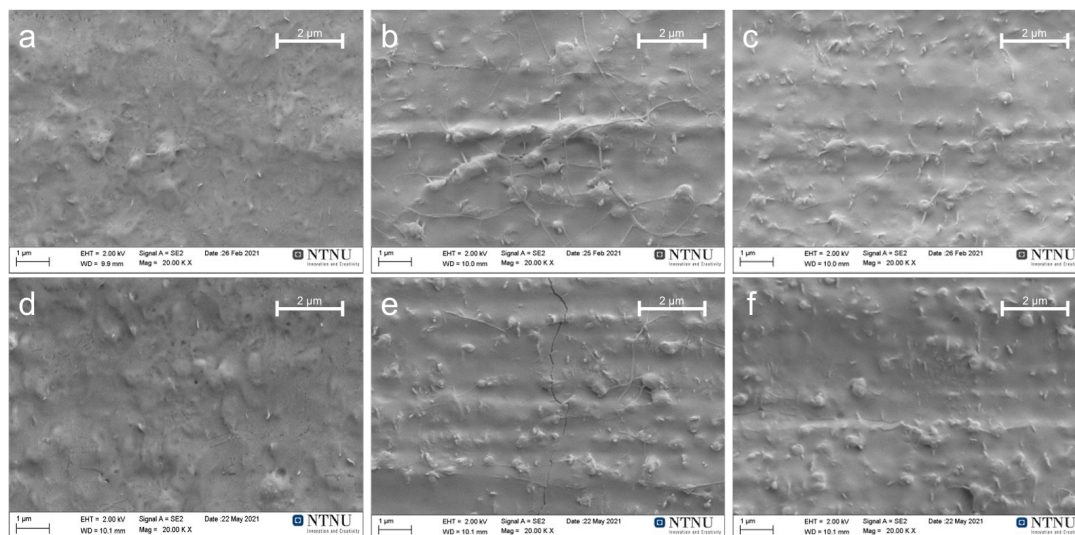
Figure 4.27: SEM micrographs of samples exposed to Phosphate Buffered Saline (PBS) solution for 1 hour imaged at 20 000 X magnification. The figure shows the first round of samples analyzed 16 days after exposure ended (*i.e.*, (a) the non-coated reference substrate, and samples coated with coatings (b) TiN (A) and (c) TiN (B)) and the second round of samples analyzed 101 days after exposure ended (*i.e.*, (d) the non-coated reference substrate, and samples coated with coatings (e) TiN (A) and (f) TiN (B)).
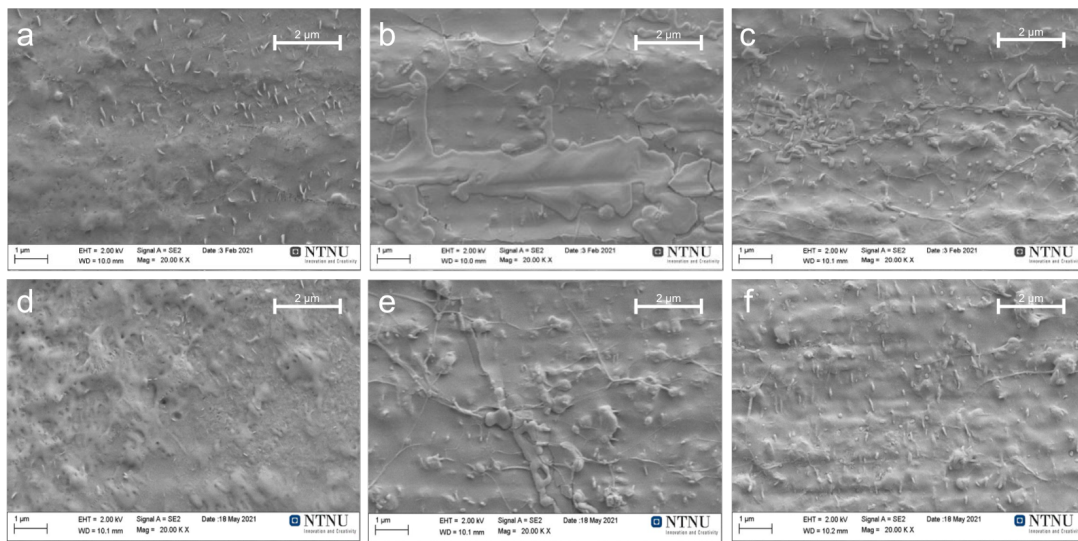
Figure 4.28: SEM micrographs of samples exposed to Phosphate Buffered Saline (PBS) solution for 24 hours imaged at 20 000 X magnification. The figure shows the first round of samples analyzed 5 days after exposure ended (*i.e.*, (a) the non-coated reference substrate, and samples coated with coatings (b) TiN (A) and (c) TiN (B)) and the second round of samples analyzed 109 days after exposure ended (*i.e.*, (d) the non-coated reference substrate, and samples coated with coatings (e) TiN (A) and (f) TiN (B)).
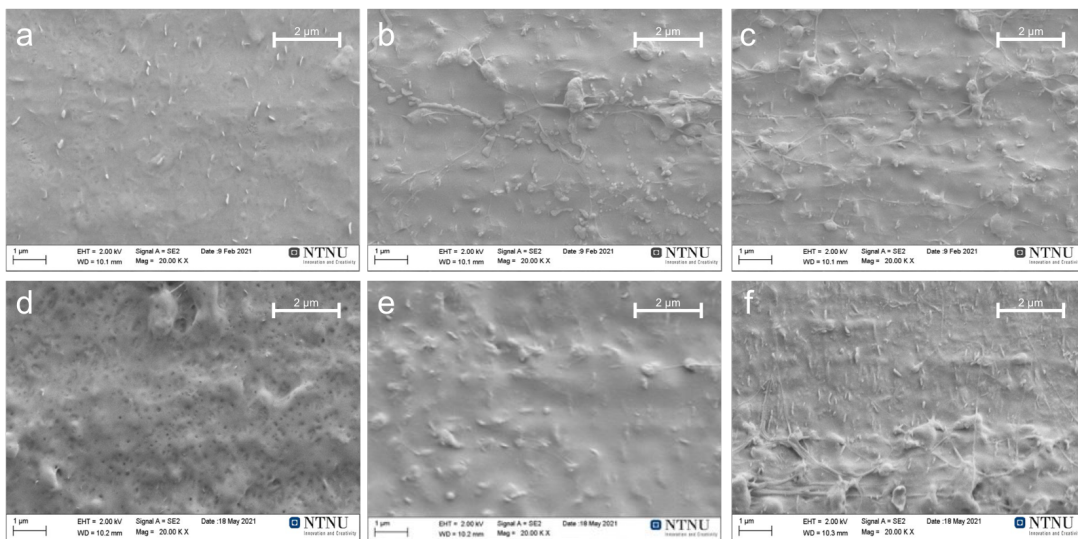
Figure 4.29: SEM micrographs of samples exposed to Phosphate Buffered Saline (PBS) solution for 7 days imaged at 20 000 X magnification. The figure shows the first round of samples analyzed 5 days after exposure ended (*i.e.*, (a) the non-coated reference substrate, and samples coated with coatings (b) TiN (A) and (c) TiN (B)) and the second round of samples analyzed 103 days after exposure ended (*i.e.*, (d) the non-coated reference substrate, and samples coated with coatings (e) TiN (A) and (f) TiN (B)).
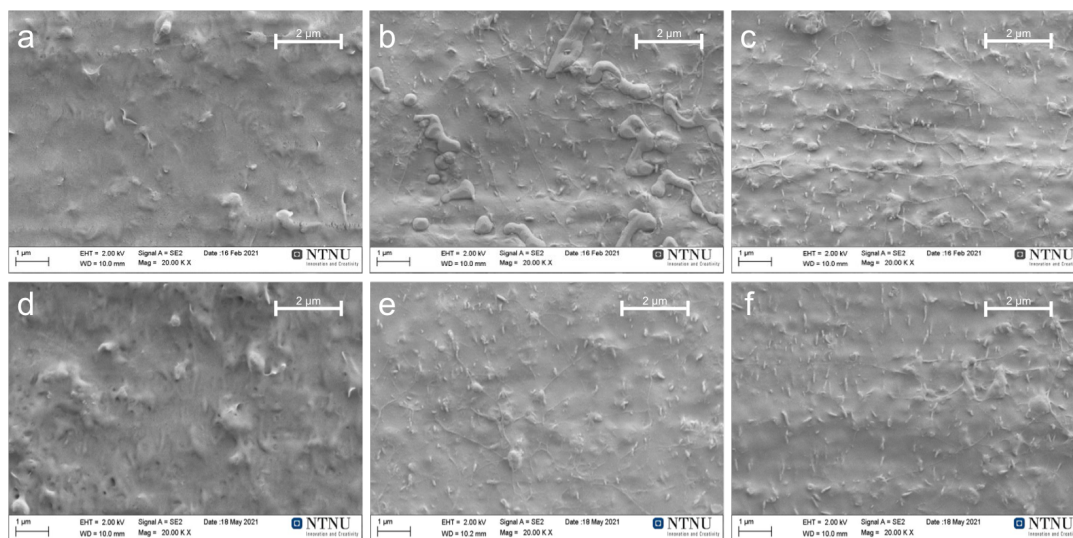
Figure 4.30: SEM micrographs of samples exposed to Phosphate Buffered Saline (PBS) solution for 30 days imaged at 20 000 X magnification. The figure shows the first round of samples analyzed 3 days after exposure ended (*i.e.*, (a) the non-coated reference substrate, and samples coated with coatings (b) TiN (A) and (c) TiN (B)) and the second round of samples analyzed 94 days after exposure ended (*i.e.*, (d) the non-coated reference substrate, and samples coated with coatings (e) TiN (A) and (f) TiN (B)).

Other irregularities observed during the SEM analysis of the samples exposed to PBS can be studied in Appendix I.

4.7.2   Chemical Stability and Potential Toxicity

The full scan of the PBS solution revealed that it contained several trace elements with varying concentrations. The baseline concentrations of S, Ti and Ba were 223 ± 7 μg/L, 3.5 ± 0.2 μg/L and 0.22 ± 0.02 μg/L respectively. A correlation between exposure time to PBS solution and barium (Ba) concentration was found from the ICP-MS analysis. The results are presented in Figure 4.31 and are normalized with respect to both solid sample weight and total exposure volume of PBS. The baseline concentration, (*i.e.*, the average Ba concentration in the PBS solution) has been subtracted. The concentration of sulfur (S) did not reveal any trends based on whether the exposed solid sample was coated, but the concentration decreased after 24 hours of exposure as seen in Figure 4.32. The concentrations of Ti showed no clear dependence on exposure time between 10 minutes and 30 days but revealed that all non-coated samples gave lower Ti concentrations than the samples coated with TiN as presented in Figure 4.33. The S and Ti concentrations are also normalized in the same manner as the Ba concentrations. Please note that the y-axis values are not equivalent for the different elements but were chosen to best show the main trends.
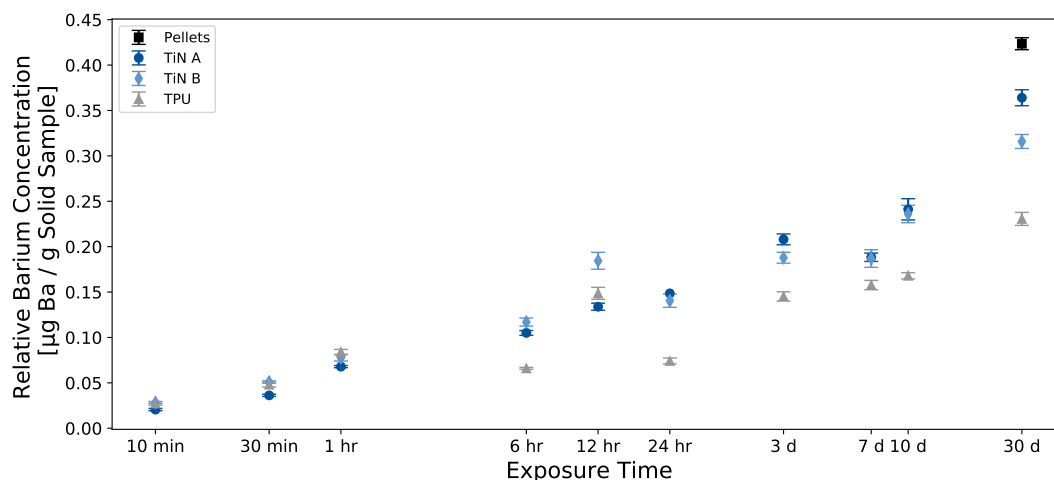
Figure 4.31: The concentration of barium released from the solid samples per gram of solid sample after exposure to PBS for various time intervals ranging from 10 minutes to 30 days. The average concentration found in the PBS solution has been subtracted and the values have been normalized with respect to the liquid volumes used and the weight of the solid samples.
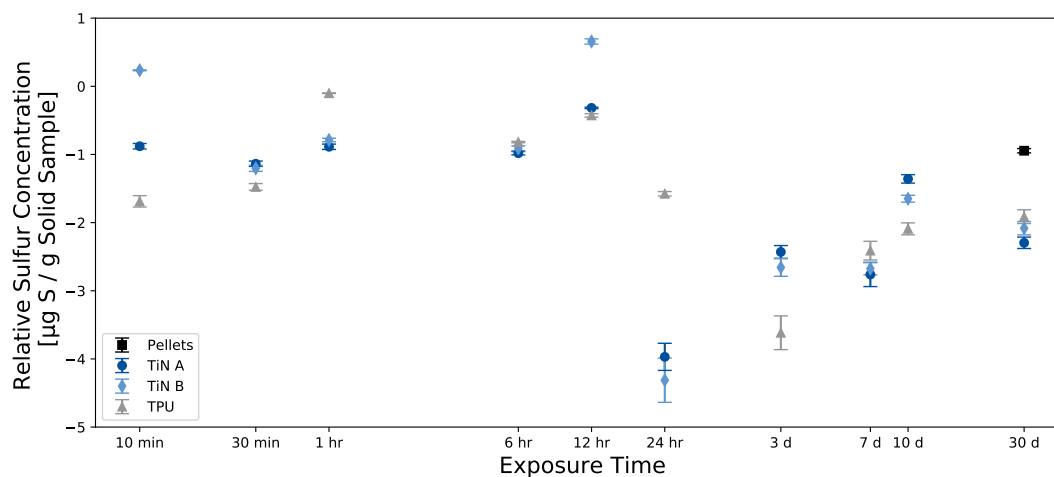
Figure 4.32: The concentration of sulfur released from the solid samples per gram of solid sample after exposure to PBS for various time intervals ranging from 10 minutes to 30 days. The average concentration found in the PBS solution has been subtracted and the values have been normalized with respect to the liquid volumes used and the weight of the solid samples.
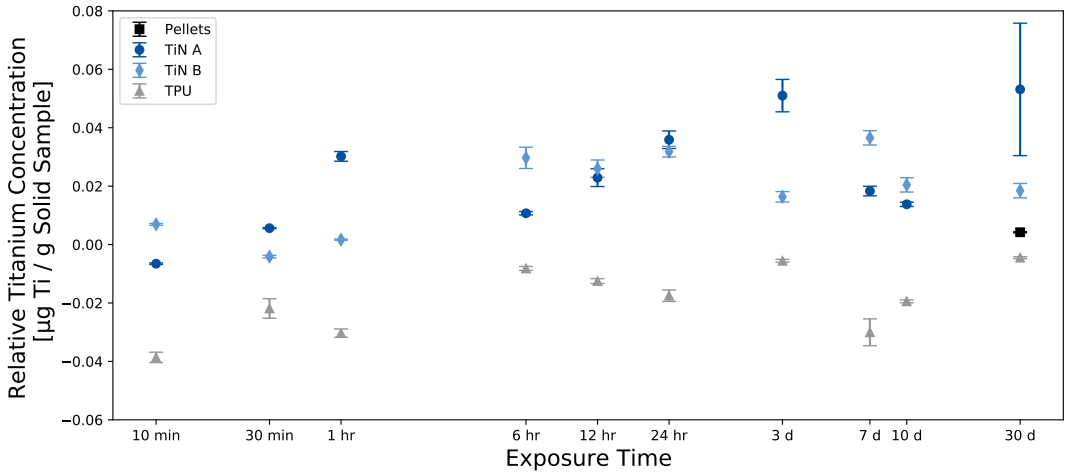
Figure 4.33: The concentration of titanium released from the solid samples per gram of solid sample after exposure to PBS for various time intervals ranging from 10 minutes to 30 days. The average concentration found in the PBS solution has been subtracted and the values have been normalized with respect to the liquid volumes used and the weight of the solid samples.

Chapter 5

Discussion

Though coating TiN (C) is a first-step optimization of coatings TiN (A) and TiN (B), it is important to note that the results from characterization of coating TiN (C) should not be directly compared to the characterization results of the first two coatings. As there are differences between the two methods for producing the substrates it is not unexpected that they show different properties (*i.e.*, surface morphology, wetting properties, and friction coefficients) when exposed to the same test conditions, even when the base material (*i.e.*, the Carbothane pellets) was the same. The properties of the substrate are also expected to significantly affect the observed properties of the coatings. As a result, the following sections are split into separate subsections depending on the substrate used.

5.1   Sputtering Process

All TiN coatings had an equivalent grey coating color (Figure 4.1). This confirms the results found in the present authors Specialization Project for coatings TiN (A) and TiN (B). The fact that the color of coating TiN (C) is indistinguishable from that of the two previously developed coatings is in accordance with expectations as only minor adjustments were made to the coating process. The color can give an indication of the coating stoichiometry, as the stoichiometric TiN phase is golden, while the grey color suggests that the nitrogen content in the coatings is lower than in the stoichiometric phase [104, 105].

The values monitored throughout the coating process were stable (Table 4.1). The deviation in the Direct Current Voltage (DCV) is only 1.6% for TiN (A), 1.5% for TiN (B) and 2.1% for TiN (C). Thus, the process is reproducible with the same input conditions, and it is reasonable to assume that samples coated with the same coating process in different process batches are equivalent.

Though polymers are vulnerable to chemical and physical changes at elevated tempera-

tures (above approximately 60° C for Carbothane), temperatures above 16° C have not been measured. However, as the monitor is mainly designed for measuring higher temperatures when the substrate heater is used, and is not directly attached to the substrate surface, the measured values may not accurately predict the temperature on the substrate surface. Despite this, the temperature is not expected to rise above 60° C [98]. This is supported by tests performed by NanoLab engineers on the same equipment with a temperature measure strip directly attached to the substrate. The substrate temperature rose to about 40° when using reactive sputtering with Ti and N_2 at 400 W for 30 minutes, and it was below 38° (*i.e.*, the lowest temperature the strip could measure) for Mo sputtering at 200 W for 19 minutes [98]. For these tests the temperature measure strip was attached to a silicon carrier wafer. The sputtering powers used for the present work (*i.e.*, 80 W and 120 W) were lower than those used for the forementioned tests, which is expected to limit the temperature increase, but the low thermal conductivity of the Carbothane substrates compared to, *e.g.*, metal substrates may also influence the results. Thus, further investigation is needed to accurately determine the temperature on the substrate surface. If local temperature increases have occurred, changes in the film growth mechanism may also have arisen.

5.2 Surface Morphology

5.2.1 Coatings TiN (A) and TiN (B)

The reproducibility of the coating procedure and the surface morphology found in previous work has been confirmed. SEM micrographs of coatings TiN (A) and TiN (B) as well as the non-coated reference substrates at 1 000 X magnification (Figure 4.2) reveal directional lines in a regular pattern. This is in accordance with was found during the initial characterization of the coatings during the present authors Specialization Project [10], and it is believed that this feature stems from teflon film uses during the processing of the substrates. Further, Figure 4.3 reveals particles of micrometer scale that are released from the surface in all samples. This is also in accordance with previous work, where chemical analysis revealed that these particles are $BaSO_4$ which is added as a filler in the Carbothane substrate material. As surface roughness on a micrometer scale has been reported to increase the protein adsorption to surfaces [32], the directional lines and $BaSO_4$ particles may lead to an increased risk of thrombosis.

As both the directional lines and $BaSO_4$ particles are observed in all samples, there are strong indications that the coatings follow the morphology of the substrate and have excellent coating coverage as is expected for magnetron sputtering techniques [73]. It is, however, not possible to tell from the SEM analysis if the coating thickness is even, though there is little reason to believe that there will be large variations. The uneven topography of the substrates in form of the directional lines could potentially give some shadowing effect, but as the distance between the substrate and the sputtering target is large (22 cm) compared to the topography differences (micrometer scale) the area affected

by such a shadowing effect would be small and thus expected to be negligible.

Like what was found in the Specialization Project, cracking in coatings TiN (A) and TiN (B) have also been observed (Figure 4.4). Though the cracks were comparatively small, they were observed on all samples at somewhat irregular intervals. The origin of the cracks is not known but they may be due to stresses induced by the coating process, or the challenges related to coating a hard coating on a soft substrate. These cracks suggest that the coating is brittle, which may negatively affect the biocompatibility. If coating fragments are released, they may travel to other parts of the body and cause adverse effects. In that case, the substrate material will once again be exposed to the corrosive environment of the human body. A local change in the surface topography of the material could potentially also be an initiation spot for setting of the paths of coagulation and/or inflammation. However, attempts of scratch testing (Appendix E) reveals that the coating adhesion is excellent, making it unlikely that coating fragments will be released. The good adhesion of magnetron sputtered thin films is also in accordance with literature [73].

5.2.2 Coatings TiN (C) and DLC

As the same large-scale surface morphology is observed in all surfaces (Figures 4.5 and 4.6) (*i.e.*, directional lines in a regular pattern), it appears that the coatings follow the morphology of the substrate. These directional lines are, like for the thicker substrates, believed to result from the substrate production process. However, the directional lines observed in the thinner substrates are much more prominent. Further, like for coatings TiN (A) and TiN (B), it is not possible to conclude that the coating thickness is even, though there is little reason to believe otherwise. Unlike the thicker substrates, there are no signs of $BaSO_4$ particles protruding the surface.

Though coating TiN (C) shows signs of cracking (Figures 4.7, 4.8, and 4.9), the coating fragments appear to still adhere to the substrate. As there are no observed cracks in the DLC coating and no surface areas observed uncovered by the coating, there are no indications of suboptimal coating adhesion. Thus, the adhesion of both coatings appears to be good, positively affecting the biocompatibility. The cracks suggests that coating TiN (C) is brittle. As such cracks were also seen on the surface of coatings TiN (A) and TiN (B), they may be a result of the general challenge of depositing a hard coating onto a soft substrate. However, the cracks seen in coating TiN (C) are also ordered in a semi-periodic pattern (Figure 4.7), in contrast to the two previously developed coatings. There was also much more cracking observed in coating TiN (C). This could be due to different stress conditions caused the new substrate, or increased stress caused by the more energetic deposition process of the latter coating. The higher sputtering power was expected to induce compressive strains in the coating, but the increase could have caused too much strain [92, 106].

The nano-scaled surface roughness also varies between the surfaces. The structure of the DLC coating, where particles have agglomerated in a distinctive pattern, appears to give

a high nano-scale surface roughness compared to the samples coated with coating TiN (C) and the non-coated reference substrate. Studies have found that the protein adsorption is lower for surfaces with nano-scaled surfaces roughness, indicating that the DLC coating could be better at resisting protein adsorption and thus reduce the probability of biofilm formation and thrombosis. However, micrometer-scaled surface roughness could according to literature cause an increased protein adsorption to the surface, and thus the directional lines found in all samples could counteract this effect. It is difficult to determine which effect will be dominant without further investigation as the effects of surface topography on protein adsorption have proven to be complex. One should thus be careful to put too much emphasis on this trend. It is also not known if such a resistance to protein adsorption would continue over time, which would be necessary for reducing complications when using medical devices implanted for longer durations.

Thus, the coating coverage is good, though coating TiN (C) has unfavorable cracks. The nano-scaled surface morphology of DLC also gives indications that the coating is more resistant to protein adsorption.

5.3   Cross Section Morphology

It is important to note that the cross section was analyzed using only one sample of each type as the analysis was preliminary. Thus, the results are vulnerable to irregularities, but the micrographs are expected to give a representative depiction of the coating-substrate interface. Figure 4.10 shows the cross section of a sample coated with coating TiN (C). In all micrographs, there are several layers. The bottom layer shows the Carbothane matrix with bright contrast $BaSO_4$ particles. The particles have inhomogeneous particle size and distribution in the matrix. Some particles are within nanometers of the surface, though without protruding it, like observed in the thicker reference substrates. The next, slightly brighter layer, is coating TiN (C), best studied at 350 000 X magnification. It is smooth, homogeneous in thickness, and follows the morphology of the substrate on a nanometer scale, which is expected from magnetron sputtering techniques as previously discussed. Only infrequent and nanometer-scaled porosity is observed between the coating and the substrate as indicated in the micrograph taken at 120 000 X magnification. This stipulates that the coating adhesion is good. There are no further indications that the coating process has damaged the Carbothane material as the material looks uniform throughout with exception of the $BaSO_4$ particles. Further, the Pt-Pd coating can be seen as a bright and inhomogeneous layer on top of coating TiN (C), followed by the carbon protection layer.

The cross section of a sample coated with DLC is presented in Figure 4.11. Please be aware that the micrographs cannot be directly compared to those of coating TiN (C) due to the differences in magnification. However, also these images show the Carbothane matrix with $BaSO_4$ particles. It is further covered by the DLC coating, the bright Pt-Pd coating, and the carbon protection layer. Much porosity is observed below the DLC

coating, which likely causes the significant surface roughness seen in the SEM micrographs of the surface morphology. There is porosity between the coating and the substrate below each wave. The porosity also makes it challenging to clearly distinguish between the DLC and Pt-Pd coatings and thus determine the homogeneity of the DLC coating thickness.

Further, it appears that the substrate is damaged approximately 500 nm into the material, in the area between the DLC coating and the white line in Figure 4.11 *a*. The damage is particularly evident when comparing the $BaSO_4$ particles in proximity to the surface and deeper into the substrate. It is likely a result of the coating process as no such degradation of the substrate material was observed in the samples coated with coating TiN (C). Because all details about the coating process are not known, it is not possible to determine the cause of such damage to the material. Nevertheless, it can be theorized that the damage is due to the process being considerably energetic which induces a temperature increase at the substrate surface, as polymers are generally sensitive to elevated temperatures. This may affect the chemical and mechanical stability of the surface and there is thus much more uncertainty related to the bio- and hemocompatibility of the coating-substrate system, which should be further investigated. There are thus indications that the coating process used for depositing the TiN coatings is more favorable than the process used for the DLC coating. It has been reported that low-temperature deposition of DLC coatings is possible [96], but even if the DLC coating procedure proves to be incompatible with polymeric materials it should not be completely written off as a coating for blood-contacting applications. Instead, it should be considered for applications where the bulk biomaterial is more resistant to the coating conditions such as metals and ceramics.

5.4 Wetting Properties

All surfaces in the present work are assumed to be sufficiently rigid and non-deformable, the temperature and humidity were controlled, and distilled water was used to obtain a consistent purity and surface tension of the liquid. Swelling of the material is not believed to occur at the relevant time scale. However, the presently studied systems have certain deviations from the ideal surfaces needed to fulfill the requirements of Young's equation. First, the surfaces have been observed to be inhomogeneous and with significant surface roughness. Grainger et. al. [77] claims that a surface which is optically or visibly featureless is generally acceptable, but the directional lines found in both substrates (though of different magnitudes) can be observed by the naked eye. Second, the thicker substrates appear to be chemically inhomogeneous due to the protruding $BaSO_4$ particles. Further, the surface mobility of the material has not been studied at this time, but many polymer surfaces do not fulfill this condition [77]. Hence, it may be an issue for the non-coated reference substrates. The coatings are furthermore expected to reduce some deviations from ideality as chemical inhomogeneities of the substrates are masked.

5.4.1   Coatings TiN (A) and TiN (B)

Both coating TiN (A) and TiN (B) have contact angles with water that are lower than that of the non-coated reference substrate, though coating TiN (A) has a significantly lower contact angle than coating TiN (B) (Figure 4.12). These wetting angles are consistently higher than those measured during the present authors Specialization Project (*i.e*, $64° \pm 7°$ for TiN (A), $78° \pm 8°$ for TiN (B), and $92° \pm 1°$ for the non-coated reference substrates) [10], but the same tendency is seen between surfaces. The deviation may be due to the 30 second pause taken between the dosing and deposition step in the procedure used during the Specialization Project (no such pause was used for the present work), as the wetting angle has been observed to decrease with time. This decrease is believed to be due to evaporation of the water leading to the contact being in receding mode [81]. The procedure used during the Specialization Project also had a longer interval for measurement (*i.e.*, 60 seconds compared to the 40 seconds used in the present work) during which the drops could further evaporate. The measured contact angle for the thicker non-coated Carbothane surface matches well with contact angles reported in literature for thermoplastic polyurethanes. Literature reports values between $99.50° \pm 4.44°$ and $95.4° \pm 1.5°$ [15, 107, 108, 109, 110] while the average value measured in the present work is $101° \pm 2°$. The variance between measurements of TPUs and the slight deviation between the values obtained in the present work and literature for the thermoplastic polyurethanes can be explained by two main factors. First, polyurethanes are a large class of polymer materials with various physical and chemical properties [111]. Even within thermoplastic polyurethanes there is thus expected to be some variation. Second, the system has certain deviations from ideality as previously explained.

The reported contact angles for TiN thin film deposited using sputtering techniques vary greatly. Sreepradha et. al. reported wetting properties ranging between a superhydrophilic state and $109.5°$ by varying the substrate temperature and sputtering bias for TiN films produced by reactive sputtering [72]. Varying the film thickness between 0.47 μm and 1.72 μm has also shown to increase the contact angle of reactively RF-pulsed magnetron sputtered TiN films between $100°$ and $118°$ [112]. A 600 nm TiN thin film sputter coated onto glass and steel substrates has been reported to give contact angles varying between $87°$ and $91°$ [113]. TiN coatings produced by other PVD techniques have also been analyzed. 50 nm TiN films deposited on glass substrates by cathodic arc evaporation gave a contact angle of $31.7°$ [114] and films produced by arc evaporation gave contact angles of approximately $60°$ [115].

As the variance of the reported contact angles for TiN coatings is substantial, it suggests that the structure and morphology of the material plays a major role in determining the contact angle and it is challenging to compare coatings deposited using different deposition conditions or methods. These reports are also promising as they confirm that the wetting properties of TiN coatings can be tailored. The deviations from an ideal surface is also valid for the sample coated with coatings TiN (A) and TiN (B), but as there are assumed to be equivalent for both coatings, it is likely not the reason for the difference in contact angle between the two coatings. The difference in contact angle between the

two coatings is believed to be a result of differences in microstructure induced by the different sputtering modes used for deposition. Unbalanced magnetron sputtering (used for coating TiN (B)) has been reported to give higher film crystallinity than balanced magnetron sputtering (used for coating TiN (A)) for SnO_2 films [74]. Shanker et. al. believed that this observation is caused by energetic argon ions bombarding the surface in the unbalanced magnetron sputtering mode which causes recrystallization.

Few of the cited articles describe the precise method for measuring the contact angles and thus it is difficult to predict the magnitude of deviance from ideality in each case. However, as the reported angles only deviate by a few degrees for the thermoplastic polyurethanes it is reasonable to assume that the general trend is valid. Such a conclusion is more challenging to make for the TiN coatings as the divergence in reported values is extensive. Nevertheless, if comparing the reported values for TPU with the results of this study, the surface roughness is only expected to deviate from ideality by a few degrees. It is important to note, however, that surface roughness is known to exaggerate wetting properties (*i.e.*, reduce the contact angle of already hydrophilic surfaces and increase the contact angle of already hydrophobic surfaces) [77, 82]. Thus, there are indications that the contact angles of the coatings deposited on ideal surfaces would be a few degrees higher than those reported in the present work. As there are other factors that could influence the coating properties as well (*e.g.*, the nano-scale surface roughness or strain conditions of the coatings), one should put more emphasis on the difference between the surfaces in the present work than in comparing the present work to literature.

As neutrally changed hydrophilic surfaces generally are the most resistant to protein adsorption, there are indications that coating TiN (A) is the most biocompatible. However, considering Xu and Siedlecki finding that the protein adhesion to LDPE did not continuously decrease with contact angle, but showed a step dependence at 60-65°, there are uncertainties to this conclusion. Though the protein adhesion does not scale directly with the contact angle, but also depends on the material itself, there are indications that increasing the hydrophilicity further could increase the biocompatibility. Taking this into account, it is indicated that the coatings (and particularly coating TiN (A)) has improved biocompatibility compared to the non-coated reference substrate with respect to wetting properties.

5.4.2 Coatings TiN (C) and DLC

The samples coated with coating TiN (C) and DLC as well as the non-coated reference substrate all show hydrophobic properties (Figure 4.14). However, these surfaces deviate from ideality more than the previous samples based on the thicker substrates due to the greater surface roughness of the thinner substrates. Though no quantification of the surface roughness has been performed at the present time, an evaluation has been done by studying the perceived scale of the directional lines in SEM micrographs and visual observations by the naked eye. The assumption is also supported by the fact that the water drops are elongated in the direction of the directional lines as described in Appendix

D, but that no such effect was observed on the thicker substrates.

The measured contact angle for the thinner non-coated reference substrates is significantly higher than the contact angle for the thicker non-coated reference substrates and the contact angles for TPU reported in literature. Though it appears that the increased sputtering power has caused changes to the surface morphology of coating TiN (C), it is challenging to determine the exact effect to the wetting properties as the surface roughness is so different between the two types of substrates, but the measured value is higher than those of coatings TiN (A) and TiN (B). The contact angles of DLC coatings are generally reported to be between 67.30° and 88° [81, 116, 117, 118]. However, superhydrophobic properties (160°) have been reported for textured surfaces [81]. Thus, the measured 97° ± 3° average for the DLC coating in the present work is slightly higher than what is reported in literature for smooth surfaces, though it is plausible that the deviation is due to surface roughness.

Appendix D describes how the contact angles vary depending on the orientation of the directional lines. (The difference is 15° ± 4° for non-coated reference substrates, 18° ± 5° for samples coated with TiN (C) and 10° ± 5° for samples coated with DLC). Thus, if the substrates had been oriented perpendicularly to the imaging direction, the coated surfaces would show hydrophilic properties. It was initially believed that the ideal contact angle value of the surface would be an approximate average of the values measured for the two orientations. However, after further comparisons with literature, it appears that contact angles measured when the directional lines are oriented perpendicularly to the imaging direction are in better accordance with literature for the non-coated reference substrate (105° ± 2°) and DLC (87° ± 3°). (The reported values for TiN vary vastly.) It is hypothesized that the directional lines contain the water droplet in the direction where the contact angle is measured when the directional lines are oriented parallel to the imaging direction, thus creating an artificially large contact angle. With the other orientation, the drop is allowed to flow unrestricted in the direction where the contact angle is measured, giving a better representation of the surface. It is worth noting, however, that general deviations from ideality due to surface roughness are likely still valid. The data collected of contact angles on the directional lines oriented perpendicular to the imaging direction is also incomplete as only two samples were analyzed for the TiN (C) and DLC coatings, and more studies should be conducted before a conclusion is reached. It is also plausible that the change in the contact angle for TPU could be caused by the new processing method altering the surface, but given the large increase, this is not deemed probable as the same molding temperature is used, though for different time spans. Further, there is very little literature mentioning the effects of such surface roughness and how such challenges have been tackled in the past.

If it is assumed that values measured when the directional lines are oriented perpendicularly to the imaging direction (Table D.1) better predicts the ideal contact angle, then there appears to have been a reduction in the contact angle from coating TiN (A) to TiN (C), *i.e.*, from 80° ± 2° to 77° ± 4° respectively, though the change is within the margin of error. Such a reduction could also be due to a general increase in surface roughness which would reduce the contact angle of already hydrophilic surfaces. Thus, there are

only weak indications that the adjustment to the sputtering process has improved the biocompatibility of the TiN coating in terms of wetting properties.

Generally, it appears that the coatings have improved the wetting properties of the material, but not sufficiently. There are indications that the TiN (C) coating has a slightly lower contact angle than the DLC coating, but the difference is not statistically significant. As mentioned earlier, the contact angle should preferably be lower to obtain biocompatibility, thus the wetting properties should be further optimized. To get an accurate representation of the wetting properties of the coatings, it could be favorable to deposit future generations of coatings onto surfaces with very low surface roughness (*e.g.*, glass slides or silicon wafers) as an additional reference.

5.5 Coating Cohesion, Adhesion and Friction Properties

The increase in the friction coefficient for the first few second seen in all samples (Figures 4.16 and 4.18) occurs as the tip-sample interaction is approaching equilibrium conditions. There is a continued increase in the friction coefficient over time for the non-coated reference substrates, which is not as rapid as in the first few seconds, suggesting a changed mechanism. The continued increase is believed to be due to a local temperature of the material increase around the tip as heat is dissipated from the sample-tip interaction, altering the properties of the substrates. This trend is not observed for any of the coated samples, possibly due to an insulating effect of the coatings. (For the thicker non-coated reference substrates, it is not necessarily a continued increase for all samples, but a continued large variation in friction properties across the surface.)

As the normal displacement is approximately two orders of magnitude larger than the thickness of the coatings (Figures 4.17 and 4.19), the tip has also deformed the substrate. However, no visible effect on the coatings is observed indicating that the coating follows the deformation of the substrate and is not damaged by the 1000 μN load applied. Thus, the coating adhesion appears to be good. [1]

5.5.1 Coatings TiN (A) and TiN (B)

Coatings TiN (A) and TiN (B) do not have statistically significant different friction coefficients, and they show approximately the same degree of measurement stability over time (Figure 4.16). This indicates that the coatings have similar friction properties. Though the friction coefficient is higher for the non-coated substrate, the difference is within the margin of error. If the difference were to be significant, it would be favorable when

---

[1]For further details on how to interpret the friction results, please contact Jianying He (jianying.he@ntnu.no) at the Department of Structural Engineering at NTNU, Trondheim, Norway.

considering the potential use of such coatings for biomedical devices. Because external force is required to insert medical devices such as catheters, guide wires or stents into blood vessels, it is favorable to minimize the force as it also minimizes the damage to the blood vessels [78]. This is done by lowering the coefficient of friction. Further, the good coating adhesion of coatings TiN (A) and TiN (B) is indicated by the scratch testing procedures described in Appendix E, and a cracked area seen in a sample coated with TiN (B) exposed to PBS solution (Appendix I). Though no quantification of the adhesion properties was achieved, it was observed that the coatings continued to adhere to the substrates at scratch loads high enough to cause significant coating cracking and permanent deformation to the substrate material.

The results for the non-coated reference substrate are also generally more unstable (Appendix H). This could be due to the inhomogeneous surface morphology observed on the non-coated surface where $BaSO_4$ particles are protruding the surface. Such particles may have different friction properties than the polymer matrix. However, a coating can mask such variations in surface chemistry and morphology. The instabilities may also be partly caused by the directional lines oriented in a regular pattern, though this would also be expected to cause instabilities in the measurements performed on the coated samples.

5.5.2 Coatings TiN (C) and DLC

The general measurement instability is lower for the thinner non-coated reference substrates than for the thicker non-coated reference substrates (Figures H.3 and H.9). This is as expected as $BaSO_4$ particles are not protruding the surface of the thinner substrates, and the samples were all oriented with the scratch direction parallel to the direction of the directional lines such that less variance in the surface topography and chemistry is expected.

The friction coefficient is lowest for the samples coated with DLC, followed by coating TiN (C) and then the non-coated reference substrate. DLC is thus the most promising coating in terms of use in biomedical devices when considering the friction properties. However, as seen in Figure 4.18, the samples coated with coating TiN (C) have more stable friction measurements which can indicate better coating adhesion. The friction measurements can also have been influenced by the more irregular surface morphology of the DLC compared to the smooth (but cracked) surface seen for the surfaces coated with coating TiN (C). Scratch testing performed on the DLC coating (described in Appendix E), supports that the coating adheres well to the substrate. Like coatings TiN (A) and TiN (B), the DLC coating continues to adhere to the substrate after scratch loads high enough to permanently deform the substrate material are applied. It is also natural to believe that coating TiN (C) has similar, and thus great, adhesion properties to coatings TiN (A) and TiN (B) as the deposition processes are similar. Thus, it appears that both coatings have good coating adhesion, though there are indications that the adhesion is better for coating TiN (C).

5.6 Mechanical Properties

As a result of the substrate, no mechanical testing has been performed on samples coated with coatings TiN (A) and TiN (B). Thus, only the mechanical properties of coatings TiN (C) and DLC will be described in this section, as well as the effects of exposing the thinner non-coated reference substrates to PBS solution.

Figure 4.20 shows that the maximum tensile stress of samples coated with coating TiN (C) and the TPU substrates exposed to PBS are within the margin of error which is expected when compared to the TPU reference substrates. The maximum strain is also within this margin of error for the TiN (C) coated samples, while the exposed samples are only slightly outside the margin. As swelling of the material cannot be ruled out, the slight increase in strain for the exposed TPU can be explained by additional chain mobility as a result of swelling and liquid molecules in between the polymer chains [119]. Even though degradation was induced in the substrate material by the DLC coating procedure, the large-scale mechanical properties of the material do not appear to be damaged. Both the maximum stress and maximum strain of the samples coated with DLC exceed the expected values, indicating that the DLC coating has positively affected the mechanical properties of the TPU material in a statistically significant way. The sample thickness varies significantly, but as calibrations are performed based on measurements of the samples, it is only expected to give a 3-5% variance [119]. Thus, the mechanical properties of Carbothane are not degraded by the coating procedures, or due to exposure to a simulated body fluid.

5.7 Effect of Exposure to PBS

As the exposure study was started at an early stage before the development of coating TiN (C), only samples coated with coatings TiN (A) and TiN (B) as well as their non-coated reference substrates were included. However, equivalent work was performed by PhD Candidate Maren K. Fossum on a 50 nm thick TiN coating produced by reactive magnetron sputtering and the commercial DLC coating coated on the thinner reference substrates, as well as the non-coated reference substrates themselves [58]. Thus, comparing with those results, the performance of the DLC coating and possible differences between the two substrates can be indicated. It should be emphasized that only two samples were analyzed at each exposure time interval for each type of sample, leaving room for some uncertainty in the results.

5.7.1 Surface Morphology

There was no direct correlation observed between the duration of the exposure to the Phosphate Buffered Saline (PBS) solution and surface morphology of the samples, though

there was variation in surface morphology between the samples. On some samples there appears to be a thin film and/or small particles covering the surface, which is believed to be salt residues. This can be seen in subfigures *b* and *d* in Figure 4.21, subfigure *b* in Figure 4.28 and subfigure *b* in Figure 4.30. More examples of such irregularities can also be found in Appendix I. It is believed that some of the PBS solution has not been completely rinsed off, and that salt has precipitated on the surface as the samples have dried. The characteristic crystallite structures of these structures also support the hypothesis that they are salt residues. There is large variation in the amount of residues, and how finely dispersed they are, but no pattern in which samples are affected by this has been identified. It is not expected that the samples will be affected by the solid salt, but it partly masks the surface of some samples making it challenging to accurately predict the surface morphology in some areas.

However, a surprising correlation was found between the time between the end of the PBS exposure and the SEM analysis for the non-coated samples (Figures 4.27, 4.28, 4.29 and 4.30). The samples that were analyzed longer after exposure end showed a more porous surface, which is a sign of material degradation. No such trend was observed for the coated samples, and nor for other non-exposed and non-coated samples stored under the same conditions for equal or longer periods of time. As no significant change to the surface morphology is seen for the coated samples, there are indications that the coatings protect the substrate material. However, it is also possible the degradation of the material has occurred under the coating, and that the coating just masks the effect. This indicates that the exposure to PBS has set off a degradation process which has not ended after the exposure to the solution is ended. The reason for this degradation is not known as Carbothane is expected to be resistant to hydrolysis and thermal degradation due to its aliphatic character [120], and that the polycarbonate fragments enhance the *in-vivo* stability compared to similar polymers with polyether fragments due to increased oxidation resistance [121]. Khan et. a.l [122] exposed four polyurethane materials to PBS solution at 37° C for 3-years, proving the excellent resistance of two of the materials and only small amounts of hydrolysis which did not markedly affected their overall properties for the two others. Considering the significantly shorter exposure period used for the present work, degradation is unexpected. Although, previous studies have shown increased porosity of CVC surfaces after both *in-vitro* and *in-vivo* exposure [58, 59], the mechanism in not believed to be the same. In the forementioned work, $BaSO_4$ particles were releasing from the surface, but the porosity found in the present work is smaller than that of the $BaSO_4$ particles, suggesting that a different mechanism causes the porosity. It also appears that $BaSO_4$ particles are still present on the surface of the degraded samples. Verbeke et. al. [59] showed that the porosity on the CVC surface resulting from the release of $BaSO_4$ particles lead to immediate and strong bacterial growth on the degraded material when exposed to the bacteria *S. epidermidis*. Despite the porosity observed in the present work being approximately one order of magnitude smaller than what Verbeke et. al. found the detected porosity may still increase the bacteria susceptibility of the Carbothane material.

The equivalent exposure study performed by Fossum did not reveal such degradation on the coated surfaces nor the thinner non-coated Carbothane substrates, even after equivalently long time periods between exposure end and SEM analysis. This suggests

that the compression molding processes of the substrates could have influenced material resistance to degradation as the compression molding type is the main difference between the two types of substrates. The fact that the thicker substrates have $BaSO_4$ particles protruding the surface, which is not found in the thinner substrates, supports that the two methods are markedly different. As the observed correlation was not expected, the study was not structured enough with respect to the time period between exposure end and SEM analysis to conclude on this effect with certainty. Thus, the possible degradation and its mechanism should be investigated further.

Some medical devices, like CVCs, are only used for limited time periods up to *e.g.*, 30 days. As no significant change has been seen in the surface morphology after exposure to PBS for 30 days, it is not given that an initiation of material degradation will impact the biocompatibility, as the degradation may occur after the use of the device has ended. It should also be emphasized that the exposure to the PBS solution is only an initial simulation of the environment in the human body, so it can only give us an indication of what could happen in the human body, and that more work on the topic is needed. However, this highlights the importance of not using medical devices for time spans longer than its approved time span for use. It also emphasizes the importance of keeping the medical devices under controlled conditions up until the point of use to avoid initiating degradation processes. Opening packaging before its needed for use will also increase the probability of the surface of the device becoming infected with unwanted microorganisms. Unfortunately, such best practice is not always followed, possibly due to the health care staff being unaware of the potential risks they are exposing patients to.

5.7.2 Chemical Stability and Potential Toxicity

The initial idea was to also determine the concentrations of several elements other than S, Ti and Ba to detect possible contamination from equipment used when handling of the samples. However, as the PBS solution contains trace elements of the elements in question, as also reported elsewhere [123], a preliminary study was performed on S, Ti and Ba only. Though carbon (C) and nitrogen (N) are key elemental components of the DLC and TiN coatings respectively, and oxygen (O) is a key component in the substrate, the concentrations of these elements are not possible to determine due to limitations with the ICP-MS technique.

The Ba concentration in the liquid samples was found to have a clear dependence with exposure time (Figure 4.31), suggesting that it is leaching from the substrate material into the PBS solution. The Ba is believed to stem from the $BaSO_4$ particles which are added to the Carbothane matrix. The concentration is continuously increasing, and it does not appear that an equilibrium is reached, which indicates that the substance would continue to leach into the solution with longer exposure times and that the solution has not been saturated. The pellets exposed to PBS solution for 30 days show a higher normalized concentration than the coated and non-coated samples exposed for 30 days. This is believed to be due to the higher surface area to weight ratio of the pellets compared to

the other samples, leaving more surface area for Ba to leach from. Some of the variation found between samples within each time interval could be accounted for by a slightly different content of $BaSO_4$ particles as the particle distribution have been shown to be inhomogeneous. Nevertheless, the concentrations after exposure for 24 hours and longer are consistently lower for the non-coated reference substrates than for the coated samples. No clear distinction can be made between samples coated with coating TiN (A) and TiN (B). As there is a trend, with quite significantly different Ba concentrations, there are indications the leaching has not been reduced by the substrate material being coated on one side. The leaching appears to rather have been increased. This could be a result of the coating process altering the chemical properties of the sample surface. However, as no damage to the Carbothane matrix was observed in the samples coated with coating TiN (C), it is deemed unlikely that the deposition of coatings TiN (A) and TiN (B) would have damaged the substrate as these deposition processes are less energetic. Thus, further investigation is needed to conclude on the mechanisms behind this observation.

There are two aspects to consider when evaluating the effect of Ba leaching into solution. First, some elements may be toxic to the human body. Exposure to high doses of Ba have shown to reduce the amount of potassium in the blood which can have detrimental effects like kidney damage, heart rate and blood pressure disturbances, muscle weakness, and paralysis [124, 125]. Other effects typically reported to occur shortly after ingestion include vomiting, abdominal cramps, and watery diarrhea. The genotoxicity and carcinogenic effects of Ba are not well investigated. However, Ba is a natural constituent in food and groundwater and studies suggest that barium exposure is safe below certain levels. The average Ba concentration in drinking water in the US is 30 μg/L, but certain regions may have Ba levels higher than the US maximum contaminant level of 2.0 mg/L. Though the limit for safe exposure appears to be dependent on the duration of the exposure, Ba generally does not accumulate in the body, and within 1-2 weeks most of the Ba that has entered the body has been removed. The toxicity of barium compounds is closely related to the solubility of those compounds in the human body as it affects the potential for adsorption. $BaSO_4$, the constituent in Carbothane, is generally less soluble than the chloride, nitrate, hydroxide and carbonate, remains essentially unabsorbed and is therefore said to be non-toxic to humans. This is the reason why $BaSO_4$ is much used in medical applications. Nevertheless, a report by the US Agency for Toxic Substances and Disease Registry states that even exposure to insoluble Ba compounds is potentially toxic if it is able to enter the blood stream, and poisoning has occurred when $BaSO_4$ used for X-ray studies have been contaminated with soluble barium, though there is no reason to believe that that has happened in this case. There is little quantitative data on the adsorption of Ba, but there is some evidence that less than 5-30% of the administered Ba dose is absorbed in the intestines. The concentrations found in this study cannot be directly related to the concentrations in drinking water. However, there is little reason to believe that the release of Ba will cause serious health problems as the concentrations obtained are many orders of magnitude lower than those found in drinking water. As CVCs are typically also only used for a limited time period, the risk is further reduced. However, as Ba may be released directly into the blood stream from such blood-contacting biomedical devices, there is increased reason for concern, and is something that should be paid attention to.

Second, leaching of continents will alter the chemistry of the material possibly leaving it more vulnerable to degradation or otherwise altering both bulk and surface properties. The leaching of Ba could have been a cause in starting the degradation process that occurred after the exposure study as discussed above which may in itself lead to changes in bio- and hemocompatibility. However, the thinner substrates that were exposed in an equivalent exposure study by PhD Maren K. Fossum, gave similar leaching of Ba, without revealing such degradation as discussed above [58], which calls for further investigation before a conclusion can be reached.

As the source of the Ba leaching is most likely the $BaSO_4$ particles, the detection of a similarly increasing S concentration could confirm that these particles had dissolved. However, the S concentration decreases for exposure times above 24 hours (Figure 4.32). Negative relative concentrations mean that the concentrations are lower than those found in the PBS solution. This does however not reject the theory that the $BaSO_4$ particles have dissolved as the baseline concentration of S (223 ± 7 μg/L) is three orders of magnitude larger in the PBS solution than the Ba concentration (0.22 ± 0.02 μg/L). A reduction in S concentration from this level rather suggests that S has been involved in a reaction after 24 hours, and that it is not possible to distinguish the effect of $BaSO_4$ dissolution from the natural variations in the S concentration as the concentration increase resulting from dissolution would be comparatively small. The detection limit for S using ICP-MS (1-10 μg/L) is several orders of magnitude higher than for Ba and Ti, and is within the same range as the measured Ba concentrations [126]. Thus, the technique may not be accurate enough to confidently confirm the presence of $BaSO_4$ leaching, even without the high baseline concentration. Because the PBS solution contains many trace elements, it is challenging to predict which chemical reactions could have caused the time-dependent concentration decrease, without also knowing the dependence of the other trace elements with exposure time. It has been hypothesized that a time-dependent precipitation of sulfur containing compounds occurred on the surface of the solid samples, but that this was not detected when examining the samples after exposure due to the rinsing of the samples with deionized water. The sulfur could also have adsorbed or absorbed directly to the surface of the solid samples. However, it is not possible to conclude without further investigation. Even if leaching of sulfur compounds from the surface were confirmed, it would not be directly harmful to the human body as daily exposure to sulfur is expected due to its presence in water and soil. It is also an essential element for humans and animals, and exposure to small doses of sulfur does is not related to carcinogenic or genotoxic effects [127].

When evaluating the normalized Ti concentrations, it can be seen that some of the concentrations are negative (Figure 4.33). This can be due to natural variations in the PBS solution trace element composition which is not properly accounted for by the calculated average Ti concentrations in the PBS solution. However, the samples exposed to PBS solution for equivalent durations were all exposed to the same batch of PBS solution, and thus they are assumed to be comparable. Consequently, a clear trend is observed. The non-coated samples always give lower Ti concentrations than the samples coated with TiN, indicating that Ti is leached from the coatings. There is no clear pattern in which of the two coatings give the highest Ti concentrations. Due to the limitations of the ICP-

MS technique it is not possible to determine if it is only Ti that leaches from coatings, or also N. The pellets, which are exposed for 30 days, show a similar Ti content as the non-coated reference substrates exposed for 30 days, and markedly lower than both TiN coatings, reinforcing the trend. As the relative concentration difference between coated and non-coated samples does not appear to increase with time, but is present already after 10 minutes exposure, it appears that the leaching process occurs quickly and reaches an equilibrium where no more Ti is released. Though further release could occur at longer exposure intervals, it appears that the coatings are quite stable in the solution. Based on the surface morphology of the coatings after exposure, there are no clear indication that the coatings are markedly damaged after the Ti leaching into solution, though this should be further investigated.

Titanium has generally been considered to be inert and biocompatible. It displays low carcinogenicity and adverse effects have not been found from the small amounts of titanium occasionally released from biomedical implants and into adjacent tissue [128]. An *in-vitro* study showed that TiN coatings are not cytotoxic [115]. However, TiN has exhibited slight fibrogenic activity in experimental studies on animal and inflammatory reactions and systemic effects have been observed in studies on Ti alloys used in implants, though no significant local effects on tissues have been indicated [128]. Extensive exposure to Ti may also lead to the development of immune dysfunction. Very rare occurrences of titanium toxicity have also been reported in relation to the use of titanium dental implants [129]. Nevertheless, the leaching of Ti nor TiN is not expected to give significant toxic effects, and though there is no data available on the possible dose-dependencies related to the systemic changes caused by titanium compounds in humans [128], the release of Ti is not expected to be to be the factor limiting the biocompatibility of the coatings.

5.8 Considerations for Optimization

As coating TiN (A) proved to have the most favorable wetting properties compared to coating TiN (B), while all other characteristics being indistinguishable, it was selected as a basis for development of coating TiN (C). The two main aims of the optimization were further reducing the contact angle with water and reducing the coating cracking. To determine how the coating properties should be altered to improve biocompatibility, the effect of various sputtering parameters was evaluated (*i.e.* sputtering power, pressure, substrate temperature, and substrate-target distance) as well as the practical possibility for altering these with the available equipment. Pang et. al. [112] reported that increasing coating thickness of TiN films from 0.5 μm to 1.7μm led to a transition from tensile to compressive stresses in the film. In turn, the films with compressive stresses showed a lower contact angle than those with tensile stresses. Though strains can make the films vulnerable for other side effects, it is expected that compressive stresses are less detrimental for the films than tensile stresses as ceramics, like TiN, are generally stronger in compression than in tension [101]. As it is desired to keep the coating thickness constant for the application in question, other ways of changing the strain properties of the coating

were investigated.

Numerous reports have been made that altering sputtering power can induce changes to the surface properties. Though no literature has been located on the influence of RF magnetron sputtering power on TiN thin films, there is literature describing the effects of varying the sputtering power on TiN thin films produced by other sputtering techniques and on other materials produced by RF magnetron sputtering. DC magnetron sputtering of 200 nm TiN thin films gave compressive stresses at high powers and low tensile stresses at lower powers [92]. There have also been reported indications that increasing the RF sputtering power has led to the development of compressive stresses at higher sputtering power for aluminium-doped zinc oxide thin films [106]. Otherwise, increasing the RF magnetron sputtering power has shown to give increased crystallinity for various materials [74, 106, 130, 131]. TiN thin films of 20-40 nm thickness deposited by HiPIMS showed denser polycrystalline films deposited at higher sputtering powers [132]. Higher sputtering power used for DC magnetron sputtering of copper also favored formation of a continuous thin film [133]. Further, increasing sputtering power has been reported to change the preferred growth orientation and decrease residual stresses in AlN thin films deposited by reactive HPPMS [134]. Though it is difficult to predict the effect of increased crystallinity, denser, more continuous films with less residual stresses are expected to improve film qualities. A higher sputtering power has also been reported to increase the deposition rate proportionally to the sputtering power [133] which is favorable for the efficiency of the process.

It appears that the exact sputtering power where the strain conditions change varies between sputtering methods, film material, and coating thickness. Thus, as a first-step optimization the sputtering power was increased from 80 W to 120 W, *i.e.*, the highest sputtering power possible for the available sputtering system [98], to examine the boundary conditions. The cracking seen in coating TiN (C) indicates that the sputtering power may have induced too much compressive strain to the system, though it is not possible to conclude on this. However, reducing the compressive strain in the coating may attribute to an increased contact angle with water which would be unfavorable in terms of biocompatibility. Thus, the main challenge for further optimization steps is to determine if the coating cracking is due to compressive strains and, if that is the case, find the optimal compromise between strain and wetting properties. Other mechanisms for reducing the contact angle, such as increasing the small-scale surface roughness could also be investigated.

In addition, it is important to keep in mind that while we cannot accurately predict the factors influencing biocompatibility, characterization of promising coating materials and techniques may contribute at a later stage. The characterization leads to a better understanding on the topic and can also give more rapid development of biocompatible coatings in the future when we have enhanced our understanding of the requirements for biocompatibility.

Chapter 6

Conclusion

In the present work thin film coatings intended for use on blood contacting biomedical devices have been characterized using a variety of techniques. Two 30 nm TiN thin film coatings (TiN (A) and TiN (B)) were reproduced using balanced and unbalanced RF magnetron sputtering, respectively, at 80 W power. An additional TiN coating (TiN (C)) was developed and produced using balanced magnetron sputtering at 120 W power as a first-step optimization of coating TiN (A). Coating TiN (C) was also compared to a 50 nm thick commercial DLC coating, and all coated samples were compared to their non-coated reference substrates. Coatings TiN (A) and TiN (B) were deposited on Carbothane substrates of 1 mm thickness, while coatings TiN (C) and DLC were deposited on Carbothane substrates of 150 μm to 500 μm thickness. The two types of substrates were produced using two different types of compression molding.

All TiN coatings had the same grey color, suggesting a lower than stoichiometric nitrogen content of the thin film. The coating processes were stable, and the substrate temperature did not rise in a manner that altered the properties of the substrate. SEM analysis revealed that all samples showed surface morphology in the form of directional lines in a regular pattern, believed to stem from the production of the substrates, though they were more prominent in the thinner substrates. All coatings followed the morphology of the substrate and appeared to have excellent coating coverage. BaSO$_4$ particles, added to the Carbothane substrate material as a filler, were observed protruding the surface of the thicker substrates, in accordance with previous work, but no such particles were seen in the thinner substrates. All TiN coatings were cracked, though the cracks in coating TiN (C) were much more frequent and regularly spaced, indicating suboptimal biocompatibility. No cracks were observed in the commercial DLC coating, which had a nano-scaled structure where particles had agglomerated in a distinctive pattern. Further, investigation of the cross section revealed that coating TiN (C) was homogeneous in thickness and followed the morphology of the substrate with only very occasional porosity between the coating and the substrate. On the other hand, the DLC coating procedure appeared to have damaged the substrate material on the substrate-coating interface, and frequent porosity was observed between the coating and the substrate, likely giving rise

to additional surface roughness.

Contact angle measurements with water confirmed that samples coated with TiN (A) ($80° \pm 2°$) had a lower contact angle than both samples coated with TiN (B) ($89° \pm 1°$) and the non-coated reference substrates ($101° \pm 2°$). The significant surface roughness may lead to exaggeration of the wetting properties. Both coating TiN (C) ($93° \pm 3°$) and DLC ($97° \pm 3°$) gave a reduction in wetting properties compared to the non-coated reference substrates ($120° \pm 3°$). However, the uncertainty in these results is greater due to the more prominent surface roughness. The directional lines proved to give asymmetrical deposition of the drops depending on the orientation, which was shown to influence the contact angles, and should be investigated further. A lower contact angle is likely favorable with respect to biocompatibility.

Both types of non-coated reference substrates showed a continued increase in friction coefficient with time, believed to be due to a local temperature effect. This behavior was not observed for the coated samples, possibly due to an insulating effect. Coatings TiN (A) and TiN (B) gave statistically equivalent coefficients of friction of 0.40 ± 0.03 and 0.39 ± 0.03 respectively, which was within the margin of error of the values measured for the non-coated reference substrate (0.44 ± 0.10). The coating measurements were stable, indicating good coating adhesion, which has also been supported by attempts at scratch testing. Coating TiN (C) had a friction coefficient of 0.42 ± 0.01, the DLC coating 0.28 ± 0.01 and 0.59 ± 0.05 for the non-coated reference substrate. The measurements performed on TiN (C) were more stable suggesting better coating adhesion, but it could also be due to the higher nano-scaled surface roughness of the DLC coatings, *i.e.*, from the agglomeration of particles in a distinctive pattern. It is believed that the coating adhesion is sufficient for all coatings as the normal displacement of the tip used for friction measurements were approximately two orders of magnitude greater than the coating thicknesses, without any damage to the coating being registered, suggesting that the coating follows the deformation of the substrate.

Tensile testing showed that the favorable mechanical properties of Carbothane are not degraded by the coating procedures nor by exposure to PBS. No direct correlation between the duration of expose and the final surface morphology of the samples was observed. However, a surprising correlation was found, in the case of the thicker non-coated reference substrates, between the time at which the exposure ended and the SEM analysis were performed, and the degree of degradation. The reason for this is at present not known and should be investigated further. A similar correlation was not found to exist for any of the coated samples, indicating that the coatings may protect the substrate material. ICP-MS analysis of the resulting liquid solution revealed that Ba leached from all samples with an increasing amount as the exposure time increased, which indicates that dissolution of $BaSO_4$ particles had occurred. The S concentration was, however, observed to decrease after 24 hours of exposure. The samples coated with TiN also consistently gave higher Ti concentrations than the non-coated samples, though without a dependence on exposure time, suggesting that Ti is leached from the coatings and reaches an equilibrium within the first 10 minutes of exposure to the PBS solution.

Though the factors influencing bio- and hemocompatibility are complex and difficult to predict, the use of TiN coatings for blood-contacting medical devices are promising, and outperform the commercial DLC coating in some aspects. However, further optimizations are needed and should focus on reducing the brittle character of the TiN coatings while enhancing hydrophilic properties.

Chapter 7

Future Work

At this time, the available characterization techniques have been applied for characterization of the developed coatings, as well as the commercial DLC coating and the non-coated reference substrates. A first-step optimization of the TiN coating has, in other words, been completed, but many more optimization steps are most likely needed before the coating can enter the verification and validation step (to ensure that the design output matches the specified design input) and later the final validation step. For this to happen, additional characterization should also be performed.

The following activities are planned, and the results will be included in a future research paper:

- The exact surface temperature of the substrate during the coating deposition process will be measured by engineers at NanoLab.

- The thrombotic properties of coatings TiN (C) and DLC will be examined using Chandler Loop testing with whole blood.

- Transmission Electron Microscopy (TEM) will be used to examine the cross section of the coated samples to give information about coating adhesion and structure and confirm the coating thickness and chemistry using Energy Dispersive X-Ray Spectroscopy (EDS) and Electron Energy Loss Spectroscopy (EELS).

- X-ray Photoelectron Spectroscopy (XPS) analysis will be performed for further chemical analysis of the coatings.

- Fourier Transform Infrared Spectroscopy (FTIR) will be applied to study potential differences in the Carbothane matrix before and after exposure to PBS.

In addition, a long-term exposure study to PBS should be performed to confirm the observed correlation between the time between the end of exposure and substrate degradation for the thicker substrates. Such a study should also investigate (1) the impact that

this degradation has on mechanical properties, (2) if it is a surface or bulk phenomenon, (3) the causative mechanisms, and (4) if the coatings prevent or limit the degradation to the substrate material. An exposure study, similar to that performed during the present work, should also be performed for samples coated with coating TiN (C).

Future optimization steps should focus on increasing coating hydrophilicity and improving coating cohesion, as well as reducing coating cracking.

In general, more work is needed on the interactions between materials and the human body to more accurately predict which material properties will give the best bio- and hemocompatibility.

Chapter 8

References

[1] "Biomaterials Science: An Introduction to Materials in Medicine". In: ed. by Buddy D. Ratner et al. Third. Academic Press, 2013. Chap. Biomaterials Science: A Multidisciplinary Endeavor.

[2] Garry Laverty, Sean Gorman, and Brendan Gilmore. "Biofilms and implant-associated infections". In: Dec. 2015, pp. 19–45. ISBN: 9780857095978. DOI: 10.1533/9780857097224.1.19.

[3] Joseph R. Davis. "Handbook of materials for medical devices". In: ed. by Joseph R. Davis. ASM International, 2003. Chap. Preface, pp. vii–viii.

[4] United Nations Department of Economic and Social Affairs. *World Population Ageing 2019*. 2019. URL: https://www.un.org/en/development/desa/population/publications/pdf/ageing/WorldPopulationAgeing2019-Report.pdf.

[5] Daniel Howdon and Nigel Rice. "Health care expenditures, age, proximity to death and morbidity: Implications for an ageing population". In: *Journal of Health Economics* 57 (2018), pp. 60–74. ISSN: 0167-6296. DOI: 10.1016/j.jhealeco.2017.11.001.

[6] OECD. *The OECD Joint Network of Senior Budget and Health Officials*. Website. Accessed: 06.06.2021. URL: https://www.oecd.org/health/sbo-health.htm.

[7] *Reducing Healthcare Associated Infections in Hospitals in England*. Tech. rep. National Audit Office, 2009. URL: https://www.nao.org.uk/wp-content/uploads/2009/06/0809560es.pdf.

[8] R. Douglas Scott II. *The Direct Medical Costs of Healthcare-Associated Infections in U.S. Hospitals and the Benefits of Prevention*. Tech. rep. Centers for Disease Control and Prevention, 2009. URL: https://www.cdc.gov/hai/pdfs/hai/scott_costpaper.pdf.

[9] Zheng Zhang and Victoria E. Wagner. "Antimicrobial Coatings and Modifications on Medical Devices". In: ed. by Zheng Zhang and Victoria E. Wagner. Springer Nature, 2017. Chap. Preface, pp. v–vii.

[10] Kari Ravnestad Kjørholt. "Development of TiN Thin Film Coatings for Biomedical Applications". MA thesis. Norwegian University of Science and Technology, Dec. 2020.

[11] V. Kumar et al. "6 - Surface analysis technique for assessing hemocompatibility of biomaterials". In: *Hemocompatibility of Biomaterials for Clinical Applications.* Ed. by Christopher A. Siedlecki. Woodhead Publishing, 2018, pp. 119–161. ISBN: 978-0-08-100497-5. DOI: 10.1016/B978-0-08-100497-5.00006-9.

[12] J. R. Davis. "Handbook of Materials for Medical Devices". In: ASM International, 2003. Chap. Physical and Mechanical Requirements for Medical Device Materials.

[13] I.R. Cooper. "1 - Introduction to biomaterials and medical device-associated infections". In: *Biomaterials and Medical Device - Associated Infections.* Ed. by L. Barnes and I.R. Cooper. Oxford: Woodhead Publishing, 2015, pp. 3–17. ISBN: 978-0-85709-597-8. DOI: 10.1533/9780857097224.1.3.

[14] P. Vermette et al. "Biomedical applications of polyurethanes". In: *Tiss. Eng. Intellig. Unit* (Jan. 2001), pp. 175–219.

[15] Patrícia Alves et al. "Surface modification of thermoplastic polyurethane in order to enhance reactivity and avoid cell adhesion". In: *Colloid and Polymer Science* 287 (Dec. 2009), pp. 1469–1474. DOI: 10.1007/s00396-009-2116-y.

[16] Anuj Kapadia et al. *Medical Devices 2030.* Tech. rep. KPMG, 2018.

[17] MedTech Europe. *The European Medical Technology in Figures, Market.* Website. Accessed: 24.03.2021. Jan. 2021. URL: https://www.medtecheurope.org/datahub/market/.

[18] U.S. Food & Drug Administration. *How to Determine if Your Product is a Medical Device.* Website. Dec. 2019. URL: https://www.fda.gov/medical-devices/classify-your-medical-device/how-determine-if-your-product-medical-device.

[19] U.S. Food & Drug Administration. *Part IV: Regulating Cosmetics, Devices, and Veterinary Medicine After 1938.* Website. Accessed: 11.04.2021. Feb. 2018. URL: https://www.fda.gov/about-fda/fdas-evolving-regulatory-powers/part-iv-regulating-cosmetics-devices-and-veterinary-medicine-after-1938.

[20] U.S. Food & Drug Administration. *Classify Your Medical Device.* Website. Accessed: 11.04.2021. Feb. 2020. URL: https://www.fda.gov/medical-devices/overview-device-regulation/classify-your-medical-device.

[21] U.S. Food & Drug Administration. *Product Classification.* Website. Accessed: 11.04.2021. Apr. 2021. URL: https://www.accessdata.fda.gov/scripts/cdrh/cfdocs/cfpcd/classification.cfm.

[22] U.S. Food & Drug Administration. *Premarket Approval (PMA).* Website. Accessed: 11.04.2021. May 2019. URL: https://www.fda.gov/medical-devices/premarket-submissions/premarket-notification-510k.

[23] U. S. Food & Drug Administration. *Premarket Notification 510(k).* Website. Accessed: 11.04.2020. Mar. 2020. URL: https://www.fda.gov/medical-devices/premarket-submissions/premarket-notification-510k.

[24] European Commission. *Overview.* Website. Accessed: 13.04.2021. URL: https://ec.europa.eu/health/md_sector/overview_en.

[25] MedTech Europe. *The European MedicalTechnology Industry - in figures 2019.* Website. Accessed: 16.04.2021. 2019. URL: https://www.medtecheurope.org/wp-content/uploads/2019/04/The-European-Medical-Technology-Industry-in-figures-2019-1.pdf.

[26] European Commission. *New Regulations.* Website. Accessed: 13.04.2021. URL: https://ec.europa.eu/health/md_sector/new_regulations_en.

[27] European Commission. *New EU Rules to Ensure Safety of Medical Devices.* Website. Accessed: 16.04.2021. 2018. URL: https://ec.europa.eu/health/sites/health/files/md_newregulations/docs/md_generic_fs_en.pdf.

[28] European Commission. *Factsheet for Manufacturers of medical devices.* Website. Accessed: 16.04.2021. Aug. 2020. URL: https://ec.europa.eu/health/sites/health/files/md_newregulations/docs/md_manufacturers_factsheet_en.pdf.

[29] European Commission. *Overview.* Website. Accessed: 13.04.2021. URL: https://ec.europa.eu/health/md_newregulations/overview_en.

[30] *Blood Basics.* Website. Accessed 15.03.2021. URL: https://www.hematology.org/education/patients/blood-basics.

[31] Manfred F. Maitz et al. "The blood compatibility challenge. Part 4: Surface modification for hemocompatible materials: Passive and active approaches to guide blood-material interactions". In: *Acta Biomaterialia* 94 (2019), pp. 33–43. ISSN: 1742-7061. DOI: 10.1016/j.actbio.2019.06.019.

[32] John L. Brash et al. "The blood compatibility challenge. Part 2: Protein adsorption phenomena governing blood reactivity". In: *Acta Biomaterialia* 94 (2019), pp. 11–24. ISSN: 1742-7061. DOI: 10.1016/j.actbio.2019.06.022.

[33] Iqbal H. Jaffer and Jeffrey I. Weitz. "The blood compatibility challenge. Part 1: Blood-contacting medical devices: The scope of the problem". In: *Acta Biomaterialia* 94 (2019), pp. 2–10. ISSN: 1742-7061. DOI: 10.1016/j.actbio.2019.06.021.

[34] Victoria E. Wagner and Nisha Gupta. "Antimicrobial Coatings and Modifications on Medical Devices". In: ed. by Zheng Zhang and Victoria E. Wagner. Springer Nature, 2017. Chap. Chapter 5 - Implantable Medical Devices Treated with Antimicrobial Agents, pp. 127–142.

[35] Juergen M Lackner et al. "Hemocompatibility of Inorganic Physical Vapor Deposition (PVD) Coatings on Thermoplastic Polyurethane Polymers". In: *Journal of functional biomaterials* 3 (Dec. 2012), pp. 283–297. DOI: 10.3390/jfb3020283.

[36] Maud Gorbet et al. "The blood compatibility challenge. Part 3: Material associated activation of blood cascades and cells". In: *Acta Biomaterialia* 94 (2019), pp. 25–32. ISSN: 1742-7061. DOI: 10.1016/j.actbio.2019.06.020.

[37] I. H. Jaffer et al. "Medical device-induced thrombosis: what causes it and how can we prevent it?" In: *Journal of Thrombosis and Haemostasis* 13.S1 (2015), S72–S81. DOI: 10.1111/jth.12961.

[38] Carlos A. Labarrere, Ali E. Dabiri, and Ghassan S. Kassab. "Thrombogenic and Inflammatory Reactions to Biomaterials in Medical Devices". In: *Frontiers in bioengineering and biotechnology* 8.123 (Mar. 2020). DOI: 10.3389/fbioe.2020.00123.

[39] National Organization for Rare Disorders. *Factor XII Deficiency.* Website. Accessed 16.03.2021. URL: https://rarediseases.org/rare-diseases/factor-xii-deficiency/.

[40] Rui Zhuo, Christopher A. Siedlecki, and Erwin A. Vogler. "Autoactivation of blood factor XII at hydrophilic and hydrophobic surfaces". In: *Biomaterials* 27.24 (2006), pp. 4325–4332. ISSN: 0142-9612. DOI: 10.1016/j.biomaterials.2006.04.001.

[41] Li-Chong Xu and Christopher A Siedlecki. "Effects of surface wettability and contact time on protein adhesion to biomaterial surfaces". In: *Biomaterials* 28.22 (Aug. 2007), pp. 3273–3283. DOI: 10.1016/j.biomaterials.2007.03.032.

[42] Sumit Parvate, Prakhar Dixit, and Sujay Chattopadhyay. "Superhydrophobic Surfaces: Insights from Theory and Experiment". In: *The Journal of Physical Chemistry* 124.8 (Jan. 2020), pp. 1323–1360. DOI: 10.1021/acs.jpcb.9b08567.

[43] M. Fischer, M.F. Maitz, and C. Werner. "7 - Coatings for biomaterials to improve hemocompatibility". In: *Hemocompatibility of Biomaterials for Clinical Applications.* Ed. by Christopher A. Siedlecki. Woodhead Publishing, 2018, pp. 163–190. ISBN: 978-0-08-100497-5. DOI: 10.1016/B978-0-08-100497-5.00007-0.

[44] O. Bazaka and K. Bazaka. "Surface modification of biomaterials for biofilm control". In: Dec. 2015, pp. 103–132. ISBN: 9780857095978. DOI: 10.1533/9780857097224.2.103.

[45] National Cancer Institute. *Central Venous Access Catheter.* Website. Accessed 15.03.2021. URL: https://www.cancer.gov/publications/dictionaries/cancer-terms.

[46] Michael S. Firstenberg et al. "Central line complications". In: *International Journal of Critical Illness and Injury Science* 5.3 (2015), p. 170. DOI: 10.4103/2229-5151.164940.

[47] *Central Venous Catheter Market Size, Share & Trends Analysis | Global | 2020-2026 | Segmented by: Product Type (Acute/Chronic, Power-Injectable, Conventional, and Antimicrobial CVCs).* Tech. rep. Accessed: 16.04.2021. iData Research, May 2020. URL: https://idataresearch.com/product/central-venous-catheter-market/.

[48] Mark A. Wood and Kenneth A. Ellenbogen. "Cardiac Pacemakers From the Patient's Perspective". In: *Circulation* 105.18 (2002), pp. 2136–2138. DOI: 10.1161/01.CIR.0000016183.07898.90.

[49] Harry G. Mond and Alessandro Proclemer. "The 11th World Survey of Cardiac Pacing and Implantable Cardioverter-Defibrillators: Calendar Year 2009–A World Society of Arrhythmia's Project". In: *Pacing and Clinical Electrophysiology* 34.8 (2011), pp. 1013–1027. DOI: 10.1111/j.1540-8159.2011.03150.x.

[50] Neal Bhatia and Mikhael El-Chami. "Leadless pacemakers: a contemporary review". In: *Journal of Geriatric Cardiology* 15.4 (Apr. 2018), pp. 249–253. DOI: `10.11909/j.issn.1671-5411.2018.04.002`.

[51] Philippe Pibarot and Jean G. Dumesnil. "Prosthetic Heart Valves". In: *Circulation* 119.7 (2009), pp. 1034–1048. DOI: `10.1161/CIRCULATIONAHA.108.778886`.

[52] Johns Hopkins Medicine. *Heart Valve Repair or Replacement Surgery*. Website. Accessed: 18.04.2021. URL: `https://www.hopkinsmedicine.org/health/treatment-tests-and-therapies/heart-valve-repair-or-replacement-surgery`.

[53] Manjula Sarkar and Vishal Prabhu. "Basics of cardiopulmonary bypass". In: *Indian Journal of Anaesthesia* 61.9 (Sept. 2017), pp. 760–767. DOI: `10.4103/ija.IJA_379_17`.

[54] J. R. Davis. "Handbook of Materials for Medical Devices". In: ASM International, 2003. Chap. Polymeric Materials.

[55] J. R. Davis. "Handbook of Materials for Medical Devices". In: ASM International, 2003. Chap. Overview of Biomaterials and Their Use in Medical Devices, pp. 1–11.

[56] J. R. Davis. "Handbook of Materials for Medical Devices". In: ASM International, 2003. Chap. Ceramic Materials, pp. 137–150.

[57] Zheng Zhang, Victoria E. Wagner, and John C. Victor. "Antimicrobial Coatings and Modifications on Medical Devices". In: ed. by Zheng Zhang and Victoria E. Wagner. Springer Nature, 2017. Chap. Chapter 1 - Antimicrobial Modifications on Critical Care Implants, pp. 1–36.

[58] Maren Kirknes Fossum. Private Communication. NTNU, Trondheim. 2021.

[59] Francis Verbeke et al. "The role of polymer surface degradation and barium sulphate release in the pathogenesis of catheter-related infection". In: *Nephrology Dialysis Transplantation* 25.4 (Nov. 2009), pp. 1207–1213. ISSN: 0931-0509. DOI: `10.1093/ndt/gfp638`.

[60] Centers for Disease Control and Prevention. *Healthcare-Associated Infections*. Website. Accessed: 11.04.2021. URL: `https://arpsp.cdc.gov/profile/infections`.

[61] Yi Wang et al. "Antimicrobial Coatings and Modifications on Medical Devices". In: ed. by Zheng Zhang and Victoria E. Wagner. Springer Nature, 2017. Chap. Chapter 2 - Antimicrobial and Anti-Biofilm Medical Devices: Public Health and Regulatory Science Challenges, pp. 37–65.

[62] Centers for Disease Control and Prevention. *Central Line-Associated Bloodstream Infections*. Website. Accessed: 11.04.2021. 2021. URL: `https://arpsp.cdc.gov/profile/infections/CLABSI`.

[63] Gunnar F. Nordberg, Bruce A. Fowler, and Monica Nordberg. "Chapter 1 - Toxicology of Metals: Overview, Definitions, Concepts, and Trends". In: *Handbook on the Toxicology of Metals (Fourth Edition)*. Ed. by Gunnar F. Nordberg, Bruce A. Fowler, and Monica Nordberg. Fourth Edition. San Diego: Academic Press, 2015, pp. 1–12. ISBN: 978-0-444-59453-2. DOI: `10.1016/B978-0-444-59453-2.00001-9`.

[64] Ronald P. Brown et al. "Chapter 5 - Toxicity of Metals Released from Implanted Medical Devices". In: *Handbook on the Toxicology of Metals (Fourth Edition)*. Ed. by Gunnar F. Nordberg, Bruce A. Fowler, and Monica Nordberg. Fourth Edition. San Diego: Academic Press, 2015, pp. 113–122. ISBN: 978-0-444-59453-2. DOI: `10.1016/B978-0-444-59453-2.00005-6`.

[65] Catarina A. Oliveira, Isabel S. Candelária, and Filipe Caseiro-Alves. "Metallosis: A diagnosis not only in patients with metal-on-metal prostheses". In: *European Journal of Radiology Open* 2 (2015), pp. 3–6.

[66] James Drummond, Phong Tran, and Camdon Fary. "Metal-on-Metal Hip Arthroplasty: A Review of Adverse Reactions and Patient Management". In: *Journal of Funtional Biomaterials* 6.3 (Sept. 2015), pp. 486–499.

[67] Thomas S. Metkus, David Zieve, and Brenda Conaway. *Thrombus*. Website. Accessed: 18.04.2021. July 2020. URL: `https://medlineplus.gov/ency/imagepages/18120.htm`.

[68] Centers for Disease Control and Prevention. *Learn About Healthcare-Associated Venous Thromboembolism*. Website. Accessed: 18.04.2021. Feb. 2020. URL: `https://www.cdc.gov/ncbddd/dvt/ha-vte.html#ref`.

[69] Jun Li, Matthew Taylor, and Zheng Zhang. "Antimicrobial Coatings and Modifications on Medical Devices". In: ed. by Zheng Zhang and Victoria E. Wagner. Springer, 2017. Chap. Anti-fouling Medical Coatings, pp. 189–214. DOI: `10.1007/978-3-319-57494-3`.

[70] James D. Bryers. "Antimicrobial Coatings and Modifications on Medical Devices". In: ed. by Zheng Zhang and Victoria E. Wagner. Springer, 2017. Chap. Anti-antimicrobial Approaches to Device-Based Infections, pp. 143–170. DOI: `10.1007/978-3-319-57494-3`.

[71] Guozhong Cao; Ying Wang. *Nanostructures and Nanomaterials*. Ed. by Mark Reed. 2nd ed. World Scientific, 2011. ISBN: 978-9814324557.

[72] E. Sreepradha et al. "Studies on Reactive Magnetron Sputtered TiN Thin Films". In: *Asian Journal of Scientific Research* 7 (2014), pp. 294–302. DOI: `10.3923/ajsr.2014.294.302`.

[73] Ioan Valentin Tudose et al. "Chapter 2 - Chemical and physical methods for multifunctional nanostructured interface fabrication". In: *Functional Nanostructured Interfaces for Environmental and Biomedical Applications*. Ed. by Valentina Dinca and Mirela Petruta Suchea. Micro and Nano Technologies. Elsevier, 2019, pp. 15–26. ISBN: 978-0-12-814401-5. DOI: `10.1016/B978-0-12-814401-5.00002-5`.

[74] Gauri Shanker et al. "Effect of balanced and unbalanced magnetron sputtering processes on the properties of SnO2 thin films". In: *Current Applied Physics* 19.6 (2019), pp. 697–703. ISSN: 1567-1739. DOI: `10.1016/j.cap.2019.03.016`.

[75] P.J Kelly and R.D Arnell. "Magnetron sputtering: a review of recent developments and applications". In: *Vacuum* 56.3 (2000), pp. 159–172. ISSN: 0042-207X. DOI: `10.1016/S0042-207X(99)00189-X`.

[76] Shaochen Lin et al. "Effects of sputtering pressure on microstructure and mechanical properties of ZrN films deposited by magnetron sputtering". In: *Materials Research Bulletin* 105 (2018), pp. 231–236. ISSN: 0025-5408. DOI: 10.1016/j.materresbull.2018.04.054.

[77] D.W. Grainger and D.G. Castner. "3.301 - Surface Analysis and Biointerfaces: Vacuum and Ambient In Situ Techniques". In: *Comprehensive Biomaterials*. Ed. by Paul Ducheyne. Oxford: Elsevier, 2011, pp. 1–22. ISBN: 978-0-08-055294-1. DOI: 10.1016/B978-0-08-055294-1.00082-9.

[78] H Zhang. "2 - Surface characterization techniques for polyurethane biomaterials". In: *Advances in Polyurethane Biomaterials*. Ed. by Stuart L. Cooper and Jianjun Guan. Woodhead Publishing, 2016, pp. 23–73. ISBN: 978-0-08-100614-6. DOI: 10.1016/B978-0-08-100614-6.00002-0.

[79] Jyotsna Chandra et al. "Modification of surface properties of biomaterials influences the ability of Candida albicans to form biofilms." In: *Applied and environmental microbiology* 71 (Dec. 2005), pp. 8795–8801. DOI: 10.1128/AEM.71.12.8795-8801.2005.

[80] Ramé-Hart Instruments Co. *Information on Contact Angle*. Website. Accessed 21.12.2020. 2020. URL: http://www.ramehart.com/contactangle.htm.

[81] Kock-Yee Law and Hong Zhao. *Surface Wetting - Characterization, Contact Angle, and Fundamentals*. Springer International Publishing, 2016. ISBN: ISBN 978-3-319-25214-8.

[82] T.T. Chau et al. "A review of factors that affect contact angle and implications for flotation practice". In: *Advances in Colloid and Interface Science* 150.2 (2009), pp. 106–115. ISSN: 0001-8686. DOI: 10.1016/j.cis.2009.07.003.

[83] SK. *Effect of drop volume on static contact angles*. Accessed 08.12.2020. Krüss. 2004. URL: https://www.kruss-scientific.com/fileadmin/user_upload/website/literature/kruss-tn310-en.pdf.

[84] *Influence of droplet volume on contact angle*. Accessed 21.12.2020. Biolin Scientific. 2016. URL: https://cdn2.hubspot.net/hubfs/516902/Pdf/Attension/Tech%20Notes/AT-TN-06-Influence-drop-volume-contact-angle-160401.pdf?t=1516102020835.

[85] Britannica, The Editors of Encyclopaedia. *Friction*. Website. Accessed 22.04.2020. May 2020. URL: https://www.britannica.com/science/friction.

[86] Engineering Toolbox. *Friction and Friction Coefficients*. Website. Accessed: 16.06.2021. 2004. URL: https://www.engineeringtoolbox.com/friction-coefficients-d_778.html.

[87] ThermoFisher Scientific. *Inductively Coupled Plasma Mass Spectrometry (ICP-MS) Information*. Website. Accessed: 19.05.2021. URL: https://www.thermofisher.com/no/en/home/industrial/spectroscopy-elemental-isotope-analysis/spectroscopy-elemental-isotope-analysis-learning-center/trace-elemental-analysis-tea-information/inductively-coupled-plasma-mass-spectrometry-icp-ms-information.html.

[88]   *The 30-Minute Guideto ICP-MS*. Tech. rep. Accessed: 19.05.2021. PerkinElmer, 2011. URL: https://www.perkinelmer.com/CMSResources/Images/44-74849tch_icpmsthirtyminuteguide.pdf.

[89]   Duanjie Li. *Understanding Coating Failures Using Scratch Testing*. Tech. rep. NANOVEA, 2013.

[90]   Cathrine Kyung Won Solem and Kari Ravnestad Kjørholt. "Rietveld Refinement of GI-XRD Diffractograms". NTNU, Trondheim. 2021.

[91]   Lubrizol LifeSciences. *Carbothane® Aliphatic TPU B20 Series*. 2016.

[92]   N.S. Lawand et al. "Thin Titanium Nitride Films Deposited using DC Magnetron Sputtering used for Neural Stimulation and Sensing Purposes". In: *Procedia Engineering* 47 (2012). 26th European Conference on Solid-State Transducers, EUROSENSOR 2012, pp. 726–729. ISSN: 1877-7058. DOI: 10.1016/j.proeng.2012.09.250.

[93]   M. Islam et al. "Nanostructured TiN thin films suitable for medical applications". In: *Materials Forum* 32 (Jan. 2007), pp. 129–136.

[94]   C.S. Geetha, A. Sabareeswaran, and P.V. Mohanan. "Pre-clinical evaluation of titanium nitride coated titanium material". In: *Toxicology Mechanisms and Methods* 22.2 (2012), pp. 144–150. DOI: 10.3109/15376516.2011.610384.

[95]   Geoffrey Dearnaley and James H. Arps. "Biomedical applications of diamond-like carbon (DLC) coatings: A review". In: *Surface and Coatings Technology* 200.7 (2005), pp. 2518–2524. ISSN: 0257-8972. DOI: 10.1016/j.surfcoat.2005.07.077.

[96]   Feng Wen, Jiaqi Liu, and Jianlu Xue. "The Studies of Diamond-Like Carbon Films as Biomaterials: Review". In: *Colloid and Surface Science* 2.3 (2017), pp. 81–95. DOI: 10.11648/j.css.20170203.11.

[97]   Hasebe T. et al. "Fluorinated diamond-like carbon as antithrombogenic coating for blood-contacting devices." In: *J Biomed Mater Res A.* 76.1 (Jan. 2006), pp. 86–94. DOI: 10.1002/jbm.a.30512..

[98]   Martijn de Roosz. Private Communication. NTNU, Trondheim. 2021.

[99]   José Antonio Santiago Varela. "Novel HiPIMS processes for DLC coatings". PhD thesis. Universidad Politécnica de Madrid, 2020.

[100]   Krüss. *Young-Laplace fit*. Website. Accessed 22.12.2020. URL: https://www.kruss-scientific.com/en/know-how/glossary/young-laplace-fit.

[101]   William D. Callister and David G Rethwisch. *Materials science and engineering / William D. Callister Jr., David G. Rethwisch*. eng. 9th ed., SI version. New York: John Wiley & Sons Asia Pte Ltd, 2015. ISBN: 9781118319222.

[102]   C.-H. Ma, J.-H. Huang, and Haydn Chen. "Nanohardness of nanocrystalline TiN thin films". In: *Surface and Coatings Technology* 200.12 (2006), pp. 3868–3875. ISSN: 0257-8972. DOI: 10.1016/j.surfcoat.2004.10.098.

[103]   AAT Bioquest, Inc. *PBS (Phosphate Buffered Saline) (1X, pH 7.4) Preparation and Recipe*. Accessed 20.01.2021. URL: https://www.aatbio.com/resources/buffer-preparations-and-recipes/pbs-phosphate-buffered-saline.

[104] Georg Reiners et al. "Decorative properties and chemical composition of hard coatings". In: *Surface and Coatings Technology* 54-55 (1992), pp. 273–278. ISSN: 0257-8972. DOI: 10.1016/S0257-8972(09)90062-7.

[105] Ph. Roquiny, F. Bodart, and G. Terwagne. "Colour control of titanium nitride coatings produced by reactive magnetron sputtering at temperature less than 100°C". In: *Surface and Coatings Technology* 116-119 (1999), pp. 278–283. ISSN: 0257-8972. DOI: 10.1016/S0257-8972(99)00076-6.

[106] Fatiha Challali et al. "Effect of RF sputtering power and vacuum annealing onthe properties of AZO thin films prepared from ceramictarget in confocal configuration". In: *Materials Science in Semiconductor Processing* (2020). DOI: ff10.1016/j.mssp.2020.105217.

[107] Timothy Douglas and Håvard Haugen. "Coating of polyurethane scaffolds with collagen: Comparison of coating and cross-linking techniques". In: *Journal of materials science. Materials in medicine* 19 (Aug. 2008), pp. 2713–9. DOI: 10.1007/s10856-008-3393-6.

[108] S. Jasmee et al. "Hydrophobicity performance of thermoplastic polyurethane coated with TiO2 under thermal aging effect". In: *Advanced Materials and Mechanical Engineering Research* (2018).

[109] S Jasmee et al. "Hydrophobicity performance of polyethylene terephthalate (PET) and thermoplastic polyurethane (TPU) with thermal effect". In: *Materials Research Express* 5.9 (2018), p. 096304. DOI: 10.1088/2053-1591/aad81e.

[110] Maurizio Villani et al. "Polyurethane-Based Composites: Effects of Antibacterial Fillers on the Physical-Mechanical Behavior of Thermoplastic Polyurethanes". In: *Polymers* 12.362 (2020). DOI: 10.3390/polym12020362.

[111] James I. Wright. *Using Polyurethanes in Medical Applications*. Website. Accessed 21.12.2020. Mar. 2006. URL: https://www.mddionline.com/materials/using-polyurethanes-medical-applications.

[112] Xiaolu Pang et al. "Residual Stress and Surface Energy of Sputtered TiN Films". In: *Xiaolu Pang, Liqiang Zhang, Huisheng Yang, Kewei Gao, and Alex A. Volinsky* 24.3 (Mar. 2015). DOI: 10.1007/s11665-015-1393-5.

[113] Jorge Estrada-Martínez et al. "Wettability modification of the AISI 304 and 316 stainless steel and glass surfaces by titanium oxide and titanium nitride coating". In: *Surface and Coatings Technology* 330 (2017), pp. 61–70. ISSN: 0257-8972. DOI: 10.1016/j.surfcoat.2017.09.059.

[114] Božana Čolović et al. "Wetting properties of titanium oxides, oxynitrides and nitrides obtained by DC and pulsed magnetron sputtering and cathodic arc evaporation". In: *Materials Science-Poland* 37 (June 2019). DOI: 10.2478/msp-2019-0031.

[115] A.P. Serro et al. "A comparative study of titanium nitrides, TiN, TiNbN and TiCN, as coatings for biomedical applications". In: *Surface and Coatings Technology* 203.24 (2009), pp. 3701–3707. ISSN: 0257-8972. DOI: 10.1016/j.surfcoat.2009.06.010.

[116] R. Costa et al. "Tribological behavior of DLC films in space and automotive oil under boundary lubrication". In: 2012.

[117] Lili Sun et al. "Comparative study on structure and wetting properties of diamond-like carbon films by W and Cu doping". In: *Diamond and Related Materials* 73 (2017). 10th International Conference on New Diamond and Nano Carbons – NDNC 2016, pp. 278–284. ISSN: 0925-9635. DOI: 10.1016/j.diamond.2016.10.022.

[118] A. A. Ogwu, T. I. T. Okpalugo, and J. A. D. McLaughlin. "The effect of PECVD plasma decomposition on the wettability and dielectric constant changes in silicon modified DLC films for potential MEMS and low stiction applications". In: *AIP Advances* 2 (2012). DOI: 10.1063/1.4742852.

[119] Christoph Burgstaller. Private Communication. Transfercenter für Kunststofftechnik GmbH (TCKT), Austria. 2021.

[120] S. Gogolewski. "Selected topics in biomedical polyurethanes. A review". In: *Colloid & Polymer Science* 267 (1989), pp. 757–785.

[121] I. Resiak and G. Rokicki. "Modified polyurethanes for biomedical applications". In: *Polimery* 9 (2000), p. 592.

[122] Imran Khan et al. "Analysis and evaluation of a biomedical polycarbonate urethane tested in an in vitro study and an ovine arthroplasty model. Part I: materials selection and evaluation". In: *Biomaterials* 26.6 (2005), pp. 621–631. ISSN: 0142-9612. DOI: 10.1016/j.biomaterials.2004.02.065.

[123] Amber Lothian et al. "Characterization of the metal status of natively purified alpha-synuclein from human blood, brain tissue, or recombinant sources using size exclusion ICP-MS reveals no significant binding of Cu, Fe or Zn†". In: *Metallomics* 11.1 (Nov. 2018), pp. 128–140. ISSN: 1756-5901. DOI: 10.1039/c8mt00223a.

[124] Agency for Toxic Substances and Disease Registry. *Toxicological Profile for Barium*. Website. Accessed: 09.06.2021. 2007. URL: https://wwwn.cdc.gov/TSP/ToxProfiles/ToxProfiles.aspx?id=327&tid=57.

[125] Agneta Oskarsson. "Chapter 29 - Barium". In: *Handbook on the Toxicology of Metals (Fourth Edition)*. Ed. by Gunnar F. Nordberg, Bruce A. Fowler, and Monica Nordberg. Fourth Edition. San Diego: Academic Press, 2015, pp. 625–634. ISBN: 978-0-444-59453-2. DOI: 10.1016/B978-0-444-59453-2.00029-9.

[126] Center for Applied Isotope Studies, University of Georgia. *Guide to Selecting The Most Suitable Technique*. Website. Accessed: 16.06.2021. URL: https://cais.uga.edu/facilities/plasma-chemistry-laboratory/guide-selecting-the-most-suitable-technique/.

[127] National Pesticide Information Center. *Sulfur*. Website. Accessed: 16.06.2021. May 2017. URL: http://npic.orst.edu/factsheets/sulfurgen.html.

[128] Taiyi Jin and Maths Berlin. "Chapter 57 - Titanium". In: *Handbook on the Toxicology of Metals (Fourth Edition)*. Ed. by Gunnar F. Nordberg, Bruce A. Fowler, and Monica Nordberg. Fourth Edition. San Diego: Academic Press, 2015, pp. 1287–1296. ISBN: 978-0-444-59453-2. DOI: 10.1016/B978-0-444-59453-2.00057-3.

[129] Kyeong Kim et al. "General review of titanium toxicity". In: *International Journal of Implant Dentistry* 5 (Mar. 2019), p. 10. DOI: 10.1186/s40729-019-0162-x.

[130] Dong Ryeol Kim et al. "Effect of Sputtering Power on the Structure and Optical Properties of Radio Frequency Sputtered-ZnS Thin Film". In: *Journal of Nanoscience and Nanotechnology* 17.7 (July 2017), pp. 5046–5049. DOI: 10.1166/jnn.2017.14277.

[131] Accarat Chaoumead, Youl-moon Sung, and Dong-Joo Kwak. "The Effects of RF Sputtering Power and Gas Pressure on Structural and Electrical Properties of ITiO Thin Film". In: *Advances in Condensed Matter Physics* (Oct. 2012). DOI: 10.1155/2012/651587.

[132] Zih-Ying Yang et al. "Room temperature fabrication of titanium nitride thin films as plasmonic materials by high-power impulse magnetron sputtering". In: *Optical Materials Express* 6.2 (Feb. 2016), p. 540. DOI: 10.1364/OME.6.000540.

[133] Kah-Yoong Chan and Bee-San Teo. "Sputtering power and deposition pressure effects on the electrical and structural properties of copper thin films". In: *Journal of Materials Science* 40 (2005), pp. 5971–5981. DOI: 10.1007/s10853-005-1362-8.

[134] D.L. Ma et al. "Optimal target sputtering mode for aluminum nitride thin film deposition by high power pulsed magnetron sputtering". In: *Vacuum* 160 (2019), pp. 410–417. ISSN: 0042-207X. DOI: 10.1016/j.vacuum.2018.11.058.

[135] Cole-Parmer. *Chemical Compatibility Database.* Website. Accessed 21.12.2020. 2020. URL: https://www.coleparmer.com/chemical-resistance.

[136] Mohammad Ibrahim. Private Communication. NTNU, Trondheim. 2020.

Appendix A

Material and Chemicals Specifications

The subsequent pages include the following information about the Carbothane pellets used to produce the substrates utilized in this work and the Phosphate Buffered Saline (PBS) used for the exposure study:

- Carbothane Safety Data Sheet

- Other Carbothane specifications from the supplier

- PBS Safety Data Sheet

SAFETY DATA SHEET

1. Identification of the substance or mixture and of the supplier

Product identifier

Product name: **CARBOTHANE™ PC-3595A-B20**

Additional identification
Chemical name: Polyurethane polymer
CAS-No.: Not applicable.

Recommended use and restriction on use

Recommended use: Catheters & IVs
Restrictions on use: None identified.

Details of the supplier of the safety data sheet

Supplier
Company Name: LUBRIZOL ADVANCED MATERIALS
EUROPE, BVBA
Address: NIJVERHEIDSSTRAAT 30
WESTERLO-OEVEL,
BE
Telephone: +32 (0) 14 24 1611

Emergency telephone number:
FOR TRANSPORT EMERGENCY CALL CHEMTREC (+1) 703 527 3887

2. Hazards identification

Classification of the substance or mixture

Prepared according to Global Harmonized System (GHS) standards.

Not classified

Label Elements Not applicable
Other hazards which do not None identified.
result in GHS classification:

3. Composition/Information on Ingredients

Mixtures

General information: No hazardous ingredients.

4. First aid measures

Description of first aid measures
Inhalation: Remove exposed person to fresh air if adverse effects are observed.

Eye contact:	Any material that contacts the eye should be washed out immediately with water. If easy to do, remove contact lenses. If hot melted material should splash into the eyes, flush eyes immediately with water for 15 minutes while holding the eyelids open. Immediately call a poison center or doctor.
Skin Contact:	Wash with soap and water. If skin irritation occurs, get medical attention. For contact with molten product, do not remove contaminated clothing. Flush skin immediately with large amounts of cold water. If possible submerge area in cold water. Pack with ice. DO NOT attempt to peel polymer from skin. Seek medical attention immediately.
Ingestion:	No specific first aid measures noted.
Personal Protection for First-aid Responders:	When providing first aid always protect yourself against exposure to chemicals or blood born diseases by wearing gloves, masks and eye protection. After providing first aid wash your exposed skin with soap and water.
Most important symptoms and effects, both acute and delayed:	See section 11.

Indication of any immediate medical attention and special treatment needed

Treatment:	Note to physician: Treat symptomatically.

5. Fire-fighting measures

General Fire Hazards:	No unusual fire or explosion hazards noted.
Extinguishing media	
Suitable extinguishing media:	Use water spray, dry chemical or foam for extinction. CO2 may be ineffective on large fires.
Unsuitable extinguishing media:	Not determined.
Specific hazard arising from the chemical:	See section 10 for additional information.
Advice for firefighters	
Special fire fighting procedures:	Thermoplastic polymers can burn. Protect product from flames; maintain proper clearance when using heat devices, etc. Irritating or toxic substances will be emitted upon burning, combustion or decomposition. Large masses of molten polymer held at elevated temperatures for extended periods of time may auto-ignite. May self-react upon long standing or exposure to heat with generation of enough heat to cause fire.
Special protective equipment for fire-fighters:	Wear full protective firegear including self-containing breathing apparatus operated in the positive pressure mode with full facepiece, coat, pants, gloves and boots.

6. Accidental Release Measures

Personal precautions, protective equipment and emergency procedures:	No data available.
Environmental Precautions:	Avoid release to the environment. Do not contaminate water sources or sewer. Environmental manager must be informed of all major spillages. Prevent further leakage or spillage if safe to do so.
Methods and material for containment and cleaning up:	Pick up free solid for recycle and/or disposal.
Reference to other sections:	See sections 8 and 13 for additional information.

7. Handling and Storage:

Precautions for safe handling:	Provide adequate ventilation. Observe good industrial hygiene practices. Wear appropriate personal protective equipment. Contact with heated material may cause thermal burns. Wash thoroughly after handling.
	Refer to Processing Guide and/or contact your local Technical Service representative for melt processing temperature range. For most thermoplastic polyurethanes, melt processing is in the range of 177 - 232 deg. C (350 - 450 deg. F), however, some products may process at different temperatures. Heating above the maximum handling temperature can generate hazardous decomposition products (see Section 10).
	Fume condensates may include hazardous contaminants from additives. Condensate may be combustible and should be periodically removed from exhaust hoods, ductwork, and other surfaces. Impervious gloves should be worn during cleanup operations to prevent skin contact.
	Post thermal processing activities necessary to produce molded articles (such as cutting, sanding, sawing, grinding, drilling, or regrinding) may create dust or "fines." Powders, dust, and/or fines may pose a dust explosion hazard. Avoid breathing dust.
	Loading and unloading operations may cause nuisance dust to form. Electrostatic buildup may occur when pouring or transferring this product from its container. The spark produced may be sufficient to ignite vapors of flammable liquids. Always transfer product by means which avoid static buildup. Avoid pouring product directly from its container into combustible or flammable solvent.
	Conduct any operations emitting fumes or vapors (including thermo-forming, heat joining, cutting and or sealing of articles and clean up) under well-ventilated conditions. Avoid breathing process vapors. Do not hold product for extended periods of time at elevated temperatures or allow thick masses of hot polymer to accumulate because they can decompose emitting hazardous gasses. Do not taste, swallow, or chew products. Wash thoroughly after processing. Do not store or consume food in processing areas. The major off-gasses from normal melt processing are expected to be water vapor and carbon dioxide. Other trace volatile organic components may also be emitted.
Maximum Handling Temperature:	260 °C

Conditions for safe storage, including any incompatibilities:	Store away from incompatible materials. See section 10 for incompatible materials. Store in dry, well ventilated place away from sources of heat and direct sunlight.
Maximum Storage Temperature:	Not determined.

8. Exposure Controls/Personal Protection

Control Parameters:

Occupational Exposure Limits

Chemical name	Type	Exposure Limit Values	Source
Barium sulfate	TWA	10 mg/m3	US. ACGIH Threshold Limit Values (03 2013)

Appropriate engineering controls:	Thermal processing operations should be ventilated to control gases and fumes given off during processing.

Individual protection measures, such as personal protective equipment

General information:	Use personal protective equipment as required.
Eye/face protection:	If contact is likely, safety glasses with side shields are recommended.
Skin protection	
Hand Protection:	Suitable gloves can be recommended by the glove supplier. To avoid burns from contact with molten product, use thermal insulating gloves.
Other:	Long sleeve shirt is recommended.
Respiratory Protection:	Consult with an industrial hygienist to determine the appropriate respiratory protection for your specific use of this material. A respiratory protection program compliant with all applicable regulations must be followed whenever workplace conditions require the use of a respirator. Under normal use conditions, respirator is not usually required. Use appropriate respiratory protection if exposure to dust particles, mist or vapors is likely. Cutting operations may create small particles from this product. If inhalation of particles cannot be avoided, wear a dust respirator.
Hygiene measures:	Always observe good personal hygiene measures, such as washing after handling the material and before eating, drinking, and/or smoking. Routinely wash work clothing to remove contaminants. Discard contaminated footwear that cannot be cleaned.

9. Physical and Chemical Properties

Information on basic physical and chemical properties

Appearance

Physical state:	solid
Form:	Pellets
Color:	White
Odor:	Slight
Odor Threshold:	No data available.
pH:	No data available.
Melting Point:	No data available.

Boiling Point:	No data available.
Flash Point:	Not applicable.
Evaporation Rate:	No data available.
Flammability (solid, gas):	No data available.
Upper/lower limit on flammability or explosive limits	
Flammability Limit - Upper (%):	No data available.
Flammability Limit - Lower (%):	No data available.
Vapor pressure:	No data available.
Vapor density (air=1):	No data available.
Relative density:	1 - 1,1 (20 °C)
Solubility(ies)	
Solubility in Water:	No data available.
Solubility (other):	No data available.
Partition coefficient (n-octanol/water):	No data available.
Autoignition Temperature:	No data available.
Decomposition Temperature:	No data available.
Viscosity:	No data available.
Explosive properties:	No data available.
Oxidizing properties:	No data available.
Pour Point Temperature	No data available.

10. Stability and Reactivity

Reactivity:	No data available.
Chemical Stability:	Material is stable under normal conditions.
Possibility of hazardous reactions:	Will not occur.
Conditions to avoid:	None known.
Incompatible Materials:	None known, avoid contact with reactive chemicals.
Hazardous Decomposition Products:	Thermal decomposition or combustion may liberate carbon oxides and other toxic gases or vapors. Nitrogen Oxides Alkyl mercaptans and sulfides may also be released. May also include isocyanates and small amounts of hydrogen cyanide.

11. Toxicological Information

Information on likely routes of exposure

Inhalation:	No data available.
Ingestion:	No data available.
Skin Contact:	No data available.
Eye contact:	No data available.

Information on toxicological effects

Acute toxicity

Oral
Product: Not classified for acute toxicity based on available data.

Dermal
Product: Not classified for acute toxicity based on available data.

Inhalation
No data available

Skin Corrosion/Irritation:
Product: Not classified as a primary skin irritant.

Serious Eye Damage/Eye Irritation:
Product: Remarks: Not classified as a primary eye irritant.

Respiratory sensitization:
No data available

Skin sensitization:
No data available

Specific Target Organ Toxicity - Single Exposure:
No data available

Aspiration Hazard:
No data available

Chronic Effects
Carcinogenicity:
No data available

Germ Cell Mutagenicity:
No data available

Reproductive toxicity:
No data available

Specific Target Organ Toxicity - Repeated Exposure:
Product: Prolonged inhalation of high levels of barium sulfate dust may cause lung damage resulting in a benign pneumoconiosis.

12. Ecological Information

Ecotoxicity
Fish
No data available

Aquatic Invertebrates
No data available

Toxicity to Aquatic Plants
No data available

Toxicity to soil dwelling organisms

No data available

Sediment Toxicity

No data available

Toxicity to Terrestrial Plants

No data available

Toxicity to Above-Ground Organisms

No data available

Toxicity to microorganisms

No data available

Persistence and Degradability
Biodegradation

No data available

Bioaccumulative Potential
Bioconcentration Factor (BCF)

No data available

Partition Coefficient n-octanol / water (log Kow)
No data available

Mobility:

No data available

Other Adverse Effects: No data available.

13. Disposal Considerations

Disposal methods: Treatment, storage, transportation, and disposal must be in accordance
with applicable Federal, State/Provincial, and Local regulations.
Since emptied containers retain product residue, follow label warnings even
after container is emptied.

Contaminated Packaging: Container packaging may exhibit hazards.

14. Transport Information

IATA
  Not regulated.

International standards
IMDG
  Not regulated.

Transport in bulk according to Annex II of MARPOL and the IBC Code
  None known.

Shipping descriptions may vary based on mode of transport, quantities, temperature of the material, package size, and/or origin and destination. It is the responsibility of the transporting organization to follow all applicable laws, regulations and rules relating to the transportation of the material. For transportation, steps must be taken to prevent load shifting or materials falling, and all relating legal statutes should be obeyed. Review classification requirements before shipping materials at elevated temperatures.

15. Regulatory Information

15.1 Safety, health and environmental regulations/legislation specific for the substance or mixture:

Inventory Status

Australia (AICS)
This product contains a substance that is not listed on the Australia Inventory of Chemical Substances.

Canada (DSL/NDSL)
Requires notification in Canada. Research and development samples must comply with CEPA R&D requirements.

China (IECSC)
This product contains a substance or polymer that has been notified and is restricted to import by the notifier.

European Union (REACh)
To obtain information on the REACH compliance status of this product, please e-mail REACH@SDSInquiries.com.

Japan (ENCS)
All components are in compliance with the Chemical Substances Control Law of Japan.

Korea (ECL)
All components are in compliance in Korea.

New Zealand (NZIoC)
This product requires notification before sale in New Zealand.

Philippines (PICCS)
All components are in compliance with the Philippines Toxic Substances and Hazardous and Nuclear Wastes Control Act of 1990 (R.A. 6969).

Switzerland (SWISS)
All components are in compliance with the Environmentally Hazardous Substances Ordinance in Switzerland.

Taiwan (TCSCA)
All components of this product are listed on the Taiwan inventory.

United States (TSCA)
All substances contained in this product are in compliance with section 5 of TSCA or are exempt. This product contains one or more polymers manufactured under the polymer exemption rule.

The information that was used to confirm the compliance status of this product may deviate from the chemical information shown in Section 3.

16. Other Information

Key literature references and sources for data: Internal company data and other publically available resources.

HMIS Hazard ID

Health	0
Flammability	1
Physical Hazards	0

Hazard rating: 0 - Minimal; 1 - Slight; 2 - Moderate; 3 - Serious; 4 - Severe; RNP - Rating not possible; *Chronic health effect

NFPA Hazard ID

■ Flammability
■ Health
■ Reactivity
□ Special hazard.
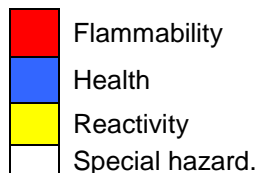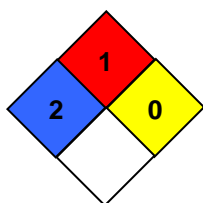
Hazard rating: 0 - Minimal; 1 - Slight; 2 - Moderate; 3 - Serious; 4 - Severe; RNP - Rating not possible

Issue Date: 24.05.2018

Disclaimer: As the conditions or methods of use are beyond our control, we do not assume any responsibility and expressly disclaim any liability for any use of this product. Information contained herein is believed to be true and accurate but all statements or suggestions are made without warranty, expressed or implied, regarding accuracy of the information, the hazards connected with the use of the material or the results to be obtained from the use thereof. Compliance with all applicable federal, state, and local regulations remains the responsibility of the user.

Carbothane® Aliphatic TPU B20 Series

Type: Radiopaque Grades – 20% loading of Barium Sulfate

Features: Medical Grade Aliphatic Polycarbonate-based TPUs which do not yellow, with excellent oxidative stability, good mechanical properties, very good chemical resistance, radiopacity and can be color-matched

Process: Extrusion, Injection Molding or Solution

Products & Properties	ASTM Test	PC-3575A-B20	PC-3585A-B20	PC-3595A-B20	PC-3555D-B20	PC-3572D-B20
Durometer (Shore Hardness)	D2240	75A	80A	92A	52D	71D
Specific Gravity	D792	1.35	1.35	1.35	1.35	1.35
Ultimate Tensile (psi)	D412	7200	8700	9400	9400	9200
Ultimate Elongation (%)	D412	530	410	400	375	300
Tensile (psi)	D412					
at 100% Elongation		300	800	1200	1975	3800
at 200% Elongation		625	1500	2050	3000	5000
at 300% Elongation		1450	4100	4900	6400	8800
Flexural Modulus (psi)	D790	2000	2200	6800	22,000	135,000
Vicat Softening Point (°C)	D1525	47	56	53	57	63
Mold Shrinkage (in/in) (1"x.25"x6" bar)	D955	0.010	0.010	0.010	0.008	0.008

Note: These test results are based on small samples of Tecothane® polyurethanes and do not necessarily represent average results from larger test samples. This information should not be used for establishing engineering or manufacturing guidelines.

Rev. 20160826 (ALL)

Handling Conditions:
Properties of all thermoplastic polyurethane products in the molten state are adversely affected by moisture. For the best results, always dry the material at least two hours at 65°C (150°F) or overnight at 57°C (135°F) in a machine mounted dehumidifying dryer (a desiccant dryer delivering air at 1 liter/sec/kg at -40°C dew point (1 cfm/lb at -40°F dew point). A dehumidifying dryer hopper or one shot loader is also recommended. Depending on the applied processing technique, the maximum moisture level should be 0.05%. Never to exceed 500°F (260°C) melt.

Processing Conditions:
Carbothane® Aliphatic TPU's can be processed on any conventional extruder or molder.

Recommended Starting <u>Extrusion</u> Temperature Profile:
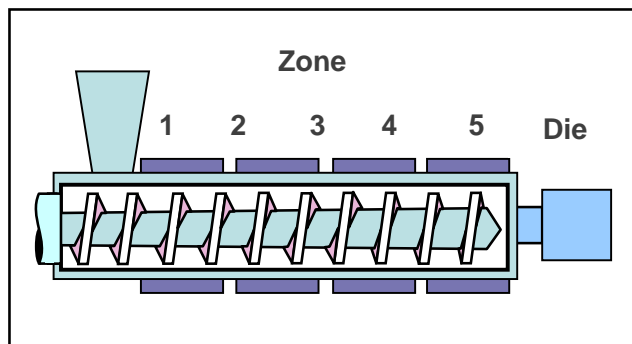
	PC-3575A-B20	PC-3585A-B20	PC-3595A-B20	PC-3555D-B20	PC-3572D-B20
	°F/°C	°F/°C	°F/°C	°F/°C	°F/°C
Zone 1	360/182	360/182	360/182	380/193	380/193
Zone 2	370/188	370/188	370/188	390/199	390/199
Zone 3	380/193	380/193	380/193	400/204	400/204
Zone 4	390/199	390/199	390/199	410/210	410/210
Adapter 5	400/204	400/204	400/204	420/216	420/216
Die	400/204	400/204	400/204	420/216	420/216

Recommended Starting Injection Molding Temperature Profile:
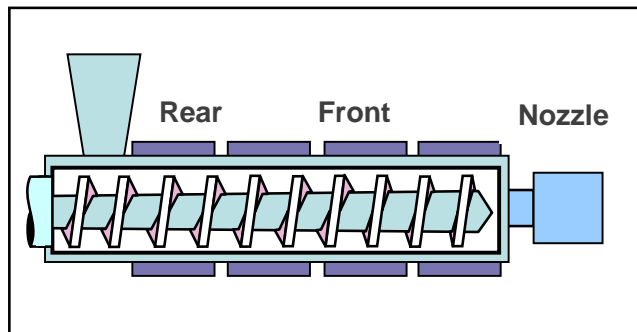
	PC-3575A-B20	PC-3585A-B20	PC-3595A-B20	PC-3555D-B20	PC-3572D-B20
	°F/°C	°F/°C	°F/°C	°F/°C	°F/°C
Rear	392/200	392/200	392/200	410/210	428/220
Front	410/210	410/210	410/210	428/220	446/230
Nozzle	428/220	428/220	428/220	446/230	464/240
Melt	410/210	410/210	410/210	428/220	446/230
Mold	50-80/10-27	50-80/10-27	50-80/10-27	50-100/10-38	60-110/16-43

For Further information, refer to Lubrizol Advanced Materials processing guides.

Sigma–Aldrich®

www.sigmaaldrich.com

Version 6.2
Revision Date 07.10.2020
Print Date 12.04.2021
GENERIC EU MSDS - NO COUNTRY SPECIFIC DATA - NO OEL DATA

SAFETY DATA SHEET
according to Regulation (EC) No. 1907/2006

SECTION 1: Identification of the substance/mixture and of the company/undertaking

1.1 Product identifiers

Product name : Phosphate buffered saline

Product Number : P4417
Brand : Sigma
REACH No. : A registration number is not available for this substance as the substance or its uses are exempted from registration, the annual tonnage does not require a registration or the registration is envisaged for a later registration deadline.

1.2 Relevant identified uses of the substance or mixture and uses advised against

Identified uses : Laboratory chemicals, Manufacture of substances

1.3 Details of the supplier of the safety data sheet

Company : Sigma-Aldrich Sweden AB
Solkraftsvagen 14C
SE-135 70 STOCKHOLM

Telephone : +46 08 742-4200
Fax : +46 08 742-4243
E-mail address : TechnicalService@merckgroup.com

1.4 Emergency telephone

Emergency Phone # : +(46)-852503403 (CHEMTREC)
Vid akut fara för liv, egendom eller miljö -
112

SECTION 2: Hazards identification

2.1 Classification of the substance or mixture

Not a hazardous substance or mixture according to Regulation (EC) No 1272/2008.

2.2 Label elements

Not a hazardous substance or mixture according to Regulation (EC) No 1272/2008.

2.3 Other hazards
This substance/mixture contains no components considered to be either persistent, bioaccumulative and toxic (PBT), or very persistent and very bioaccumulative (vPvB) at levels of 0.1% or higher.

SECTION 3: Composition/information on ingredients

3.2 Mixtures

Synonyms   :   PBS

No components need to be disclosed according to the applicable regulations.

SECTION 4: First aid measures

4.1 Description of first-aid measures

If inhaled
After inhalation: fresh air.

In case of skin contact
In case of skin contact: Take off immediately all contaminated clothing. Rinse skin with water/ shower.

In case of eye contact
After eye contact: rinse out with plenty of water. Remove contact lenses.

If swallowed
After swallowing: make victim drink water (two glasses at most). Consult doctor if feeling unwell.

4.2 Most important symptoms and effects, both acute and delayed
The most important known symptoms and effects are described in the labelling (see section 2.2) and/or in section 11

4.3 Indication of any immediate medical attention and special treatment needed
No data available

SECTION 5: Firefighting measures

5.1 Extinguishing media

Suitable extinguishing media
Use extinguishing measures that are appropriate to local circumstances and the surrounding environment.

Unsuitable extinguishing media
For this substance/mixture no limitations of extinguishing agents are given.

5.2 Special hazards arising from the substance or mixture
Oxides of phosphorus, Hydrogen chloride gas, Potassium oxides, Sodium oxides
Oxides of phosphorus, Hydrogen chloride gas, Potassium oxides, Sodium oxides
Not combustible.
Ambient fire may liberate hazardous vapours.

5.3 Advice for firefighters
In the event of fire, wear self-contained breathing apparatus.

5.4 Further information
Suppress (knock down) gases/vapors/mists with a water spray jet. Prevent fire extinguishing water from contaminating surface water or the ground water system.

SECTION 6: Accidental release measures

6.1 Personal precautions, protective equipment and emergency procedures
Advice for non-emergency personnel: Avoid inhalation of dusts. Evacuate the danger area, observe emergency procedures, consult an expert.
For personal protection see section 8.

6.2 Environmental precautions
Do not let product enter drains.

6.3 Methods and materials for containment and cleaning up
Cover drains. Collect, bind, and pump off spills. Observe possible material restrictions (see sections 7 and 10). Take up dry. Dispose of properly. Clean up affected area. Avoid generation of dusts.

6.4 Reference to other sections
For disposal see section 13.

SECTION 7: Handling and storage

7.1 Precautions for safe handling
For precautions see section 2.2.

7.2 Conditions for safe storage, including any incompatibilities
No data available

7.3 Specific end use(s)
Apart from the uses mentioned in section 1.2 no other specific uses are stipulated

SECTION 8: Exposure controls/personal protection

8.1 Control parameters

Ingredients with workplace control parameters

8.2 Exposure controls

Appropriate engineering controls
Change contaminated clothing. Wash hands after working with substance.

Personal protective equipment

Eye/face protection
Use equipment for eye protection tested and approved under appropriate government standards such as NIOSH (US) or EN 166(EU). Safety glasses

Skin protection
This recommendation applies only to the product stated in the safety data sheet, supplied by us and for the designated use. When dissolving in or mixing with other substances and under conditions deviating from those stated in EN374 please contact the supplier of CE-approved gloves (e.g. KCL GmbH, D-36124 Eichenzell, Internet: www.kcl.de).

Full contact
Material: Nitrile rubber
Minimum layer thickness: 0,11 mm
Break through time: 480 min
Material tested:KCL 741 Dermatril® L

Splash contact
Material: Nitrile rubber
Minimum layer thickness: 0,11 mm
Break through time: 480 min
Material tested:KCL 741 Dermatril® L

Respiratory protection
required when dusts are generated.
Our recommendations on filtering respiratory protection are based on the following
standards: DIN EN 143, DIN 14387 and other accompanying standards relating to
the used respiratory protection system.

Control of environmental exposure
Do not let product enter drains.

SECTION 9: Physical and chemical properties

9.1 Information on basic physical and chemical properties

a)	Appearance	Form: solid
b)	Odor	No data available
c)	Odor Threshold	No data available
d)	pH	7,2 - 7,6 at 25 °C
e)	Melting point/freezing point	No data available
f)	Initial boiling point and boiling range	No data available
g)	Flash point	Not applicable
h)	Evaporation rate	No data available
i)	Flammability (solid, gas)	The product is not flammable.
j)	Upper/lower flammability or explosive limits	No data available
k)	Vapor pressure	No data available
l)	Vapor density	No data available
m)	Relative density	No data available
n)	Water solubility	No data available
o)	Partition coefficient: n-octanol/water	No data available
p)	Autoignition temperature	Not applicable
q)	Decomposition temperature	No data available
r)	Viscosity	No data available

s) Explosive properties   No data available

t) Oxidizing properties   No data available

9.2 Other safety information
No data available

SECTION 10: Stability and reactivity

10.1 Reactivity
No data available

10.2 Chemical stability
The product is chemically stable under standard ambient conditions (room temperature) .

10.3 Possibility of hazardous reactions
No data available

10.4 Conditions to avoid
no information available

10.5 Incompatible materials
Strong oxidizing agents, Strong acids

10.6 Hazardous decomposition products
Hazardous decomposition products formed under fire conditions. - Oxides of phosphorus,
Hydrogen chloride gas, Potassium oxides, Sodium oxides
Other decomposition products - No data available
Hazardous decomposition products formed under fire conditions. - Oxides of phosphorus,
Hydrogen chloride gas, Potassium oxides, Sodium oxides
In the event of fire: see section 5

SECTION 11: Toxicological information

11.1 Information on toxicological effects

Acute toxicity
No data available

Dermal: No data available

Skin corrosion/irritation
No data available

Serious eye damage/eye irritation
No data available

Respiratory or skin sensitization
No data available

Germ cell mutagenicity
No data available

Carcinogenicity

IARC: No ingredient of this product present at levels greater than or equal to 0.1% is
identified as probable, possible or confirmed human carcinogen by IARC.

Reproductive toxicity
No data available

Specific target organ toxicity - single exposure
No data available

Specific target organ toxicity - repeated exposure
No data available

Aspiration hazard
No data available

Additional Information
RTECS: Not available

Vomiting, Diarrhea, Dehydration and congestion may occur in internal organs. Hypertonic salt solutions can produce inflammatory reactions in the gastrointestinal tract., To the best of our knowledge, the chemical, physical, and toxicological properties have not been thoroughly investigated.

Hazardous properties cannot be excluded but are unlikely when the product is handled appropriately.

SECTION 12: Ecological information

12.1 Toxicity
No data available

12.2 Persistence and degradability
No data available

12.3 Bioaccumulative potential
No data available

12.4 Mobility in soil
No data available

12.5 Results of PBT and vPvB assessment
This substance/mixture contains no components considered to be either persistent, bioaccumulative and toxic (PBT), or very persistent and very bioaccumulative (vPvB) at levels of 0.1% or higher.

12.6 Other adverse effects
No data available

SECTION 13: Disposal considerations

13.1 Waste treatment methods

Product
See www.retrologistik.com for processes regarding the return of chemicals and containers, or contact us there if you have further questions.

SECTION 14: Transport information

14.1 UN number
ADR/RID: -　　　　　　　IMDG: -　　　　　　　IATA: -

14.2 UN proper shipping name

ADR/RID: Not dangerous goods
IMDG: Not dangerous goods
IATA: Not dangerous goods

14.3 Transport hazard class(es)

ADR/RID: -   IMDG: -   IATA: -

14.4 Packaging group

ADR/RID: -   IMDG: -   IATA: -

14.5 Environmental hazards

ADR/RID: no   IMDG Marine pollutant: no   IATA: no

14.6 Special precautions for user

Further information
Not classified as dangerous in the meaning of transport regulations.

SECTION 15: Regulatory information

15.1 Safety, health and environmental regulations/legislation specific for the substance or mixture

This material safety data sheet complies with the requirements of Regulation (EC) No. 1907/2006.

15.2 Chemical Safety Assessment

For this product a chemical safety assessment was not carried out

---

SECTION 16: Other information

Further information
The above information is believed to be correct but does not purport to be all inclusive and shall be used only as a guide. The information in this document is based on the present state of our knowledge and is applicable to the product with regard to appropriate safety precautions. It does not represent any guarantee of the properties of the product. Sigma-Aldrich Corporation and its Affiliates shall not be held liable for any damage resulting from handling or from contact with the above product. See www.sigma-aldrich.com and/or the reverse side of invoice or packing slip for additional terms and conditions of sale.

Copyright 2020 Sigma-Aldrich Co. LLC. License granted to make unlimited paper copies for internal use only.
The branding on the header and/or footer of this document may temporarily not visually match the product purchased as we transition our branding. However, all of the information in the document regarding the product remains unchanged and matches the product ordered. For further information please contact mlsbranding@sial.com.

The life science business of Merck operates as MilliporeSigma in the US and Canada

Appendix B

Substrate Cleaning Procedure

The following procedure for cleaning the medical grad polyurethane (Carbothane) substrates was developed by PhD Candidate Maren K. Fossum affiliated at the Department of Materials Science and Engineering at NTNU in Trondheim to reduce the effect of extrinsic impurities as much as possible [58]. This reduces the uncertainty of the experiments and ensures reliable and reproducible results [14]. All substrates used throughout the work with this Thesis were cleaned according to the procedure before further processing and/or characterization.

The substrates were completely emerged for at least 30 seconds in five different beakers containing distilled water and ethanol of 96% and 70% concentrations. To avoid further contamination, nitrile gloves were worn, and thoroughly cleaned tweezers and metal spoons were used to transfer the substrates between the beakers. The further details of the procedure are presented in Table B.1. The last two steps were employed to wash away all remaining ethanol as it is known to degrade polyurethane materials [135]. The metal spoons and tweezers were changed between beaker 3 and 4 to transfer as little ethanol as possible to the final beakers filled with distilled water. However, it is unlikely that any remaining ethanol would affect this specific polyurethane material greatly as it has been shown that Carbothane does not shows signs of degradation even after being emerged in 70% ethanol for over 24 hours [136].

Following the cleaning, the substrates were transferred onto laboratory grade aluminum foil and left to dry in a fume hood for 2 hours. They were then stored in plastic sample boxes with separate compartments for each sample. These sample boxes had also been thoroughly cleaned with soap, ethanol and distilled water.

Table B.1: The cleaning procedure used when cleaning the substrates before further processing and characterization.

Beaker	Beaker Content	Purpose of Cleaning Step	Comments
1	Distilled Water	Remove loosely attached surface contamination	Content replaced for every 5th substrate
2	96% Ethanol	Remove grease contamination or compounds leached from the polymer	Content replaced for every 5th substrate
3	70% Ethanol	Sterilization	Content replaced for every 5th substrate
4	Distilled Water	Wash away remaining ethanol	Content replaced for every 2nd substrate
5	Distilled Water	Wash away remaining ethanol	Content replaced for every 2nd substrate

Appendix C

Measurement of Gold Coater Sputter Rate

To find the thickness of the conductive gold coating deposited on the samples before SEM-analyzes, three silicon wafers were covered with a piece of tape across the center. They were then coated using an Edwards Sputter Coater S150B for 5 minutes with the coating parameters otherwise equal to that used for the SEM sample preparation technique (*i.e.*, 18 kV, 20 mA, 0.15 atm Ar pressure).

The tape was then removed from the wafers, which created steps between the coated and non-coated sections of the surface. The height of this step was measured in NanoLab using a Veeco Dektak 150 with a 12.5 μm tip radius, a scan length of 1000 μm, a scan time of 30 s and a hills and valleys profile. At least three measurements were performed on each side of the previously taped areas for each of the three samples, and the results are presented in Table C.1. The resulting coating rate is thus 0.20 ± 0.04 nm/s and the coating thickness 3.9 ± 0.7 nm for the coating applied to the samples before SEM analyzes.

Table C.1: The average thickness of the gold coating as measured by the Veeco Dektak 150 in NanoLab at NTNU.

Sample	Average Coating Thickness
1	61 ± 10 nm
2	59 ± 11 nm
3	57 ± 11 nm
Average	59 ± 11 nm

Appendix D

Factors Affecting Contact Angle Measurements

D.1   Effect of Orientation of Directional Lines

While performing contact angle measurements, an asymmetrical drop shape was observed on the samples with the thinner substrates. The asymmetry was expected to be due to the surface roughness caused by the directional lines found in these substrates, and the asymmetrical drop behavior is illustrated in Figure D.1. The drops are elongated in the direction parallel to the directional lines. Thus, measurements were performed to confirm whether the orientation of the directional lines affected the measured contact angle values.
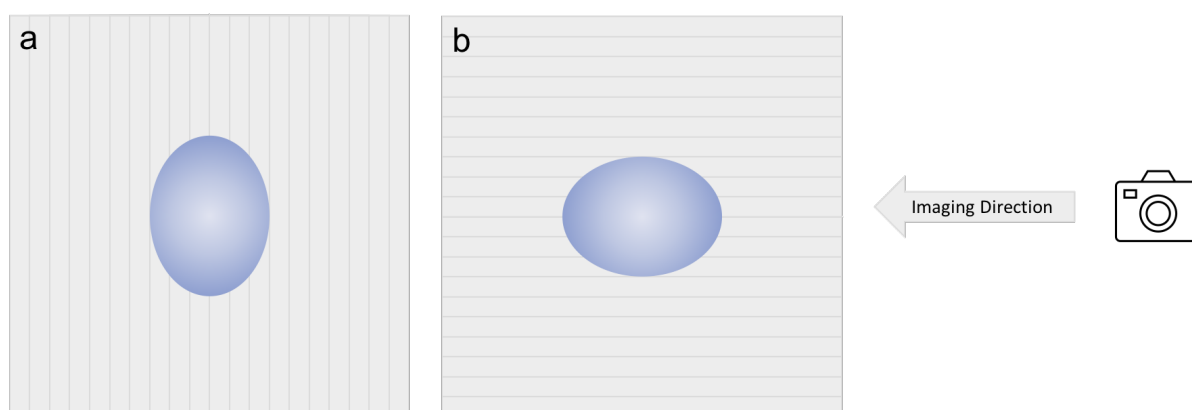
Figure D.1: The deposited drop showed asymmetrical behavior based on the orientation of the directional lines. The drops are elongated in the direction parallel to the directional lines. Measurements were performed to determine if the contact angle measurements depend on whether the directional lines are oriented (a) perpendicular or (b) parallel to the imaging direction.

Four non-coated reference substrates were analyzed. For each sample, three drops were

deposited with the directional lines oriented perpendicular and parallel to the imaging direction respectively. To check if the dependence also applied to the coated substrates, samples coated with coating TiN (C) and DLC were analyzed with both orientations represented with at least two samples. At least three drops were deposited on each sample. The resulting measurements are presented in Figure D.2.

All samples with directional lines oriented parallel to the imaging direction showed significantly higher contact angle values than the drops deposited on the same samples oriented in the other direction. The average difference between the two orientations is $15° \pm 4°$ for non-coated reference substrates, $18° \pm 5°$ for samples coated with TiN (C) and $10° \pm 5°$ for samples coated with DLC as seen in Table D.1. Thus, it is crucial to use the same orientation for all measurements to get comparable results between samples. All measurements on the thinner substrates have therefore been performed with the directional lines oriented parallel to the imaging direction. Asymmetrical drop behavior was not observed on the thicker substrates, and therefore such measurements were not performed on those substrates.
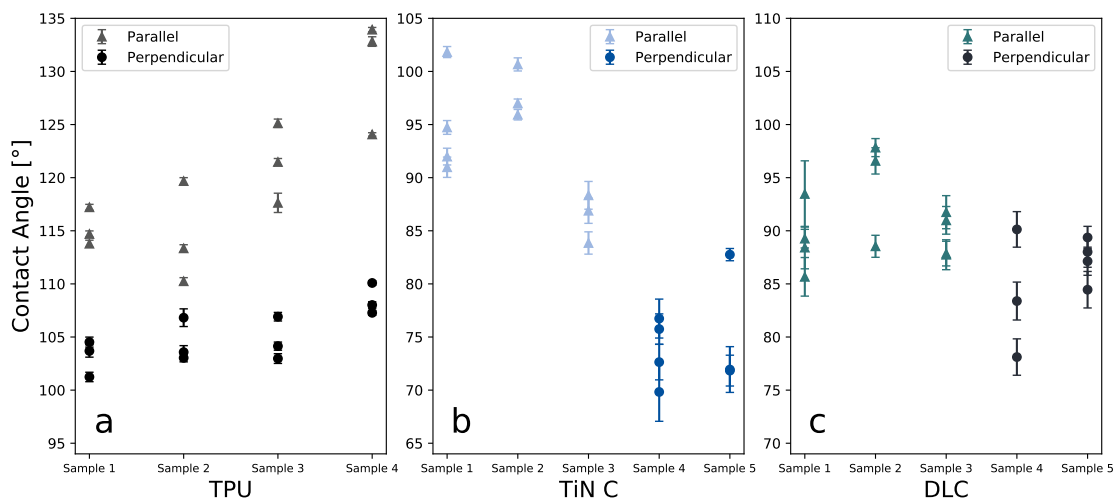
Figure D.2: The contact angles of the drops deposited on the (a) non-coated thinner reference substrates, (b) samples coated with coating TiN (C), and (c) DLC. The samples were oriented with the directional lines parallel or perpendicular to the imaging direction.

Table D.1: The contact angles with water of the non-coated reference substrate, and samples coated with coating TiN (C) and DLC at 25°C and 50% humidity depending on the orientation of the directional lines in the substrate. The contact angle values for the TiN (C) and DLC coated samples with the directional lines perpendicularly orientated to the imaging direction are only based on two samples.

Orientation of Directional Lines	Parallel to Imaging Direction	Perpendicular to Imaging Direction	Average Difference
TPU	$120.3° \pm 3.4°$	$105.2° \pm 1.6°$	$15° \pm 4°$
TiN (C)	$93.0° \pm 3.0°$	$74.6° \pm 4.47°$	$18° \pm 5°$
DLC	$96.6° \pm 3.4°$	$86.7° \pm 3.4°$	$10° \pm 5°$

D.2 Effect of Temperature

As the material is intended for use in the human body, which holds 37°C, contact angle measurements were also performed at this temperature to determine if the increased temperature gives a significant change in the wetting properties. The non-coated thinner substrates were used as a reference to determine a potential difference. Three samples were analyzed with three drops at 25°C and 37°C respectively. The humidity was kept constant at 50%. Between the measurements performed at the two different temperatures, the samples were stored in a desiccator for 10 days to ensure that the surfaces were completely dry prior to analysis. The results are presented in Table D.2. As the average differences are lower than the corresponding standard deviations, no statistically significant difference has been found between measurements at the two temperatures.

Table D.2: The average contact angles of the thinner non-coated reference substrates measured at 25°C and 37°C as well as the average difference between the two temperatures. The humidity was kept at 50% for all measurements.

Orientation of Directional Lines	25°C	37°C	Average Difference
Parallel to Imaging Direction	$117° \pm 3°$	$118° \pm 7°$	$-0.6° \pm 7°$
Perpendicular to Imaging Direction	$104° \pm 2°$	$102° \pm 3°$	$2° \pm 3°$

Appendix E

Developing a Scratch Testing Procedure

Coating adhesion and cohesion were early identified as key coating properties, and scratch testing was identified as a key method for testing them. However, not much literature was found on a procedure for scratch testing soft substrates with a hard coating of nanometer-scaled thickness. Thus, the work of developing such a method began as part of the present author Specialization Project. The following methods and results are not without limitations and work remains on developing a method that gives reliable and reproducible quantitative results. Despite this, the following procedures and results are included as they give qualitative indications of the performance of coatings TiN (A) and B as well as the DLC coating. The work can also form a basis for developing an improved procedure for similar samples (*i.e.*, give indications on which equipment and scratching loads should be used).

E.1 SEM Analysis of Samples Scratch Tested During Specialization Project

During the present author's Specialization Project [10] samples coated with TiN coating A and B, as well as the non-coated samples were subjected to a scratching procedure. The load was linearly increasing from 1000 mN to 5000 mN over a 3 mm distance with a scratching speed of 2 mm per minute using an Anton Paar Micro Scratch Tester with a 100 μm radius Rockwell L-157 diamond indenter. However, it was not possible to conclude on the effects of this procedure based on the optical microscope built into the instrument as only magnifications of 5 X and 20 X were available. Thus, the surface morphology has been analyzed using a Zeiss Supra 55VP Low Vacuum Field Emission Scanning Electron Microscope (LVFESEM) after being stored in a closed plastic container for 56 to 57 days. The micrographs were secured through secondary electron analyses using the same

parameters as described in Section 3.4.1.

Three samples of each of the coatings and the non-coated reference substrate had been scratched, and several micrographs were taken at a chosen range of magnifications for each sample, *i.e.* at 50 000 X, 20 000 X, 10 000 X, 5000 X, 3000 X, 1000 X and 100 X, to ensure that the results were representative of the morphology in the scratched area. Micrographs with magnifications 10 000 X, 5000 X and 500 X were also taken of parts of the surfaces that were not affected by the scratch testing as a reference to ensure that the surface had not changed during the storage period. The micrographs most representative of the surfaces have been selected for the figures included in this section.

The thin film coatings showed significant cracking after being exposed to the scratching procedure, as can be seen in Figures E.1 and E.2. These micrographs also reveal that the non-coated substrates appear to have been plastically deformed. These findings are further supported by the micrographs in Figures E.3 and E.4 where the difference between the scratched areas and the non-affected surfaces can be seen. Though the coatings show brittle behavior, the coating-substrate adhesion appears to be excellent. The coatings are not removed from the surface, even when a force large enough to cause plastic deformation in the substrates is applied. As can be seen in Figure E.5 the impact to the surface is not trivial to identify even at 1 000 X magnification.
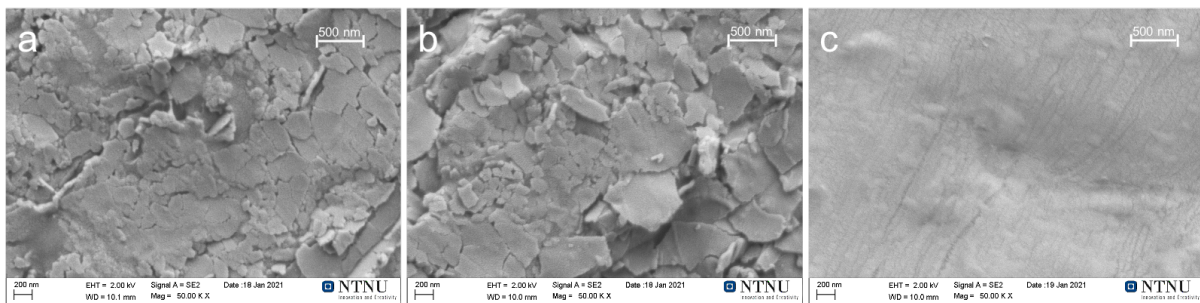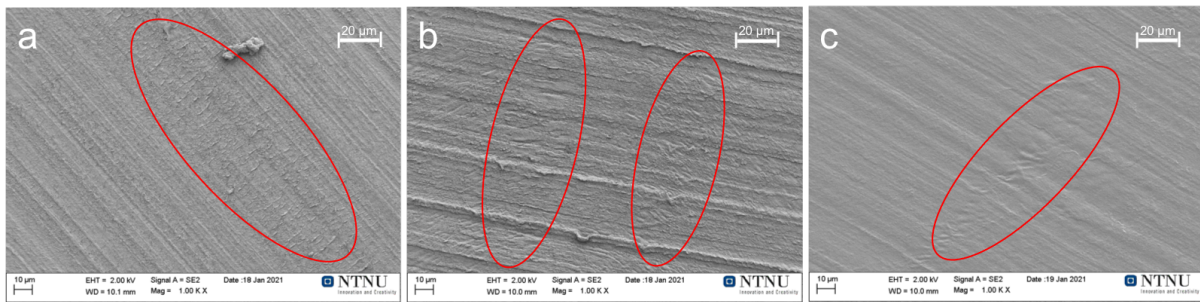

Figure E.1: SEM micrographs of the scratched area of samples with (a) coating TiN (A), (b) coating TiN (B) and (c) the non coated reference substrate imaged 50 000 X magnification. The samples were scratched with a load ranging from 1000 mN to 5000 mN.
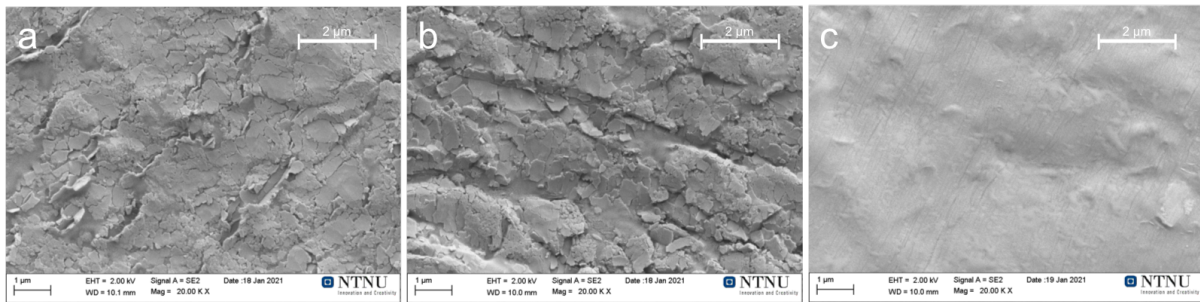
Figure E.2: SEM micrographs of the scratched area of samples with (a) coating TiN (A), (b) coating TiN (B) and (c) the non coated reference substrate imaged 20 000 X magnification. The samples were scratched with a load ranging from 1000 mN to 5000 mN.
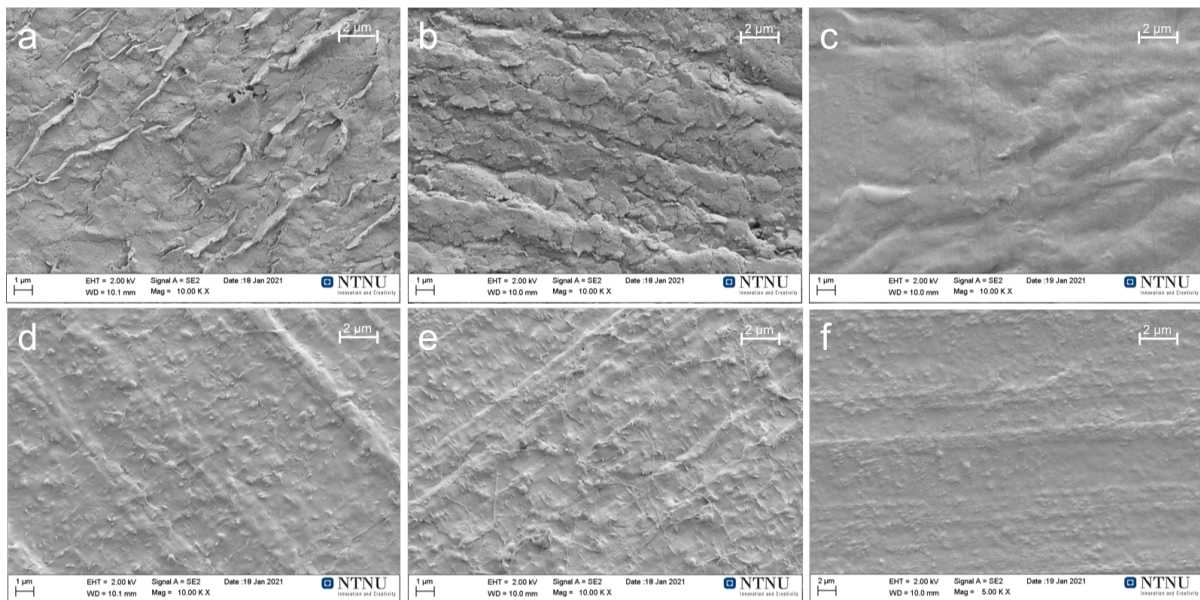
Figure E.3: SEM micrographs of the scratched area of samples with (a) coating TiN (A), (b) coating TiN (B) and (c) the non coated reference substrate. The unaffected surface of samples with (d) coating TiN (A), (e) coating TiN (B) and (f) the non-coated reference substrate. All micrographs are taken at 10 000 X magnification and the samples were scratched with a load ranging from 1000 mN to 5000 mN.
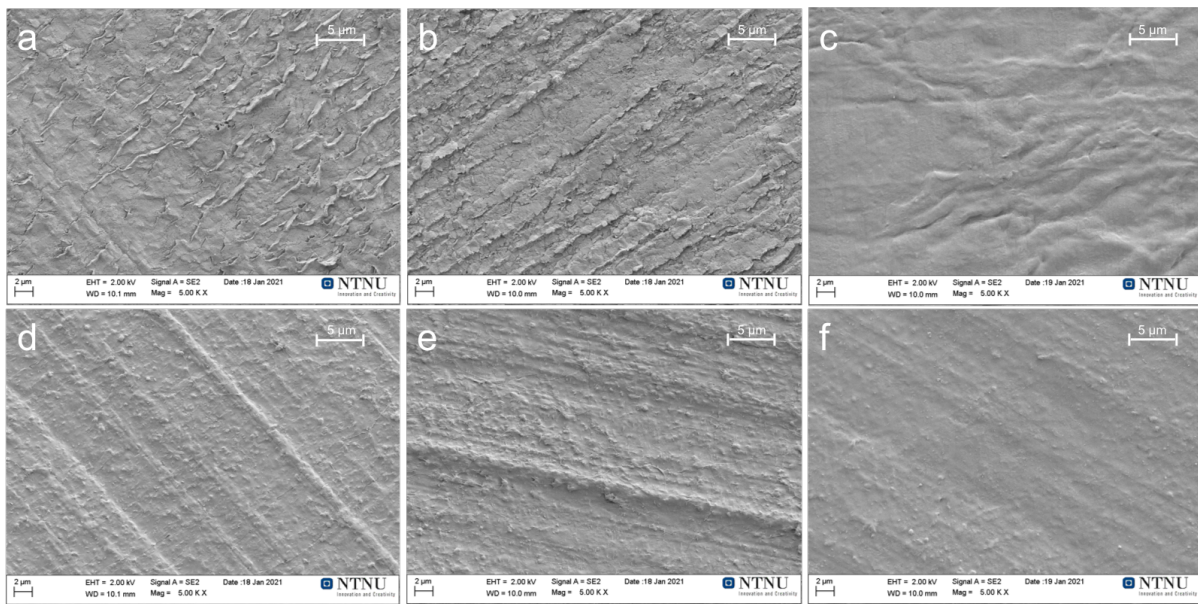
Figure E.4: SEM micrographs of the scratched area of samples with (a) coating TiN (A), (b) coating TiN (B) and (c) the non coated reference substrate. The unaffected surface of samples with (d) coating TiN (A), (e) coating TiN (B) and (f) the non-coated reference substrate. All micrographs are taken at 5 000 X magnification and the samples were scratched with a load ranging from 1000 mN to 5000 mN.

In the areas of the samples that have been imaged, coating TiN (B) appears to crack into slightly smaller flakes than coating TiN (A). However, one should be careful to draw strong conclusions from this as there is great uncertainty. First of all, the scratching load increased across the scratch, but it was not possible to confidently identify the area of the scratch where the highest load had been applied. Thus, it is possible that an averagely higher load had been applied to the areas of coating TiN (B). Secondly, some of the samples (with both coatings) showed several parallel scratches as seen for coating TiN (B) in Figure E.5. It was hypothesized that it could be due to tip damage, but investigations in light microscope confirmed that the tip was in good condition. The split scratch could also be due to cushioning effects in the substrate or the carbon tape that is used to attach the samples to the sample holder. Thus, a conclusion was not reached on what caused this phenomenon, but it is likely that these parallel scratches will differ in the true load applied to the coating.

Figure E.5: SEM micrographs of the scratched area of samples with (a) coating TiN (A), (b) coating TiN (B) and (c) the non coated reference substrate imaged 1 000 X magnification. The samples were scratched with a load ranging from 1000 mN to 5000 mN.

To reduce the possible effect of the substrate, to be more certain of the applied load in the analyzed area and to find the critical loads needed for the coatings to start cracking, a new approach was tried as described in the following section.

E.2 Micro Scratch Testing at Constant Load

E.2.1 Coatings TiN (A) and TiN (B)

The Anton Paar Micro Scratch Tester was used to scratch sample coated with coating TiN (A) and TiN (B) as well as the non-coated reference substrates at a constant load of 1000 mN. Otherwise, the same test conditions as above where used. Three samples of each surface were scratched at each load for statistical significance.

Figure E.6 shows the optical microscopy images from the microscope built into the scratch tester at 5 X magnification. The selected images are the most representative for each surface, but there were significant variations between samples in how visible the scratches were, though they were always more visible on the coated surfaces. It is believed that the damaged coatings gave the dark scratch, but that the deformation of the non-coated substrates was too insignificant to cause similar effects.
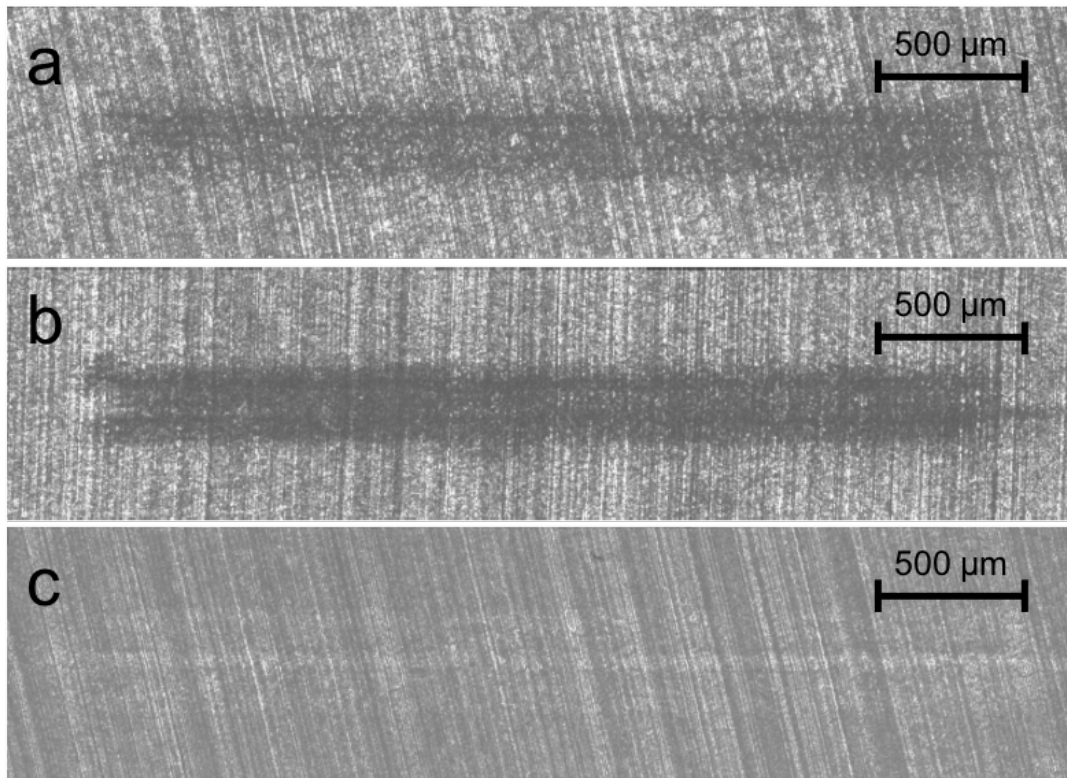
Figure E.6: Images retrieved with the built-in optical microscope at 5 X magnification of (a) coating TiN (A), (b) coating TiN (B) and (c) the non-coated substrate after scratch testing at 1000 mN constant load.

The samples were analyzed using SEM and the parameters described in Section 3.4.1. Unaffected areas were also imaged at 20 000 X, 10 000 X and 5 000 X magnification as a reference. Though the samples were cut into pieces of approximately 0.5 cm x 0.5 cm around the scratches to aid in identifying the scratched areas, it was not possible to confidently identify the scratched areas on any of the non-coated reference substrates. Thus, only micrographs of coating TiN (A) and TiN (B) are presented in the following figures. Figure E.7 (50 000 X magnification) reveals significant cracking in the coatings in the scratched areas, but that the coating does not appear to peel off the surface. Figures E.8 (20 000 X magnification), E.9 (10 000 X magnification), and E.10 (5 000 X magnification) also shows this tendency and compares the scratched areas to non-affected areas of the surface.
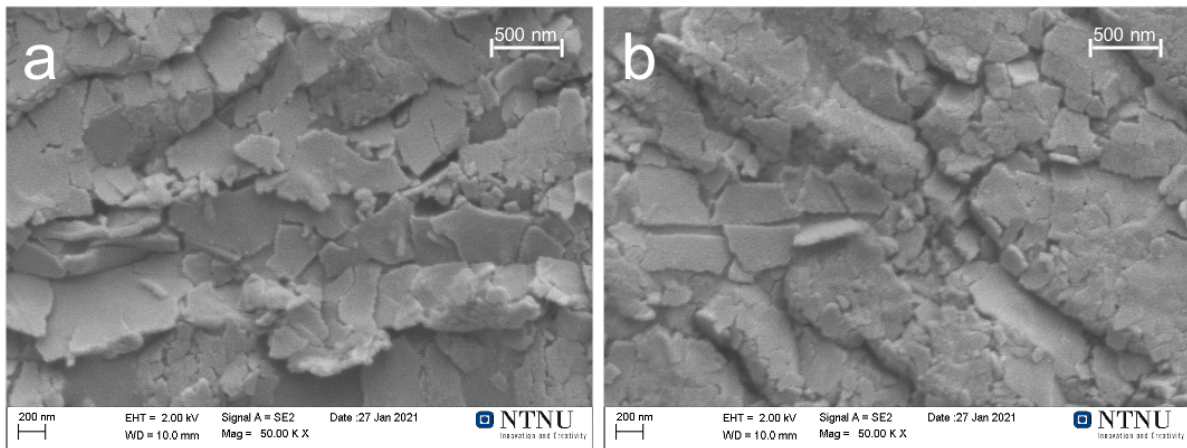
Figure E.7: SEM micrographs of coatings (a) TiN (A) and (b) TiN (B) scratched at a constant load of 1000 mN imaged at 50 000 X magnification.
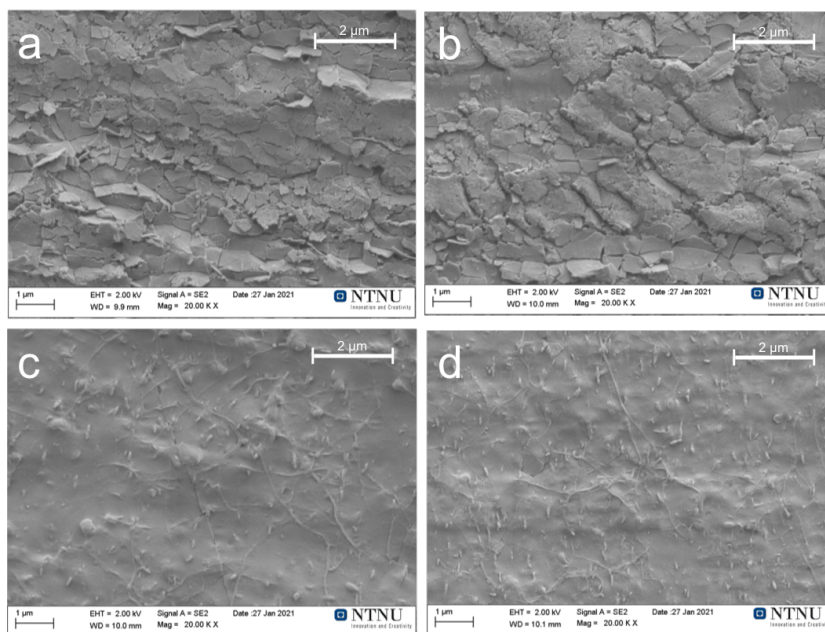
Figure E.8: SEM micrographs of coatings (a) TiN (A) and (b) TiN (B) scratched at a constant load of 1000 mN as well as the non-affected surface of (c) coating TiN (A) and (d) TiN (B) imaged at 20 000 X magnification.
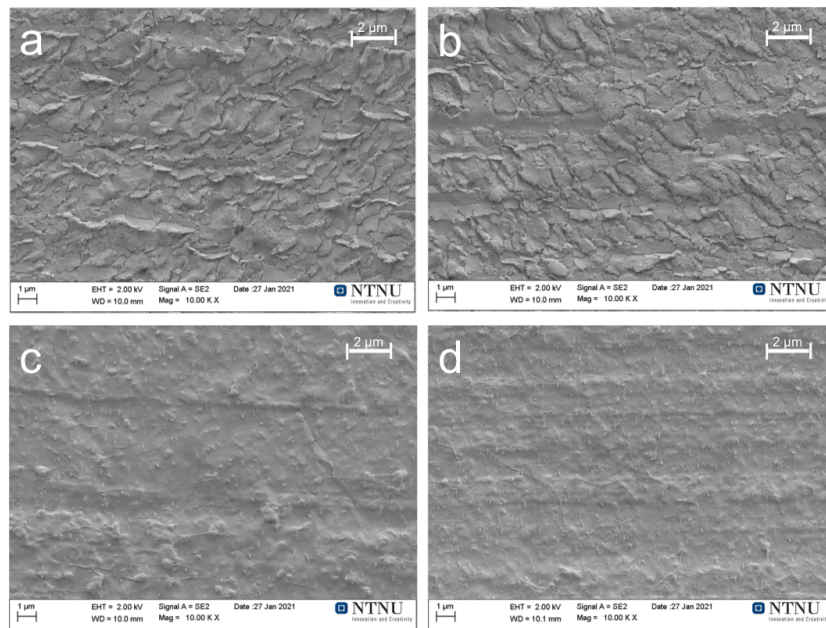
Figure E.9: SEM micrographs of coatings (a) TiN (A) and (b) TiN (B) scratched at a constant load of 1000 mN as well as the non-affected surface of (c) coating TiN (A) and (d) TiN (B) imaged at 10 000 X magnification.
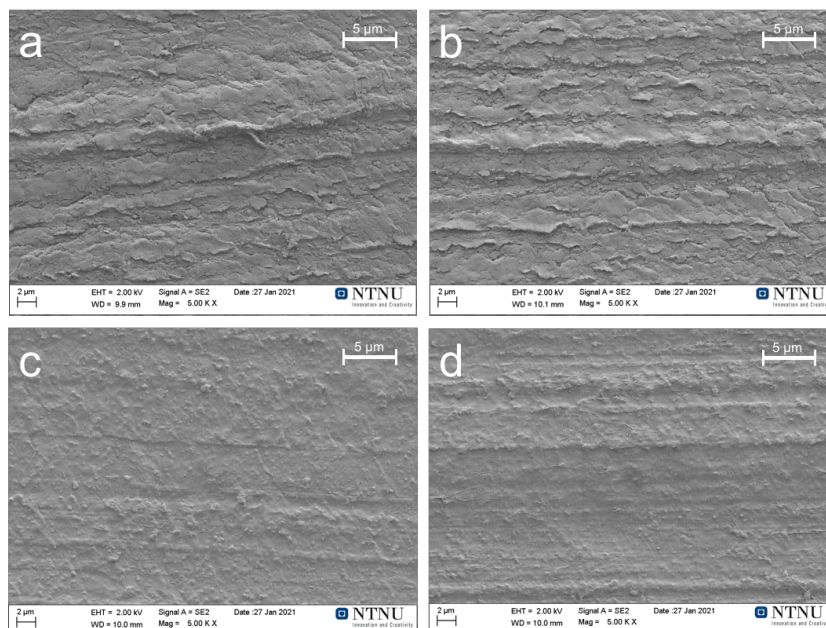
Figure E.10: SEM micrographs of coatings (a) TiN (A) and (b) TiN (B) scratched at a constant load of 1000 mN as well as the non-affected surface of (c) coating TiN (A) and (d) TiN (B) imaged at 5 000 X magnification.

E.2.2 Coating TiN (A) Exposed to PBS Solution

To determine if scratch testing would also be a suitable characterization technique for the samples exposed Phosphate Buffered Saline (PBS) solution, a few test scratches were performed. Samples coated with coating TiN (A) were exposed to PBS solution for 30 days and scratch tested at constant loads of 1000 mN and 2500 mN. Two scratches were performed at each load at each of the two samples. Figures E.11 and E.12 show that the coating cracks significantly at both loads, but that the scratches are much more visible at lower magnifications for the higher load. One of the scratches performed at 2500 mN clearly gives several parallel scratches, as seen in the micrograph with 1 000 X magnification in Figure E.12.
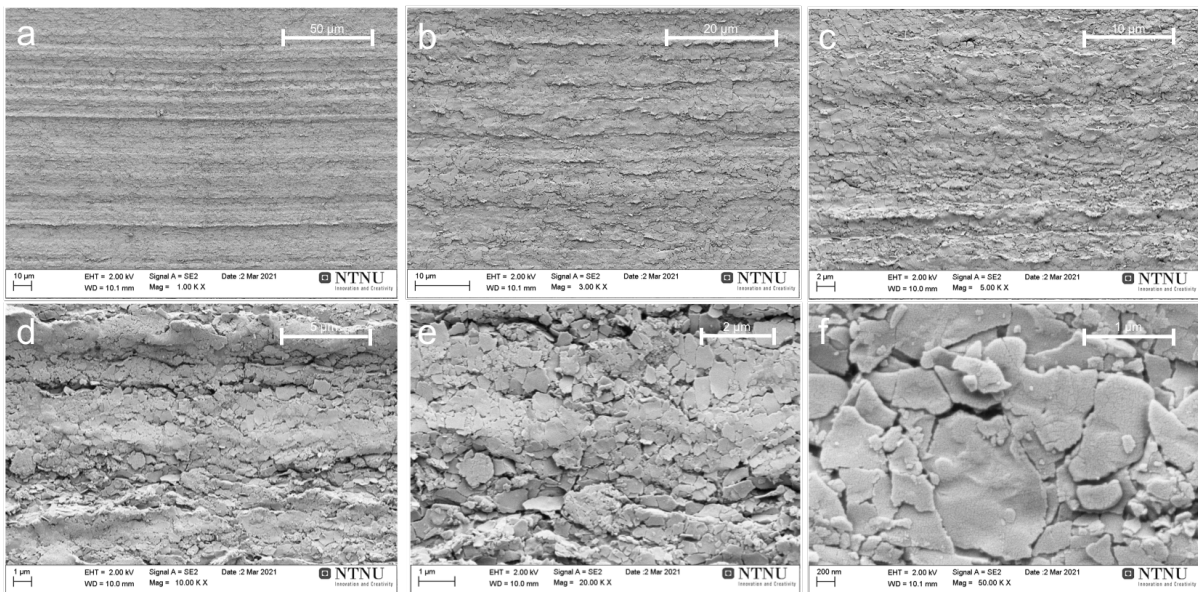
Figure E.11: SEM micrographs of samples coated with coating TiN (A) imaged at (a) 1 000 X, (b) 3 000 X, (c) 5 000 X, (d) 10 000 X, (e) 20 000 X, and (f) 50 000 X magnification. The samples were exposed to Phosphate Buffered Saline (PBS) solution for 30 days and scratch tested at 1000 mN.
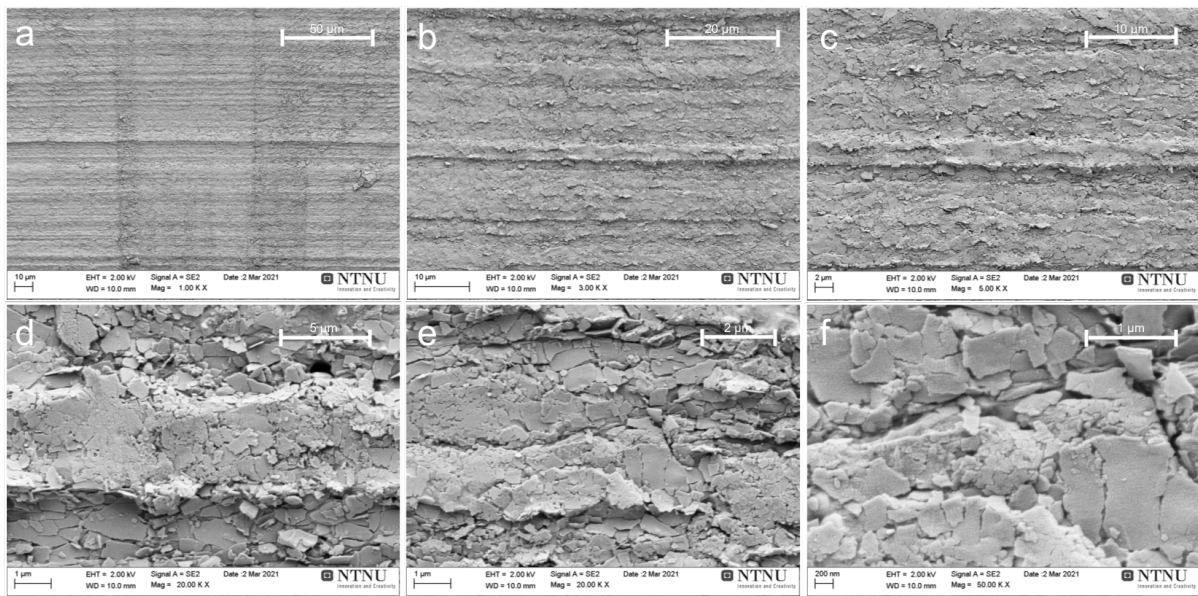
Figure E.12: SEM micrographs of samples coated with coating TiN (A) imaged at (a) 1 000 X, (b) 3 000 X, (c) 5 000 X, (d) 10 000 X, (e) 20 000 X, and (f) 50 000 X magnification. The samples were exposed to Phosphate Buffered Saline (PBS) solution for 30 days and scratch tested at 2500 mN.

E.2.3   DLC Coating

Samples coated with DLC were also scratched using the same method, but with constant loads of 500 mN, 1000 mN and 2500 mN. Two samples were scratched for each load and analyzed using the same SEM parameters. Two scratches were performed for each load on each sample. Only the areas scratched at 2500 mN could be confidently identified using SEM. Figure E.13 shows micrographs of the scratched surface at various magnifications, and reveals cracking, but no coating delamination. The micrograph with 1 000 X magnification also shows the parallel scratches which have been observed earlier.
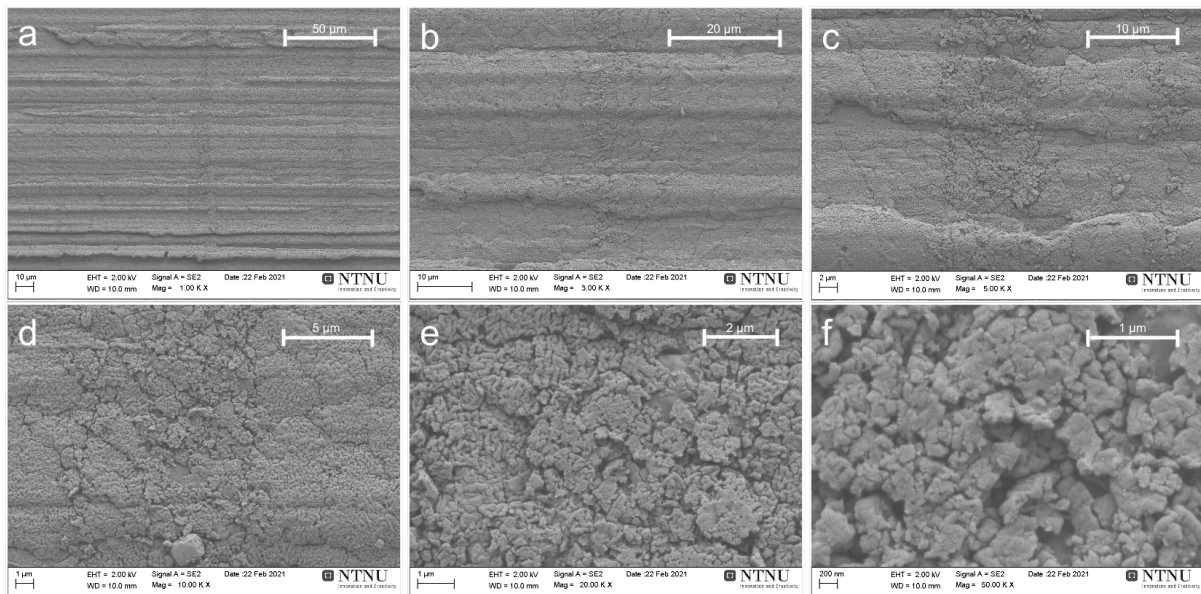
Figure E.13: SEM micrographs of samples coated with DLC and scratch tested at 2500 mN imaged at (a) 1 000 X, (b) 3 000 X, (c) 5 000 X, (d) 10 000 X, (e) 20 000 X, and (f) 50 000 X magnification.

E.3 Attempts at Nano Scratch Testing

Due to several possible large inaccuracies in predicting the coating adhesion and cohesion with the methods described above (*i.e.*, the parallel scratches of unknown origin, and the possible cushioning effect of the carbon tape and the soft substrates), a decision was made to try a smaller indenter which literature describes should be more suitable for the thin film coatings. Thus, a Hysitron TI 950 TriboIndenter with a Berkovich tip 20 μm in diameter was used. The standard scratch testing program for the instrument was tested with a variety of loads. However, it was not possible to observe a scratch in the coatings for any of the loads tested. This could be due to the tip not being sharp enough for the coating system or because of a cushioning effect in the substrate. Therefore, the attempt at establishing a reliable and reproducible scratch testing procedure for the coatings have not been successful.

Appendix F

ICP-MS Instrument Parameters

The instrument parameters used for ICP-MS analysis are presented in Table F.1. Helium was mixed with oxygen for better sensitivity. The instrument uses S-lenses, and the mass shifts utilized for increased measurement accuracy are shown in Table F.2. A matrix matched 0.1 M HNO_3 standard solution was used to calibrate the instrument before use.

Table F.1: The instrument parameters utilized for ICP-MS analysis.

Parameter	Value
RF Power	1600 W
Nebulizer Gas	0.80 L/min
Makeup Gas	0.41 L/min
Oxygen Gas Mix	44%
Helium Gas Flow	4.4 mL/min
Octopole Bias	-20.0 V
Octopole RF	200 V
Energy Discrimination	-8.5 V

Table F.2: The mass shifts utilized in the ICP-MS analysis for increased measurement accuracy.

Element	Q1	Q2
S	32	48
Ti	47	63
Ba	137	137

Appendix G

Additional Micrographs of Surface Morphology

G.1 Coatings TiN (A) and TiN (B)

Figures G.1, G.2 and, G.3 show the surface morphology of samples coated with coatings TiN (A) and TiN (B) as well as the non-coated reference substrate at 10 000 X, 5 000 X and, 3 000 X magnification respectively. The presented micrographs are selected as the most representative of the surfaces.
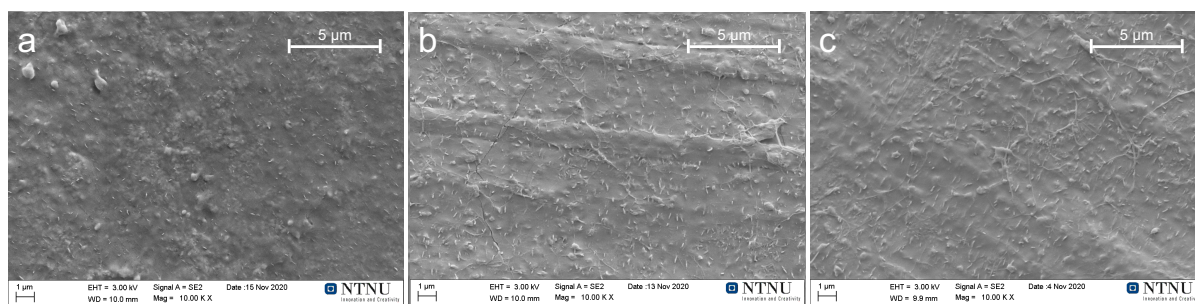
Figure G.1: SEM micrographs of (a) the non-coated reference substrate, (b) samples coated with coating TiN (A) and (c) coating TiN (B) imaged at 10 000 X magnification.
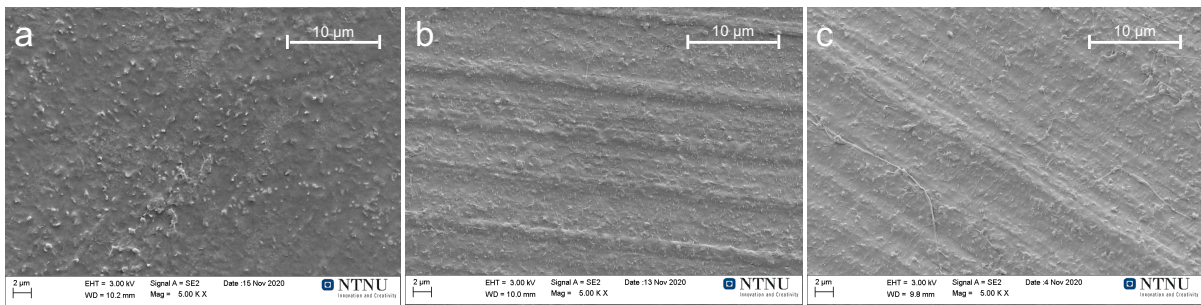
Figure G.2: SEM micrographs of (a) the non-coated reference substrate, (b) samples coated with coating TiN (A) and (c) coating TiN (B) imaged at 5 000 X magnification.
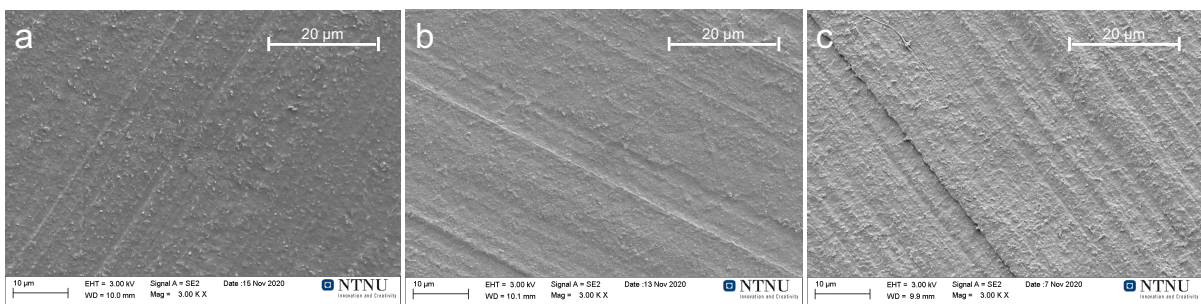
Figure G.3: SEM micrographs of (a) the non-coated reference substrate, (b) samples coated with coating TiN (A) and (c) coating TiN (B) imaged at 3 000 X magnification.

G.2 Coatings TiN (C) and DLC

G.2.1 Additional Magnifications

Figures G.4 and G.5 show the surface morphology of samples coated with coating TiN (C) and DLC as well as the non-coated reference substrate at 5 000 X and 3 000 X magnification respectively. The presented micrographs are selected as the most representative of the surfaces.
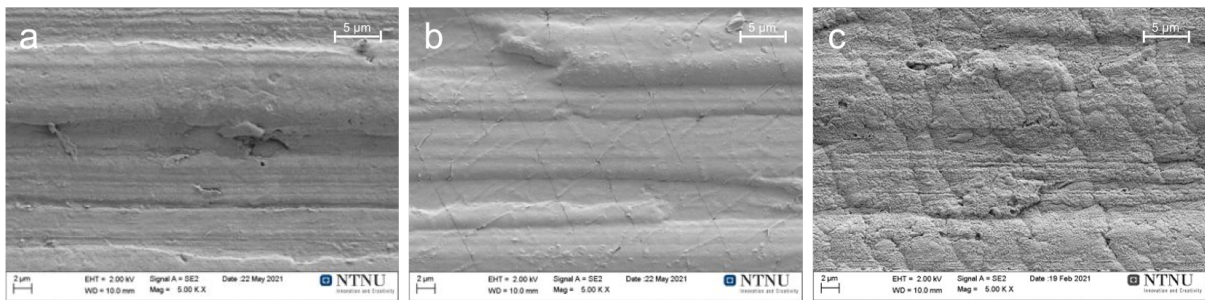
Figure G.4: SEM micrographs of (a) the non-coated reference substrate, (b) samples coated with coating TiN (C) and (c) DLC imaged at 5 000 X magnification.
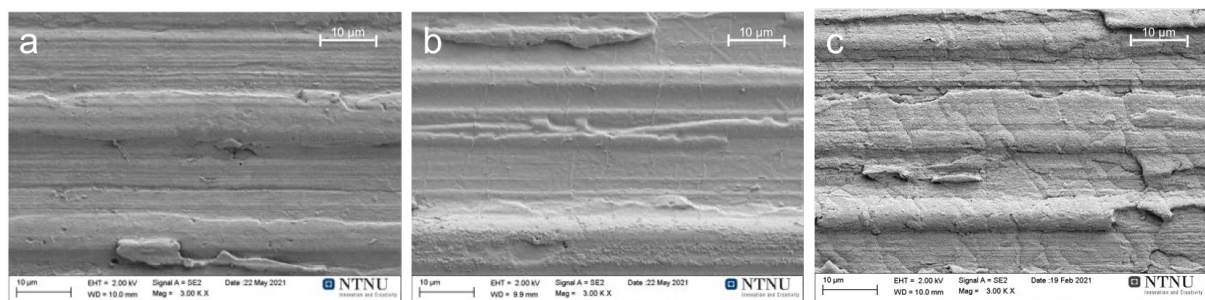
Figure G.5: SEM micrographs of (a) the non-coated reference substrate, (b) samples coated with coating TiN (C) and (c) DLC imaged at 3 000 X magnification.

G.2.2 Irregularity

Figure G.6 shows an irregularity observed on the surface of a non-coated reference substrate. It appears that some material is peeling of the surface, probably the Carbothane material itself. The origin of this irregularity is not known.
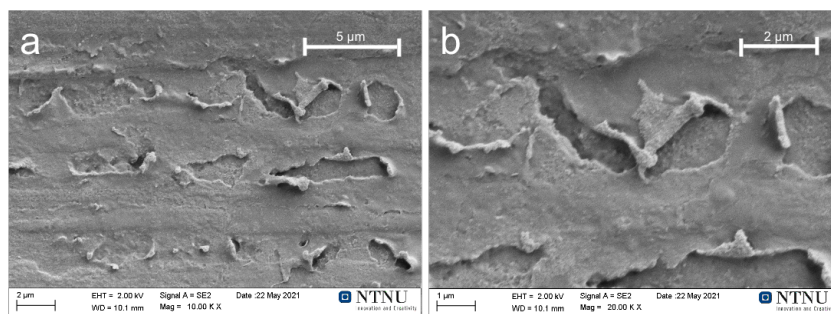
Figure G.6: SEM micrographs of an irregularity observed in the the non-coated reference substrate imaged at (a) 10 000 X and (b) 20 000 X magnification.

Appendix H

Additional Friction Coefficient Results

H.1 Coatings TiN (A) and TiN (B)

H.1.1 Friction Coefficients

The friction coefficients of the samples coated with coating TiN (A) and TiN (B) as well as the non-coated reference substrates are presented in Figures H.1, H.2, and H.3, respectively. The average friction coefficient values between when equilibrium conditions are reached for the respective surface and 50 seconds for each sample are shown in Table H.1. Equilibrium conditions are determined to be reached after 25 seconds for the coated surfaces and after 28 seconds for the non-coated reference substrates.
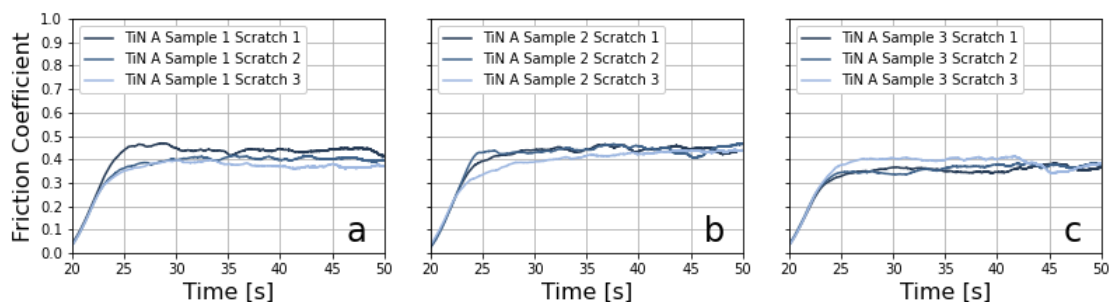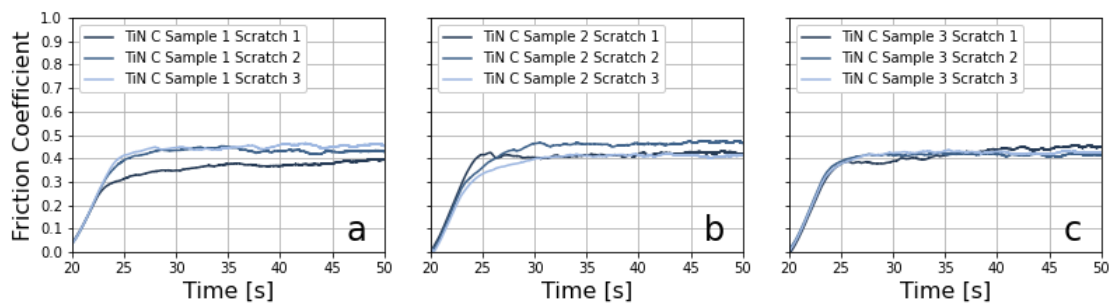

Figure H.1: The friction coefficients of samples coated with coating TiN (A) obtained from (a) sample 1, (b) sample 2 and (c) sample 3.
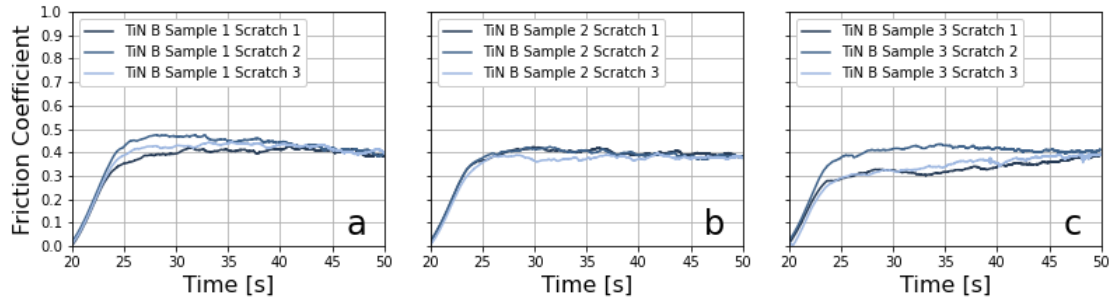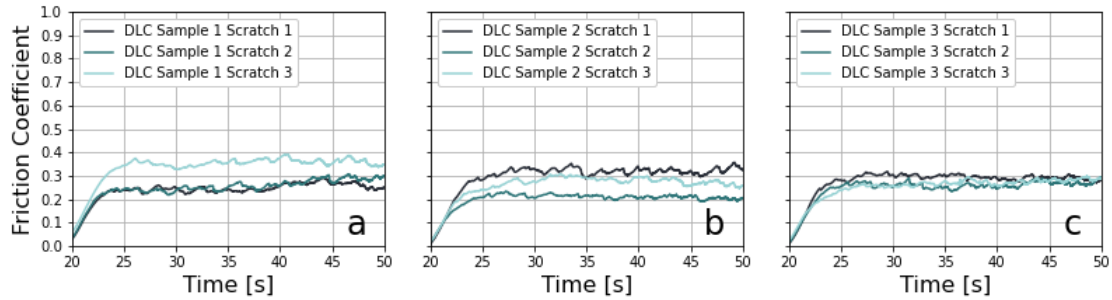
Figure H.2: The friction coefficients of samples coated with coating TiN (B) obtained from (a) sample 1, (b) sample 2 and (c) sample 3.
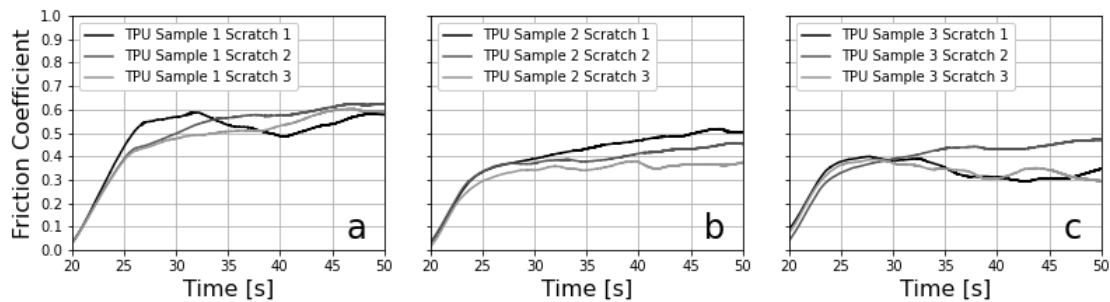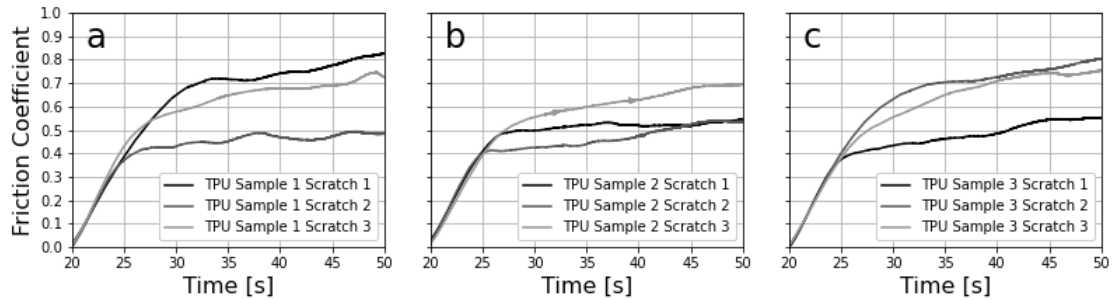

Figure H.3: The friction coefficients of the thicker non-coated reference substrates obtained from (a) sample 1, (b) sample 2 and (c) sample 3.

Table H.1: Average friction coefficient of each sample for samples coated with coating TiN (A), TiN (B) and the non-coated reference substrate (TPU). The average is obtained from the friction coefficient values between when the equilibrium conditions are reached and 50 s.

Sample	TPU	TiN (A)	TiN (B)
1	0.55 ± 0.04	0.41 ± 0.01	0.42 ± 0.02
2	0.41 ± 0.03	0.43 ± 0.02	0.39 ± 0.01
3	0.37 ± 0.03	0.37 ± 0.02	0.37 ± 0.02
Average	0.44 ± 0.10	0.40 ± 0.03	0.39 ± 0.03

H.1.2   Normal Displacement

The normal displacement of the samples coated with coating TiN (A) and TiN (B) as well as the non-coated reference substrates are presented in Figures H.4, H.5, and H.6, respectively.
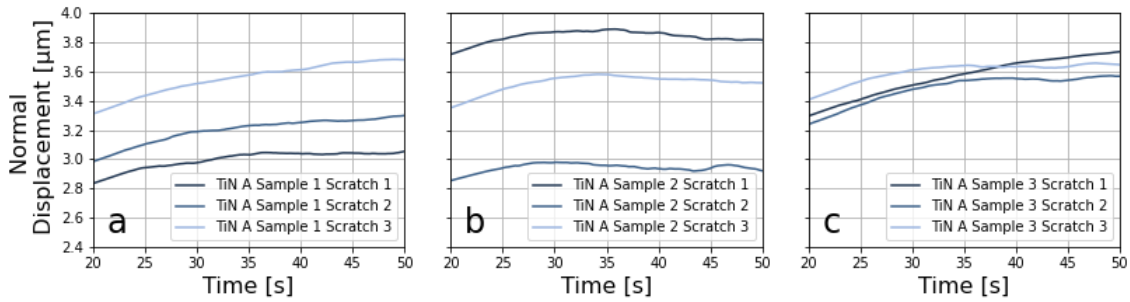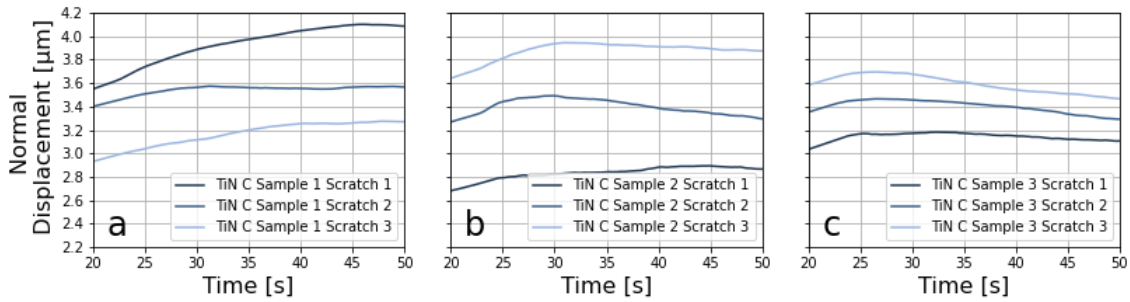

Figure H.4: The normal displacement of samples coated with coating TiN (A) obtained from (a) sample 1, (b) sample 2 and (c) sample 3.
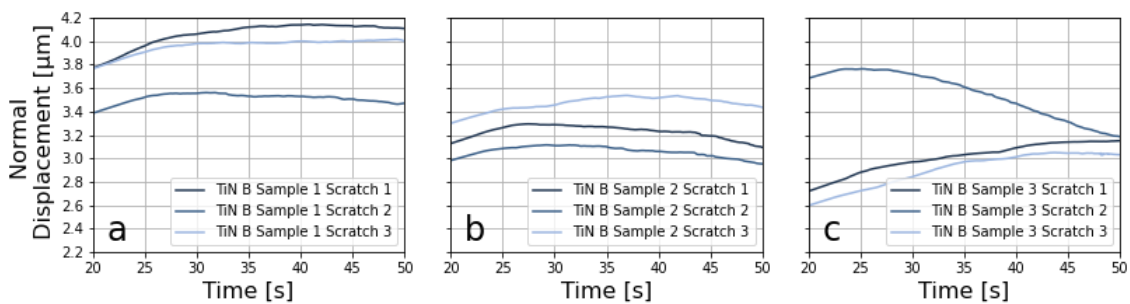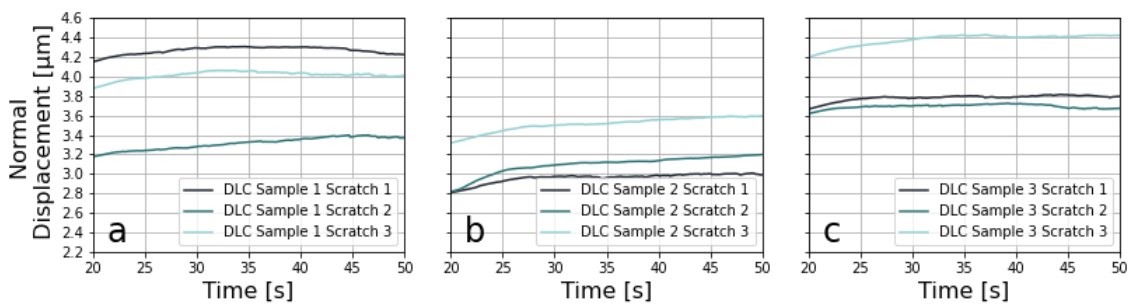

Figure H.5: The normal displacement of samples coated with coating TiN (B) obtained from (a) sample 1, (b) sample 2 and (c) sample 3.
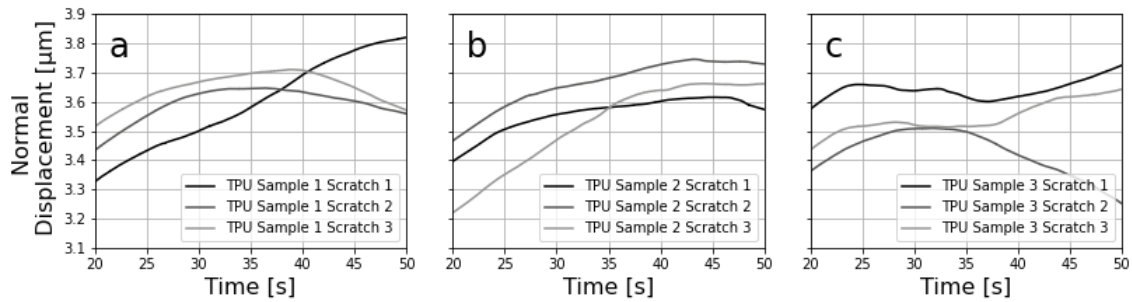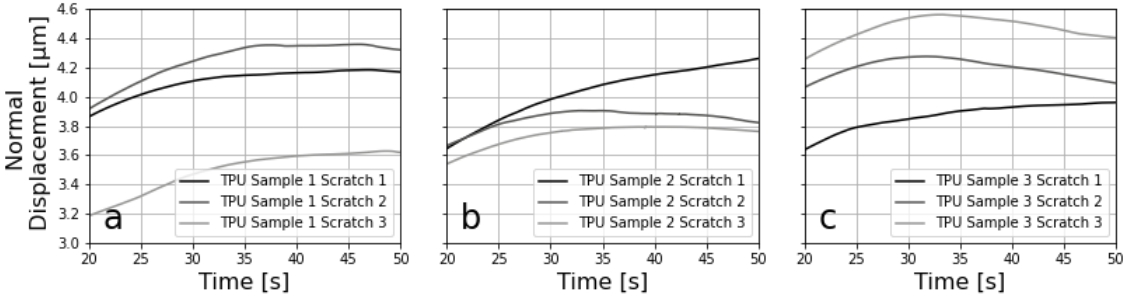
Figure H.6: The normal displacement of the thicker non-coated reference substrates obtained from (a) sample 1, (b) sample 2 and (c) sample 3.

H.2 Coatings TiN (C) and DLC

H.2.1 Friction Coefficients

The friction coefficients of the samples coated with coating TiN (C) and DLC as well as the non-coated reference substrates are presented in Figures H.7, H.8, and H.9, respectively. The average friction coefficient values between when equilibrium conditions are reached for the respective surface 50 seconds for each sample are shown in Table H.2. Equilibrium conditions are determined to be reached after 25 seconds for the samples coated with coating TiN (C), after 24 s for samples coated with DLC and after 28 seconds for the non-coated reference substrates.

Figure H.7: The friction coefficients of samples coated with coating TiN (C) obtained from (a) sample 1, (b) sample 2 and (c) sample 3.

Figure H.8: The friction coefficients of samples coated with DLC obtained from (a) sample 1, (b) sample 2 and (c) sample 3.

Figure H.9: The friction coefficients of the thinner non-coated reference substrates obtained from (a) sample 1, (b) sample 2 and (c) sample 3.

Table H.2: Average friction coefficient of each sample for samples coated with coating TiN (C), DLC and the non-coated reference substrate (TPU). The average is obtained from the friction coefficient values between when the equilibrium conditions are reached and 50 s.

Sample	TPU	TiN (C)	DLC
1	0.62 ± 0.04	0.42 ± 0.01	0.29 ± 0.02
2	0.54 ± 0.04	0.42 ± 0.02	0.27 ± 0.01
3	0.63 ± 0.06	0.42 ± 0.02	0.27 ± 0.01
Average	0.59 ± 0.05	0.42 ± 0.01	0.28 ± 0.01

136

H.2.2 Normal Displacement

The normal displacement of the samples coated with coating TiN (A) and TiN (B) as well as the non-coated reference substrates are presented in Figures H.10, H.11, and H.12, respectively.

Figure H.10: The normal displacement of samples coated with coating TiN (C) obtained from (a) sample 1, (b) sample 2 and (c) sample 3.

Figure H.11: The normal displacement of samples coated with DLC obtained from (a) sample 1, (b) sample 2 and (c) sample 3.

Figure H.12: The normal displacement of the thinner non-coated reference substrates obtained from (a) sample 1, (b) sample 2 and (c) sample 3.

Appendix I

Additional Results from Exposure Study

I.1 Additional Magnifications

The following micrographs are deemed to be the most representative of the respective surfaces, exposure times and magnifications. All micrographs are taken of the first round of samples analyzed using SEM. The figures in this subsection presents samples that are exposed to Phosphate Buffered Saline (PBS) solution for 1 hour, 24 hours, 7 days and 30 days. Figures I.1, I.2 and I.3 show SEM micrographs of samples with coating TiN (A), TiN (B) and non-coated substrates, respectively, imaged at 50 000 X magnification.
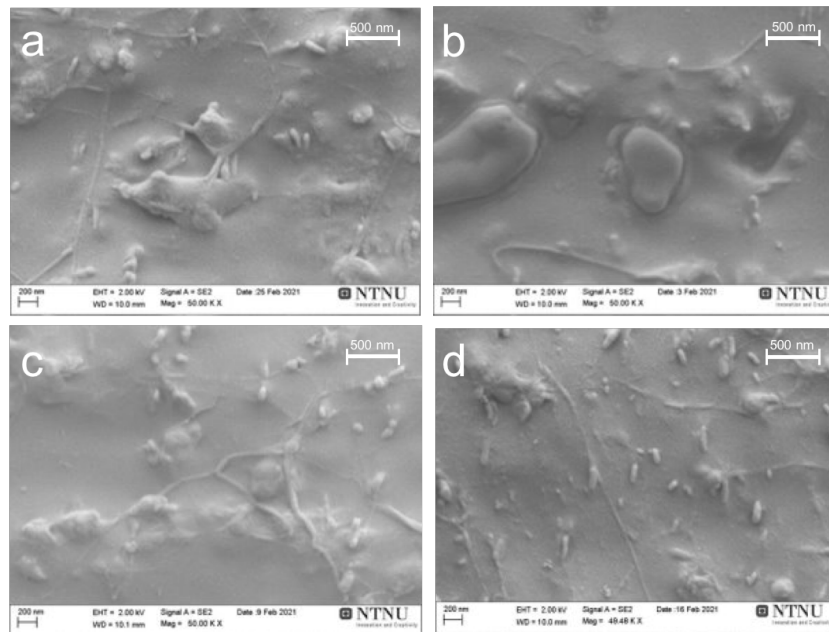
Figure I.1: SEM micrographs of samples with coating TiN (A) exposed to PBS for (a) 1 hour, (b) 24 hours, (c) 7 days and (d) 30 days imaged at 50 000 X magnification.
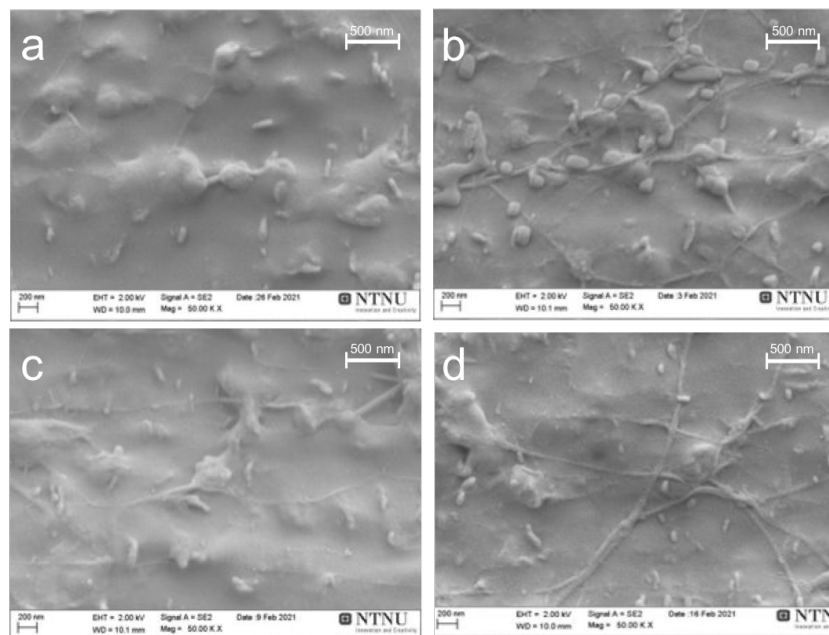
Figure I.2: SEM micrographs of samples with coating TiN (B) exposed to PBS for (a) 1 hour, (b) 24 hours, (c) 7 days and (d) 30 days imaged at 50 000 X magnification.
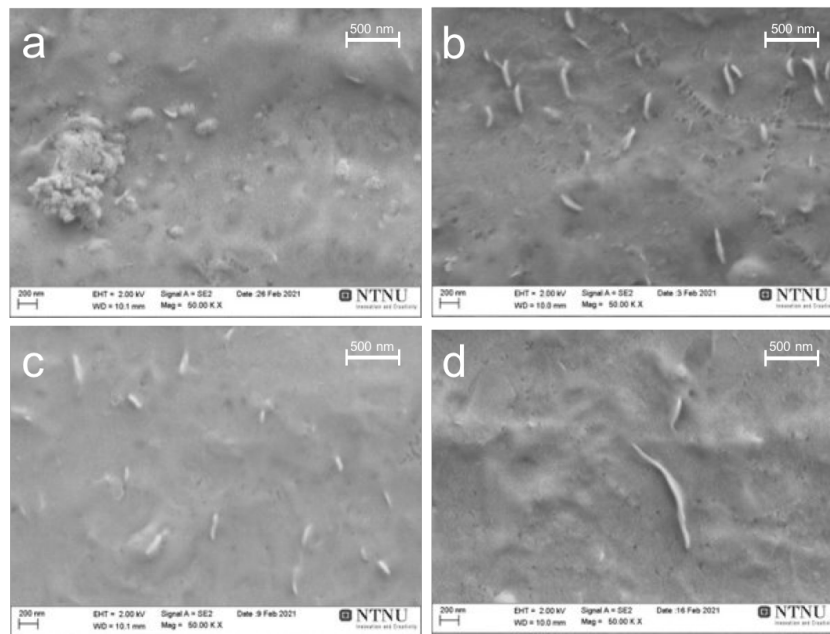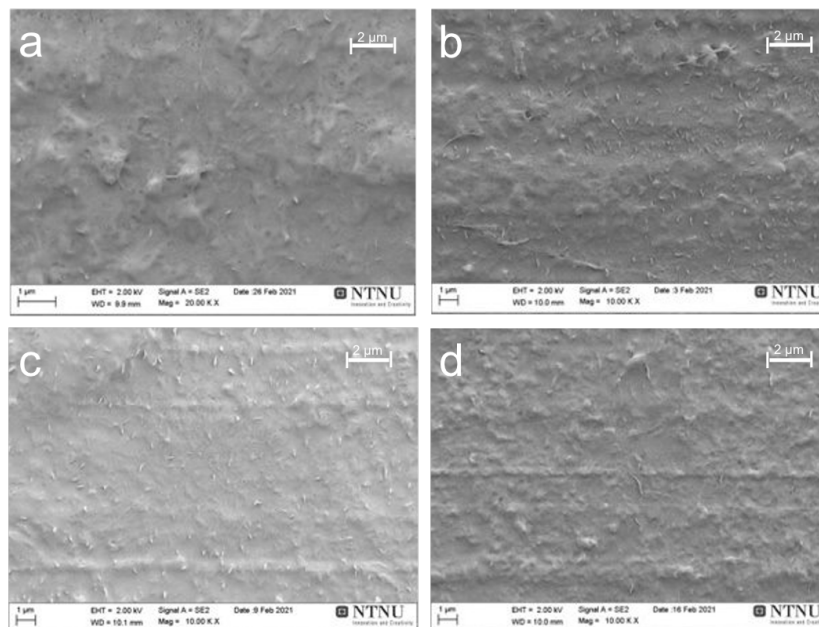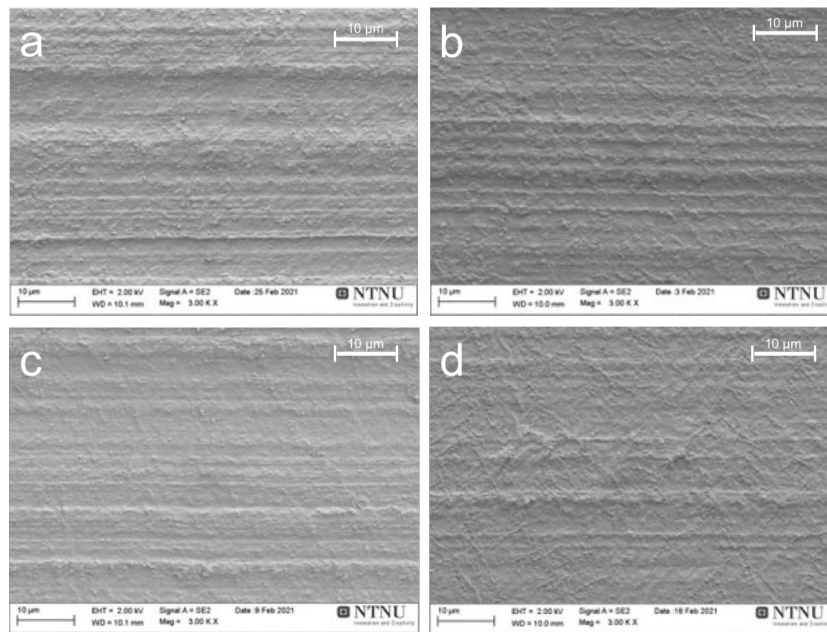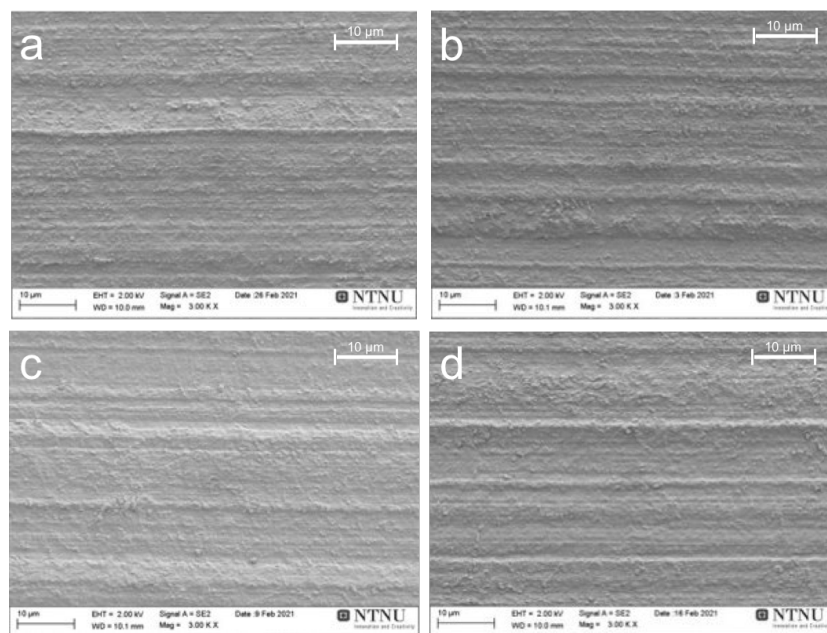
Figure I.3: SEM micrographs of non-coated substrates exposed to PBS for (a) 1 hour, (b) 24 hours, (c) 7 days and (d) 30 days imaged at 50 000 X magnification.

Figures I.4, I.5 and I.6 show SEM micrographs of samples with coating TiN (A), TiN (B) and non-coated substrates, respectively, imaged at 10 000 X magnification.
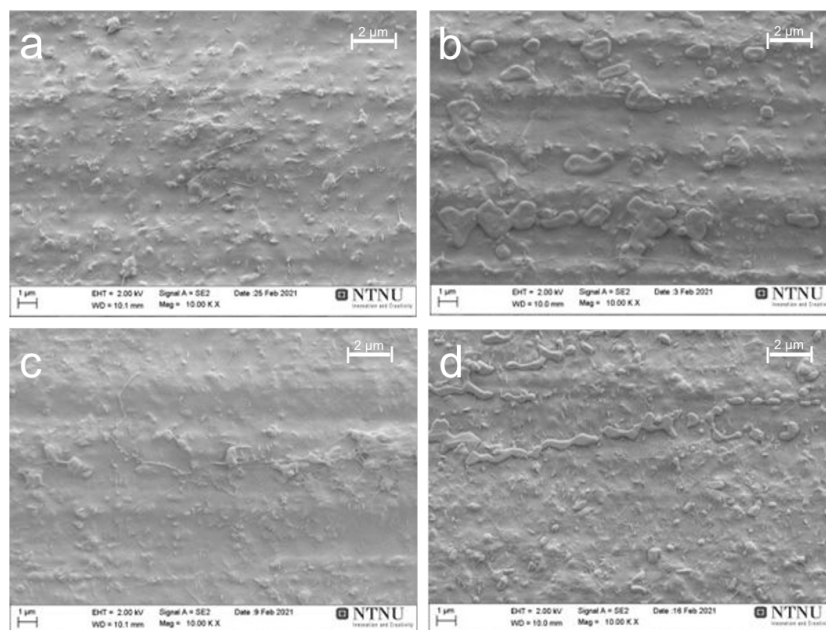
Figure I.4: SEM micrographs of samples with coating TiN (A) exposed to PBS for (a) 1 hour, (b) 24 hours, (c) 7 days and (d) 30 days imaged at 10 000 X magnification.
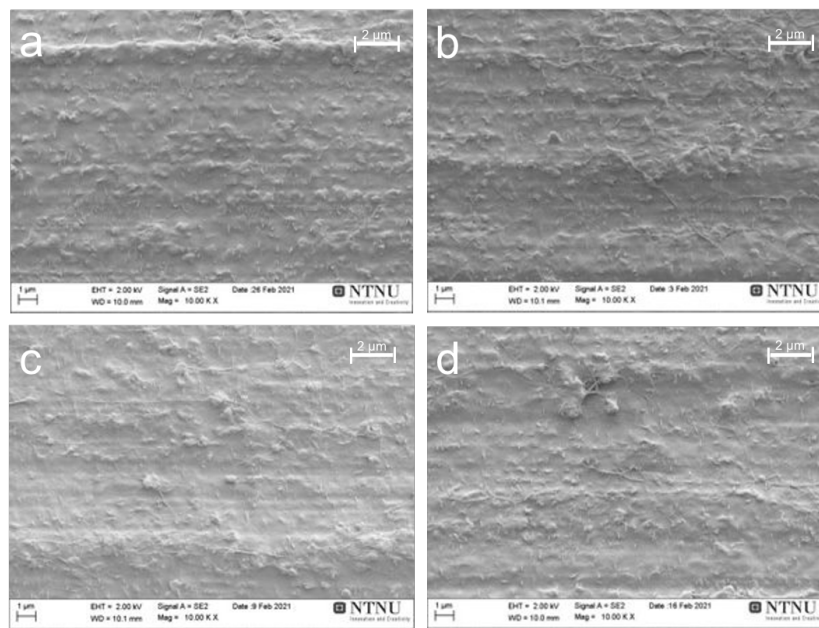
Figure I.5: SEM micrographs of samples with coating TiN (B) exposed to PBS for (a) 1 hour, (b) 24 hours, (c) 7 days and (d) 30 days imaged at 10 000 X magnification.
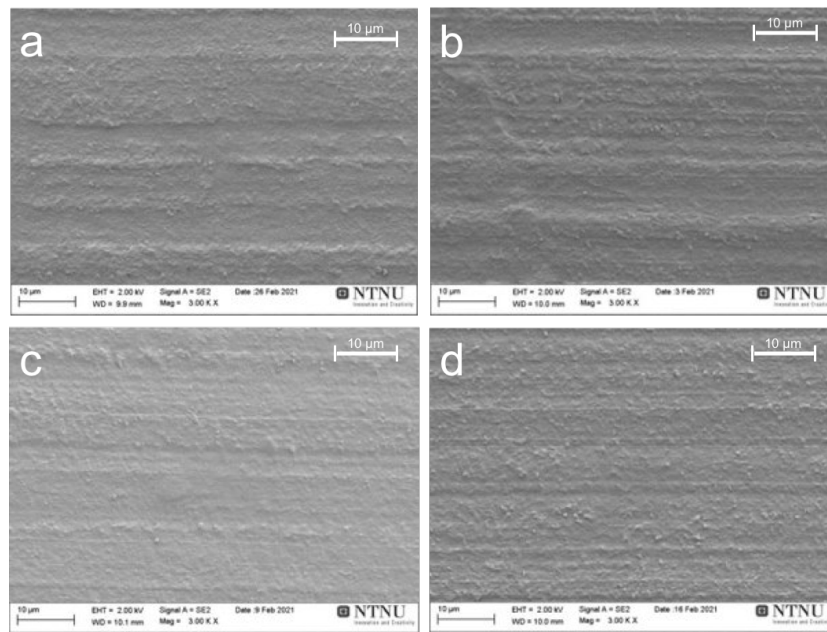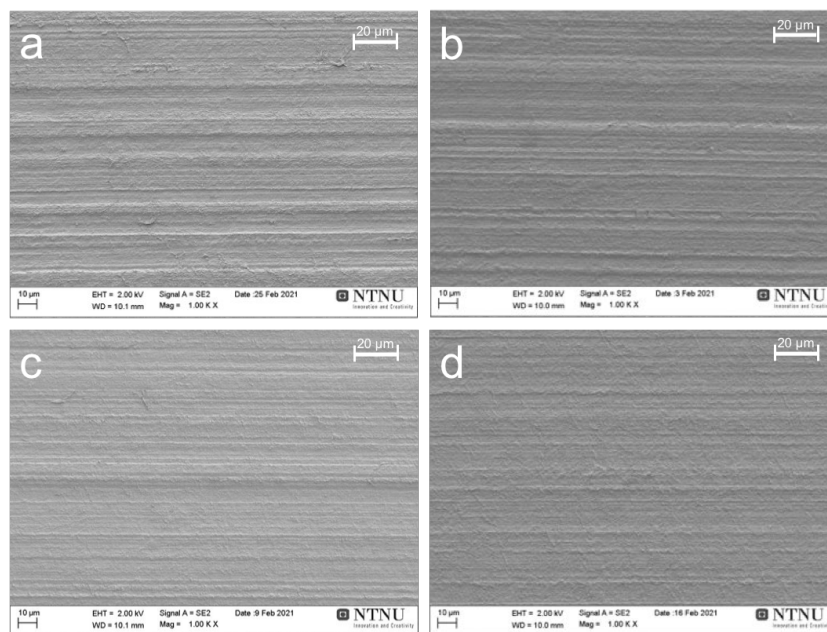

Figure I.6: SEM micrographs of non-coated substrates exposed to PBS for (a) 1 hour, (b) 24 hours, (c) 7 days and (d) 30 days imaged at 10 000 X magnification.

Figures I.7, I.8 and I.9 show SEM micrographs of samples with coating TiN (A), TiN (B) and non-coated substrates, respectively, imaged at 3 000 X magnification.

Figure I.7: SEM micrographs of samples with coating TiN (A) exposed to PBS for (a) 1 hour, (b) 24 hours, (c) 7 days and (d) 30 days imaged at 3 000 X magnification.
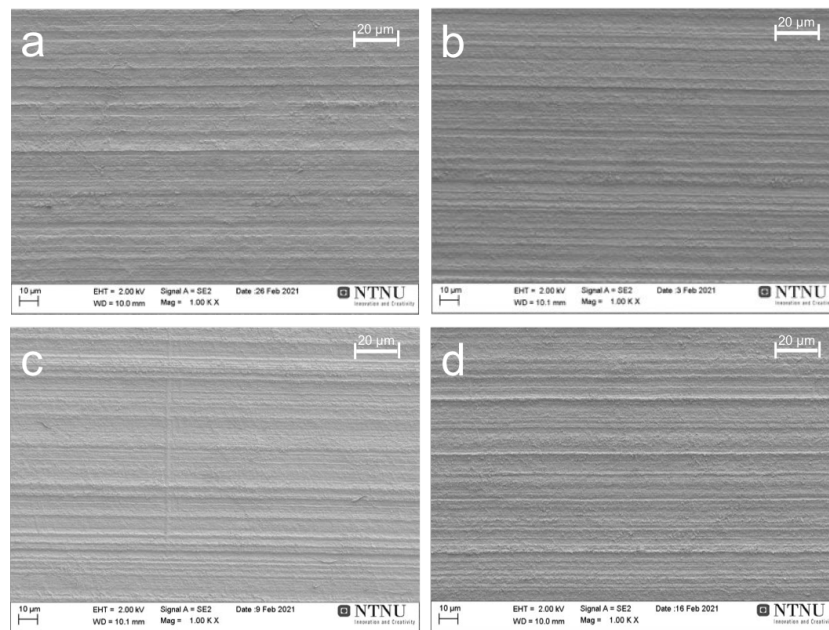

Figure I.8: SEM micrographs of samples with coating TiN (B) exposed to PBS for (a) 1 hour, (b) 24 hours, (c) 7 days and (d) 30 days imaged at 3 000 X magnification.
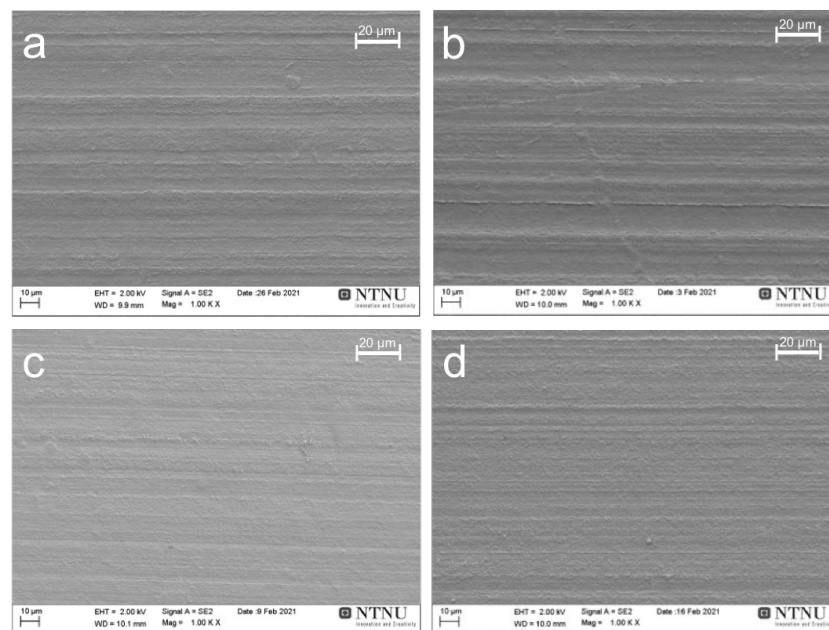
Figure I.9: SEM micrographs of non-coated substrates exposed to PBS for (a) 1 hour, (b) 24 hours, (c) 7 days and (d) 30 days imaged at 3 000 X magnification.

Figures I.10, I.11 and I.12 show SEM micrographs of samples with coating TiN (A), TiN (B) and non-coated substrates, respectively, imaged at 1 000 X magnification.
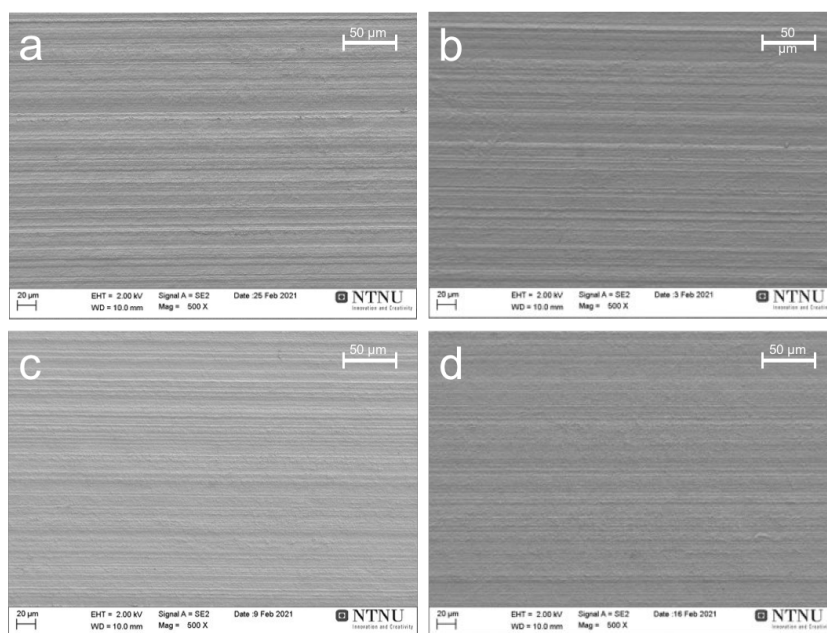

Figure I.10: SEM micrographs of samples with coating TiN (A) exposed to PBS for (a) 1 hour, (b) 24 hours, (c) 7 days and (d) 30 days imaged at 1 000 X magnification.
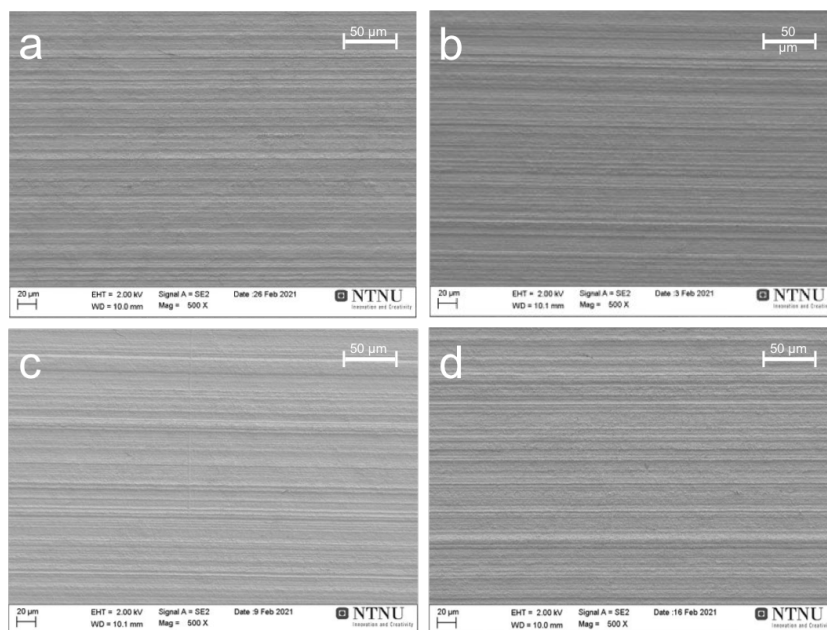
Figure I.11: SEM micrographs of samples with coating TiN (B) exposed to PBS for (a) 1 hour, (b) 24 hours, (c) 7 days and (d) 30 days imaged at 1 000 X magnification.

Figure I.12: SEM micrographs of non-coated substrates exposed to PBS for (a) 1 hour, (b) 24 hours, (c) 7 days and (d) 30 days imaged at 1 000 X magnification.

Figures I.13, I.14 and I.15 show SEM micrographs of samples with coating TiN (A), TiN (B) and non-coated substrates, respectively, imaged at 500 X magnification.

Figure I.13: SEM micrographs of samples with coating TiN (A) exposed to PBS for (a) 1 hour, (b) 24 hours, (c) 7 days and (d) 30 days imaged at 500 X magnification.

Figure I.14: SEM micrographs of samples with coating TiN (B) exposed to PBS for (a) 1 hour, (b) 24 hours, (c) 7 days and (d) 30 days imaged at 500 X magnification.
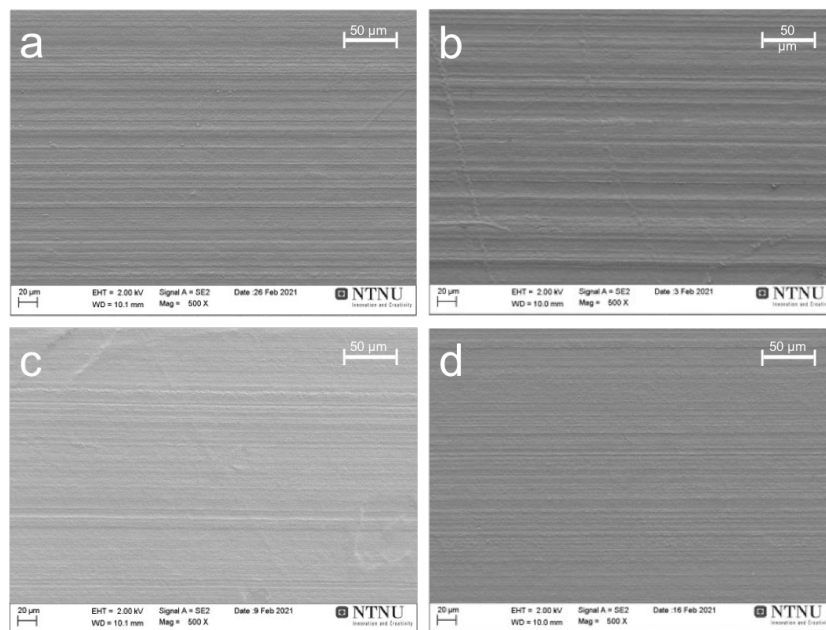
Figure I.15: SEM micrographs of non-coated substrates exposed to PBS for (a) 1 hour, (b) 24 hours, (c) 7 days and (d) 30 days imaged at 500 X magnification.

I.2 Additional Exposure Intervals

Figures I.16, I.17 and I.18 show SEM micrographs at 20 000 X magnification of samples with coating TiN (A), TiN (B) and non-coated substrates, respectively. All ten exposure intervals included in the exposure study are represented in all figures in this subsection.
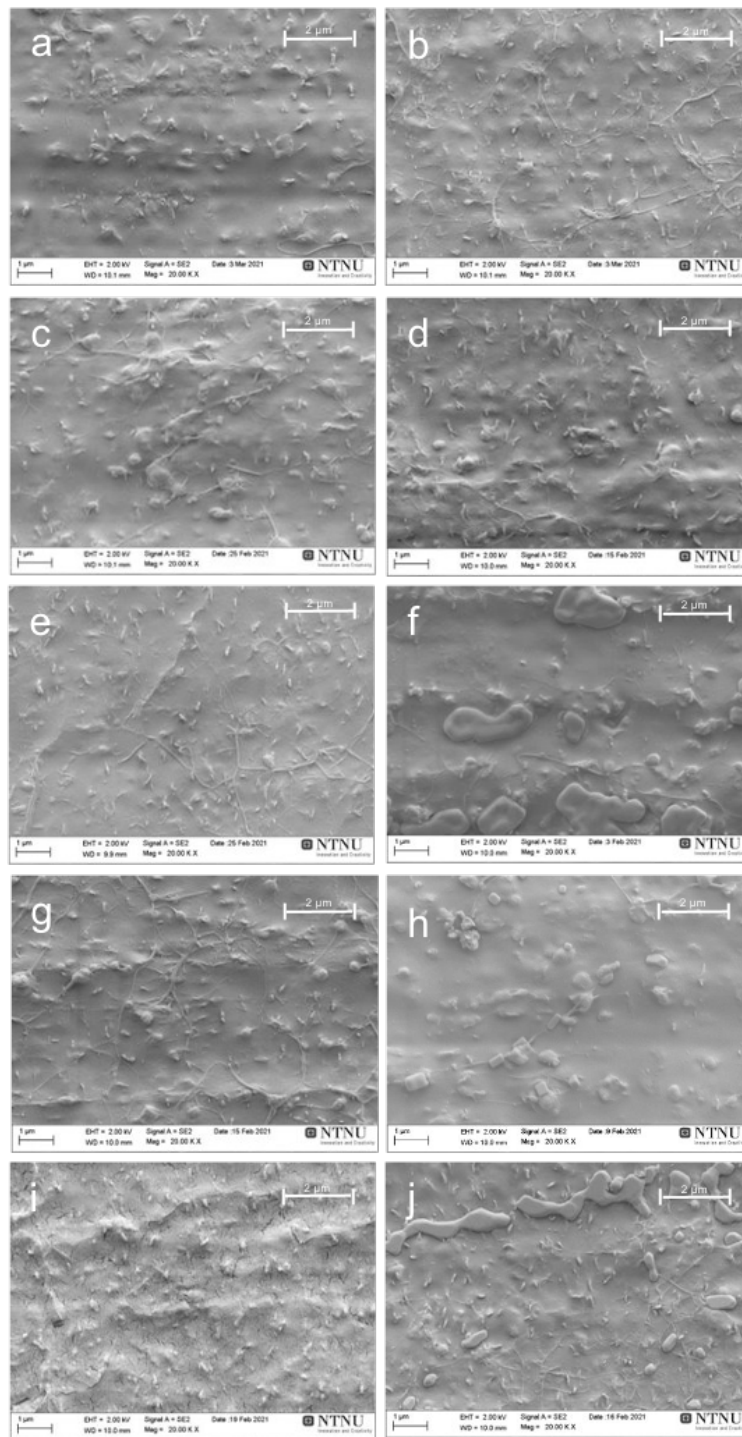
Figure I.16: SEM micrographs of samples with coating TiN (A) exposed to PBS for (a) 10 min, (b) 30 min, (c) 1 hr and (d) 6 hours, (e) 12 hrs, (f) 24 hrs, (g) 3 days, (h) 7 days, (i) 10 days, and (j) 30 days imaged at 20 000 X magnification.
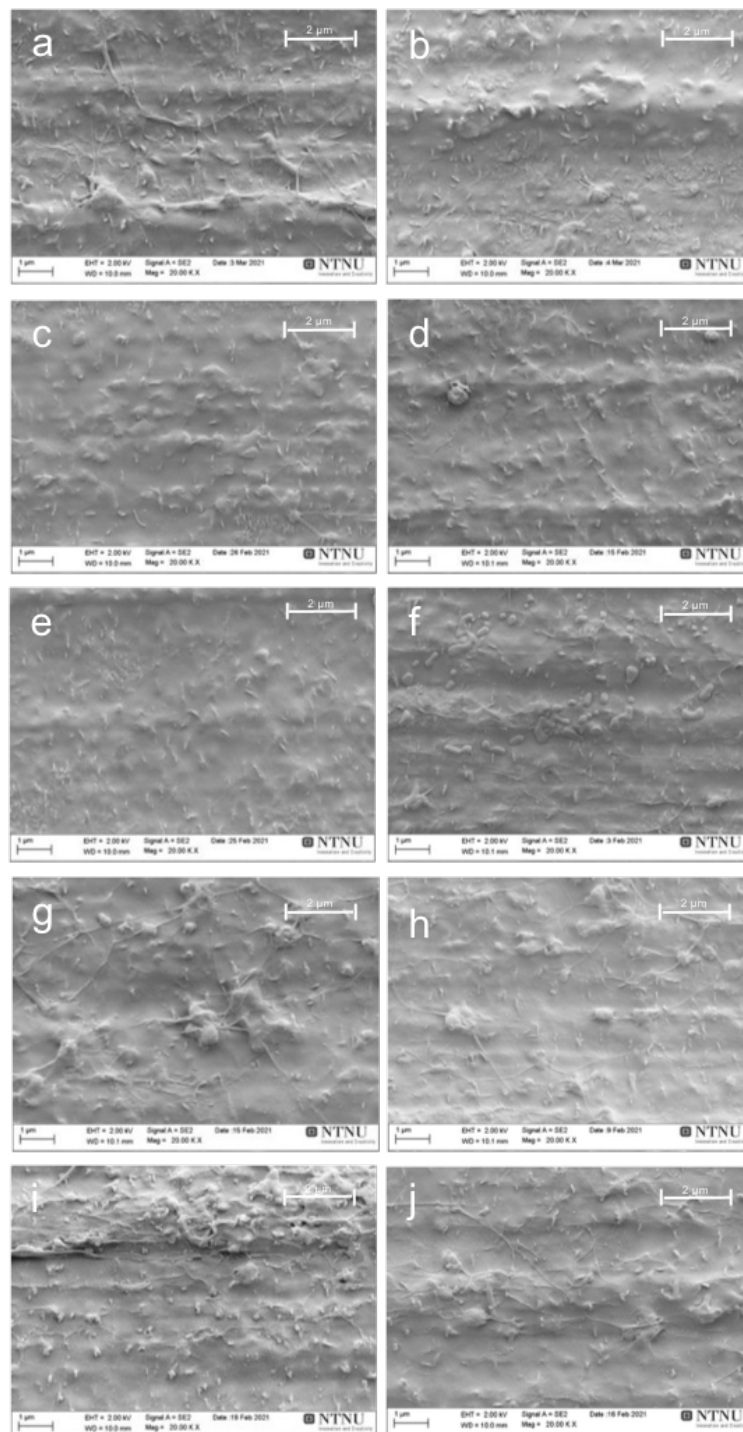
Figure I.17: SEM micrographs of samples with coating TiN (B) exposed to PBS for (a) 10 min, (b) 30 min, (c) 1 hr and (d) 6 hours, (e) 12 hrs, (f) 24 hrs, (g) 3 days, (h) 7 days, (i) 10 days, and (j) 30 days imaged at 20 000 X magnification.
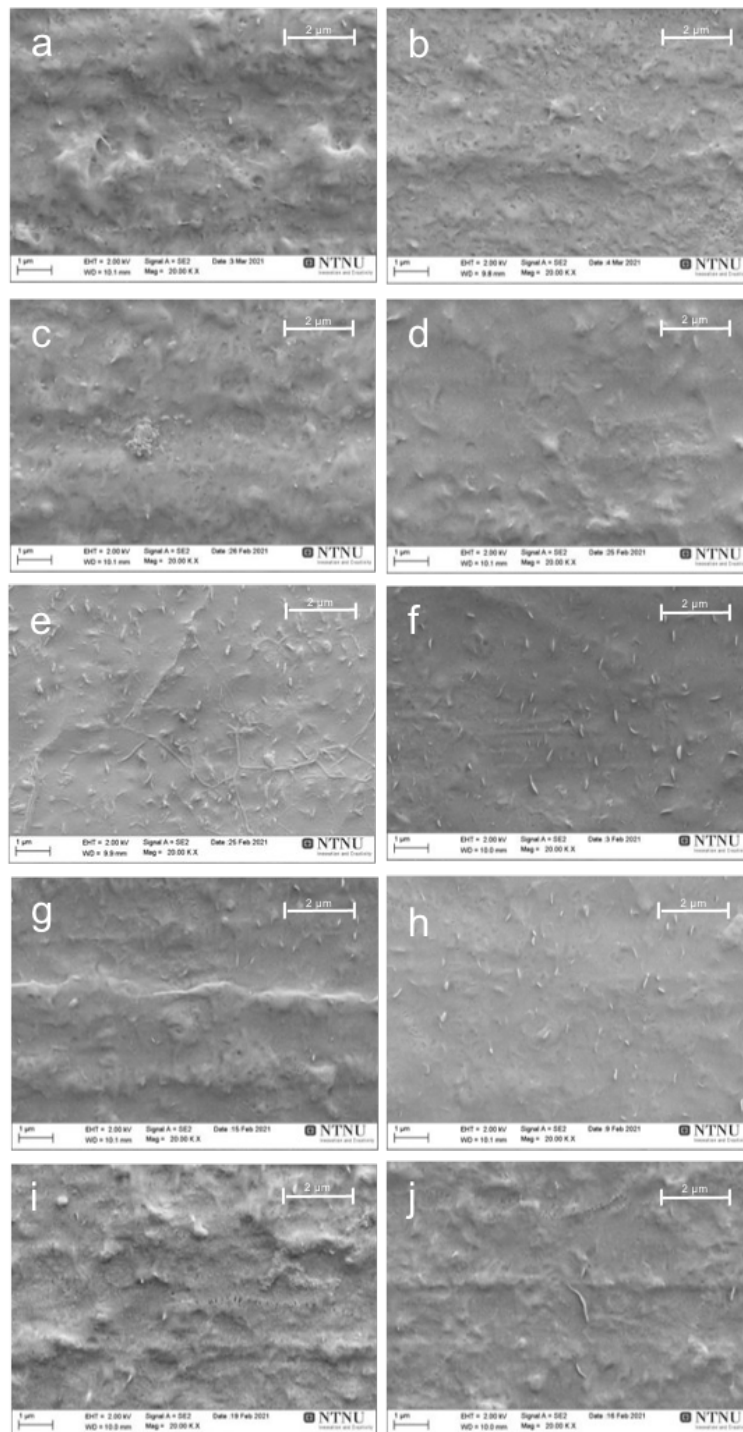
Figure I.18: SEM micrographs of non-coated substrates exposed to PBS for (a) 10 min, (b) 30 min, (c) 1 hr and (d) 6 hours, (e) 12 hrs, (f) 24 hrs, (g) 3 days, (h) 7 days, (i) 10 days, and (j) 30 days imaged at 20 000 X magnification.

Figures I.19, I.20 and I.21 show SEM micrographs at 5 000 X magnification of samples with coating TiN (A), TiN (B) and non-coated substrates, respectively.
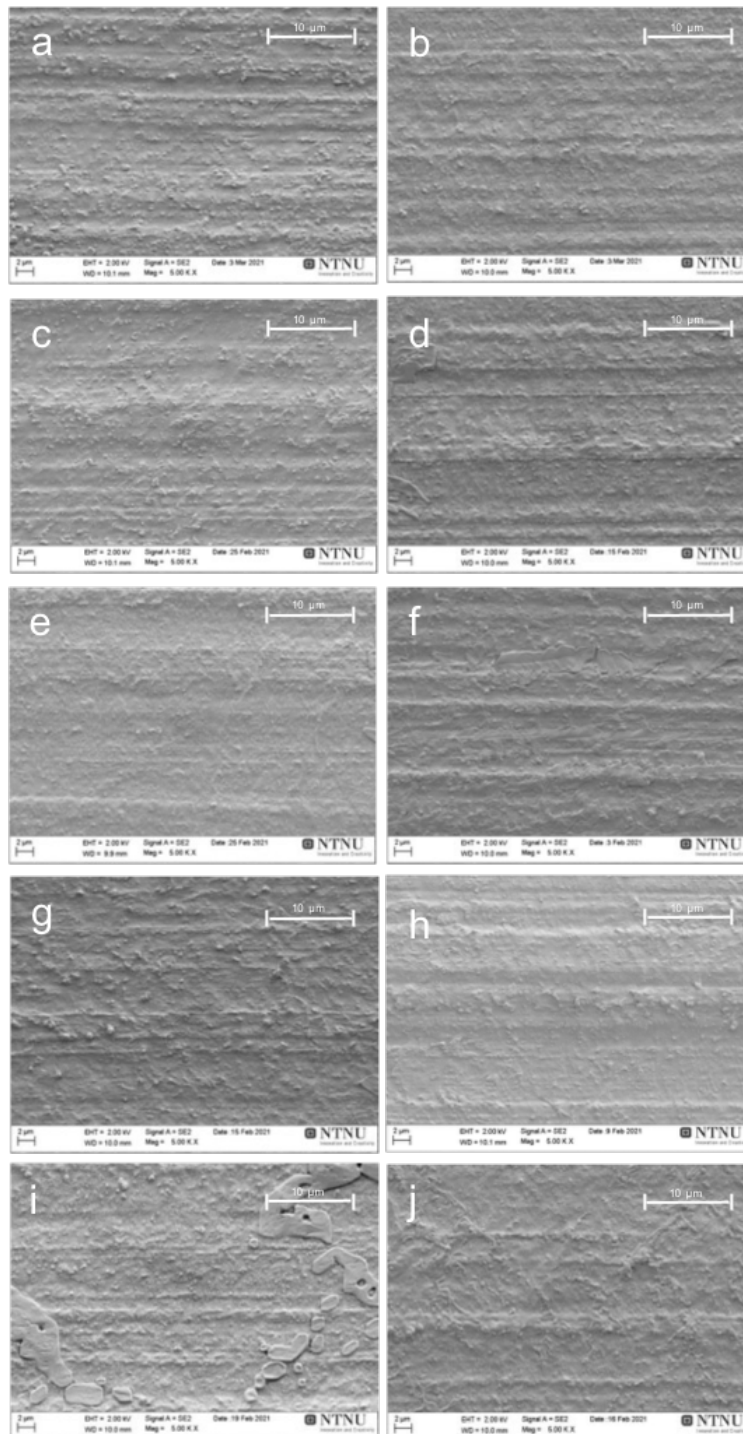

Figure I.19: SEM micrographs of samples with coating TiN (A) exposed to PBS for (a) 10 min, (b) 30 min, (c) 1 hr and (d) 6 hours, (e) 12 hrs, (f) 24 hrs, (g) 3 days, (h) 7 days, (i) 10 days, and (j) 30 days imaged at 5 000 X magnification.
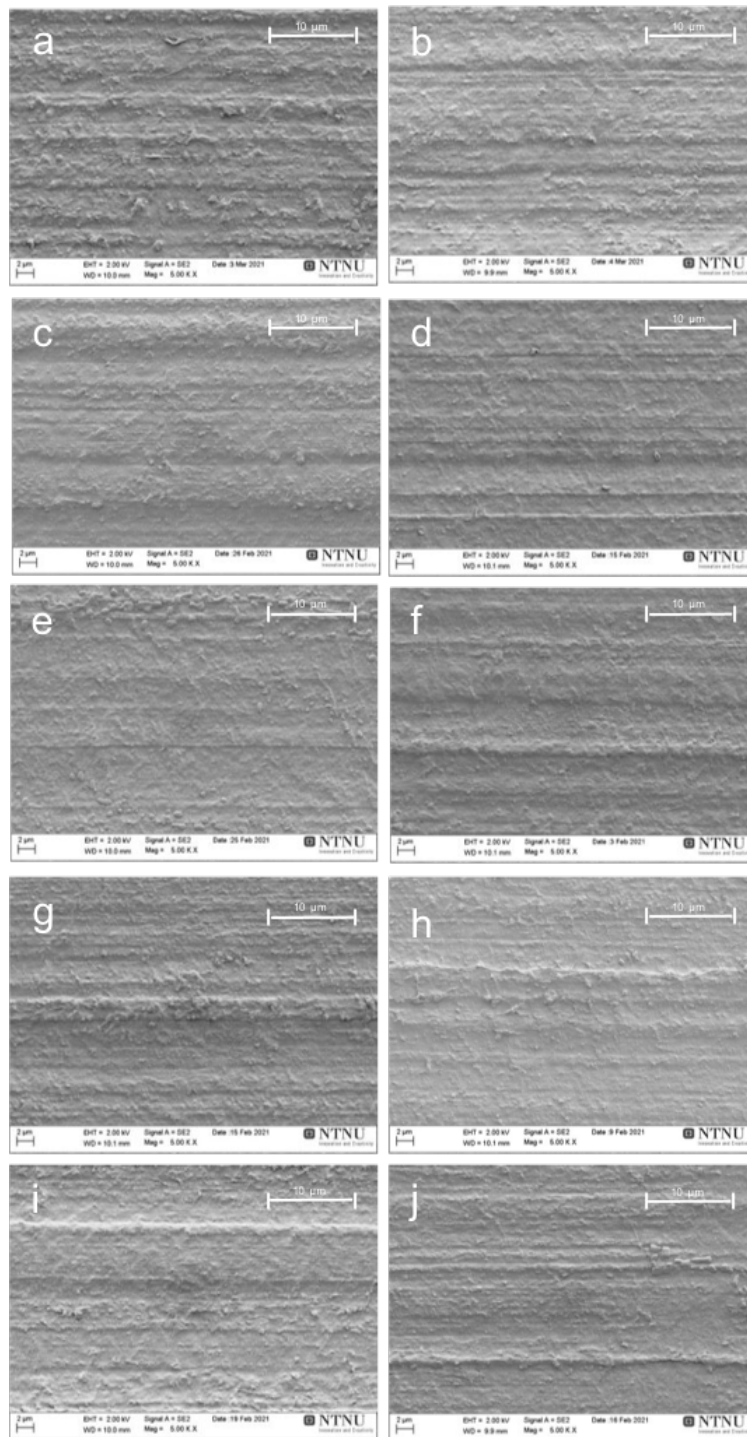
Figure I.20: SEM micrographs of samples with coating TiN (B) exposed to PBS for (a) 10 min, (b) 30 min, (c) 1 hr and (d) 6 hours, (e) 12 hrs, (f) 24 hrs, (g) 3 days, (h) 7 days, (i) 10 days, and (j) 30 days imaged at 5 000 X magnification.
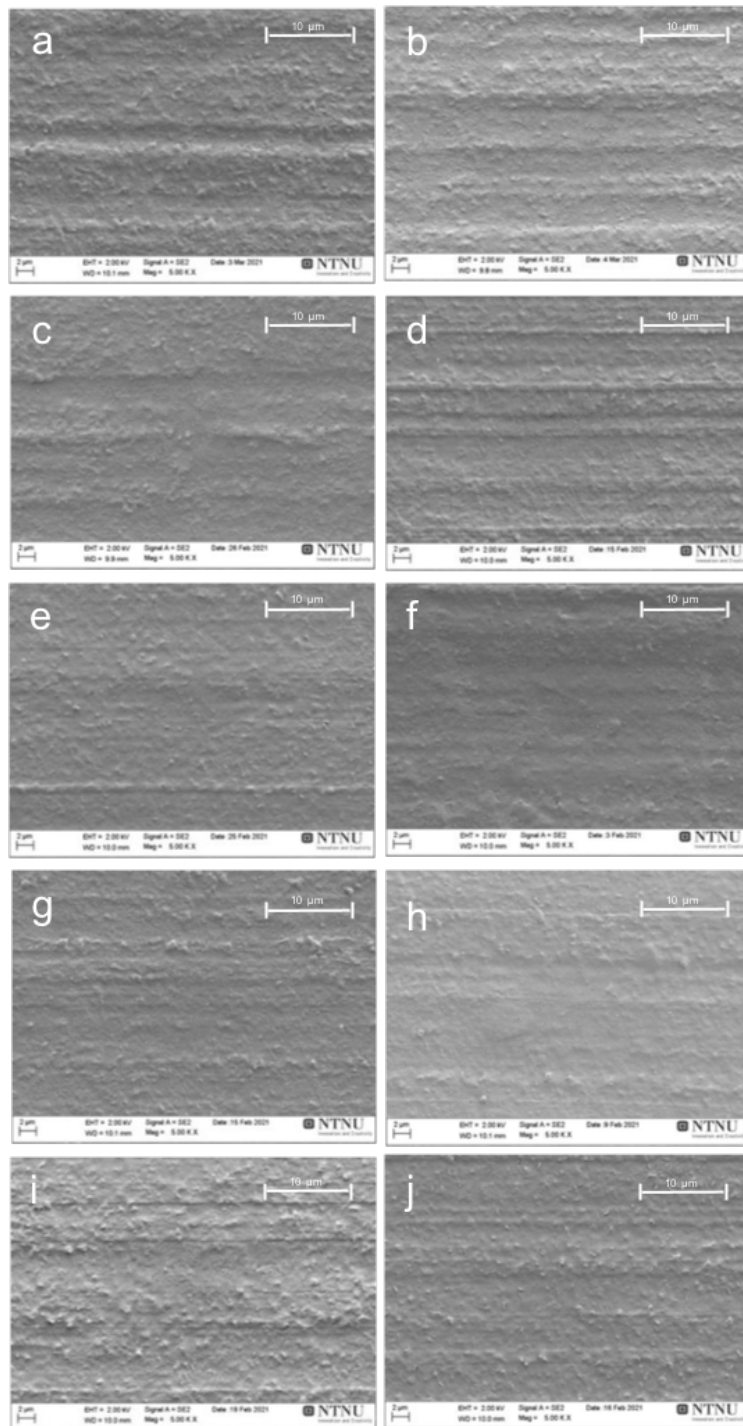
Figure I.21: SEM micrographs of non-coated substrates exposed to PBS for (a) 10 min, (b) 30 min, (c) 1 hr and (d) 6 hours, (e) 12 hrs, (f) 24 hrs, (g) 3 days, (h) 7 days, (i) 10 days, and (j) 30 days imaged at 5 000 X magnification.

I.3   Irregularities

Crystalline structures have been observed on the surface of some of the sample after exposure to PBS solution as presented in Figure I.22. These structures are believed to be salt residues from the PBS solution which was not completely washed away by the rinsing procedure after exposure end. The quantity of salt residues on the surface greatly varies from sample to sample. The residues have been more frequently observed as more evenly distributed crystal structures with crystals of micrometer scale as seen in Figure I.23.
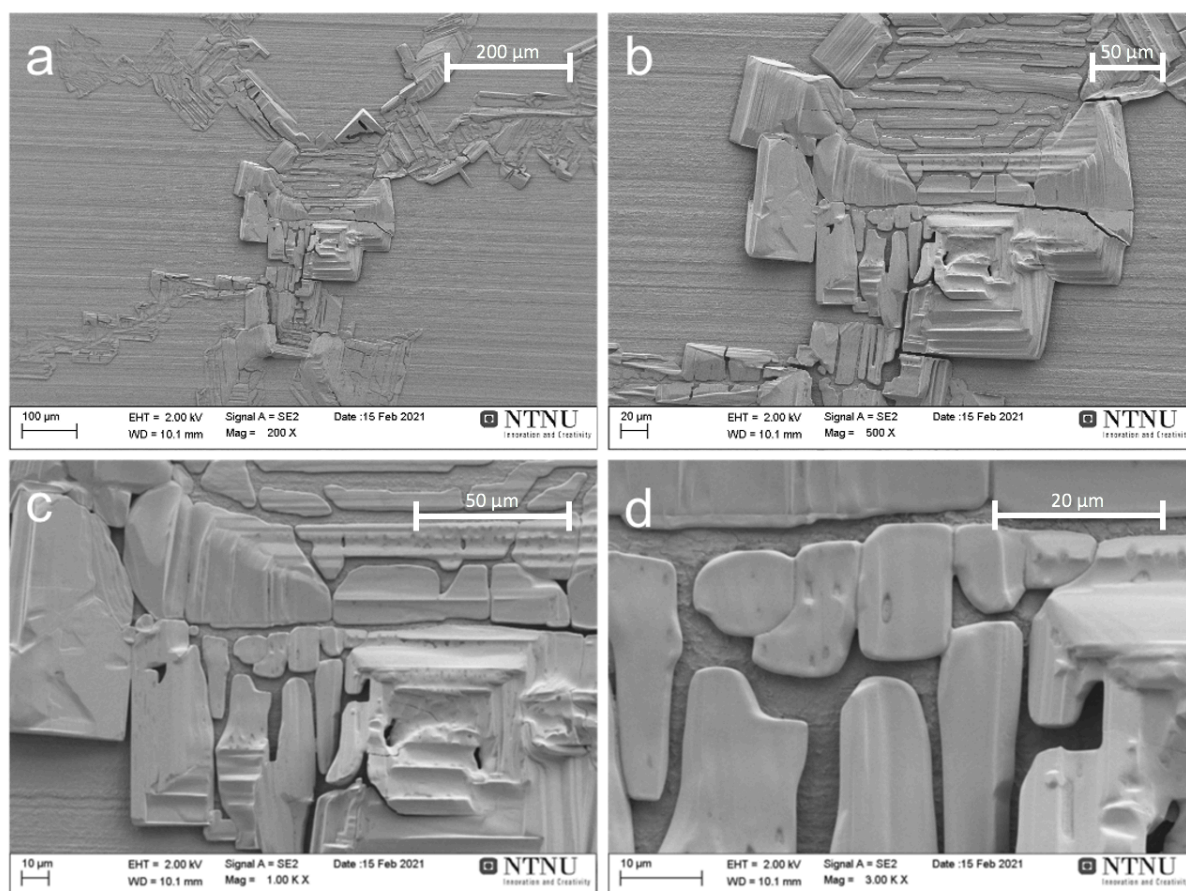

Figure I.22: SEM micrograhs of salt crystals observed on the surface of a sample coated with coating TiN (A) and exposed to PBS solution for 10 days. The sample is imaged at (a) 200 X, (b) 500 X, (c) 1 000 X, and (d) 3 000 X.

On a sample coated with coating TiN (B) and exposed to PBS solution for 3 days a bulge in the sample was observed as shown in Figure I.24. The sample bulge is accompanied by local cracks in the substrate material and in the coating. The coating appears to adhere to the substrate surface.
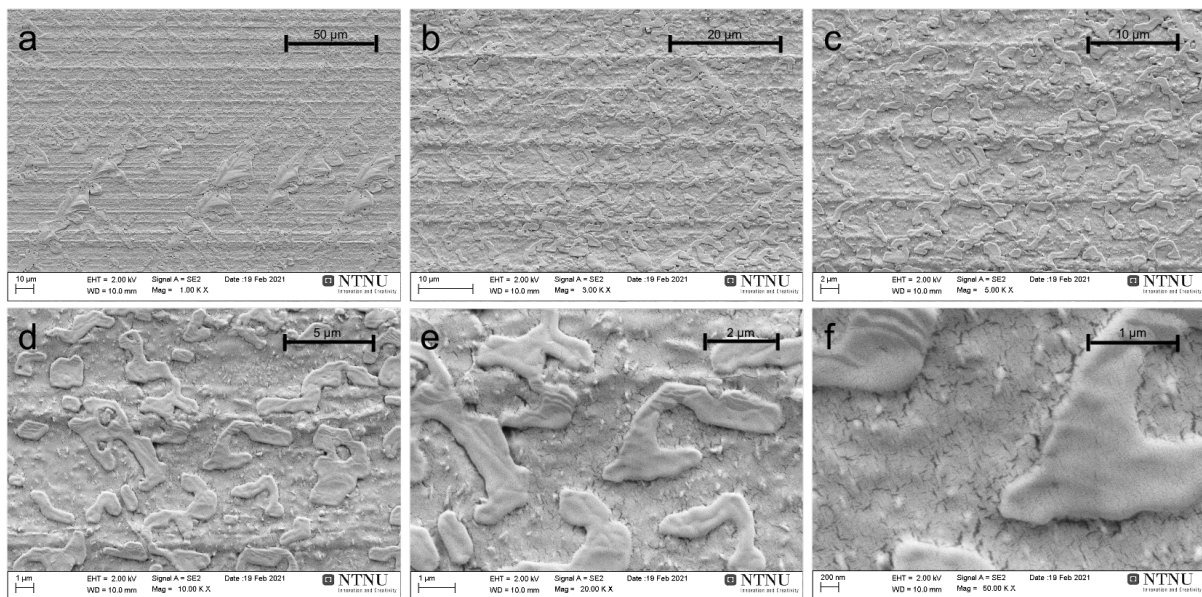
Figure I.23: SEM micrograhs of salt crystals observed on the surface of a sample coated with coating TiN (A) and exposed to PBS solution for 3 days. The sample is imaged at (a) 1 000 X, (b) 3 000 X, (c) 5 000 X, (d) 10 000 X, (e) 20 000 X, and (f) 50 000 X.
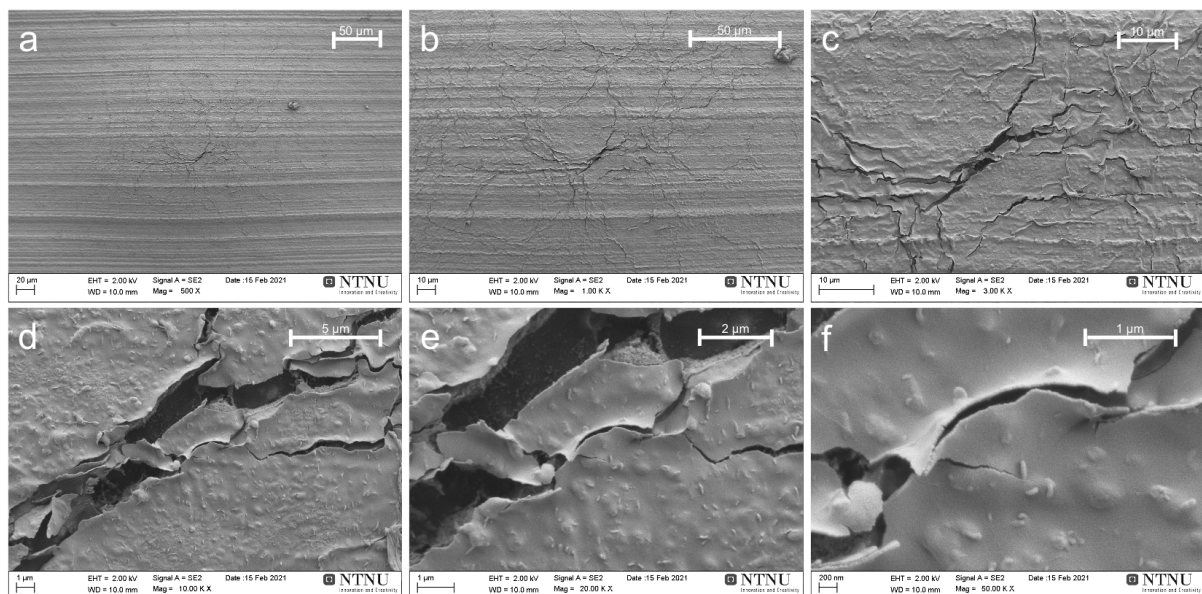

Figure I.24: SEM micrographs of a bulge on the surface of a sample coated with coating TiN (B) and exposed to PBS solution for 3 days. The sample is imaged at (a) 500 X, (b) 1 000 X, (c) 3 000 X, (d) 10 000 X, (e) 20 000 X, and (f) 50 000 X, and the micrographs reveal cracks in the coating.

I.4   Timespan Between End of Exposure Study and SEM Analysis

As it was not expected that the samples would change significantly after ended exposure to PBS, there were varying time intervals between the end of exposure and the SEM analysis of the solid samples. The dates of these events and the timespan between them are presented in Table I.1. The timespan was between 3 days and 28 days for the first round of samples analyzed. A second round of analysis on a second sample was performed for selected time intervals (*i.e.*, 1 hour, 24 hours, 7 days and 30 days), and for these samples the timespan ranged from 94 days to 109 days.

Table I.1: The dates when the exposure study was ended and for when SEM analysis was performed for each of the samples including the time between these events.

Exposure Interval	Exposure End	SEM Analysis	Time Between Events
10 min	10.02.2021	03.03.2021	21 days
30 min	10.02.2021	03.03.2021	21 days
1 hour	10.02.2021	26.02.2021 22.05.2021	16 days 101 days
6 hours	12.02.2021	15.02.2021	3 days
12 hours	13.02.2021	25.02.2021	12 days
24 hours	29.01.2021	03.02.2021 18.05.2021	5 days 109 days
3 days	11.02.2021	15.02.2021	4 days
7 days	04.02.2021	09.02.2021 18.05.2021	5 days 103 days
10 days	22.01.2021	19.02.2021	28 days
30 days	13.02.2021	16.02.2021 18.05.2021	3 days 94 days

Kari Ravnestad Kjørholt, 2021

Optimization of Hemocompatible Thin Film Coatings for Biomedical Applications

NTNU

Norwegian University of
Science and Technology